Metamorphic fluids at extreme pressure conditions

and their significance for element transfer in subduction zones:

A multidisciplinary study on metamorphic veins

in UHP/HP eclogites from Dabieshan, China

Dissertation

submitted to

the Mathematic-Scientific Faculties

of the Georg-August-University Göttingen

in partial fulfillment of the requirements

for the doctoral degree (Dr. rer. nat.)

according to the doctoral program

of the Georg-August University School of Science (GAUSS)

presented by

Nina Albrecht

from Hameln

Göttingen 2017

Thesis committee:

Supervisor: Prof. Dr. Gerhard Wörner (GZG, Dep. Geochemistry)

Co-supervisor: Prof. Dr. Andreas Pack (GZG, Dep. Isotope Geology)

Examination committee:

Prof. Dr. Gerhard Wörner (GZG, Dep. Geochemistry)

Prof. Dr. Andreas Pack (GZG, Dep. Isotope Geology)

Prof. Dr. Yilin Xiao (USTC, School of Earth and Space Sciences Hefei)

Dr. A.M. van den Kerkhof (GZG, Dep. Applied Geology)

Prof. Dr. Sharon Webb (GZG, Dep. Mineralogy)

Prof. Dr. Jonas Kley (GZG, Dep. Structural Geology)

Day of defense:

05. April 2017

Abstract

The present study provides a comprehensive geochemical dataset on ultra-/high pressure (UHP/HP) eclogites and enclosed, fluid-deposited metamorphic veins. It targets to broaden our understanding of the nature and extent of fluid-rock interaction in deep subduction environments, and to evaluate the capability of metamorphic fluids at high pressures to producing elemental fractionations which may account for global mass imbalances such as the enigmatic lead- and niobium paradoxes. This is approached by bringing together geochemistry, isotope geology and a fluid inclusion study to reconstructing fluid origin and compositional evolution as well as fluid-assisted element transport and fractionation in subducting basaltic rocks.

The occurrence of different vein generations records multiple stages of fluid flow during deep subduction and exhumation of continental crust. 1st generation quartz-rutile veins are identified to represent internal remnants of prograde, virtually "dry" eclogite dehydration. The precipitating Si-, and HFSE-bearing aqueous fluids solidify in a closed system at UHP peak conditions, without evidence of retrogression in the host eclogite or detectable compositional fluid evolution.

Fluids that precipitate mineralogical complex 2nd generation veins are found to form at the onset of exhumation from UHP eclogite facies depths. Based on chemical and isotopic fingerprinting, their initial source is determined to be external fluids that are derived from prograde dehydration of bedrock gneisses.

Given the starting situation of a felsic crust with intercalated basaltic bodies being conjointly subducted, a petrogenetic multistage model in consistence with the collected data is reconstructed:

(1) Shallow fluid-rock interaction of comparatively "soft" felsic crust and isotopically light meteoric glaciation waters prior to subduction, while "resistant" basaltic blocks remain widely unaffected.

(2) Prograde dehydration of felsic bedrock (later gneisses) during subduction, resulting in fluid-assisted Ca-, Al-, REE-, LILE-, HFSE-, OH- metasomatism of basalt, that selectively occurs at the gneiss-basalt interface and is most likely explained by lawsonitization.

(3) Conjoint eclogitization of partly metasomatized and partly pristine basalt bodies, producing epidote- and phengite-bearing eclogites that adopt gneissic signatures, alongside pristine grt + omp ± qtz eclogites that retain their precursors geochemical fingerprints.

(4) In-situ formation of 1st generation veins in pristine, ±dry eclogites at the metamorphic UHP peak.

(5) Formation of 2nd generation veins and concurrent pervasive eclogite retrogression, restricted to metasomatized eclogite portions, and supplied by decompressional lawsonite breakdown and by external remnants of gneissic fluids at the onset of exhumation.

(6) Occasional replacement of 2nd generation veins during late retrograde stages, resulting in 3rd generation veins with amphibolite facies mineralogy and eventually greenschist facies overprint.

Fluid inclusion characteristics, vein mineralogy and mineral chemistry document a compositional evolution of post-peak 2nd generation vein-forming fluids, proceeding in three stages.

The initial fluid, derived from lawsonite breakdown, is dominated by Ca, Al, OH, and is rich in REE and most trace elements. It is trapped in primary and possibly early pseudosecondary fluid inclusions found in eclogite and vein minerals during an early retrograde crystallization stage at the onset of exhumation.

This fluid is successively diluted towards the amphibolite facies stage due to element partitioning into newly forming, retrograde (REE-rich) epidote group minerals, either in veins or in retrogressed eclogite. It is trapped at variable stages in pseudo-secondary fluid inclusions.

Secondary fluid inclusions and late (REE-poor) epidote record highly evolved, low salinity fluids that experienced negligible influx of meteoric waters.

Element fractionation is common in the investigated UHP/HP rocks. Nb/Ta is profoundly elevated in rutile of retrogressively affected eclogites relative to Nb/Ta in pristine samples. Fluid-affected eclogites, i.e. rutile therein, are thus identified to be a potential high-Nb- high Nb/Ta candidate to theoretically balance the global niobium deficiency. However, whether or not the crust-mantle vs. eclogite mass balance can be closed depends on the mass of such a reservoir, which is presently unknown.

U/Pb is lowered in retrogressively affected eclogites relative to pristine samples, resulting in shifting of retrogressed eclogites towards unradiogenic $^{206}Pb/^{204}Pb$ compositions. High pressure retrogressed eclogites, as described in this study, are thus a potential candidate to balancing the global lead-paradox. A theoretical residuum after fluid-rock interaction could provide a conceptual explanation for the enigmatic HIMU source.

Acknowledgments

A doctoral thesis is always the final outcome of constructive interaction of various persons with both scientific and non-scientific background, whose contributions shall be acknowledged at this point.

First of all, I convey my sincere gratitude to my supervisor Gerhard Wörner for raising the funding (DFG project WO 362/45-1) and for providing me with this topic. His passion for science and his continuous and encouraging support with fresh ideas and optimism paved my way to working on this thesis with curiosity and confidence.

Yilin Xiao (USTC Hefei) is thanked for initiating this project in the course of a collaboration with the Geoscience Center Göttingen and for conducting the field work in China that left a deep and memorable impression on me.

Andreas Pack is thanked for co-supervising this thesis and for providing me with a research assistant sideline position in his working group alongside my doctoral studies. Working in the stable isotope lab has always been a welcomed change from my PhD project.

My research would not have been possible without the help and reliable support of my colleagues:

Erwin Schiffczyk, Reinhold Przybilla, Harald Tonn, Angelika Reitz and Gabriele Mengel were indispensable helpers in the course of sample preparation and they substantially supported my lab work. Erwin Schiffczyk is especially thanked for his generous helpfulness in the clean lab.

Contents

List of abbreviations

ab	albite
aln	allanite
ap	apatite
ath	anthophyllite
brs	barroisite
BSE	backscattered electron
BX	Bixiling
chl	chlorite
cum	cummingtonite
EMP	electron microprobe
ep/(c-)zo	epidote/(clino-)zoisite
FI	fluid inclusion
fs	femtosecond
grt	garnet
hbl	hornblende
HP/LT	high pressure/low temperature
HW	Huwan
ky	kyanite
LA-ICP-MS	laser ablation inductively coupled plasma mass spectrometry
mhb	magnesio-hornblende
omp	omphacite
pg	paragonite
phe	phengite
PI	primary inclusion
PPL	plane polarized light
PSI	pseudosecondary inclusion
qtz	quartz
rt	rutile
SH	Shuanghe
SI	secondary inclusion
TIMS	Thermal Ionization Mass Spectrometry
ts	tschermakite
(U-)HP	(ultra-)high pressure
UV	ultraviolet
XPL	crossed polarized light
XRF	x-ray fluorescence
ZJC	Zhujiachon
zrn	zircon

1. Introduction

The presence of aqueous fluids and/or melts is a necessary condition for the effective transport of elements during metamorphism, particularly in a cold subduction environment. The present work is dedicated to the investigation of fluid-mediated, geochemical processes and especially mass transfer that occur under ultrahigh pressure (UHP) and high pressure (HP) conditions. Except for rare impact events, these conditions are naturally realized only in deep and comparatively cold subduction zones that are characteristically found along the Earth's major collision belts. Some of such UHP lithologies were tectonically exhumed and provide today's most direct access to high-grade metamorphic fluid processes.

This study provides a multidisciplinary approach, based on metamorphic mineral veins in UHP/HP eclogites from the Dabie UHP terrain in China, to reconstruct fluid origin, compositional fluid evolution and fluid-assisted element fractionation in deep subduction environments. In order to assess these issues, petrographic evidence, bulk and mineral chemistry, a fluid inclusion study, and stable as well as radiogenic isotopes are combined for a systematical characterization of different vein generations and their host eclogites.

1.1 Ultrahigh-pressure metamorphism

1.1.1 History of ultrahigh-pressure metamorphism

Subduction of continental crust into the mantle has been precluded from the conceptual framework of plate tectonics for a long time. The expected buoyancy of crustal lithosphere with respect to denser mantle rocks resulted in a general consensus that the crust-mantle boundary, namely the Mohorovičić discontinuity, limits the burial depth of continental lithologies. A widely endorsed model by ENGLAND AND THOMPSON (1984) proposed a blockade of subduction in the case of continental collision, but crustal duplication by underplating and stacking instead. Seismic imaging supported this theory by providing that continental crust is typically about 20–40 km thick and can be thickened up to about 60–80 km in continental collision zones, such as the Alps, Andes and Himalayas. Corresponding lithostatic pressures at the root of such orogens were thus expected not to exceed 2 GPa.

The report of coesite and diamond microinclusions in highly metamorphosed continental crust by CHOPIN (1984), SMITH (1984), XU ET AL. (1992), (2003) and SOBOLEV AND SHATSKY (1990) conflicted with these considerations. Coesite is a high-pressure polymorph of quartz and its formation requires 2.7–2.8 GPa at about 700°C (BOHLEN AND BOETTCHER, 1982; BOSE AND GANGULY, 1995; MIRWALD AND MASSONNE, 1980) and the occurrence of diamond indicates formation pressures of >3.5 GPa at 700°C (BERMAN, 1979; KENNEDY AND KENNEDY, 1976). With these pressures corresponding to burial depths of at least 100–120 km it became evident that continental lithosphere can be both subducted into the upper mantle as well as returned from mantle depths.

The findings launched a revision of the previous notion of plate tectonics and the limits of continental-collision-type regional metamorphism. The classical metamorphic facies diagram was extended towards pressures >2 GPa and the phase transformation from quartz to coesite was defined to distinguish the high-pressure (HP) quartz-eclogite facies where quartz is stable from the ultrahigh-pressure (UHP) coesite-eclogite facies where coesite is stable (**Figure 1.1**). In the following decades, UHP metamorphic rocks were reported from numerous collision belts worldwide (**Figure 1.2**) (ZHANG ET AL., 2009 and references therein) and deep continental subduction and related UHP

2

metamorphism emerged as being a regular part of the metamorphic cycle, rather than an exotic phenomenon.
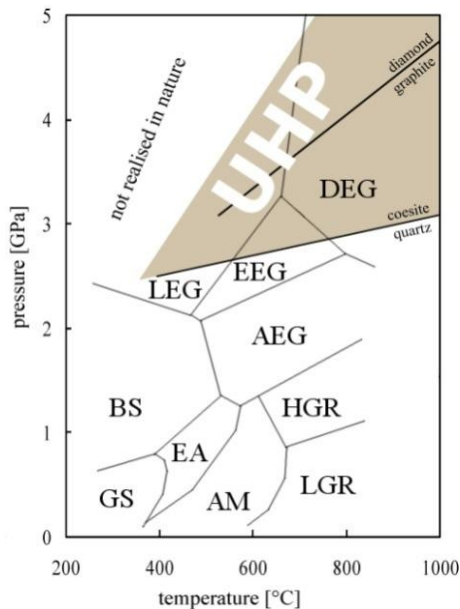
← **Figure 1.1 S**ketch of the classical metamorphic facies fields for crustal rocks (modified after HERMANN AND RUBATTO, 2014). Ultrahigh and high pressure (UHP/HP) metamorphic conditions are defined to be distinguished by the quartz-coesite phase transformation. GS. greenschist, BS: blueschist, AM: amphibolite, EA: epidote amphibolite, GR: granulite, the eclogite-facies are subdivided into amphibole eclogite, epidote eclogite, lawsonite eclogite, and dry eclogite sub-facies.

UHP belts are spatially tied to continental collision terrains and exhibit consistently Phanerozoic ages. The absence of older UHP rocks is well explained by the secular decrease of the estimated subduction zone geotherm through geologic times. UHP metamorphism became possible only after the geotherm fell below the wet solidus of MORB at about 600 Ma, which inhibited regional slab melting (MARUYAMA AND LIOU, 2005). Exposed UHP rocks that evolved from oceanic crust are rare, which is due to the higher density of the mafic oceanic rocks in contrast to felsic continental crust. While the latter remains, at least in the upper mantle, buoyant with respect to mantle rocks, high-grade metamorphosed oceanic lithosphere has similar or higher densities than mantle material and is thus improbable to be exhumed (AGARD ET AL., 2009; GERYA ET AL., 2002).

The occurrence of index minerals and their relics in UHP lithologies seemed to be restricted to rare metabasites (primarily eclogites) at first. Because regional metamorphic belts mainly comprise quartzo-feldspathic lithologies with sedimentary or granitic origin, interpretations of allochthonous formation mechanisms of mafic UHP units prevailed first (CONG ET AL., 1995), explaining the juxtaposition of mafic and gneissic lithologies by tectonic melange environments.
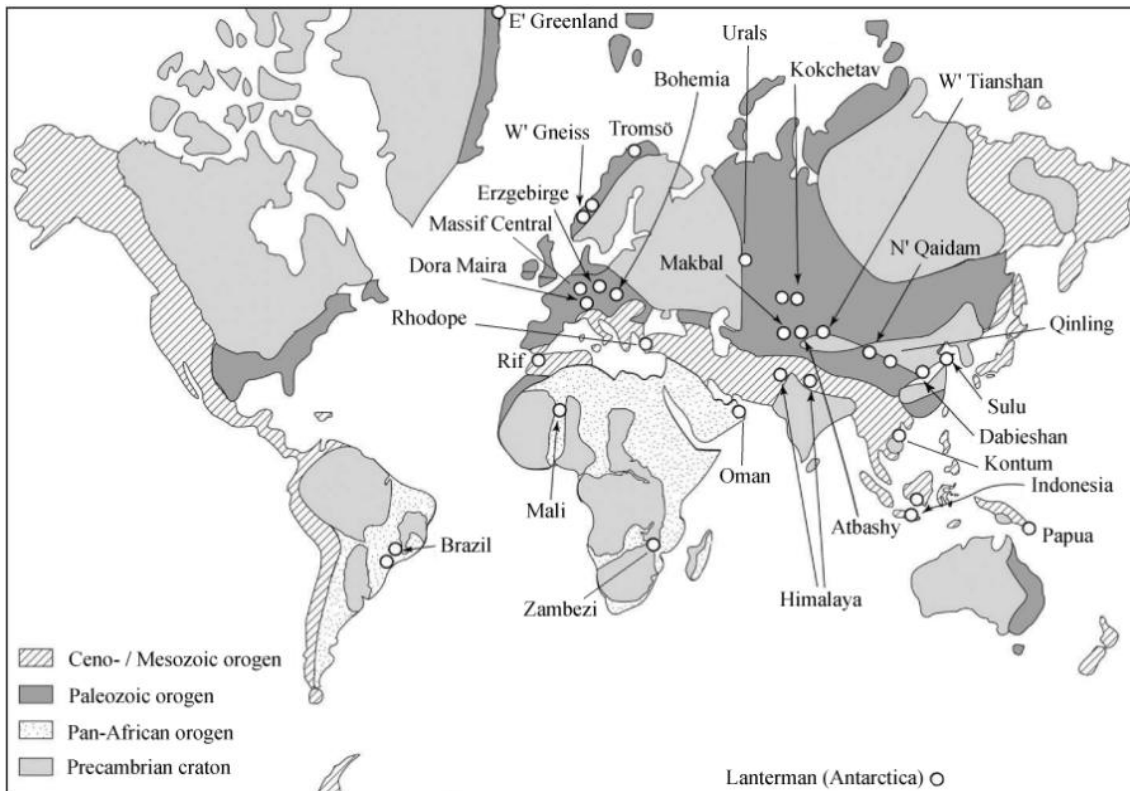
↑ Figure 1.2 Global distribution of UHP metamorphic rocks, partly modified after MARUYAMA ET AL. (2010) and GILOTTI (2013). The occurrence of UHP terrains correlates to the world's major collision belts. About 30 UHP localities worldwide are known today, identified either by the presence of coesite and diamond, or inferred by respective pseudomorphs.

Later studies identified microcoesite and -diamond also in zircon crystals from the ubiquitous felsic lithologies, pointing at a coherent subduction theory where granitic and sedimentary rocks as well as the metabasite precursors have jointly undergone HP-UHP metamorphism (KATAYAMA ET AL., 2000; KANEKO ET AL., 2003; LIU ET AL., 2001; RUMBLE ET AL., 2003; TABATA ET AL., 1998; YE ET AL., 2000). The apparent predominance of metabasitic UHP occurrences is merely owed to the fact that the prograde UHP record has been widely obliterated by retrograde overprinting within less robust gneissic parageneses. Refractory minerals like zircon, eclogitic garnet and clinopyroxene behave as rigid containers to UHP indicators and their relics (CARSWELL ET AL., 2000; MASAGO ET AL., 2010), and thus mafic rocks preserve UHP features better than felsic lithologies.

1.1.2   Deep continental subduction

The evolution of UHP metamorphic belts is complex and depends on the individual interplay of tectonic forces, buoyancy effects and surface processes while the emphasis of involved mechanisms as well as the external and internal conditions may vary over time. The modern understanding of regional and associated UHP metamorphism is consistently based on three common processes: (i) deep subduction and dehydration of continental lithosphere as a result of regional continental-collision-type metamorphism, (ii) exhumation from mantle depths to mid-crustal levels along with the circulation of hydrous fluids and ongoing amphibolite-facies retrogression, (iii) mountain building that exposes the metamorphic units to the surface. For reviews on regional UHP metamorphism see MARUYAMA ET AL. (2010), HERRMANN AND RUBATTO (2014), and references therein.

Deep subduction of continental crust may be initiated by the subduction of attached, dense oceanic crust, as it is the case at passive continental margins (BELTRANDO ET AL., 2010; CLOOS, 1993). Once subducted, this slab-pull process may subsequently be maintained by another slab-pull force that is generated at mantle depths beyond pressures of 9 GPa, where the density of quartzo-feldspathic rocks becomes higher relative to mantle material (IRIFUNE ET AL., 1994). Buoyancy effects in shallower levels are assumed to be, however, ineffective due to the comparably small size and low aspect ratio of regional metamorphic belts, and are assumed to not impede the subduction process (MARUYAMA ET AL., 2010).

Exhumation mechanisms that attempt to explain the uplift of continental UHP metamorphic slices from mantle depths generally base upon scenarios that include the detachment of an UHP slice from the down going slab (HERRMANN AND RUBATTO, 2014). In case of passive continental margin subduction, a slab break-off of the denser oceanic slab would lead to an increase of buoyant forces within the remaining continental slab and thus trigger exhumation. Wedge extrusion models that propose tectonic upward 'squeezing' of the regional belt during its insertion between a rigid mantle and slab wedge and concomitant shallowing of the subduction angle (MARUYAMA ET AL., 1996) are also conceivable. In this regard, the association of mafic UHP lithologies to less dense and less rigid

materials (eg. serpentinite) is furthermore supposed to promote exhumation (HERMANN ET AL., 2000). GEYRA ET AL. (2002) developed a numerical model and propose a forced return flow of low-viscosity material (eg. eclogite) within a subduction channel that is progressively widened by hydration of the mantle wedge. Once the crustal level is reached, UHP tectonic blocks are assumed to be emplaced as high-temperature solid intrusions, similar to magma intrusions (KATAYAMA ET AL., 2001; TERABAYASHI ET AL., 2002). According to MARUYAMA ET AL. (2010) and references therein, the initial idea of a rapid exhumation of UHP units has been relativized. The exhumation rate of UHP units to the mid-crustal level is in the range of 5–35 mm/year and thus one order of magnitude slower than recent uplift rates measured in the Himalayas.

Final mountain building and folding is temporarily unrelated to the initial exhumation stage and is mainly driven by doming and related faulting, and finally modified by late surface processes linked to erosion (KANEKO ET AL., 2003).

1.2 Fluids during deep subduction

1.2.1 Aqueous fluids in deep subduction environments

While melting within, usually cold, UHP slabs occurs only locally, the presence of hydrous fluids during deep continental subduction and subsequent exhumation is ubiquitous (SCAMBELLURI AND PHILIPPOT, 2001). The down going slab is continuously dehydrated as subjected to increasing P–T conditions and the availability of fluids during exhumation from mantle depths to crustal levels is reflected by extensive intermediate facies hydration-recrystallization.

The occurrence of primary fluid inclusions in UHP/HP eclogitic minerals provides evidence for the existence of prograde fluids during eclogitization (eg. ANDERSEN ET AL., 1993; GIARAMITA AND SORENSEN, 1994; KLEMD ET AL., 1992; PHILIPPOT AND SELVERSTONE, 1991; SCAMBELLURI ET AL., 1998; TOURET, 1992), and the incidence of hydroxyl-bearing phases such as epidote, zoisite, phengite, talc and lawsonite as part of peak metamorphic assemblages in coesite-bearing eclogites (eg. CARSWELL, 1997; GUO ET AL., 2013; LIOU AND ZHANG, 1995; NAGASAKI AND ENAMI, 1998; ZHANG ET AL., 1995) refutes the previously prevalent notion of dry conditions during eclogitization and related UHP metamorphism. Numerous findings of hydrous phase-bearing mineral veins (eg. BECKER ET AL., 1999; CASTELLI ET AL., 1998; FRANZ ET AL., 2001; GUO ET AL., 2012; JOHN ET AL., 2008; WU ET AL., 2009; XIAO ET AL., 2011; ZHANG ET AL., 2008; ZHENG ET AL., 2007) in UHP/HP rocks from different metamorphic stages furthermore demonstrate a substantial involvement of fluid phases during metamorphic evolution.

The main source of aqueous fluids during prograde metamorphism are rock-forming hydrous minerals from within the subducting slab lithologies, such as mica, amphibole, chlorite, talc, epidote, or pumpellyite (HACKER ET AL., 2003; POLI AND SCHMIDT, 2002; THOMPSON, 1992). These phases are progradely destabilized due to increasing P–T conditions during ongoing subduction, resulting in a gradually release of aqueous fluids over a depth range of 65–90 km (SCHMIDT AND POLI, 1998). At subsolidus conditions the transport of water to greater depths is tied to UHP-stable hydrous phases

such as phengite, zoisite-clinozoisite, lawsonite, talc, clinohumite, staurolite or antigorite (LIOU ET AL., 1995; PAWLEY AND HOLLOWAY, 1993; SCHMIDT AND POLI, 1998; SCHREYER ET AL., 1988; ULMER AND TROMMSDORFF, 1995; ZHANG ET AL., 1995), or trapped pore fluids along grain boundaries and microfractures (ZHENG, 2009, 2012). While part of the water released during early mica and amphibole breakdown will return to the Earth's surface via magmatism, some fractions are incorporated into the above-mentioned UHP hydrous phases within the subducting slab. These phases are able to store water far beyond 200 km in mature, ie. cold, subduction zones (COMODI AND ZANAZZI, 1996; DOMANIK AND HOLLOWAY, 1996; POLI AND SCHMIDT, 1995). Further feasible pathways for water to great depths are structurally bound hydroxyl that may be contained in nominally anhydrous minerals (eg. omphacite, garnet and rutile) up to contents of 1000 ppm under high pressure conditions (HIRSCHMANN ET AL., 2005; SU ET AL., 2002; ZHANG ET AL., 2001), or fluid inclusions (PHILIPPOT AND SELVERSTONE, 1991; ZHENG, 2004).

Possible sources of retrograde fluids include recycled prograde fluids, fluids that are liberated by decompressional dehydration of hydrous HP phases during uplift (eg. talc and lawsonite), exsolution of water from nominally anhydrous minerals, or external water derived from surrounding host rocks (ZONG ET AL., 2010). Such fluids have the potential to trigger partial melting and retrograde reactions within the host rock and can be the source of metamorphic veins. Meteoric waters that may infiltrate the Earth's crust along fault zones to depths of several kilometers can be involved at the final stage of exhumation (eg. FRICKE ET AL., 1992; MORRISON, 1994; UPTON ET AL., 1995).

The initial composition of aqueous UHP/HP fluids apparently depends on the nature of the dehydrating protolith as well as ambient conditions, whereas the composition of the infiltrated host rock and proceeding dissolution-precipitation reactions can influence the element inventory. Observed compositions range from dilute aqueous solutions to high-salinity brines and supercritical liquids possibly preserved as multiphase solid inclusions - all with variable concentrations of fluid-mobile, incompatible trace elements (ZHENG AND HERMANN, 2014).

YARDLEY AND GRAHAM (2002) compiled that prograde fluids liberated from continental crust bear higher solute contents compared to fluids derived from oceanic crust. In general, the mineral

assemblage of the host rock to a coexisting fluid phase controls especially the fluid's trace element signature. LILE are mainly controlled by the presence of phengite, garnet is the major host of HREE, epidote group minerals are major carriers of LREE, Th, U, and Sr, and rutile hosts almost all HFSE (ZHENG AND HERMANN, 2014 and references therein). PHILIPPOT (1993) and BUREAU AND KEPPLER (1999) propose, that the early dehydration breakdown of amphibole at shallower levels will release mobile and low-salinity fluids with little dissolved silica on a large scale, whereas the decomposition of HP hydrous phases at greater (UHP) depths will rather result in a release of heterogeneous, high-silica fluids with significant element load.

The major modification processes of such metamorphic fluids include scavenging of the infiltrated host rock (JOHN ET AL., 2008) and metamorphic mineral reactions. Hydration reactions induce a 'distillation' of the metamorphic fluid, potentially accounting for observed concentrated brines (SCAMBELLURI ET AL., 1997; SCAMBELLURI ET AL., 1998; SVENSEN ET AL 1999). Dehydration reactions and accompanying mineral decomposition are expected to add both water and part of the elemental inventory of the destabilized minerals to the fluid. The precipitation of metamorphic mineral veins with often hydrous mineral inventory could partially consume the fluid phase and potentially result in element fractionation in the residual fluids.

1.2.2   The role of UHP/HP fluids in global element recycling

Subduction zones are powerful factories of fluid-mediated mass transfer, element recycling and redistribution. It is well documented for subducted crust, that significant element fractionation and differentiation can occur during partial melting and, to a lesser extent, by interaction with aqueous fluids. For reviews on the geochemical nature of subduction-related fluids refer to HACK ET AL. (2007), HERMANN ET AL. (2006), HERMANN AND RUBATTO (2014), MANNING (2004), POLI AND FUMAGALLI (2003), ZHENG AND HERMANN (2014).

Subduction of continental crust, in contrast to oceanic crust, holds striking differences: metamorphosed continental crust may be returned to the Earth's surface, continental subduction zones are cold since the geothermal gradient is generally low, and a free fluid phase is comparatively scarce.

Melting in a continental slab during UHP metamorphism is thus reliant on water supplying dehydration reactions, the virtual absence of phengite and sufficient temperatures (RUBATTO AND HERMANN, 2014). These conditions are commonly not fulfilled for UHP terrains. Although fine-scale anatectic melting linked to decompression and in-situ breakdown of hydrous minerals on the retrograde metamorphic path is possible (eg. ZHENG ET AL., 2011; WANG ET AL., 2014), and gneissic migmatites occur within UHP terrains, extensive melting within UHP lithologies remains largely absent.

Fluids that are liberated in oceanic subduction zones at mantle depths trigger large-scale partial melting in the overlying wedge and can be indirectly accessed by investigation of arc volcanics (eg. MCCULLOCH AND GAMBLE, 1991 ; PEARCE AND PEATE, 1995; STERN, 2002; TATSUMI AND EGGINS, 1995). The direct rock record in the form of exhumed blueschist- to eclogite-facies lithologies is, however, limited from depths <80 km (AGARD, 2009). Continental subduction zones lack considerable volcanism, but UHP terrains provide a direct rock record from depths far beyond 100 km and play an outstanding role in deciphering deep fluid-rock interaction.

Element partitioning experiments using synthetic MORB compositions have demonstrated that extreme pressures as well as temperatures result in both the enhancement of trace element solubilities in the fluid phase of up to two orders of magnitude and in fractionation of especially REE (KESSEL ET AL., 2005). Fluids under UHP conditions may even mobilize HFSE (eg. SCAMBELLURI AND PHILIPPOT, 2001), and studies on natural UHP eclogites and enclosed rutile-bearing mineral veins confirmed not only the apparent mobility of Ti, Nb, Ta, Zr and Hf, but also a fractionation among these elements (eg. BECKER ET AL., 1999; BECKER ET AL., 2000; GAO ET AL., 2007; HUANG ET AL., 2012; JOHN ET AL., 2004; LIANG ET AL., 2009; XIAO ET AL., 2006) that were traditionally regarded as being immobile throughout subduction (PEARCE AND PEATE, 1995). The presence of halogen group elements enhances these effects (KEPPLER, 1996; RAPP, 2010). Fractionation depends on an interplay of ambient conditions, the amount and nature of fluid, as well as host rock composition. Partition coefficients $D_{fluid-mineral}$ at UHP/HP conditions are, however, difficult to constrain and are only sparsely available for UHP eclogite and associated complex (magmatic) vein parageneses (eg. FOLEY, 2005;

JENNER ET AL., 1993; KESSEL, 2005). Appropriate knowledge of partitioning between minerals and an aqueous fluid phase may hold clues on the deciphering of enigmatic questions such as the apparent imbalance in the Earth's Nb/Ta budget (eg. PFÄNDER ET AL., 2007) and the source for HIMU magmas (eg. STRACKE ET AL., 2005), but the determination is not straight forward since mineral veins that precipitated from aqueous fluid cannot be handled as a closed system.

A major unsettled issue is the nature of UHP fluids. The ambient conditions that UHP rocks (and fluids) experience along the metamorphic path can fall beyond the estimated critical point of the schematic phase diagram of an average continental crust composition (HERMANN ET AL., 2006; MANNING, 2004). It is thus possible that UHP fluids adopt a supercritical state, revoking the distinction between a hydrous melt and a solute-rich aqueous fluid. Supercritical liquids are expected to be the qualitatively most effective agents of mass transport in UHP regimes (KEPPLER, 1996), but natural examples of multiphase solid inclusions potentially trapping such fluids are rare (FERRANDO ET AL., 2005; STÖCKHERT ET AL., 2001; VAN ROERMUND ET AL., 2002; MALASPINA ET AL., 2006). For a review on supercriticality during UHP metamorphism refer to ZHENG ET AL.(2011).

UHP/HP fluids are mostly interpreted to form in-situ and to be mobile on a small scale only. Consequently, the fluid's element load should be tied to dissolution reactions of the respective host rock (eg. PHILIPPOT AND SELVERSTONE, 1991; SCAMBELLURI AND PHILIPPOT, 2001; SPANDLER, 2003) within a virtually closed system. BARNICOAT AND CARTWRIGHT (1995) , GAO ET AL. (2007) and JOHN ET AL. (2008) instead give evidence that fluids in high-pressure environments can move over long distances along focused and permeable reaction zones, and that, a sufficient fluid-rock ratio provided, they are able to scavenge the rocks they are passing through and to precipitate their element load far off.

The amount of water that is initially buried in suduction zones exceeds the amount of water that is released through magmatic and volcanic systems (SCHMIDT AND POLI, 1998; ANGIBOUST AND AGARD, 2010), and certain portions of prograde fluids may be trapped and retained within the subducting lithologies during burial (SCAMBELLURI AND PHILIPPOT, 2001). Channels of fluid escape

towards the surface other than volcanism and to a minor extent the formation of retrograde (ie. hydrated) rocks are not known yet, and based on the observation of deep-focus earthquakes at mantle depths, MEADE AND JEANLOZ (1991) propose a partial recycling of subducted fluid into the mantle. Considering fluid and element mobility as well as element partitioning, devolatilization-induced UHP/HP fluids are ascribed an important role in controlling the elemental budget and mass transport between crust and mantle in subduction zones. They may account for the transfer of slab signatures to the overlying mantle wedge, and for leaving behind either metasomatised rocks or residual rocks after dehydration for deeper subduction. Their sources and element load, pathways within the slab, timing during the subduction process, and the conditions and extents of element partitioning, however, hold fundamental questions that can promisingly be addressed through the study of UHP fluid-rock interaction on the basis of exhumed UHP rocks.

1.2.3 Deep fluid-rock interaction recorded by UHP/HP metamorphic veins

Solid evidence for hydrous fluid activity in a rock during metamorphism is provided by metamorphic mineral veins enclosed in UHP/HP lithologies. These veins precipitated from aqueous fluids and can be distinguished from solidified partial melts by structural and petrographic evidence. Their usually polymineralic assemblages often comprise quartz, refractory minerals like rutile, HP phases such as omphacite, phengite and kyanite, as well as hydrous epidote group minerals, talc, clinohumite and amphibole (eg. FRANZ ET AL., 2001; GUO ET AL., 2015; ZHANG ET AL., 2008; ZHENG ET AL., 2007). The formation of such veins has been diversely interpreted to be either related to prograde dehydration reactions (eg. BECKER ET AL., 1999; CASTELLI ET AL., 1998; ZHANG ET AL., 2008), to eclogitization (JOHN ET AL., 2008; GAO AND KLEMD, 2001), or to the local retrograde breakdown of UHP stable hydrous phases (eg. CHEN ET AL., 2012; FRANZ ET AL., 2001; GUO ET AL., 2015; SHENG ET AL., 2013). Next to rare multiphase solid inclusions (FERRANDO ET AL., 2005), primary aqueous inclusions with variable compositions have been repeatedly identified within UHP rocks and associated veins (FU ET AL., 2002; PHILIPPOT AND SELVERSTONE, 1991; LI ET AL., 2006; XIAO ET AL., 2000; ZHANG ET AL., 2008). They provide an even more direct approach to the original fluid than vein minerals. Although

high-grade metamorphic conditions lead to density re-equilibration of the inclusions during exhumation in most cases (VITYK AND BODNAR, 1995), changes affect fluid inclusion volume rather than causin significant modification of content by leakage or diffusion (STERNER AND BODNAR 1989; GAO AND KLEMD 2001).

1.3   Approach of the present study

This project targets to contribute to a better understanding of the nature and extent of fluid-rock interaction in deep subduction environments, using metamorphic veins as proxies for processes that occur during deep subduction and UHP/HP conditions.

Although metamorphic mineral veins unequivocally represent only vestiges of the fluid present at the time of their precipitation rather than the fluid itself, they arguably allow the most robust access to the nature of deep fluids. Their mineral inventories as well as the alteration in the adjacent host rock basically display the range of elements that were mobilized by the circulating fluid. Detailed characterization of vein mineral and element inventories and associated country rock may provide host rock/ fluid partition coefficients. This theoretical approach is, however, complicated by the fact that vein precipitation may proceed via multiple dissolution-precipitation reactions in a small-scale open system rather than from continuous precipitation from a bulk fluid volume (ZHENG AND HERMANN, 2014). But analogous to inferring a melt composition from an igneous rock, a metamorphic vein formed by fluids can be considered to reflect a residue after a series of complex processes. Although the bias of this residue throughout the metamorphic evolution can be expected to be distinctly more pronounced compared to a plutonic rock, metamorphic veins are expectedly the best attempt to decipher U/HP fluid composition and related fluid-rock interaction.

The basis of the present case study are samples from a set of high-grade polymineralic metamorphic veins enclosed within UHP eclogites from various localities in the Dabieshan in Eastern Central China. These veins formed at different metamorphic stages between peak and late retrograde

conditions and can be assigned to different generations via structural and petrographic evidence. The related host eclogites vary from pristine to strongly retrogressed rocks.

Chapter 2 presents an introduction to the geological setting and the P-T-t evolution of the sampling sites.

Chapter 3 provides a structural and petrographic characterization of the investigated samples. Both chapters serve as a common basis for the following main sections, that are otherwisely self-contained.

Chapter 4 targets to quantify the element budget of UHP/HP veins and eclogites and fluid-assisted fractionation. It aims to assess the compositional characteristics of the vein-forming U/HP fluids. This is done by detailed characterization of the major and trace element inventories of the different vein generations and adjacent host rocks by means of electron microprobe (EMP), and laser ablation inductively coupled plasma mass spectrometry (LA-ICPMS) on bulk samples and single minerals. Mass-balancing of bulk vein model compositions is done in order to derive the potential of the underlying fluids to transport and fractionate trace elements in subducted basaltic rocks, and how they affect their hosting eclogites. Element fractionation is investigated with special emphasis on and the Earth's enigmatic Nb-anomaly, and Pb and Sr isotopic compositions are used to test if fluid-affected, residual UHP/HP rocks are eligible sources for global HIMU magma signatures.

Chapter 5 intends to trace back the evolution of UHP/HP fluids along the metamorphic path. This is approached through linking of mineral chemistry and fluid inclusion evidence. The textural relations of fluid inclusions and the related distinction of different inclusion assemblages, their individual compositions derived from Raman spectroscopy, microthermometry and ultraviolet femtosecond laser ablation inductively coupled plasma mass spectrometry (UV-fs-LAICPMS) and estimates on the ambient P–T conditions during their formation record distinct compositional changes of the vein-forming fluids between peak and late retrograde metamorphic stages. Basically depending on the UHP/HP host rock mineralogy, these changes can be qualitatively related to changing ambient conditions and accompanying metamorphic reactions on the prograde as well as on the retrograde path. Possible sources of the vein-forming fluids are addressed via stable oxygen isotope and radiogenic isotope signatures (Rb-Sr, Pb) of both vein and eclogitic minerals as well as bulk eclogites.

1.4   References

Agard P, Yamato P, Jolivet L, Burov E (2009) Exhumation of oceanic blueschists and eclogites in subduction zones: Timing and mechanisms. *Earth Sci Rev 92*: 53–79.

Andersen T, Austrheim H, Burke EAJ, Elvevold S (1993) N_2 and CO_2 in deep crustal fluids: evidence from the Caledonides of Norway. *Chem Geol 108*: 113–132.

Angiboust S, Agard P (2010) Initial water budget: The key to detaching large volumes of eclogitized oceanic crust along the subduction channel? *Lithos 120(3)*: 453–474.

Barnicoat AC, Cartwright I (1995) Focused fluid flow during subduction: oxygen isotope data from high-pressure ophiolites of the western Alps. *Earth Planet Sci Lett 132(1)*: 53–61.

Becker H, Jochum KP, Carlson RW (1999) Constraints from high-pressure veins in eclogites on the composition of hydrous fluids in subduction zones. *Chem Geol 160*: 291–308.

Becker H, Jochum KP, Carlson RW (2000) Trace element fractionation during dehydration of eclogites from high-pressure terranes and the implications for element fluxes in subduction zones. *Chem Geol 163(1)*: 65–99.

Beltrando M, Compagnoni R, Lombardo B (2010) (Ultra-) high-pressure metamorphism and orogenesis: An Alpine perspective. *Gondwana Res 18*: 147–166.

Berman R (1979) Thermal properties. *In: The properties of diamond.* Academic Press, London: 3–22.

Bohlen SR, Boettcher AL (1982) The Quartz $\leftrightarrows$ Coesite Transformation: A precise determination and the effects of other components. *J Geophys Res* 87: 7073–7078.

Bose K, Ganguly J (1995) Quartz-coesite transition revisited – Reversed experimental determination at 500–1200°C and retrieved thermochemical properties. *Am Mineral* 80: 231–238.

Bureau H, Keppler H (1999) Complete miscibility between silicate melts and hydrous fluids in the upper mantle: experimental evidence and geochemical implications. *Earth Planet Sci Lett 165(2)*: 187–196.

Carswell DA, O'Brien PJ, Wilson RN, Zhai M (1997) Thermobarometry of phengite-bearing eclogites in the Dabie Mountains of Central China. *J Metamorph Geol 15*: 239–252.

Carswell DA, Wilson RN, Zhai M (2000) Metamorphic evolution, mineral chemistry and thermobarometry of schists and orthogneisses hosting ultra-high pressure eclogites in the Dabieshan of central China. *Lithos 52*: 121–155.

Castelli D, Rolfo F, Compagnoni R, Xu ST (1998) Metamorphic veins with kyanite, zoisite and quartz in the Zhujiachong eclogite, Dabie Shan, China. *Isl Arc 7*: 159–173.

Chen RX, Zheng YF, Hu Z (2012) Episodic fluid action during exhumation of deeply subducted continental crust: geochemical constraints from zoisite–quartz vein and host metabasite in the Dabie orogen. *Lithos 155*: 146–166.

Chopin C (1984) Coesite and pure pyrope in high-grade blueschists of the Western Alps: A first record and some consequences. *Contrib Mineral Petrol 86*: 107–118.

Cloos M (1993) Lithospheric buoyancy and collisional orogenesis: Subduction of oceanic plateaus, continental margins, island arcs, spreading ridges, and seamounts. *Geol Soc Am Bull 105*: 715–737.

Comodi P, Zanazzi PF (1996) Effects of temperature and pressure on the structure of lawsonite. *Am Mineral 81*: 533–841.

Cong BL, Zhai MG, Carswell DA, Wilson RN, Wang QC, Zhao ZY, Windley BF (1995) Petrogenesis of ultrahigh-pressure rocks and their country rocks at Shuanghe in the Dabie Mountains, Central China. *Eur J Mineral 7*: 119–138.

Domanik KJ, Holloway JR (1996) The stability and composition of phengitic muscovite and associated phases from 5.5 to 11 GPa: implications for deeply subducted sediments. *Geochim Cosmochim Ac 60*: 4133–4150.

England PC and Thompson AB (1984) Pressure–Temperature–Time Paths of Regional Metamorphism I. Heat Transfer during the Evolution of Regions of Thickened Continental Crust. *J Petrol 25(4)*: 894–928.

Ferrando S, Frezzotti ML, Dallai L, Compagnoni R (2005) Multiphase solid inclusions in UHP rocks (Su-Lu, China): remnants of supercritical silicate-rich aqueous fluids released during continental subduction. *Chem Geol 223(1)*: 68–81.

Franz L, Romer RL, Klemd R, Schmid R, Oberhansli R, Wagner T, Shuwen D (2001) Eclogite-facies quartz veins within metabasites of the Dabie Shan (eastern China): pressure-temperature-time-deformation path, composition of the fluid phase and fluid flow during exhumation of high-pressure rocks. *Contrib Mineral Petrol 141(3)*: 322–346.

Fricke HC, Wickham SM, O'Neil JR (1992) Oxygen and hydrogen isotope evidence for meteoric water infiltration during mylonitization and uplift in the Ruby Mountains-East Humboldt Range core complex, Nevada. *Contrib Mineral Petr 111(2)*: 203–221.

Foley SF, Barth MG, Jenner GA (2000) Rutile/melt partition coefficients for trace elements and an assessment of the influence of rutile on the trace element characteristics of subduction zone magmas. *Geochim Cosmochim Ac 64(5)*: 933–938.

Fu B, Zheng YF, Touret JL (2002) Petrological, isotopic and fluid inclusion studies of eclogites from Sujiahe, NW Dabie Shan (China). *Chem Geol 187(1)*: 107–128.

Gao J, Klemd R (2001) Primary fluids entrapped at blueschist to eclogite transition: evidence from the Tianshan meta-subduction complex in northwestern China. *Contrib Mineral Petrol 142(1)*: 1–14.

Gao J, John T, Klemd R, Xiong X (2007) Mobilization of Ti–Nb–Ta during subduction: evidence from rutile-bearing dehydration segregations and veins hosted in eclogite, Tianshan, NW China. *Geochim Cosmochim Ac 71(20)*: 4974–4996.

Gerya T, Stöckhert B, Perchuck A (2002) Exhumation of high-pressure metamorphic rocks in a subduction channel: A numerical simulation. *Tectonics 21(6)*: 1056–1082.

Giaramita MJ, Sorensen SS (1994) Primary fluids in low-temperature eclogites: evidence from two subduction complexes (Dominican Republic, and California, USA). *Contrib Mineral Petrol 117*: 279–292.

Gilotti JA (2013) The realm of ultrahigh-pressure metamorphism. *Elements 9(4)*: 255–260.

Guo S, Ye K, Chen Y, Liu J, Mao Q, Ma Y (2012) Fluid–rock interaction and element mobilization in UHP metabasalt: Constraints from an omphacite–epidote vein and host eclogites in the Dabie orogen. *Lithos 136*: 145–167.

Guo S, Ye K, Wu TF, Chen Y, Yang YH, Zhang LM, Liu JB, Mao Q, Ma YG (2013) A potential method to confirm the previous existence of lawsonite in eclogite: the mass imbalance of Sr and LREEs in multistage epidote (Ganghe, Dabie UHP terrane). *J Metamorph Geol 31*: 415–435.

Guo S, Chen Y, Ye K, Su B, Yang Y, Zhang L, Liu J, Mao Q (2015) Formation of multiple high-pressure veins in ultrahigh-pressure eclogite (Hualiangting, Dabie terrane, China): Fluid source, element transfer, and closed-system metamorphic veining. *Chem Geol 417*: 238–260.

Hack AC, Hermann J, Mavrogenes JA (2007) Mineral solubility and hydrous melting relations in the deep earth: Analysis of some binary A–H2O system pressure-temperature-composition topologies. *Am J Sci 307(5)*: 833–855.

Hacker BR, Abers GA, Peacock SM (2003) Subduction factory 1. Theoretical mineralogy, densities, seismic wave speeds, and H_2O contents. *J Geophys Res 108*: 2029–2054.

Hermann J, Müntener O, Scambelluri M (2000) The importance of serpentinite mylonites for subduction and exhumation of oceanic crust. *Tectonophysics 327*: 225–238.

Hermann J, Spandler C, Hack A, Korsakov AV (2006) Aqueous fluids and hydrous melts in high-pressure and ultra-high pressure rocks: implications for element transfer in subduction zones. *Lithos 92(3)*: 399–417.

Hermann J, Rubatto D (2014) Subduction of continental crust to mantle depth: Geochemistry of ultra-high pressure rocks. In: *Treatise on Geochemistry 2(4) The Crust*: 309. Oxford: Elsevier.

Hirschmann MM, Aubaud C, Withers AC (2005) Storage capacity of H_2O in nominally anhydrous minerals in the upper mantle. *Earth Planet Sci Lett 236*: 167–181.

Huang J, Xiao Y, Gao Y, Hou Z, Wu W (2012) Nb–Ta fractionation induced by fluid-rock interaction in subduction-zones: constraints from UHP eclogite-and vein-hosted rutile from the Dabie orogen, Central-Eastern China. *J Metamorph Geol 30(8)*: 821–842.

Irifune T, Ringwood AE, Hibberson WO (1994) Subduction of continental crust and terrigenous and pelagic sediments: an experimental study. *Earth Planet Sc Lett 126:* 351–368.

Jenner GA, Foley SF, Jackson SE, Green TH, Fryer BJ, Longerich HP (1993) Determination of partition coefficients for trace elements in high pressure-temperature experimental run products by laser ablation microprobe-inductively coupled plasma-mass spectrometry (LAM-ICP-MS). *Geochim Cosmochim Ac 57(23)*: 5099–5103.

John T, Scherer E, Haase KM, Schenk V (2004) Trace element fractionation during fluid-induced eclogitization in a subducting slab: trace element and Lu–Hf/Sm–Nd isotope systematics. *Earth Planetary Sci Lett 227*: 441–456.

John T, Klemd R, Gao J, Garbe-Schönberg CD (2008) Trace-element mobilization in slabs due to non steady state fluid–rock interaction: Constraints from an eclogite-facies transport vein in blueschist (Tianshan, China). *Lithos 103*:1–24.

Kaneko Y, Katayama I, Yamamoto H, Misawa K, Ishikawa M, Rehman HU, Shiraishi K (2003) Timing of Himalayan ultrahigh-pressure metamorphism: sinking rate and subduction angle of the Indian continental crust beneath Asia. *J Metamorph Geol 21(6)*: 589–599.

Katayama I, Zayachkovsky A, Maruyama S (2000) Progressive P–T records from zircon in Kokchetav UHP–HP rocks, northern Kazakhstan. *Isl Arc 9*: 417–428.

Katayama I, Maruyama S, Parkinson CD, Terada K, Sano Y (2001) Ion micro-probe U–Pb zircon geochronology of peak and retrograde stages of ultrahigh-pressure metamorphic rocks from the Kokchetav massif, northern Kazakhstan. *Earth Planet Sc Lett 188*: 185–198.

Kennedy CS and Kennedy GC (1976) Equilibrium boundary between graphite and diamond. *J Geophs Res* 81: 2467–2470.

Keppler H (1996) Constraints from partitioning experiments on the composition of subduction-zone fluids. *Nature 280*: 237–240.

Kessel R, Schmidt MW, Ulmer P, Pettke T (2005) Trace element signature of subduction-zone fluids, melts and supercritical liquids at 120–180 km depth. *Nature 437*: 724–727.

Klemd R, van den Kerhof AM, Horn EE (1992) High-density CO_2–N_2 inclusions in eclogite–facies metasediments of the Munchberg gneiss complex. *Contrib Mineral Petrol 111*: 409–419.

Li X, Xiaoming S, Wei Z, Jinlong L, Yeheng L, Kun S, Zeming Z, Qian T (2006) Fluid inclusions in quartz veins from HP-UHP metamorphic rocks, Chinese Continental Scientific Drilling (CCSD) project. *Int Geol Rev 48(7)*: 639–649.

Liang JL, Ding X, Sun XM, Zhang ZM, Zhang H, Sun WD (2009) Nb/Ta fractionation observed in eclogites from the Chinese Continental Scientific Drilling project. *Chem Geol 268(1)*: 27–40.

Liu J, Ye K, Maruyama S, Cong B, Fan H (2001) Mineral inclusions in zircon from gneisses in the ultrahigh pressure zone of the Dabie Mountains, China. *J Geol 109*: 523–535.

Liou JG, Zhang RY (1995) Significance of ultrahigh-pressure talc-bearing eclogite assemblages. *Mineral Mag 59*: 93–102.

Malaspina N, Hermann J, Scambelluri M, Compagnoni R (2006) Polyphase inclusions in garnet–orthopyroxenite (Dabie Shan, China) as monitors for metasomatism and fluid-related trace element transfer in subduction zone peridotite. *Earth Planet Sci Lett 249(3)*: 173–187.

Manning, C. E. (2004) The chemistry of subduction-zone fluids. *Earth Planet Sci Lett 223(1)*: 1–16.

Maruyama S, Liou JG, Terabayashi M (1996) Blueschists and eclogites of the world and their exhumation. *Int Geol Rev 38*: 485–494.

Maruyama S, Liou JG (2005) From snowball to Phanerozoic Earth. *Int Geol Rev 47*: 775–791.

Maruyama S, Masago H, Katayama I, Iwase Y, Toriumi M, Omori S, Aoki K (2010) A new perspective on metamorphism and metamorphic belts. *Gondwana Res 18*: 106–137.

Masago H, Omori S, Maruyama S (2010) Significance of retrograde hydration in collisional metamorphism: a case study of water infiltration in the Kokchetav ultrahigh-pressure metamorphic rocks, northern Kazakhstan. *Gondwana Res 18*: 205–212.

McCulloch MT, Gamble JA (1991) Geochemical and geodynamical constraints on subduction zone magmatism. *Earth Planet Sci Lett 102(3)*: 358–374.

Meade C, Jeanloz R (1991) Deep-focus earthquakes and recycling of water into the Earth's mantle. *Science 252*: 68–72.

Mirwald PW and Masonne HJ (1980) The low-high quartz and quartz-coesite transition to 40 kbar between 600 °C and 1600°C and some reconnaissance data on the effect of $NaAlO_2$ component on the low quartz-coesite transition. *J Geophys Res 85*: 6983–6990.

Morrison J (1994) Meteoric water-rock interaction in the lower plate of the Whipple Mountain metamorphic core complex, California. *J Metamorph Geol 12*: 827–840.

Nagasaki A, Enami M (1998) Sr-bearing zoisite and epidote in ultra-high pressure (UHP) metamorphic rocks from the Su-Lu province, eastern China: An important Sr reservoir under UHP conditions. Am Mineral 83: 240–247.

Pawley AR, Holloway JR(1993) Water sources for subduction-zone volcanism: new experimental and constraints. *Science 260*: 664–667.

Pearce JA, Peate DW (1995) Tectonic implications of the composition of volcanic arc magmas. *Annu Rev Earth Planet Sci Lett 23*: 251–285.

Pfänder JA, Münker C, Stracke A, Mezger K (2007) Nb/Ta and Zr/Hf in ocean island basalts –implications for crust–mantle differentiation and the fate of Niobium. *Earth Planet Sci Lett 254(1)*: 158–172.

Philippot P, Selverstone J (1991) Trace element-rich brines in eclogitic veins: implications for fluid composition and transport during subduction. *Contrib Mineral Petrol 106*: 417–430.

Philippot P (1993) Fluid-melt-rock interaction in mafic eclogites and coesite-bearing metasediments: constraints on volatile recycling during subduction. *Chem Geol 108(1)*: 93–112.

Poli S, Fumagalli P (2003) Mineral assemblages in ultrahigh pressure metamorphism: a review of experimentally determined phase diagrams. In: *EMU Notes in Mineralogy 5(10) Ultrahigh Pressure Metamorphism*: 307. Budapest: Eötvös University Press.

Poli S, Schmidt MW (1995) H_2O transport and release in subduction zones: experimental constraints on basaltic and andesitic systems. *J Geophys Res 100*: 22299–22314.

Poli S, Schmidt MW (2002) Petrology of subducted slabs. *Annu Rev Earth Pl Sc 30*: 207–235.

Rapp JF, Klemme S, Butler IB, Harley SL (2010) Extremely high solubility of rutile in chloride and fluoride-bearing metamorphic fluids: an experimental investigation. Geology 38(4): 323–326.

Rumble D, Liou JG, Jahn BM (2003) Continental crust subduction and ultrahigh pressure metamorphism. In: *Treatise on Geochemistry 1(3) The Crust*: 293–319. Oxford: Elsevier.

Scambelluri M., Piccardo GB, Philippot P, Robbiano A, Negretti, L (1997) High salinity fluid inclusions formed from recycled seawater in deeply subducted alpine serpentinite. *Earth Planet Sci Lett 148*: 485–500.

Scambelluri M, Philippot P, Pennacchioni G (1998) Salt-rich aqueous fluids formed during eclogitization of metabasites in the Alpine continental crust (Austroalpine Mt. Emilius unit, Italian Western Alps). *Lithos 43*: 151–161.

Scambelluri M, Philippot P (2001) Deep fluids in subduction zones. *Lithos 55(1)*: 213–227.

Schmidt MW, Poli S (1998) Experimentally based water budgets for dehydrating slabs and consequences for arc magma generation. *Earth Planet Sci Lett 163*: 361–379.

Schreyer W (1988) Experimental studies on metamorphism of crustal rocks under mantle pressures. *Mineral Mag 364*: 1–36.

Sheng YM, Zheng YF, Li SN, Hu Z (2013) Element mobility during continental collision: insights from polymineralic metamorphic vein within UHP eclogite in the Dabie orogen. J *Metamorph Geol 31(2)*: 221–241.

Smith DC (1984) Coesite in clinopyroxene in the Caledonides and its implications for geodynamics. *Nature* 310: 641–644.

Sobolev NV, Shatsky VS (1990) Diamond inclusions in garnets from metamorphic rocks: a new environment for diamond formation. *Nature 343*: 742–746.

Spandler CJ, Hermann J, Arculus RJ, Mavrogenes JA (2003) Redistribution of trace elements during prograde metamorphism from lawsonite blueschis to eclogie facies: implications for deep subduction-zone processes. *Contrib Mineral Petrol 146:* 205–222.

Stern RJ (2002) Subduction zones. Rev *Geophys 40(4)*: 1–38.

Sterner SM, Bodnar RJ (1989) Synthetic fluid inclusions-VII. Re-equilibration of fluid inclusions in quartz during laboratory-simulated metamorphic burial and uplift. *J Metamorph Geol 7(2)*: 243–260.

Stöckhert B, Duyster J, Trepmann C, Massonne HJ (2001) Microdiamond daughter crystals precipitated from supercritical COH^+ silicate fluids included in garnet, Erzgebirge, Germany. *Geology 29(5)*: 391–394.

Stracke A, Hofmann AW, Hart SR (2005) FOZO, HIMU, and the rest of the mantle zoo. *Geochem Geophy Geosy 6*, Q05007, doi:10.1029/2004GC000824.

Su W, You Z, Cong B, Ye K, Zhong Z (2002) Cluster of water molecules in garnet from ultrahigh-pressure eclogite. *Geology 30*: 611–614.

Svensen H, Jamtveit B, Yardley BW, Engvik AK, Austrheim H, Broman C (1999) Lead and Bromine enrichment in eclogite facies fluids: extreme fractionation during lower crustal hydration. *Geology 27*: 467–470.

Tabata H, Yamauchi K, Maruyama S, Liou JG (1998) Tracing the extent of a UHP metamorphic terrane: Mineral-inclusion study of zircons in gneisses from the Dabie Shan. In: *When Continents Collide: Geodynamics and Geochemistry of Ultrahigh-Pressure Rocks*. Springer, Amsterdam: 261–273.

Tatsumi Y, Eggins S (1995) Subduction zone magmatism. Wiley, Weinheim.

Terabayashi M, Ota T, Yamamoto H, Kaneko Y (2002) Contact metamorphism of the Daulet Suiteby solid-state emplacement of the Kokchetav UHP-HP metamorphic slab. *Int Geol Rev 44*: 819–830.

Touret JLR (1992) Fluid inclusions in subducted rocks. *Proc Koninklijke Ned Akad van Wetensch 95*: 385–403.

Ulmer P, Trommsdorff V (1995) Serpentine stability to mantle depths and subduction-related magmatism. *Science 268*: 858–861.

Upton P, Koons PO, Cahmberlain CP (1995) Penetration of deformation-driven meteoric water into ductile rocks: isotopic and model observations from the Southern Alps, New Zealand. *New Zeal J Geol Geop 38*: 535–543.

van Roermund HL, Carswell DA, Drury MR, Heijboer TC (2002) Microdiamonds in a megacrystic garnet websterite pod from Bardane on the island of Fjørtoft, western Norway: evidence for diamond formation in mantle rocks during deep continental subduction. *Geology 30(11)*: 959–962.

Vityk MO, Bodnar RJ (1995) Do fluid inclusions in high-grade metamorphic terranes preserve peak metamorphic density during retrograde decompression? *Am Mineral 80(7)*: 641–644.

Wang L, Kusky TM, Polat A, Wang S, Jiang X, Zong K, Wang J, Deng H, Fu J (2014) Partial melting of deeply subducted eclogite from the Sulu orogen in China. *Nature Communications 5604*: doi:10.1038/ncomms6604

Wu YB, Gao S, Zhang HF, Yang SH, Liu XC, Jiao WF, Liu YS, Yuan HL, Gong HJ, He MC (2009) U–Pb age, trace-element, and Hf-isotope compositions of zircon in a quartz vein from eclogite in the western Dabie Mountains: constraints on fluid flow during early exhumation of ultrahigh-pressure rocks. *Am Mineral 94*:303–312.

Xia QK, Sheng YM, Yang XZ, Yu HM (2005) Heterogeneity of water in garnets from UHP eclogites, eastern Dabieshan, China. *Chem Geol 224(4)*: 237–246.

Xiao Y, Hoefs J, van den Kerkhof AM, Fiebig J, Zheng YF (2000) Fluid history of UHP metamorphism in Dabie Shan, China: a fluid inclusion and oxygen isotope study on the coesite-bearing eclogite from Bixiling. *Contrib Mineral Petr 139*: 1–16.

Xiao Y, Sun W, Hoefs J, Simon K, Zhang Z, Li S, Hofmann AW (2006) Making continental crust through slab melting: constraints from niobium–tantalum fractionation in UHP metamorphic rutile. *Geochim Cosmochim Ac 70(18)*: 4770–4782.

Xiao Y, Hoefs J, Hou Z, Simon K, Zhang Z (2011) Fluid/rock interaction and mass transfer in continental subduction zones: constraints from trace elements and isotopes (Li, B, O, Sr, Nd, Pb) in UHP rocks from the Chinese Continental Scientific Drilling Program, Sulu, East China. *Contrib Mineral Petrol 162*:797–819.

Xu S, Okay AI, Shouyuan J, Sengör AMC, Wen S, Yican L, Laili J (1992) Diamond from the Dabie Shan metamorphic rocks and its implication for tectonic setting. *Science 256*: 80.

Xu S, Liu Y, Chen G, Compagnoni R, Rolfo F, He M, Liu H (2003) New finding of micro-diamonds in eclogites from Dabie-Sulu region in central-eastern China. *Chinese Sci Bull 48(10)*: 988–994.

Yardley BWD, Graham JT (2002) The origins of salinity in metamorphic fluids. *Geofluids 2(4)*: 249–256.

Ye K, Yao Y, Katayama I, Cong BL, Wang QC, Maruyama S (2000) Large area extent of ultrahigh-pressure metamorphism in the Sulu ultrahigh-pressure terrane of East China: new implications from coesite and omphacite inclusions in zircon of granitic gneiss. *Lithos 52*: 157–164.

Zhang RY, Hirajima T, Banno S, Cong B, Liou JG (1995) Petrology of ultrahigh-pressure rocks from the southern Su-Lu region, eastern China. J *Metamorph Geol 13(6)*: 659–675.

Zhang RY, Liou JG, Cong BL (1995) Talc-, magnesite-and Ti-clinohumite-bearing ultrahigh-pressure meta-mafic and ultramafic complex in the Dabie Mountains, China. *J Petrol 36(4)*: 1011-1037.

Zhang J, Jin Z, Green HW, Jin S (2001) Hydroxyl in continental deep subduction zone: Evidence from UHP eclogites of the Dabie Mountains. *Chinese Sci Bull 46*:592–596.

Zhang ZM, Shen K, Sun WD, Liu YS, Liou JG, Shi C, Wang JL (2008) Fluids in deeply subducted continental crust: petrology, mineral chemistry and fluid inclusion of UHP metamorphic veins from the Sulu orogen, eastern China. *Geochim Cosmochim Ac 72*:3200–3228.

Zhang RY, Liou JG, Ernst WG (2009) The Dabie-Sulu continental collision zone: a comprehensive review. *Gondwana Res 16*: 1–26.

Zheng YF, Fu B, Gong B, Li L (2003) Stable isotope geochemistry of ultrahigh pressure metamorphic rocks from the Dabie–Sulu orogen in China: implications for geodynamics and fluid regime. *Earth Sci Rev 62(1)*: 105–161.

Zheng, YF (2004) Fluid activity during exhumation of deep-subducted continental plate. *Chinese Sci Bull 49*: 985–998.

Zheng YF, Gao TS, Wu YB, Gong B, Liu XM (2007) Fluid flow during exhumation of deeply subducted continental crust: zircon U–Pb age and O–isotope studies of a quartz vein within ultrahigh-pressure eclogite. *J Metamorph Geol 25*:267–283.

Zheng YF (2009) Fluid regime in continental subduction zones: petrological insights from ultrahigh-pressure metamorphic rocks. *J Geol Soc 166(4)*: 763–782.

Zheng YF, Xia QX, Chen RX, Gao XY (2011) Partial melting, fluid supercriticality and element mobility in ultrahigh-pressure metamorphic rocks during continental collision. *Earth Sci Rev 107(3)*: 342–374.

Zheng YF (2012) Metamorphic chemical geodynamics in continental subduction zones. *Chem Geol 328*: 5–48.

Zheng YF, Hermann J (2014) Geochemistry of continental subduction-zone fluids. *Earth Planets Space 66(1)*: 1–16.

Zong K, Liu Y, Hu Z, Kusky T, Wang D, Gao C, Wang J (2010) Melting-induced fluid flow during exhumation of gneisses of the Sulu ultrahigh-pressure terrane. *Lithos 120(3)*: 490–510.

2. Geological setting

Among all UHP terrains, the Dabie-Sulu collision zone in Central Eastern China is the largest area of exposed UHP lithologies worldwide and provides an exceptional natural laboratory for studying high pressure metamorphic processes. It became an active field of research since the first discovery of coesite in 1989 (OKAY ET AL., 1989; WANG ET AL., 1989) and is still extensively investigated. For summaries on the evolution and geology of the Dabie-Sulu metamorphic belt refer to eg. MARUYAMA ET AL. (1994), ZHANG ET AL. (2009), ZHENG ET AL. (2008).

2.1 Tectonometamorphic evolution of the Dabie-Sulu UHP belt

The Dabieshan low mountain range is located in central eastern China about 550 km west of Shanghai (**Figure 2.1a**). Together with its geological equivalents, the northern Sulu from which it is tectonically divided by the NE–SW tending, sinistral Tan Lu strike-slip fault, and the western Qinling-Hong'an, it constitutes the eastern extension of an orogenic chain that stretches in a WNW–ESE direction curvilinearly for about 4000 km throughout China. The formation of this tectonic suture resulted from a Triassic continent-continent collision that took place progressivly from west to east and induced a northward deep subduction of the Proterozoic Yangtze craton (also: South China craton) beneath the Sinokorean lithospheric plate (also: North China craton) (HACKER ET AL., 2004).

The Dabie-Sulu region (**Figure 2.1b**), as a part of this suture, comprises an area of more than 30000 km^2. It represents the deep portion of the ancient continental deep subduction zone, which has been
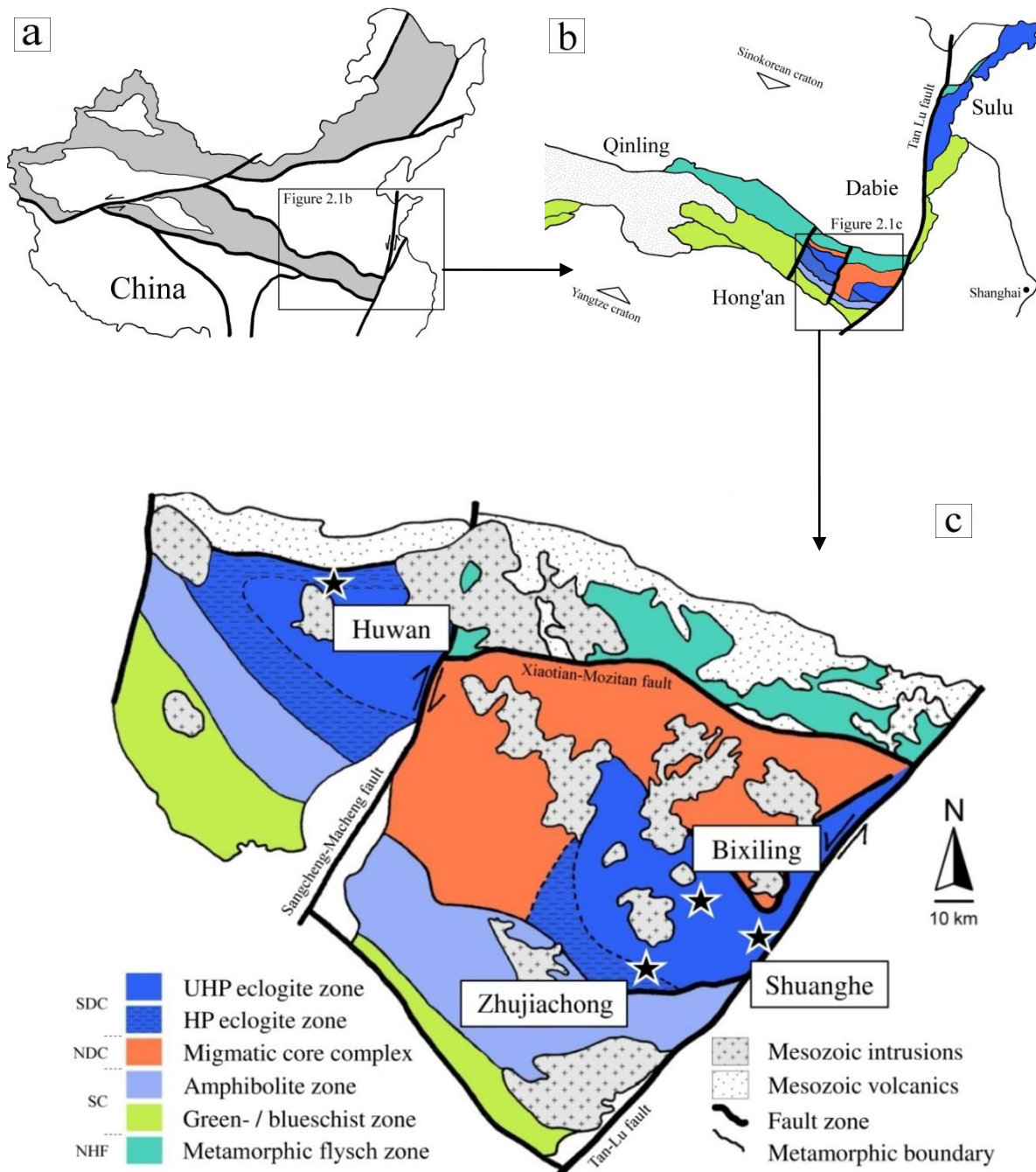
↑ **Figure 2.1 a** Simplified tectonic map of China, showing the major orogenic belts (shaded) associated to suture zones that resulted from the Triassic collision of the northern Sinokorean craton and the southern Yangtze craton. Modified after ZHANG ET AL. (2009) **b** Schematic sketch of the Dabie-Sulu orogen and its subdivision into main geological units (cf. legend of Figure 2.1c). Modified after ZHENG ET AL. (2003). **c** The Hong'an block and the Dabie block and their division into the common petrotectonic units. Sample localities of this study (labelled with asteriks) are within the UHP regions of Central Dabie Shan (Bixling, Shuanghe), and in the border areas between the UHP and HP eclogite zones (Zhujiachong, Huwan). Modified after ZHANG ET AL. (2009). SDC: South Dabie Complex, NDC: North Dabie Complex, SC: Susong Metamorphic Complex, NHF: North Huaiyang Flysch (explanation in **Chapter 2.2**).

exhumed due to slab-breakoff, wedge extrusion, Cretaceous plate margin transtension and erosion (HACKER ET AL., 1995; ZHENG ET AL., 2008) with exhumation rates between 5–10 mm/a (ZHANG ET AL., 2009). It is bounded by three main strike-slip fault zones against Hong'an in the west, Sulu in the northeast and against the Hefei basin in the north and the Yangtze basin in the south. The latter two basically comprise a Palaeozoic low-grade metamorphic greenschist facies basement, which is by intruded by Mesozoic granites and largely covered by (volcano-)clastic rocks, as well as younger Cenozoic sediments (eg. LI ET AL., 2006).

The Hong'an-Dabie-Sulu belt exposes mainly granulites and amphibolite-facies, quartzofeldspathic gneisses of granitic and minor sedimentary origin, with the highest grade metamorphic lithologies in the center of the belt. The gneisses are in part migmatized and intercalated with layers, blocks and lenses of marble, amphibolites and typical, mafic UHP lithologies such as eclogite, garnet peridotite and -pyroxenite as well as jadeite-quartzite (TABATA ET AL., 1998A), accompanied by younger granitic intrusions and volcanics. Coesite and its pseudomorphs are widespread as inclusions in both eclogitic minerals and gneissic zircons (LIU ET AL., 2002; OKAY ET AL., 1989; TABATA ET AL., 1998B; WANG ET AL., 1989; WANG AND LIOU, 1991; YE ET AL., 2000) and even mircodiamond has been found in eclogites, garnet-pyroxenites and jadeitites (XU ET AL., 1992, 2003).This testifies the UHP metamorphic history of the terrane and points to a conjoint and regional metamorphism of the eclogites and their country rocks, as a result of large scale deep subduction of felsic crust down to 120 km during continental collision.

The continental collision that induced the regional burial down to UHP conditions and accounts for the formation of the indicator minerals was dated to 210–230 Ma by Sm-Nd analyses of eclogitic minerals and U-Pb analyses of zircon (AMES ET AL. 1993; HACKER ET AL., 1998; LI ET AL. 1993; ROWLEY ET AL. 1997).

Peak metamorphism within the Dabie-Sulu UHP belt was bracketed between 242±2 Ma and 227±2 Ma with SHRIMP U-Pb ages of zircons from eclogite, gneiss, peridotite and pyroxenite from different UHP localities (LIU ET AL., 2004A, 2006; WAN ET AL., 2005; YANG ET AL., 2003). Two episodes of

zircon growth were correlated to the incipient UHP metamorphism at 242±2 Ma and the beginning

exhumation at 219±3. Peak metamorphic P-T conditions have been estimated to 2.8–4.0 GPa and 630–

850 °C (eg. CARSWELL ET AL., 1997; CONG ET AL., 1995; LI ET AL., 2004) (**Figure 2.2**).
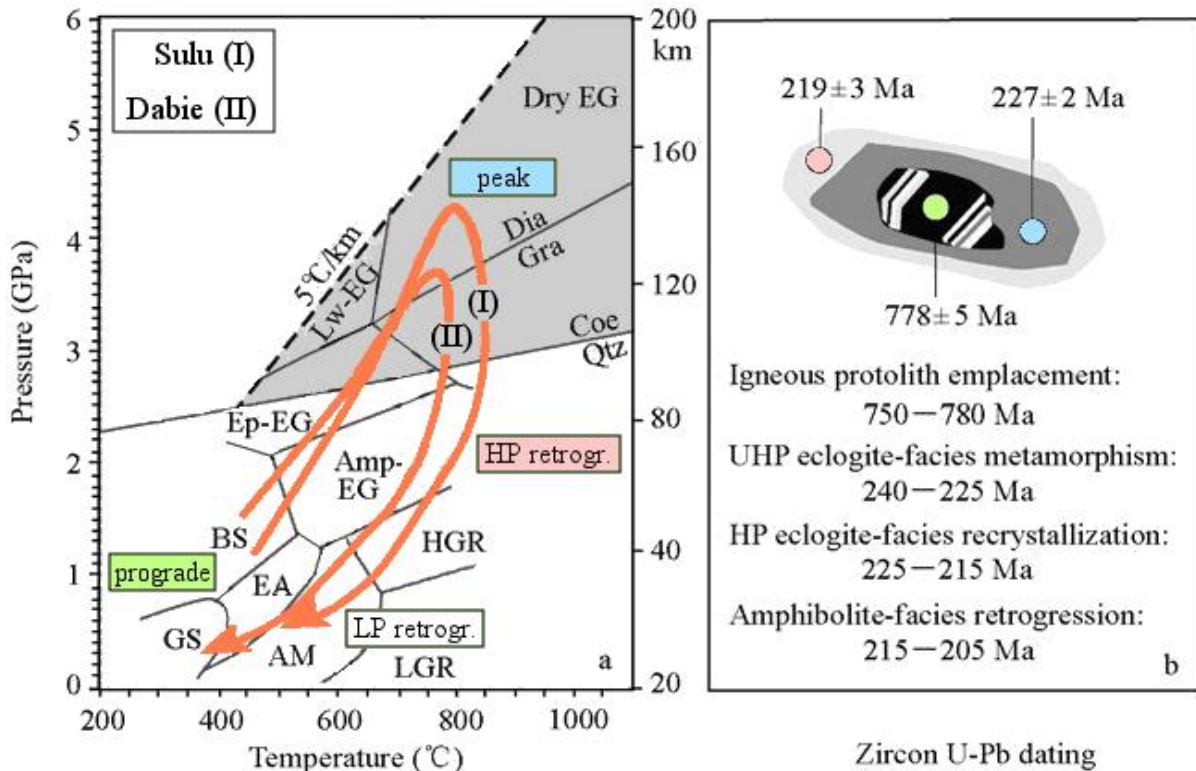
↑ **Figure 2.2 a** Schematic P-T-t evolution of different terrains along major metamorphic facies fields according to **b** Representative zircon U-Pb ages for UHP metamorphic rocks in the Dabie-Sulu orogenic belt. Modified after ZHENG (2008), who compiled the data according to the references cited. P-T-t data: Sulu (I) from ZHANG ET AL. (1995C, 2006); ZHU ET AL. (2007), Dabie (II) from CARSWELL AND ZHANG (1999).

Based on the distribution of U-Pb ages among UHP lithologies, HACKER ET AL. (2006) and LIOU ET AL. (2009) proposed a three-stage recrystallization of Dabie-Sulu UHP rocks. Peak UHP facies recrystallization has been related to 240–225 Ma, HP eclogite facies recrystallization during early retrograde exhumation has been estimated at 225–215 Ma by petrographic and geochronological studies (LIU ET AL., 2006; LIU ET AL., 2008; ZHAO ET AL., 2006), and a late amphibolite-facies retrogression was identified between 215–205 Ma (LIU ET AL., 2004B; LIU ET AL., 2008).

2.2   Petrology of the Dabie Complex

The Dabie orogenic belt has been divided into four main complexes on the basis of lithotectonic associations and their metamorphic evolution (eg. OKAY ET AL., 1993; HACKER ET AL., 1998; HIRAJIMA AND NAKAMURA, 2003; LIOU ET AL., 1996; ZHANG ET AL., 1996). As is typical for continental collision belts, the UHP unit is sandwiched between lower grade metamorphic lithologies. The units are, from the northeast to the southwest: (1) the low-grade metamorphic North Huaiyang Flysch (NHF), (2) the multistage metamorphic North Dabie Complex (NDC), (3) the South Dabie Complex (SDC) that records UHP conditions, and (4) the low-grade metamorphic Susong Complex(SC) (cf. **Figure 2.1c**).

The NHF (1) comprises greenschist facies metapelites with interlayered orthoquartzite, marble and Mesozoic intrusions as well as volcanic rocks (WANG ET AL., 2002 and references therein). The metasediments are assumed to have formed from a flysch sequence of sand- and mudstones, and locally also experienced amphibolite facies conditions in the late Palaeozoic. The northern boundary against the non-metamorphic lithologies of the Hefei Basin is the Xinyang-Shucheng fault.

The NDC (2) belt is characterized by the occurrence of orthogneisses, migmatites, metasediments, eclogites, granulites, ultramafic rocks as well as Mesozoic granitoids, and underwent multistage metamorphism from eclogite facies to retrograde granulite facies and late amphibolite facies (MALASPINA ET AL., 2006). No UHP indicating minerals have been identified within the NDC. It is bounded against the NHF by the Xiaotian-Mozitan fault. Due to structural and geochemical similarities, BRYANT ET AL. (2004) interpreted the Northern Dabie Complex to be a part of the SDC that was unaffected by ultrahigh-pressure metamorphism.

The SDC (3) has been sampled for this work. It exhibits, next to Mesozoic granitoids, ultrahigh pressure lithologies in the form of coesite-and microdiamond-bearing eclogites, ultramafics such as garnet pyroxenites, jadeite-quartzites and marbles (OKAY ET AL., 1989; WANG ET AL., 1989; WANG AND LIOU, 1991; XU ET AL., 1991, 2003; ZHANG ET AL., 1995A). These UHP lithologies a embedded as lenses, blocks or layers within widespread gneissic rocks that are comparable to those found within

the NDC. They are interpreted to be mostly of Neoproterozoic intraplate basaltic origin and to have been subjected to UHP conditions conjointly with their country rock during the Triassic (eg. LIU ET AL., 2001; RUMBLE ET AL., 2003; TABATA ET AL., 1998; YE ET AL., 2000). The SDC is commonly subdivided into a UHP coesite-eclogite zone ('hot eclogite'), and a HP quartz-eclogite zone ('cold eclogite'), that lacks UHP indicating minerals and is bound by the Shuihou-Wuhe fault in the north and the Taihu-Mamiao fault in the south.

The origin of the eclogitic bodies is discussed either to be in-situ, related to former intraplate basalts (for review refer to HIRAJIMA & NAKAMURA, 2003), or tectonic emplacement as exotic blocks (eg. CONG ET AL., 1995) (cf. **Chapter 1.1.1**). Since (i) coesite inclusions in zircons are regionally distributed within the whole Dabie-Sulu area in several different metamorphic rock types, and (ii) U-Pb dating of zircons from both eclogites and surrounding country rocks yield consistent Triassic ages, the in-situ model is widely established (for references see ZHANG ET AL., 2009).

The SC (4), the southernmost part of the Dabie complex, exposes mostly meatsediments and Mesozoic granitic bodies with medium to high pressure greenschist, amphibolite and blueschist facies metamorphic overprint. Exposed lithologies comprise meta-sandstones, mica-schists, orthogneisses and marbles, while the degree of metamorphism progressively decreases from the northeast to the southwest. The SC is bound to the southern and non-metamorphic Yangtze Basin by the Xiangfan-Guangji fault.

As sketched in **Figure 2.1c**, the petrotectonic units of the Hong'an Block correspond to the classification of the Dabie Block. Although the Hong'an-Dabie-Sulu collisional belt undoubtedly occupies the suture between the Yangtze craton and the Sinokorean craton, the exact suture boundary has long been debated. ZHANG ET AL. (1996) proposed the border between the SDC and the NDC, while more recent workers suggest it to trend along the Xiaotian-Mozitan fault (BRYANT ET AL., 2004; HACKER ET AL, 1998; ZHENG ET AL., 2005).

U-Pb dating on the Hong'an-Dabie-Sulu rock suite revealed that the majority of lithologies have Neoproterozoic igneous and minor sedimentary protoliths with ages between 740–780 Ma (AMES ET AL., 1996; HACKER ET AL., 1998; ROWLEY ET AL., 1997; ZHENG ET AL., 2003). A conspicuous feature

of many UHP/HP rocks in the Dabie region are low $\delta^{18}O$ values down to -10 ‰. These low oxygen isotope signatures are widespread over the whole metamorphic belt and have been confirmed down to depths of 3000 m in the China Continental Scientific Drilling (CCSD) project. The lowest $\delta^{18}O$ values were detected in three CCSD sections close to granitic gneiss layers that are assumed to correspond to paleofault systems (CHEN ET AL., 2007; XIAO ET AL., 2006). The oxygen isotopic depletion is commonly interpreted to be inherited from regional hydrothermal alteration of the protoliths with extremely low $\delta^{18}O$ waters that were common during Neoproterozoic 'Snowball Earth' (HOFFMANN ET AL., 1998) equatorial glaciations (BAKER ET AL., 1997; FU ET AL., 1999; HERWARTZ ET AL., 2015; TANG ET AL., 2008; YUI ET AL., 1995; ZHENG ET AL., 1998, 2003, 2004).

Geochemical characteristics of the Dabie-Sulu UHP eclogites indicate that their precursors predominantly evolved from basaltic island arc (LI ET AL., 1993) or continental intraplate magmatism within the subducting Yangtze basement (JAHN, 1999, 2005; LIU ET AL., 2004C; HACKER ET AL., 2000; ZHENG ET AL., 2006).

2.3 Geology and P-T-t evolution of sampling sites

Sampling was carried out at four localities in the Dabieshan that expose UHP/HP eclogites. The outcrops at Shuanghe and Bixiling are located within the UHP coesite-eclogite region of the Dabie block, Zhujiachong is located in the transition zone towards the HP quartz-eclogite belt (cf. **Figure 2.1c**). Huwan is located in the HP quartz-eclogite region in the northern area of Hong'an block.

2.3.1 Shuanghe (Dabie UHP region)

**Outcrop SH-A:** [30°38'03,77"N, 116°24'44,16"E], near the dam of the reservoir lake

Outcrop SH-B: [30°37'03,62"N, 116°24'36,98"E], riverbed 0.9 km downstream from SH-A

Outcrop SH-C: [30°37'00,85"N, 116°24'41,26"E], river bend 1.0 km downstream from SH-A

The coesite-bearing eclogite from Shuanghe occurs as intercalated lenses within in a NNW–SSE striking thrust slab that is occasionally exposed over a length of about 1500 m. The eclogite layers mostly do not show macroscopic evidence of retrogression. They are embedded within structurally concordant paragneissic schists and crosscut by a strike-slip fault with a dextral offset of ~ 500 m. Next to mica-gneisses and -schists and eclogite, which both constitute the main lithologies of the slab, minor jadeite quartzite with coesite inclusions and impure marble are exposed. The entire slab is embedded within orthogneissic country rock (**Figure 2.3**).

CONG ET AL. (1995) favor tectonic emplacement of UHP slab eclogites and paragneisses in a lower pressure granitic gneiss host rock. Findings of coesite in both zircons from surrounding orthogneisses and eclogitic garnet and omphacite, however, indicate that the Shuanghe slab has been subjected to UHP metamorphic conditions conjointly with the country rock gneiss (CARSWELL ET AL., 2000; YE ET AL., 2000).

The precursors of the Shuanghe UHP slab are mafic and minor sedimentary lithologies that preserved a clockwise polymetamorphic history with three preserved metamorphic stages: (i) Peak UHP metamorphism, (ii) an amphibolite-eclogite recrystallization stage, (iii) a symplectic stage that records amphibolite facies retrogression (CONG ET AL., 1995; FU ET AL., 2001; LIOU ET AL., 1997).
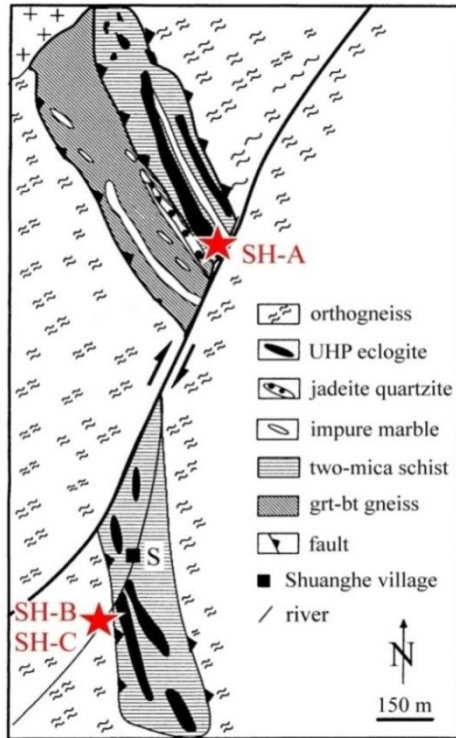
← **Figure 2.3** Geological map sketch of the Shuanghe UHP metamorphic slab and its country rocks, modified after CONG ET AL.(1995). The two-mica schist can contain epidote as well as minor garnet-biotite gneiss sections, whereas the garnet-biotite gneiss can contain minor two-mica schist. Sampled localities are labeled with stars.

Sm–Nd isotopic chronology for gneissic minerals revealed peak conditions at 226.3±3.2 Ma (LI ET AL., 2000), coinciding with U-Pb ionprobe ages of 229–234 Ma (CHAVAGNAC ET AL., 1999). CARSWELL ET AL. (1997) inferred temperatures of 700±50 °C and corresponding pressures of 3.1–3.2 GPa for the UHP stage for the Shuanghe eclogites. Rb–Sr and Ar–Ar data from gneisses give ages of 226–219 Ma for the early retrograde recrystallization stage at 1.3–1.8 GPa and 630–700 °C, as well as ages of 190–170 Ma for the late amphibolite facies retrogression at 0.6–0.8 GPa at 470–570 °C (CONG ET AL., 1995; LI ET AL., 2000).

2.3.2 Zhujiachong (Dabie UHP/HP region)

Outcrop ZJC: [30°27'20,55"N, 116°11'57,17"E], along the road between Lidu and Zhujiachong

The eclogite body from Zhujiachong (sometimes the locality is also referred to as 'Lidu' or 'Huangzhen') forms an elongated, E–W striking block of about 500 m in length and 200 m in width (**Figure 2.4**). The sampled outcrop exposes an eclogite block over a length of about 50 m and is located shortly behind the bridge across the Zhucong river along the road towards the village Lidu.

The amphibolitized eclogite is structurally concordant embedded within the two-mica epidote- and garnet-bearing gneiss, pointing to in-situ metamorphism of the HP and the country rock. Coesite has not been observed within Zhujiachong lithologies.

CARSWELL ET AL. (1997) derive conditions of 2.2–2.3 GPa at 600–620 °C for the peak metamorphism of the Zhujiachong area via thermobarometry. CASTELLI ET AL. (1998) estimated the peak metamorphism to HP conditions of 2.4 GPa and ~700 °C, based on petrographic observations and thermodynamic calculations regarding the observed mineral assemblages. The authors propose a multistage metamorphic model based on preserved mineral assemblages and symplectites. They conclude HP epidote-eclogite facies conditions during the peak stage and subduction to depths of <90km. The subsequent inset of an initially rapid (quasi-adiabatic) decompression resulted in an early retrograde amphibolite facies stage, followed by cooling and greenschist facies recrystallization at distinctly lower exhumation rates, being consistent with geochronological data of MARUYAMA ET AL. (1994) from the Dabie HP quartz-eclogite area.
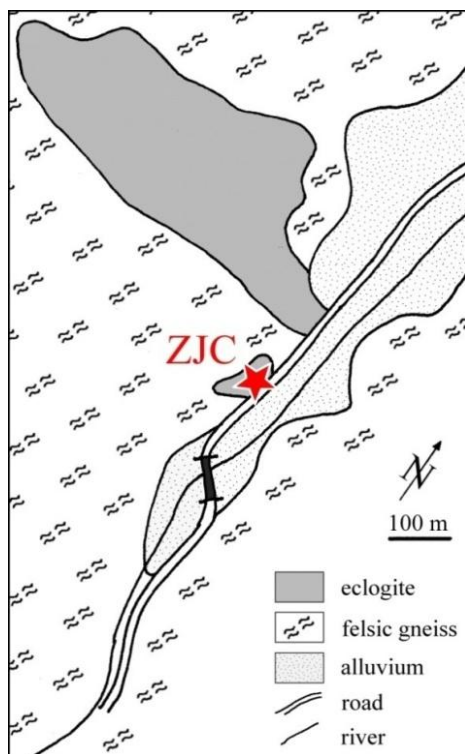
← **Figure 2.4** Geological map sketch of the Zhujiachong U/HP eclogite bodies about 1 km north of the village Zhujiachong. Modified after CASTELLI ET AL. (1998). Sampling spot labeled with star.

LI ET AL. (2004) identified coesite pseudomorphs in garnet from the Zhujiachong area and suggest the re-evaluation of the HP quartz-eclogite unit towards an UHP coesite-eclogite unit. The authors derived revised formation conditions of 3.3 GPa at 670°C.

2.3.3 Bixiling (Dabie UHP region)

Outcrop BX: [30°44'11,16"N, 116°17'00,75"E], road outcrop

The UHP eclogite from Bixiling occurs as a tectonic block of ~1.5 km^2 in size in the eastern part of the Dabie UHP unit and represents one of the largest coesite-bearing eclogite bodies in Dabieshan. It is enclosed within foliated quartzofeldspathic gneisses and contains numerous lenticular, subparallel lenses of mafic to ultramafic lithologies, such as garnet peridotite and pyroxenite that are in gradational contact to the eclogite (**Figure 2.5**). The conditions of exposed eclogites range from slightly retrogressed to pristine, whereas retrogressed rocks predominantly occur towards the boundaries of the complex (XIAO ET AL., 2000). The Bixiling complex is interpreted to be of cumulate origin and gradual contacts between the different lithologies indicate a conjoint UHP metamorphism of the entire UHP block (ZHANG ET AL., 1995B). The boundary between the complex and country rock shows tectonic contact relations whereas their metamorphic ages are, however, similar.
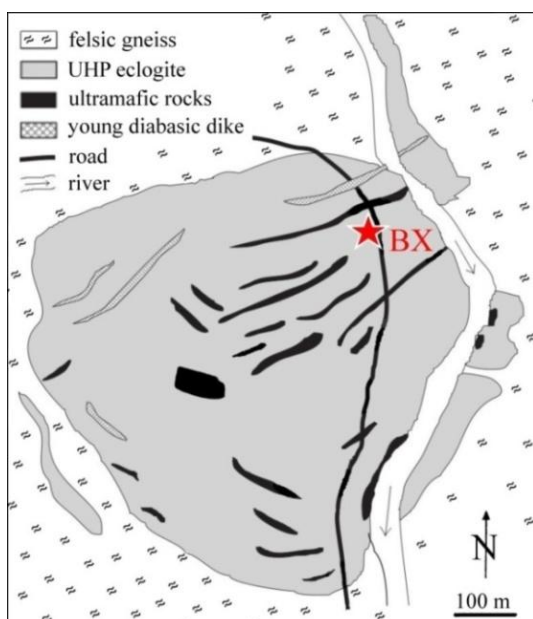
← **Figure 2.5** Geological map sketch of the Bixiling eclogite complex and its country rock, modified after XIAO ET AL. (2000). Sampling spot labeled with star.

Sm–Nd ages on garnet and omphacite from eclogite and garnet peridotite give ages of 210–218 Ma (CHAVAGNAC AND JAHN, 1996), and 209 Ma for eclogites as well as 217 Ma for the gneissic country rock (XIAO ET AL., 1995).

Peak metamorphic UHP conditions were constrained by thermobarometry to be >2.7 GPa at 610–700°C. A retrograde stage, characterised by amphibolite facies symplectic recrystallization, provides P-T estimates of 0.6–1.5 GPa at temperatures <600 °C (ZHANG ET AL., 1995B).

2.3.4 Huwan (Hong'an HP region)

Outcrop HW: [31°43'39,27"N, 114°52'35,78"E], road outcrop

The sample site Huwan is situated in the HP quartz-eclogite metamorphic unit of the northern part of the Hong'an block. The outcrop shows textural and tectonic characteristics of a shear zone and bounds the Hong'an UHP eclogite unit against the low-grade metamorphic flysch in the north.

The Huwan HP area exposes felsic gneisses with minor schists and amphibolites. HP quartz-eclogites contain epidote and occur as concordantly intercalated bands (YE ET AL., 1994; EIDE AND LIOU, 2000; FU ET AL., 2002; LIU ET AL., 2004D) with marked post-eclogitic deformation. Three different protolith types, including MORB (LI ET AL., 2001; FU ET AL., 2002; GAO ET AL., 2002; WU ET AL., 2009), island arc basalts (LI ET AL., 2001) and Neoproterozoic continental crust (HACKER ET AL., 2000; LIU ET AL, 2004C; JAHN ET AL., 2005) have been proposed.

The eclogites sampled for the present study are assumed to originate from former oceanic crust protoliths that evolved in a continental margin environment and experienced variable contamination with continental material. Peak metamorphic conditions were constrained to540–730 °C and 1.4–2.1 GPa, whereas the timing of eclogite facies metamorphism and protolith formation is still debated.

WU ET AL., 2009 reported U-Pb metamorphic ages of 309±4 Ma for Huwan, which are dinstinctly older than the eclogite facies metamorphism at 242–227 Ma derived for Dabieshan (cf. **Chapter 2.1**). The authors propose a multistage amalgamation model for the collision of the Yangtze and Sinokorean cratons that includes both a Carboniferous collisional event at the first stage that is preserved in the Hong'an block, and a Triassic tectonic event that is preserved in Dabieshan.

2.4   References

Ames L, Tilton G, Zhou G (1993) Timing of collision of the Sino-Korean and Yangtse cratons: U-Pb zircon dating of coesite-bearing eclogites. *Geology 21(4)*: 339–342.

Ames L, Gaozhi Z, Baocheng X (1996) Geochronology and isotopic character of ultrahigh-pressure metamorphism with implications for collision of the Sino-Korean and Yangtze cratons, central China. *Tectonics 15(2)*: 472–489.

Baker J, Matthews A, Mattey D, Rowley D, Xue F (1997) Fluid-rock interactions during ultra-high pressure metamorphism, Dabie Shan, China. *Geochim Cosmochim Ac 61(8)*: 1685–1696.

Bryant DL, Ayers JC, Gao S, Miller CF, Zhang H (2004) Geochemical, age, and isotopic constraints on the location of the Sino–Korean/Yangtze Suture and evolution of the Northern Dabie Complex, east central China. *Geol So Am Bull 116(5)*: 698–717.

Carswell DA, O'Brien PJ, Wilson RN, Zhai M (1997) Thermobarometry of phengite-bearing eclogites in the Dabie Mountains of central China. *J Metamorph Geol 15(2)*: 239–252.

Carswell DA, Zhang RY, (1999) Petrographic characteristics and metamorphic evolution of ultra-high pressure eclogites in plate collision belts. *Int Geol Rev 41*: 781–798.

Carswell DA, Wilson RN, Zhai, MG (2000) Metamorphic evolution, mineral chemistry and thermobarometry of schists and orthogneisses hosting ultra-high pressure eclogites in the Dabieshan of central China. *Lithos 52(1)*: 121–155.

Castelli D, Rolfo F, Compagnoni R, Xu S (1998) Metamorphic veins with kyanite, zoisite and quartz in the Zhu-Jia-Chong eclogite, Dabie Shan, China. *Isl Arc 7(1-2)*: 159–173.

Chavagnac V, Jahn BM (1996) Coesite-bearing eclogites from the Bixiling Complex, Dabie Mountains, China: Sm–Nd ages, geochemical characteristics and tectonic implications. *Chem Geol 133(1)*: 29–51.

Chavagnac V, Jahn BM, Villa IM Whitehouse MJ (1999) Multi-chronometric study of the country gneisses of UHP eclogites of Dabieshan: evidence for 'in-situ' tectonic relationship. *Journal of Conference Abstracts (EUG-10) 4*: 102.

Chen RX, Zheng YF, Gong B, Zhao ZF, Gao TS, Chen B, Wu YB (2007) Oxygen isotope geochemistry of ultrahigh-pressure metamorphic rocks from 200–4000 m core samples of the Chinese Continental Scientific Drilling. *Chem Geol 242(1)*: 51–75.

Cong BL, Zhai M, Carswell DA, Wilson RN, Wang Q, Zhao Z, Windley BF (1995) Petrogenesis of ultrahigh-pressure rocks and their country rocks at Shuanghe in Dabieshan, central China. *Eur J Mineral 7*: 119–138.

Eide EA, Liou JG (2000) High-pressure blueschists and eclogites in Hong'an: a framework for addressing the evolution of high-and ultrahigh-pressure rocks in central China. *Lithos 52(1)*: 1–22.

Fu B, Zheng YF, Wang Z, Xiao Y, Gong B, Li S (1999) Oxygen and hydrogen isotope geochemistry of gneisses associated with ultrahigh pressure eclogites at Shuanghe in the Dabie Mountains. *Contrib Mineral Petrol 134(1)*: 52–66.

Fu B, Touret JLR, Zheng YF (2001) Fluid inclusions in coesite-bearing eclogites and jadeite quartzite at Shuanghe, Dabie Shan (China). *J Metamorph Geol 19(5)*: 531–547.

Fu B, Zheng YF, Touret JL (2002) Petrological, isotopic and fluid inclusion studies of eclogites from Sujiahe, NW Dabie Shan (China). *Chem Geol 187(1)*: 107–128.

Gao S, Qiu Y, Ling W, McNaughton NJ, Zhang B, Zhang G, Suo S (2002) SHRIMP single zircon U–Pb geochronology of eclogites from Yingshan and Xiongdian. *Earth Sci 27*: 558–564.

Hacker BR, Ratschbacher L, Webb L, Shuwen D (1995) What brought them up? Exhumation of the Dabie Shan ultrahigh-pressure rocks. *Geology 23(8)*: 743–746.

Hacker BR, Ratschbacher L, Webb L, Ireland T, Walker D, Shuwen D (1998) U/Pb zircon ages constrain the architecture of the ultrahigh-pressure Qinling–Dabie Orogen, China. *Earth Planet Sci Lett 161(1)*: 215–230.

Hacker BR, Ratschbacher L, Webb L, McWilliams MO, Ireland T, Calvert A, Dong S, Wenk HR, Chateigner D (2000) Exhumation of ultrahigh-pressure continental crust in east central China: Late Triassic-Early Jurassic tectonic unroofing. *J Geophys Res: Solid Earth 105(B6)*: 13339–13364.

Hacker BR, Ratschbacher L, Liou JG (2004) Subduction, collision and exhumation in the ultrahigh-pressure Qinling-Dabie orogen. *Geol Soc Spec Pub 226(1)*: 157–175.

Hacker BR, Wallis SR, Ratschbacher L, Grove M, Gehrels G (2006) High-temperature geochronology constraints on the tectonic history and architecture of the ultrahigh-pressure Dabie-Sulu Orogen. *Tectonics, 25(5)*: DOI: 10.1029/2005TC001937.

Herwartz D, Pack A, Krylov D, Xiao Y, Muehlenbachs K, Sengupta S, Di Rocco T (2015) Revealing the climate of snowball Earth from Δ17O systematics of hydrothermal rocks. *P Natl Acad Sci USA 112(17)*: 5337–5341.

Hirajima T, Nakamura D (2003) The Dabie Shan–Sulu orogen. In: *EMU Notes in Mineralogy 5*: 105–144. Eötvös Univ. Press, Budapest.

Hoffman PF, Kaufman AJ, Halverson GP, Schrag DP (1998) A Neoproterozoic snowball earth. *Science 281(5381)*: 1342-1346.

Jahn BM (1998) Geochemical and isotopic characteristics of UHP eclogites and ultramafic rocks of the Dabie orogen: implications for continental subduction and collisional tectonics. In: *When continents collide: geodynamics and geochemistry of ultrahigh-pressure rocks*: 203–239. Springer, Amsterdam.

Jahn BM, Liu X, Yui TF, Morin N, Bouhnik-Le Coz M (2005) High-pressure/ultrahigh-pressure eclogites from the Hong'an Block, East-Central China: geochemical characterization, isotope disequilibrium and geochronological controversy. *Contrib Mineral Petrology 149(5)*: 499–526.

Li S, Xiao Y, Liou D, Chen Y, Ge N, Zhang Z, Sun S, Cong B, Zhang R, Hart S, Wang S (1993) Collision of the North China and Yangtze Blocks and formation of coesite-bearing eclogites: timing and processes. *Chem Geol 109(1)*: 89–111.

Li S, Jagoutz E, Chen Y, Li Q (2000) Sm–Nd and Rb–Sr isotopic chronology and cooling history of ultrahigh pressure metamorphic rocks and their country rocks at Shuanghe in the Dabie Mountains, Central China. *Geochim Cosmochim Ac 64(6)*: 1077–1093.

Li SG, Huang F, Nie YH, Han WL, Long G, Li HM, Zhang ZH (2001) Geochemical and geochronological constraints on the suture location between the North and South China Blocks in the Dabie orogen, central China. *Phys Chem Earth, Part A: Solid Earth and Geodesy 26(9)*: 655–672.

Li XP, Zheng YF, Wu YB, Chen F, Gong B, Li YL (2004) Low-T eclogite in the Dabie terrane of China: petrological and isotopic constraints on fluid activity and radiometric dating. *Contrib Mineral Petrol 148(4)*: 443–470.

Li R, Wan Y, Cheng Z, Zhou J, Li S, Jin F, Meng Q, Li Z, Jiang M (2005) Provenance of Jurassic sediments in the Hefei Basin, east-central China and the contribution of high-pressure and ultrahigh-pressure metamorphic rocks from the Dabie Shan. *Earth Planet Sci Lett 231(3)*: 279–294.

Liou JG, Zhang RY, Eide EA, Maruyama S, Wang X, Ernst WG (1996) Metamorphism and tectonics of high-P and ultrahigh-P belts in Dabie-Sulu Regions, eastern central China. *The tectonic evolution of Asia*, 300–343. Cambridge Univ. Press, Cambridge.

Liou JG, Zhang RY, Jahn BM (1997) Petrology, geochemistry and isotope data on a ultrahigh-pressure jadeite quartzite from Shuanghe, Dabie Mountains, East-central China. *Lithos 41(1)*: 59–78.

Liou JG, Ernst WG, Zhang RY, Tsujimori T, Jahn BM (2009) Ultrahigh-pressure minerals and metamorphic terranes–the view from China. *J Asian Earth Sci 35(3)*: 199–231.

Liu J, Ye K, Maruyama S, Cong B, Fan H (2001) Mineral inclusions in zircon from gneisses in the ultrahigh pressure zone of the Dabie Mountains, China. *J Geol 109*: 523–535.

Liu F, Xu Z, Katayama I, Masago H, Maruyama S, Yang J (2002) Ultrahigh-pressure mineral inclusions in zircons from gneissic core samples of the Chinese Continental Scientific Drilling Site in eastern China. *Eur J Mineral 14(3)*: 499–512.

Liu F, Xu Z, Xue H (2004a) Tracing the protolith, UHP metamorphism, and exhumation ages of orthogneiss from the SW Sulu terrane (eastern China): SHRIMP U–Pb dating of mineral inclusion-bearing zircons. *Lithos 78(4)*: 411–429.

Liu F, Xu Z (2004b) Fluid inclusions hidden in coesite-bearing zircons in ultrahigh-pressure metamorphic rocks from southwestern Sulu terrane in eastern China. *Chinese Sci Bull 49(4)*: 396–404.

Liu X, Jahn BM, Liu D, Dong S, Li S (2004c) SHRIMP U–Pb zircon dating of a metagabbro and eclogites from western Dabieshan (Hong'an Block), China, and its tectonic implications. *Tectonophysics 394(3)*: 171–192.

Liu D, Jian P, Kröner A, Xu S (2006) Dating of prograde metamorphic events deciphered from episodic zircon growth in rocks of the Dabie–Sulu UHP complex, China. *Earth Planet Sci Lett 250(3)*: 650–666.

Liu F, Gerdes A, Zeng L, Xue H (2008) SHRIMP U–Pb dating, trace elements and the Lu–Hf isotope system of coesite-bearing zircon from amphibolite in the SW Sulu UHP terrane, eastern China. *Geochim Cosmochim Ac 72(12)*: 2973–3000.

Malaspina N, Hermann J, Scambelluri M, Compagnoni R (2006) Multistage metasomatism in ultrahigh-pressure mafic rocks from the North Dabie Complex (China). *Lithos 90(1)*: 19–42.

Maruyama S, Liou JG, Zhang R (1994) Tectonic evolution of the ultrahigh-pressure (UHP) and high-pressure (HP) metamorphic belts from central China. *Isl Arc 3(2)*: 112–121.

Maruyama S, Masago H, Katayama I, Iwase Y, Toriumi M, Omori S (2010) A new perspective on metamorphism and metamorphic belts. *Gondwana Res 18(1)*: 106–137.

Okay AI, Xu S, Sengor AC (1989) Coesite from the Dabie Shan eclogites, central China. Eur J Mineral1(4): 595–598.

Okay AI (1993) Petrology of a diamond and coesite-bearing metamorphic terrain: Dabie Shan. China. *Eur J Mineral 5*: 659–675.

Rowley DB, Xue F, Tucker RD, Peng ZX, Baker J, Davis A (1997) Ages of ultrahigh pressure metamorphism and protolith orthogneisses from the eastern Dabie Shan: U/Pb zircon geochronology. *Earth Planet Sci Lett 151(3)*: 191–203.

Rumble D, Liou JG, Jahn BM (2003) Continental crust subduction and ultrahigh pressure metamorphism. In: *Treatise on Geochemistry 1(3) The Crust*: 293–319. Oxford: Elsevier.

Tabata H, Maruyama S, Shi Z (1998a) Metamorphic zoning and thermal structure of the Dabie ultrahigh-pressure–high-pressure terrane, central China. *Isl Arc 7(1)*: 142–158.

Tabata H, Yamauchi K, Maruyama S, Liou JG (1998b) Tracing the extent of a UHP metamorphic terrane: Mineral-inclusion study of zircons in gneisses from the Dabie Shan. In: *When Continents Collide: Geodynamics and geochemistry of ultrahigh-pressure rocks*: 261–273. Springer Netherlands.

Tang J, Zheng YF, Gong B, Wu YB, Gao TS, Yuan H, Wu FY (2008) Extreme oxygen isotope signature of meteoric water in magmatic zircon from metagranite in the Sulu orogen, China: implications for Neoproterozoic rift magmatism. *Geochim Cosmochim Ac 72(13)*: 3139–3169.

Wan Y, Li R, Wilde SA, Liu D, Chen Z, Yan L, Song T, Yin X (2005) UHP metamorphism and exhumation of the Dabie Orogen, China: evidence from SHRIMP dating of zircon and monazite from a UHP granitic gneiss cobble from the Hefei Basin. *Geochim Cosmochim Ac 69(17)*: 4333–4348.

Wang X, Liou JG, Mao HK (1989) Coesite-bearing eclogite from the Dabie Mountains in central China. *Geology 17(12)*: 1085–1088.

Wang X, Liou JG (1991) Regional ultrahigh-pressure coesite-bearing eclogitic terrane in central China: evidence from country rocks, gneiss, marble, and metapelite. *Geology 19(9)*: 933–936.

Wang Y, Fan W, Guo F (2002) K-Ar dating of late Mesozoic volcanism and geochemistry of volcanic gravels in the North Huaiyang Belt, Dabie orogen: Constraints on the stratigraphic framework and exhumation of the northern Dabie orthogneiss complex. *Chinese Sci Bull 47(20)*: 1688–1695.

Wang X, Liou JG (1991) Regional ultrahigh-pressure coesite-bearing eclogitic terrane in central China: evidence from country rocks, gneiss, marble, and metapelite. *Geology 19(9)*: 933–936.

Wu YB, Hanchar JM, Gao S, Sylvester PJ, Tubrett M, Qiu HN, Wijbrans JR, Brouwer FM, Yang, SH, Liu YS, Yuan HL (2009) Age and nature of eclogites in the Huwan shear zone, and the multi-stage evolution of the Qinling-Dabie-Sulu orogen, central China. *Earth Planet Sci Lett 277(3)*: 345–354.

Xiao YL, Li SG, Jagoutz E, Cheng W (1995) P-T-t path for coesite-bearing peridotite-eclogite association in the Bixiling, Dabie Mountains. *Chin Sci Bull 40*: 156–158.

Xiao Y, Hoefs J, van den Kerkhof AM, Fiebig J, Zheng Y (2000) Fluid history of UHP metamorphism in Dabie Shan, China: a fluid inclusion and oxygen isotope study on the coesite-bearing eclogite from Bixiling. *Contrib Mineral Petrol 139(1)*: 1–16.

Xiao Y, Zhang Z, Hoefs J, van den Kerkhof A (2006) Ultrahigh-pressure metamorphic rocks from the Chinese Continental Scientific Drilling Project: II Oxygen isotope and fluid inclusion distributions through vertical sections. *Contrib Mineral Petrol 152(4)*: 443–458.

Xu S, Okay AI, Shouyuan J, Sengör AMC, Wen S, Yican L, Laili J (1992) Diamond from the Dabie Shan metamorphic rocks and its implication for tectonic setting. *Science 256*: 80.

Xu S, Liu Y, Chen G, Compagnoni R, Rolfo F, He M, Liu H (2003) New finding of micro-diamonds in eclogites from Dabie-Sulu region in central-eastern China. *Chinese Sci Bull 48(10)*: 988–994.

Yang, JS, Wooden JL, Wu CL, Liu FL, Xu ZQ, Shi RD, Katayama I, Liou JG, Maruyama S (2003) SHRIMP U–Pb dating of coesite-bearing zircon from the ultrahigh-pressure metamorphic rocks, Sulu terrane, east China. *J Metamorph Geol 21(6)*: 551–560.

Ye BD, Jiang P, Xu J, Cui F, Li Z, Zhang Z (1994) Timing of the Sujiahe group in the Tongbai–Dabie orogenic belt. *Res Isotope Geochem*: 175–186.

Ye K, Yao Y, Katayama I, Cong B, Wang Q, Maruyama S (2000) Large areal extent of ultrahigh-pressure metamorphism in the Sulu ultrahigh-pressure terrane of East China: new implications from coesite and omphacite inclusions in zircon of granitic gneiss. *Lithos 52(1)*: 157–164.

Yui TF, Rumble D, Lo CH (1995) Unusually low δ 18 O ultra-high-pressure metamorphic rocks from the Sulu Terrain, eastern China. *Geochim Cosmochim Ac 59(13)*: 2859–2864.

Zhang, RY, Liou JG, Ernst WG (1995a) Ultrahigh-pressure metamorphism and decompressional P-T paths of eclogites and country rocks from Weihai, eastern China. *Isl Arc 4(4)*: 293–309.

Zhang RY, Liou JG, Cong BL (1995b) Talc-, magnesite-and Ti-clinohumite-bearing ultrahigh-pressure meta-mafic and ultramafic complex in the Dabie Mountains, China. *J Petrol 36(4)*: 1011–1037.

Zhang RY, Hirajima T, Banno S, Cong B, Liou JG (1995c) Petrology of ultrahigh-pressure rocks from the southern Sulu region, eastern China. *J Metamorph Geol 13*: 659–675.

Zhang RY, Liou JG, Tsai CH (1996) Petrogenesis of a high-temperature metamorphic terrane: a new tectonic interpretation for the north Dabieshan, central China. *J Metamorph Geol 14(3)*: 319–333.

Zhang Z, Xiao Y, Xu Z, Hoefs J, Yang J, Liu F, Liou JG (2006) UHP metamorphic rocks from the main hole (0–2050 m) of Chinese Continental Scientific Drilling Project – I. Petrology and geochemistry. *Contrib Mineral Petrol 152*: 421–441.

Zhang RY, Liou JG, Ernst, WG (2009) The Dabie–Sulu continental collision zone: a comprehensive review. *Gondwana Res 16(1)*: 1–26.

Zhao ZF, Zheng YF, Gao TS, Wu YB, Chen B, Chen FK, Wu FY (2006) Isotopic constraints on age and duration of fluid-assisted high-pressure eclogite-facies recrystallization during exhumation of deeply subducted continental crust in the Sulu orogen. *J Metamorph Geol 24(8)*: 687–702.

Zheng YF, Fu B, Li Y, Xiao Y, Li S (1998) Oxygen and hydrogen isotope geochemistry of ultrahigh-pressure eclogites from the Dabie Mountains and the Sulu terrane. *Earth Planet Sci Lett 155(1)*: 113–129.

Zheng YF, Fu B, Gong B, Li L (2003) Stable isotope geochemistry of ultrahigh pressure metamorphic rocks from the Dabie–Sulu orogen in China: implications for geodynamics and fluid regime. *Earth Sci Rev 62(1)*: 105–161.

Zheng YF, Wu YB, Chen FK, Gong B, Li L, Zhao ZF (2004) Zircon U-Pb and oxygen isotope evidence for a large-scale [18]O depletion event in igneous rocks during the Neoproterozoic. *Geochim Cosmochim Ac 68(20)*: 4145–4165.

Zheng YF, Zhou JB, Wu YB, Xie Z (2005) Low-grade metamorphic rocks in the Dabie-Sulu orogenic belt: A passive-margin accretionary wedge deformed during continent subduction. *Int Geol Rev 47(8)*: 851–871.

Zheng YF, Zhao ZF, Wu YB, Zhang SB, Liu X, Wu FY (2006) Zircon U–Pb age, Hf and O isotope constraints on protolith origin of ultrahigh-pressure eclogite and gneiss in the Dabie orogen. *Chem Geol 231(1)*: 135–158.

Zheng Y (2008) A perspective view on ultrahigh-pressure metamorphism and continental collision in the Dabie-Sulu orogenic belt. *Chinese Sci Bull 53(20)*: 3081–3104.

Zhu YF, Massonne HJ, Theye T (2007) Eclogite from the Chinese continental scientific drilling borehole: their petrology and different P–T evolutions. *Isl Arc 16*: 508–535.

3. Petrography and field relations

3.1   Sampling and vein classification

A set of UHP/HP eclogites, that record fluid-rock interaction in the form of enclosed metamorphic veins, has been collected. Sampled lithologies comprise both pristine and retrogressed eclogites as well as different bulk veins in contact to eclogite (specimen dimension approximately 15 x 15 x 15 cm) and selective metamorphic vein drill core samples (core dimension approximately 2.5 x 6 cm). Eclogites and veins were collected in Shuanghe and Zhujiachong. Bixiling and Huwan eclogites did not expose any metamorphic veins, but each a representative pristine eclogite was sampled. Rocks with macroscopic evidence of alteration were categorically excluded with the exception of Huwan, where the eclogite is entirely altered due to strong deformation.

Structural relations of veins and associated eclogites as well as vein mineral assemblages were used for a fundamental classification of the metamorphic veins. Three types of veins were characterized:

(1)   Small-scale quartz-rutile veins (widths: 1–5 cm, lengths: 0.2–2 m) that occur strictly parallel to the eclogite foliation and did not trigger retrogression in the eclogite. They are referred to as **1st generation**, since they are apparently related to eclogitization and with this to be the oldest of all observed veins.

(2) Medium-scale (widths: 10–30 cm, lengths: >3 m), heterogeneous and polymineralic veins that crosscut the eclogitic foliation and are slightly deformed along with the host rock. They contain HP phases such as omphacite, kyanite and phengite and caused minor retrograde reaction zones <10 cm in the adjacent eclogite. They are referred to as **2nd generation**, since they clearly post-date the eclogitization.

(3) Large-scale (widths: 60 cm, lengths: >1 m), heterogeneous and polymineralic veins that crosscut the foliation of eclogite and lack evidence of conjoint deformation. They predominantly contain low-grade metamorphic phases such as plagioclase, chlorite and hornblende whereas HP phases are absent, and show distinct retrogression for about 60 cm at the host margins. They are referred to as **3rd generation**, since their mineral assemblages and structural relations point to a late retrograde formation.

Conspicuously, no 2nd and 3rd generation veins were observed within outcrop-scale distances (~25 m) to the sampled, pristine eclogites. These veins are generally only observed at outcrops of eclogites that show retrograde overprint.

Table 3.1 provides an overview on samples selected for this study with associated locations, rock types, mineral assemblages, and an index of fluid inclusion-bearing minerals. As most veins are heterogeneous, samples were selected with the aim to cover their complete mineralogy. Thin sections (40 μm) of all samples were prepared for petrographic study and in-situ trace element analyses.

3.2   Eclogites

3.2.1   Shuanghe (samples: SH-B56, -A59)

Sample **SH-A59** represents a pristine and unaltered UHP coesite-eclogite. It was collected at location SH-A. The outcrop resulted from road building and exposes a massive, medium-grained and poorly deformed eclogite with a mineral assemblage of garnet (45%) + omphacite (45%) + quartz (8%) + rutile (1–2%) ± phengite ± zircon. The eclogite partly exhibits a centimeter-scaled banding of garnet- and omphacite-dominated layers both of which may be occasionally rich in quartz (up to 30 vol%), but is homogeneous on the outcrop scale of about 25 m. It was sampled about 15 m away from a swarm of 1st generation quartz-rutile veins.

Garnet occurs as euhedral to subhedral crystals and shows abundant intragranular microcracks, euhedral to subhedral omphacite crystals show a preferred orientation coinciding with the rocks foliation. Structural relations of quartz, such as equilibrated grain boundaries and 'pushing apart' of former garnet-omphacite fabrics (**Figure 3.1a, b**), suggest a recrystallization after coesite. The eclogite is almost devoid of retrogression, except for occasional thin (<1 mm) symplectic rims of plagioclase and fibrous amphibole around omphacite. Transgranular cracks on a macroscopic scale are rare, indicating little deformation along the exhumation path. Rutile and zircon occur both as inclusions in omphacite and garnet and as eclogitic accessories. Apatite has not been identified as mineral inclusion, whereas phengite solely occurs as rare inclusion in garnet or omphacite. Fluid inclusions of mainly secondary character are abundant in quartz, but are rarely also found as primary inclusions in garnet and quartz. Numerous pseudomorphic quartz inclusions after coesite are observed in garnet and omphacite (**Figure 3.1c**).

Sample **SH-B56** represents an UHP coesite-eclogite that experienced retrograde recrystallization. It was collected at SH-B in the form of blocky rocks that accumulated along a shallow riverbed 1 km south of SH-A. Next to numerous gneissic blocks, a vein-bearing eclogite fragment (approximately 60 x 60 x 60 cm) with distinct amphibolitization has been found. It exhibits sharp jagged edges and lacks
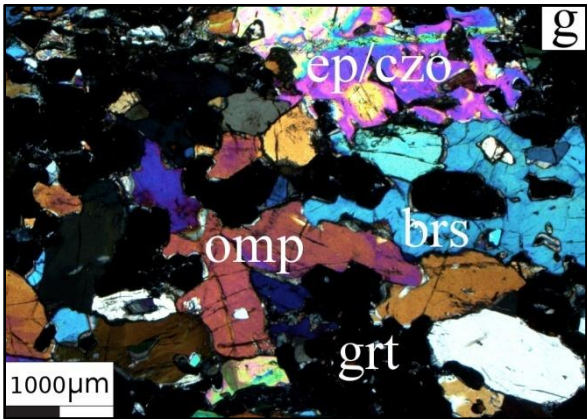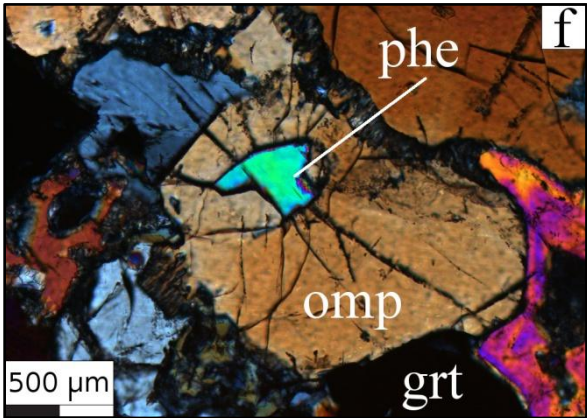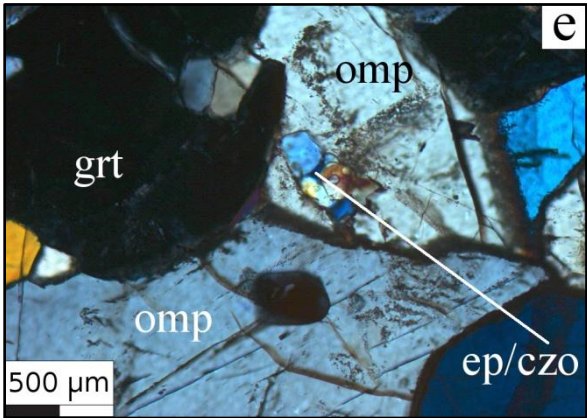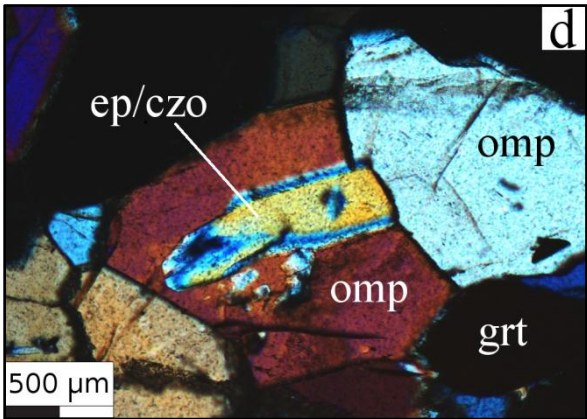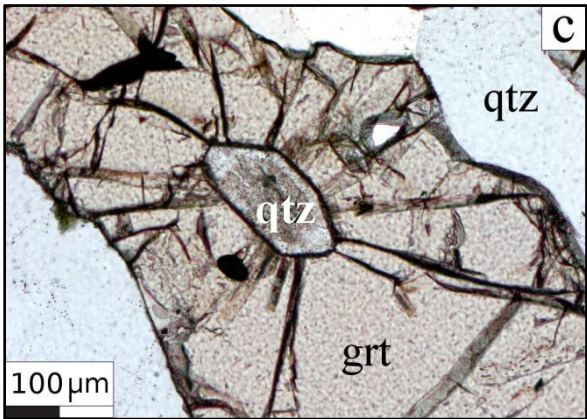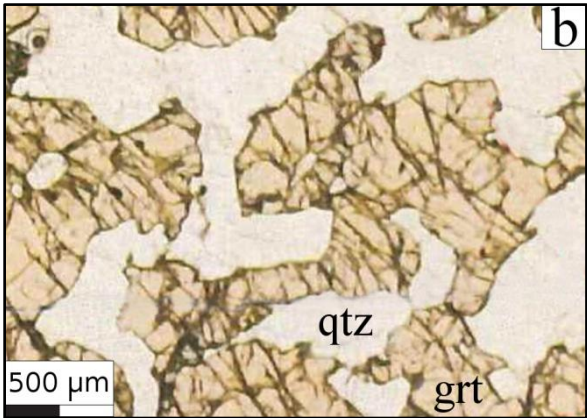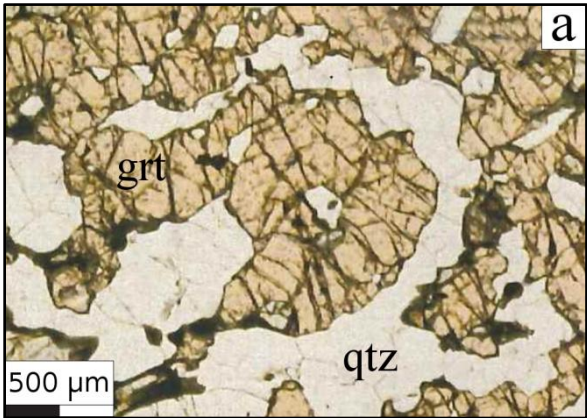
↑ **Figure 3.1 (previous page) a, b** Quartz in between garnet crystals with mostly congruent grain boundaries indicates a 'pushing apart' of the initial mineral association due to quartz recrystallization after coesite in the pristine UHP eclogite from Shuanghe SH-A59. Plane polarized light (PPL). **c** Representative inclusion of recrystallized quartz after coesite in garnet from SH-A59, showing indicative radial cracks in the host mineral that developed as a result of volume expansion during the coesite-quartz transition (PPL). **d-f** Epidote/clinozoisite and phengite inclusions in omphacite attesting their affiliation to the peak metamorphic assemblage. **g** Representative section of the Shuanghe eclogite with retrograde overprint (SH-B56), displaying overgrowth of epidote and amphibole over garnet and omphacite, as well as diffuse zoning in ep/czo. Cross polarized light (XPL). Mineral abbreviations after WHITNEY AND EVANS (2010).

macroscopic evidence of secondary alteration features (**Figure 3.5a**), indicating fresh fracturing and negligible transportation. The eclogite sample from this fragment has been taken in a distance of about 50 cm away from the enclosed metamorphic vein.

The fine-grained, homogeneous and slightly foliated eclogite exhibits a mineral assemblage of garnet (35%) + omphacite (35%) + barroisite (15%) + epidote/clinozoisite (10%) + phengite (4%) ± ky (1%) ± apatite ± rutile ± pyrite ± zircon. Omphacite and garnet occur anhedral to subhedral and omphacites exhibit a preferred orientation according to the eclogitic foliation. Inclusions of phengite and epidote/clinozoisite (**Figure 3.1d-f**) attest their affiliation to the peak paragenesis. Anhedral barroisite and epidote/clinozoisite texturally overgrow the peak assemblage, as indicated by numerous inclusions of garnet, omphacite and phengite, and ep/czo often exhibit a diffuse zoning pattern under crossed polarized light (**Figure 3.1g**). Rutile and zircon inclusions are common in all minerals. The eclogite is pervaded by few transgranular microcracks on a length scale of centimeters that are filled with hornblendic amphibole and record tectonic stress. Quartz pseudomorphs after coesite are rarely found in garnet and omphacite, while unequivocally identifiable fluid inclusions have not been observed at all.

3.2.2 Zhujiachong (sample: ZJC-16)

Sample **ZJC-16** represents a HP quartz-eclogite with distinct retrograde overprint. Outcrop ZJC resulted from road construction and exposes a fine-grained and homogeneous eclogite with a slight

foliation parallel to the foliation of the gneissic country rock. A slight undulation of this foliation points to tectonic stress resulting in marginal deformation. The sample was collected ~10 m away from each the margin towards the host gneiss and towards metamorphic veins, aiming to minimize the retrograde exchange with the country rock and the potential influence of fluid-rock interaction induced by the vein-forming fluids.

The foliated and weakly deformed eclogite consists of garnet (25%) + omphacite (13%) + epidote/clinozoisite (10%) + phengite (5%) + paragonite (5%) + barroisite (5%) + quartz (5%) + zoisite (2%) ± apatite ± rutile ± zircon, in a fine-grained and slightly deformed matrix (30%) of albite and amphibole. Garnet occurs as mainly euhedral porphyroblasts in three different modes (**Figure 3.2a, b**): (i) annular atoll garnet, (ii) annular atoll garnet enclosing anhedral garnet, (iii) full garnet without atoll texture and numerous inclusions of rutile, omphacite, phengite and epidote/clinozoisite in the crystal mantle region, while core and rim are devoid of inclusions. Type (i) and (ii) atoll garnet envelop phengite, quartz, omphacite, epidote/clinozoisite and rutile.
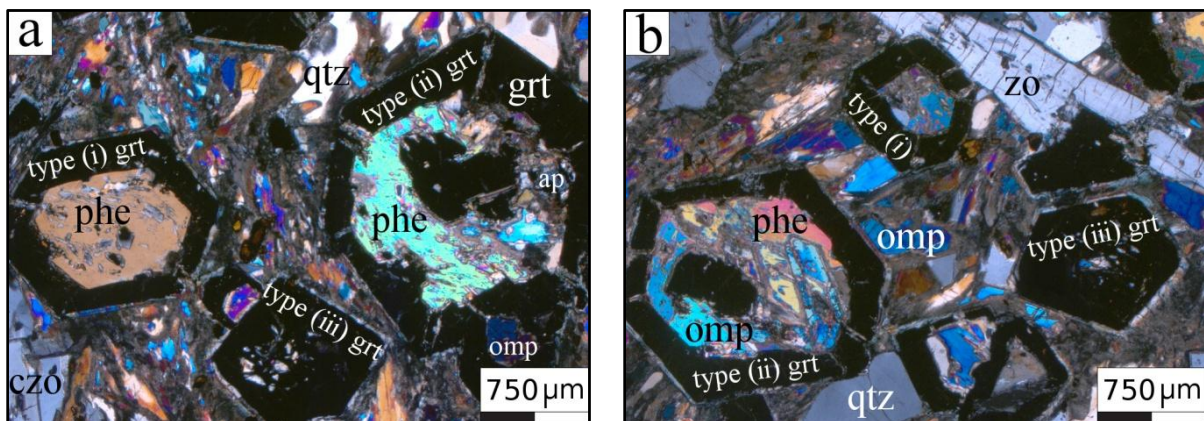
↑ **Figure 3.2 a, b** Three types of atoll garnet with multiple inclusions in the retrograded eclogite from ZJC. Along with relictic omphacite and zoisite porphyroblasts, they are embedded in a fine-grained and partly deformed and sheared matrix of amphibole and plagioclase (XPL).

The initial eclogitic assemblage comprises garnet + omphacite + phengite + epidote/clinozoisite (preserved as inclusions in omphacite and garnet) ± rutile. A second generation of porphyroblastic zoisite and texturally coexisting epidote/clinozoisite, paragonite, as well as interstitially recrystallized

quartz with equilibrated grain boundaries and barroisite postdates the eclogitic peak assemblage. These minerals both occur within and outside atoll garnets. Their growth is likely related to the introduction of a fluid phase that triggered the atoll-like garnet modification and accounted for the hydrous mineral inclusions (eg. ep/czo) in the mantles of type (iii) garnets. Neither pseudomorphed quartz after coesite nor any fluid inclusions have been identified within the sample, and thus a UHP metamorphic origin of this eclogite, as proposed by LI ET AL. (2004), cannot be confirmed by petrographic evidence.

3.2.3   Bixiling (sample: BX-07)

The bulk sample **BX-07** is a pristine and unaltered UHP coesite-eclogite that has been collected at the road outcrop BX. The medium- to coarse-grained, unfoliated and homogeneous eclogite virtually lacks retrogression, except for occasional and marginal symplectic rims around garnet and omphacite and occasional poiciloblastic zoisite, and it does not show any evidence of secondary alteration. The mineral assemblage comprises garnet (50%) + omphacite (45%) + quartz (3%) + phengite (<1%) + zoisite (<1%) ± rutile ± zircon ± pyrite.

Euhedral to subhedral garnet and omphacite crystals show equilibrated grain boundaries and host few and tiny phengite, rutile and zircon inclusions. Omphacite, garnet and phengite represent the initial eclogitic assemblage, whereas quartz and zoisite recrystallized dispersedly distributed within the rock. Anhedral zoisite exhibits poicilitic overgrowth of garnet and omphacite and formed only locally on the expense of phengite, garnet and omphacite. Quartz occurs interstitially with mainly equilibrated grain boundaries and several inclusions of the eclogitic minerals. Radial microcracks in garnet and omphacite around circular quartz domains (**Figure 3.3a,b**) likely reflect the existence of coesite during UHP conditions that recrystallized to quartz after the UHP peak. Pseudomorphic quartz inclusions after coesite in both omphacite and garnet are abundant, fluid inclusions were not identifiable at all.
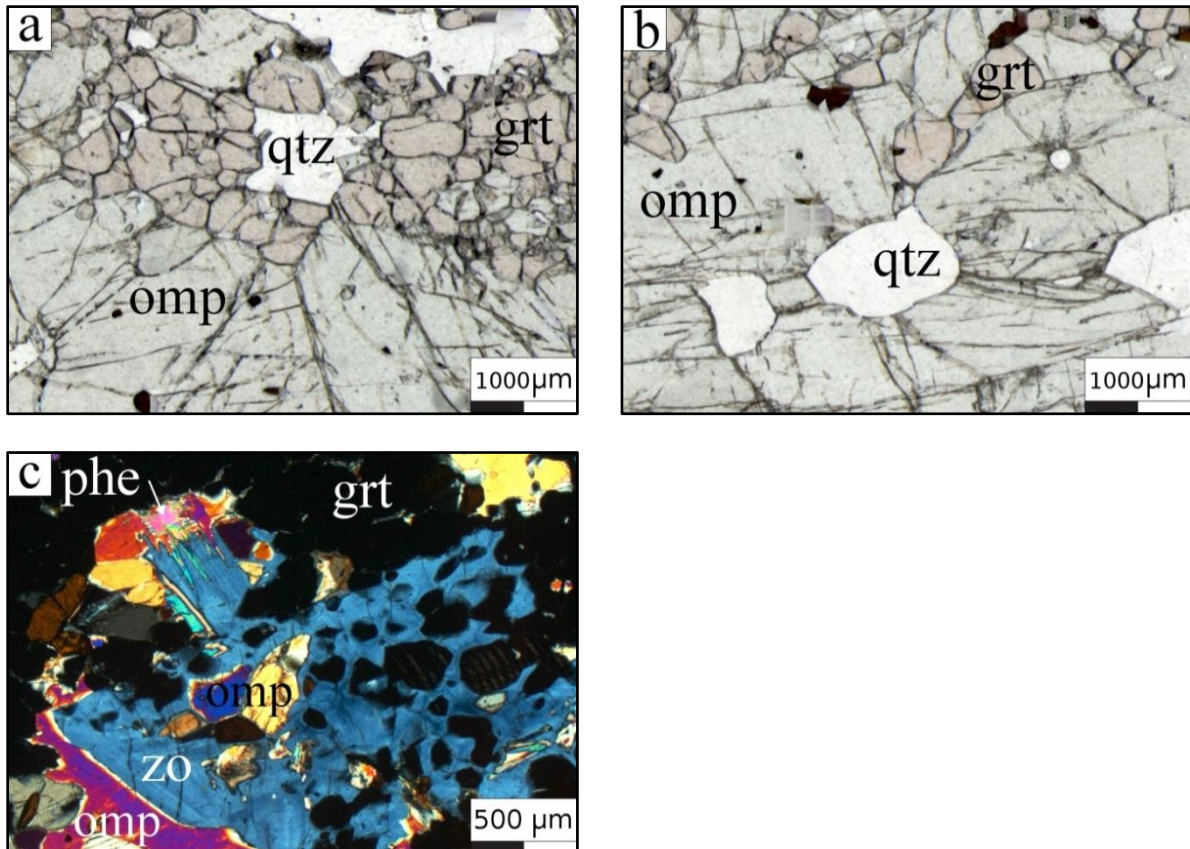
↑ **Figure 3.3 a**,**b** Garnet-omphacite fabric in pristine eclogite with qtz-domains surrounded by radial fractures. Fracturing is interpreted to result from volume expansion of quartz, related to the coesite-quartz transformation . A pseudomorphic quartz inclusion in omphacite in the proper sense is depicted in the upper right part of (b) (PPL). **c** Zoisite occurs solely in contact to phengite on the expense of garnet, omphacite and phengite (XPL).

3.2.4 Huwan (sample: HW-42)

Sample **HW-42** represents a strongly altered eclogite from outcrop HW that shows distinct deformation features. Retrogression is limited to the decomposition of garnet and omphacite towards a fine-grained, plagioclase-rich matrix. The retrograde formation of eg. epidote group minerals and phengite is virtually absent. The mineral assemblage is garnet (25%) + omphacite (13%) + phengite (1%) + zoisite (1%) rutile ± zircon ± pyrite in a fine-grained matrix (60%) of amphibole, pyroxene and plagioclase.

Garnet porphyroblasts occur as euhedral but strongly corroded, microcrystalline aggregates with sizes between 1–5 mm and may include rutile. Relictic and anhedral omphacite exhibits pronounced

symplectic rims or is completely decomposed. Phengite and relictic zoisite are occasionally observed as dispersedly distributed, anhedral and isolated crystals of sizes <1 mm. The fine- to superfine-grained, amphibole- and plagioclase-dominated matrix often exhibits an undulating deformed texture, recording distinct tectonic stress and deformation. Pseudomorphic quartz after coesite, as well as mineral and fluid inclusions have not been identified.

3.3 Metamorphic veins

3.3.1 Shuanghe (samples: SH-B44, -B55, -C58, -A60)

Sample **SH-A60** is a 1st generation quartz-rutile vein in contact to the pristine host eclogite from outcrop SH-A. The outcrop exposes medium-grained quartz-rutile veins with widths of 1–5 cm that occur parallel to the slightly deformed foliation of a coesite-bearing eclogite (**Figure 3.4c**). They consist of quartz with 1–2 vol% of subhedral single crystals of rutile (up to 2 cm in size), and show a macroscopically sharp and microscopically gradual transition towards the eclogite without triggering retrogression (**Figure 3.4a, b**). Structural relations of quartz, such as triple-point grain boundaries and 'breaking apart' of former garnet-omphacite fabrics, suggest a recrystallization of possibly former coesite along garnet and omphacite grain boundaries (cf. **Figure 3.4b**).

51
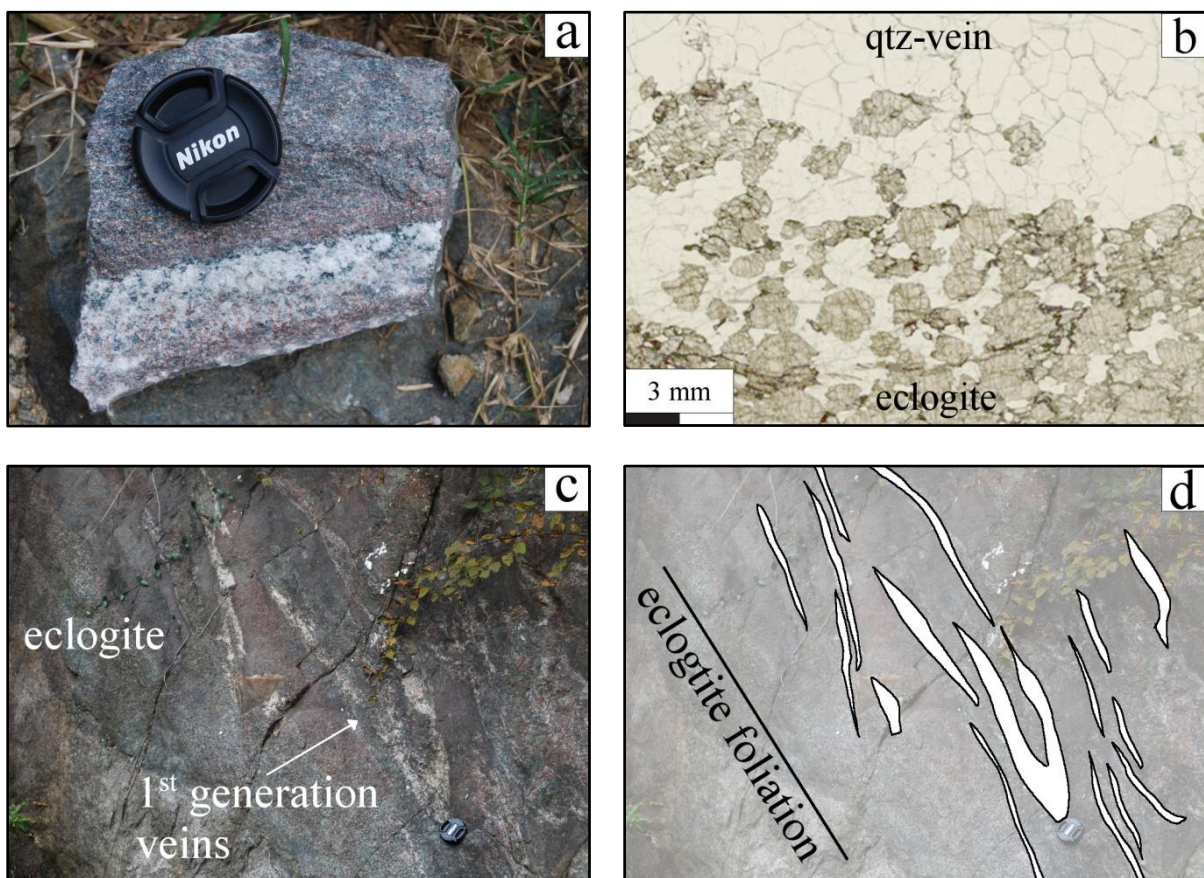
↑ **Figure 3.4 (previous page) a** Handspecimen SH-A60 of a 1st generation vein from Shuanghe, representing its contact to the eclogite **b** Vein-eclogite contact on a microscopic scale. The quartz apparently expands into the host rock by pushing apart its original omp-grt assemblage, pointing to a previous existence of coesite (PPL) **c, d** Photograph and schematic sketch of a 1st generation vein in the outcrop. The contact to the eclogitic foliation is at very low angles. Lense cover for scale (5cm).

Quartz crystals occur subhedrally and exhibit mainly equilibrated grain boundaries. Minor interlobate crystal contacts are observed in association with re-equilibrated microcracks. Fluid inclusions are abundant in quartz.

Samples **SH-B44** and **SH-B55** represent 2nd generation polymineralic, coarse-grained veins collected from two rock fragments along the riverbed at SH-B. The vein widths are in the range of decimeters. SH-B55 was taken from the same rock fragment as the retrogressed Shuanghe bulk eclogite (SH-B56) (**Figure 3.5a**), while SH-B44 originates from another, similar block. The veins as a whole are irregular concerning width and orientation. They clearly crosscut the eclogitic foliation at high angles and exhibit undulating contacts towards the eclogite. Both vein samples contain the same, and heterogeneously distributed, mineral assemblage of amphibole (50%) + epidote/clinozoisite (30%) + phengite (5%) + apatite (5%) + quartz (5%) + omphacite (3%) + rutile (2%) ± zircon ± pyrite. Due to the variability of mineral abundances in the vein samples, the estimation of modal contents has high uncertainties.

The vein contacts towards eclogite are gradual for about 5–10 cm, showing vein minerals (mainly amphibole) to apparently propagate into the eclogite by poicilitic overgrowth of the eclogitic assemblage. In these transitional zones, garnet shows pronounced resorption rims, and omphacite relics are largely decomposed.

Megacrystic amphibole with sizes up to several centimeters is the major constituent of all veins. Indicated by glaring blue to dark green interference colours, it is identified as HP-stable barroisite. They structurally overgrow all other vein minerals and especially epidote/clinozoisite, omphacite and quartz occasionally show distinct symplectic resorption rims in contact to amphibole. Barroisite sometimes shows poicilitic overgrowth textures and is transformed to hornblende in retrogressively
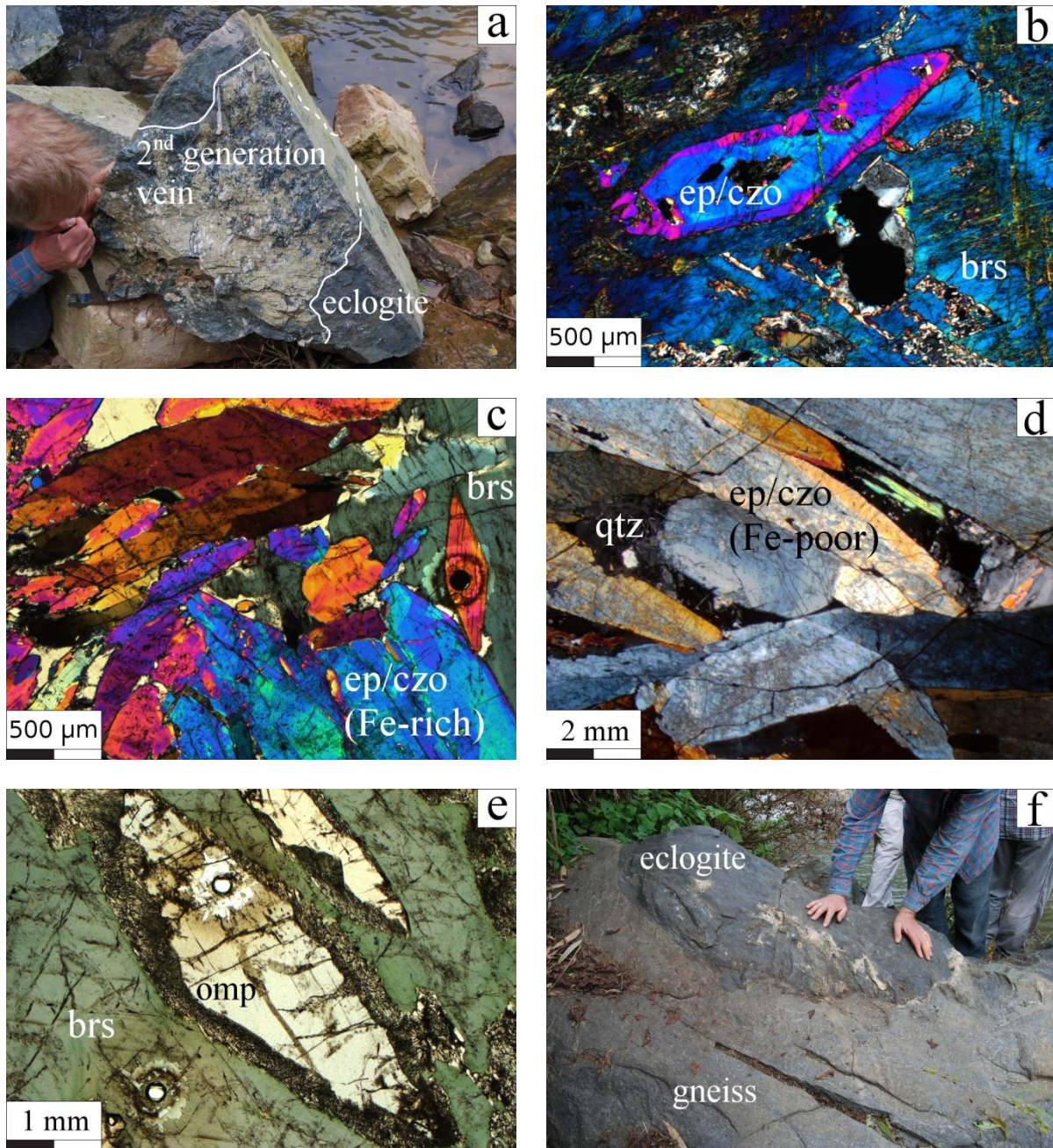
↑ **Figure 3.5 a** 2nd generation ep/czo + brs + omp + phe + qtz vein from SH-B, white lines trace the contact towards the eclogite **b** Subhedral ep/czo with two stage zonation (XPL) **c** Aggregation of epidote-endmember-rich (Fe-rich) ep/czo, exhibiting glaring and colourful interference colours (XPL) **d** Aggregation of clinozoisite-endmember-rich (Fe-poor) ep/czo exhibiting pale blue and yellow interference colours (XPL). The minerals show distinct alteration as well as numerous fluid inclusions, resulting in a turbid appearance. **e** Vein omphacite occurs as euhedral crystals with pronounced reaction rims (PPL). Circular structures are LA-ICPMS spots. **f** Eclogite lens in gneissic country rock. The sharp contact and the vein that does not propagate from the eclogite into the gneiss indicate tectonic mingling as well as the affiliation of vein formation to the eclogitic host and a closed-system, eclogite internal veining.

altered regions (eg. related to microfractures). Filled microfractures contain fibrous hornblende and fine-grained Fe-rich epidote.

Epidote/clinozoisite occur in two modes: (i) Coarse-grained (0.5–50 mm) clinozoisite-rich, subhedral to anhedral crystals which are distinctly altered and thus appear turbid (**Figure 3.5d**). They generally exhibit low (mostly anomalous blue) interference colours in the core and higher (mostly yellow) interferences towards the rim and along microfractures and are not in textural equilibrium with overgrowing barroisite. (ii) Coarse-grained (2–10 mm) epidote-rich euhedral to subhedral crystals that often exhibit two-step zoning patterns (**Figure 3.5b**) and comparatively higher (glaring and variable) interference colours than type (i) (**Figure 3.5c**). They are in textural equilibrium with barroisite. The zoned crystals usually show higher interferences towards the rim. Both ep/czo types predominantly occur aggregated and the apparently younger type (i) is occasionally overgrown by type (ii). Type (i) occasionally contains fluid inclusions with multiple daughter crystals.

Medium-grained omphacite occurs as isolated, euhedral to subhedral crystals with distinct symplectic rims consisting of pyroxene, albite and amphibole (**Figure 3.5e**). All observed omphacites are surrounded by megacrystic barroisite.

Subhedral phengite is found dispersed within the vein as isolated flakes, or in the form of aggregated crystal layers that are occasionally slightly sheared along grain boundaries.

Apatite occurs as individual, mainly sub- to anhedral crystals reaching sizes in the range of several millimeters. Plagioclase occurs solely as exsolution products in association with secondary hornblende, pyroxene and epidote. Anhedral and often polycrystalline rutiles reach sizes of up to 2 cm.

Sample **SH-C58** has been collected at outcrop SH-C. Along a river bend, two vein-bearing eclogite bodies of decimeters to meters in size are exposed in direct contact with the surrounding gneiss. The sampled, coarse-grained 2nd generation vein approximately contains quartz (45%) + kyanite (25%) + zoisite (15%) + phengite (15%) ± anthophyllite ± rutile ± zircon ± apatite. The eclogite in contact to the vein is characterized by a gradual increase of amphibole, as well as increasing retrograde decomposition of strongly relictic garnet and omphacite.

Euhedral to subhedral lath-shaped kyanite with lengths up to 2 cm occurs intergrown with subhedral zoisite and quartz, and shows slight resorptive rims. While fluid inclusions are remarkably abundant in quartz, kyanite provides rare tubular inclusions with daughter minerals. Anthophyllitic amphibole is a minor, secondary component, often related to slightly sheared grain boundaries. Subhedral to anhedral rutile reaches sizes of up to 2 cm. Along with phengite, rutile is predominantly observed along the vein margin and in the transitional, strongly amphibolitized (barroisite) eclogite.

The second eclogite body encloses an irregular, coarse-grained quartz + phengite + kyanite + zoisite $\pm$ rutile 2nd generation vein that was not sampled. The vein does not propagate into the gneissic country rock (**Figure 3.5f**), indicating both a tectonic mingling of eclogite into the gneiss and a predating, eclogite-related HP vein formation in a virtually closed system and in the stability field of phengite and kyanite.

3.3.2   Zhujiachong (samples: ZJC-02, -03, -04, -05, -06, -07, -08, -09, -10, -11, -12, -13)

Sampling of veins at ZJC was carried out in-situ in the form of drill cores. Samples **ZJC-02** to **-08** represent 3rd generation vein including strongly retrogressed eclogite in contact to the vein, whereas **ZJC-09** to **-13** represent a 2nd generation vein. A swarm of 1st generation veins was not sampled due inaccessibility in the outcrop.

The 1st generation, planar quartz-rutile veins with <5 cm widths and maximum lengths of about 100 cm occur strictly parallel to the eclogitic foliation (**Figure 3.6a**). Macroscopically visible hydration of the epidote- and phengite-lacking host eclogite along the margins to the veins is characteristically absent. This textural context suggests that they are related to eclogitization. Sampling was not possible due to inaccessibility in the outcrop.

The medium- to coarse-grained, heterogeneous 2nd generation vein approximately contains quartz (50%) + zoisite (15%) + kyanite (5%) + phengite (20%) + paragonite (5%) + barroisite (5%) $\pm$ anthophyllite/ cummingtonite $\pm$ apatite $\pm$ rutile $\pm$ zircon. It shows widths up to 10 cm and is exposed over a length of about 1.5 m, crosscutting the eclogitic foliation (**Figure 3.6b**). Vein mineralogy

attests a formation at HP conditions, while it obviously precipitated later than the texturally concordant 1st generation quartz-rutile veins. The contact to the host is at high angles to the foliation of the eclogite and shows irregular and undulating vein margins. The eclogite in direct contact (up to 10 cm) to the vein shows retrogression in the form of amphibolitization and phengitization, and the extent of retrograde recrystallization is distinctly higher than in the retrogressed eclogite bulk sample (ZJC-16). The vein exhibits a distinct zoning in some sections, with phengite accumulated at the eclogite contact, palisade-like oriented zoisite and barroisite towards the vein margins and predominantly quartz in the vein center (**Figure 3.6c,d**).
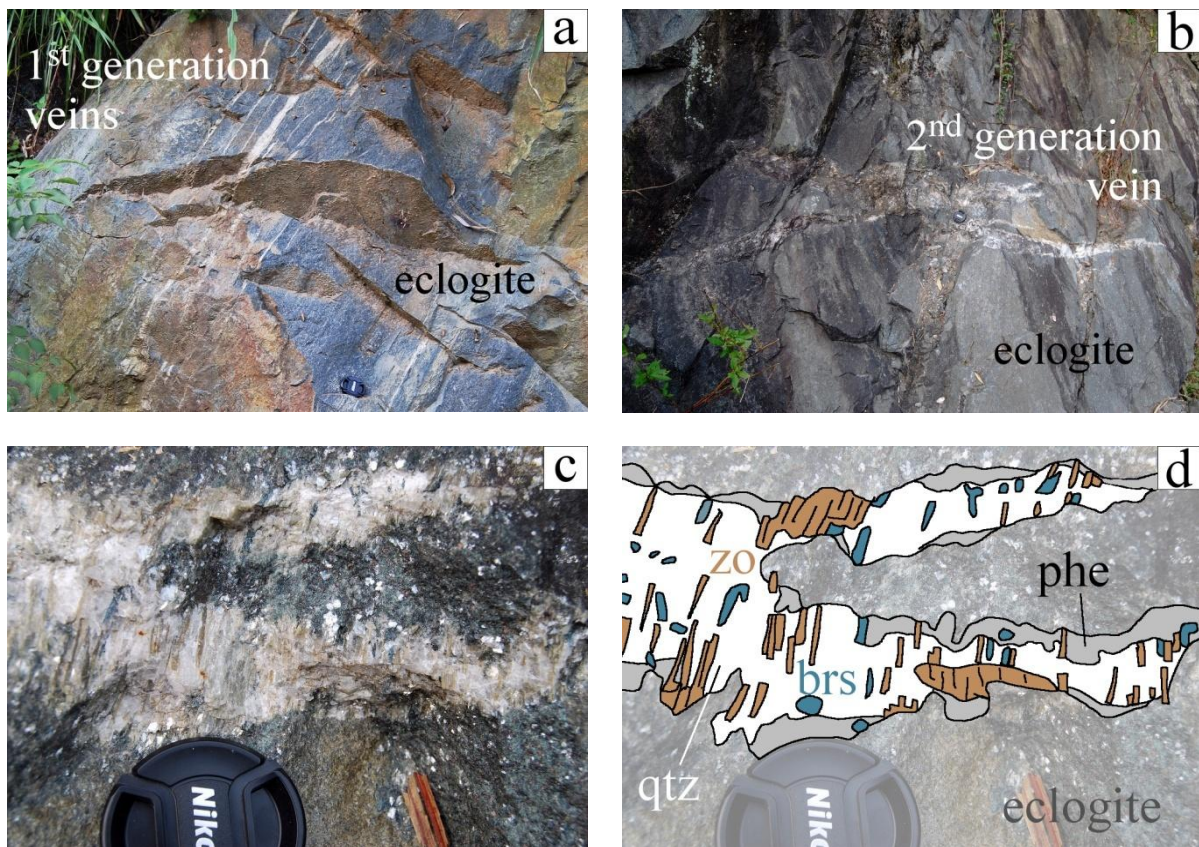
↑ **Figure 3.6 a** A swarm of planar 1st generation qtz + rutile veins at ZJC parallel to the eclogitic foliation. In contrast to the sampled eclogite (ZJC-16), the eclogite in contact to the 1st generation veins does not contain epidote and phengite. **b** 2nd generation phe + pg + zo + brs + qtz vein at ZJC that crosscuts the eclogitic foliation **c** Close-up of the 2nd generation vein, displaying an internal zoning with mainly quartz in the vein center, tabular barroisite (blue) and zoisite (brown) towards the rim and phengite (grey) predominantly at the vein-eclogite contact. The eclogite in direct vein contact is strongly phengitized **d** Sketch of c, highlighting the internal vein zoning.

Quartz occurs in monomineralic, equigranular associations with grain sizes of about 5 mm, interlobate grain boundaries and often undulating extinction. Next to abundant secondary fluid inclusions with sizes <20 μm, it is devoid of mineral inclusions. Euhedral to subhedral, tabular zoisite is often intergrown with phengite. Subhedral barroisite and kyanite have sizes up to 15 mm and they mainly occur in zoisite-rich sections of the vein. Phengites occur as subhedral and often aggregated crystals that are intergrown with zoisite. Paragonite is always accumulated in monomineralic, fine-grained and undirected aggregates.

The eclogitic host rock is strongly retrogressed at the contact to the vein, with tiny corroded garnets and relictic phengite as well as rutile being the only minerals which are in parts preserved in a superfine-grained matrix of mainly plagioclase and amphibole.

The coarse-grained, 0.6 m thick 3rd generation vein irregularly crosscuts the eclogitic foliation with macroscopically sharp contacts towards the eclogite. The former eclogite is strongly retrogressed to amphibolite for about 50 cm towards the vein margins. This is reflected by an almost entire replacement of the eclogitic assemblage with amphibole and plagioclase. This transitional zone contains porphyroblastic epidote/clinozoisite and is gradually pervaded by plagioclase-rich layers (**Figure 3.7a**). The vein approximately contains ab-rich plagioclase (80%) + hornblende (5%) + quartz (5%) + chlorite (5%) + phengite (3%) + calcite (2%) ± apatite ± rutile ± zircon ± pyrite.
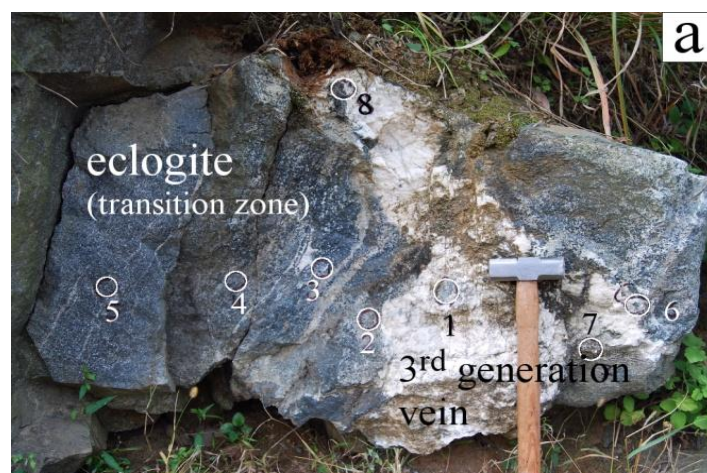
↑ **Figure 3.7 a** Outcrop of the 3rd generation ab + qtz + ep/czo + hbl + chl + cal + phe vein at ZJC. The transition zone is characterized by gradually retrogressed eclogite. Drill core sample location are labeled with circels.
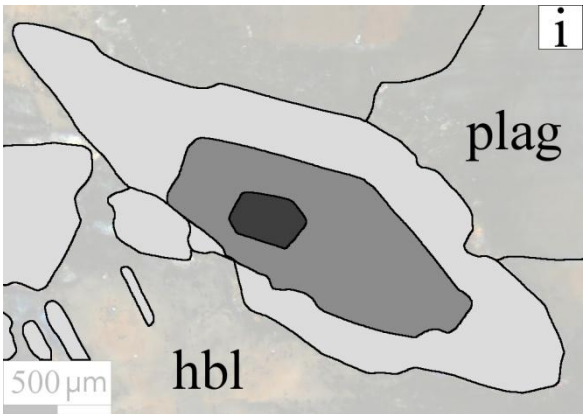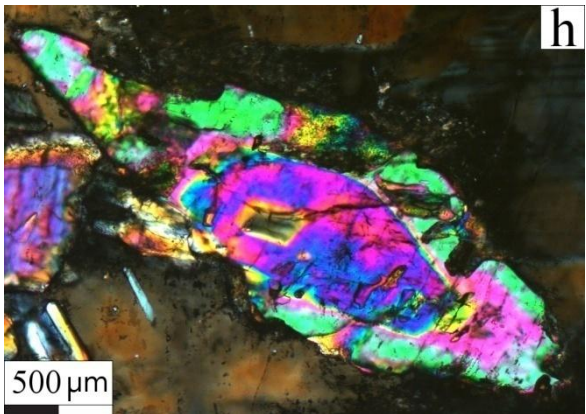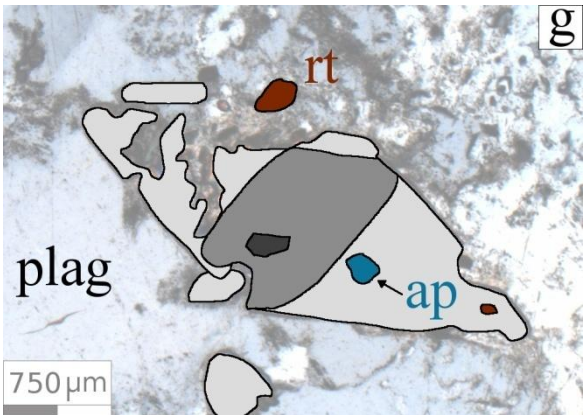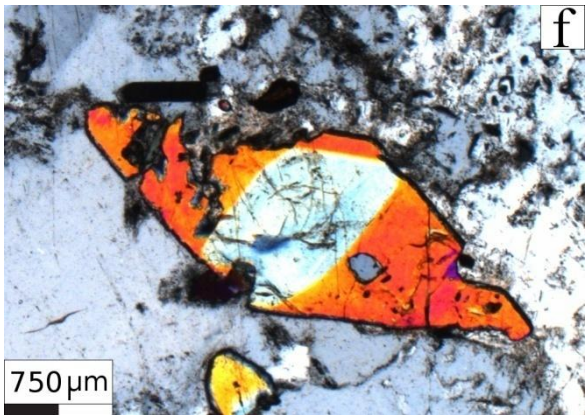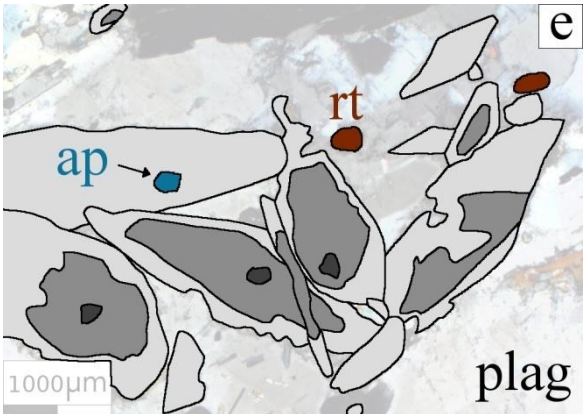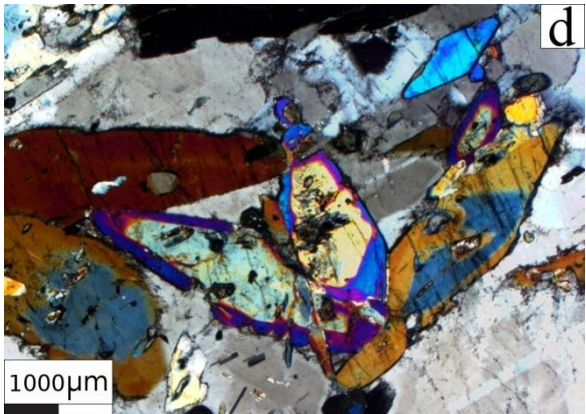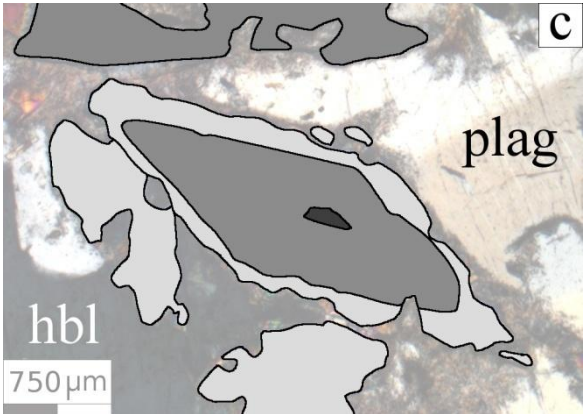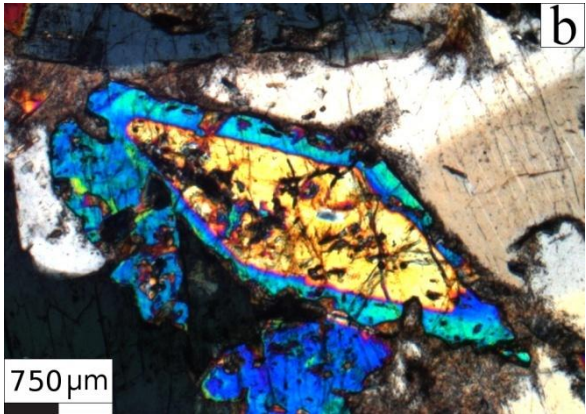
↑ Figure 3.7 (previous page) b – i Epidote/clinozoisite from the eclogite transition zone adjacent to the 3rd generation vein form ZJC (left: XPL, right: sketches) that display the zoning patterns in grayscale colouring: dark grey: cores, medium grey: mantles, light grey: rims or late idioblasts. They are overgrown by plagioclase and hornblende and show distinct resorption. The zoning patterns consistently reflect three growth stages, whereas the core is often not preserved due to resorptive alteration. Note that the thin section thickness in (h) is greater (>60 μm) than for the other pictures (40-50 μm).

The transitional zone is characterized by corroded garnet and omphacite relics (1%), porphyroblastic epidote/clinozoisite (15%), chlorite (3%), quartz (5%), poiciloblastic hornblende (10-40%), plagioclase (10-40%) and phengite (2%).

Albite-rich plagioclase occurs with pronounced saussuritization and often exhibits distinct bending. It is in textural equilibrium with deformed (ie. cracked) hornblende and both minerals texturally overgrow epidote/clinozoisite, phengite and quartz. Euhedral to subhedral epidote/clinozoisite with distinct resorption features exclusively occur in the transitional zone, rather than in the vein itself. They occur in two modes: (i) as subhedral to anhedral, tabular poiciloblasts with sizes up to 5 mm and homogeneous clinozoisite-rich compositions (comparably low, mainly anomalous blue interferences), or (ii) as euhedral to subhedral rhombic often aggregated crystals that show two- and three-stage zoning with consistently higher interferences towards the crystal rim (**Figure 3.7b-i**). Epidote group minerals often contain phengite inclusions and vice versa.

Chlorite and calcite occur as fine-grained aggregates in micro-cavities. Rutile and apatite appear both as inclusions in epidote and amphibole and in the matrix. Fluid inclusions were identified in quartz.

Table 3.1 Sample overview on rock type, mineralogy and occurrence of fluid inclusions (FI). Modified sample names were used in this thesis and original field sample designations are given in (brackets). Mineral abbreviations after WHITNEY AND EVANS (2010). † LI ET AL. (2004), * indicates pseudomorphed quartz after coesite observed in omphacite and garnet.

Location	Sample	Initial field name	Type	Lithology	Mineral assemblage [vol%]	Accessories	FI
Zhujiachong	**ZJC-16**	(DBS-10-16)	bulk	retrogressed (U†)HP eclogite	grt [25] + omp [13] + zo [10] + ep/czo [2] + brs [5] + phe [5] + qtz [5] + pg [5] + matrix [30]	ap + rt + zrn +hbl	-
	ZJC-06 – -08	(DBS-10-06 – -08)	drill core	3rd generation vein	ab [80] + qtz [5] + hbl [5] + chl [5] + phe [3] + cal [2]	rt + zrn + py + ap	qtz
	ZJC-09 – -13	(DBS-10-09 – -13)	drill core	2nd generation vein (type I)	qtz [50] + zo [15] + phe [13] + pg [12] + brs [5] + ky [5]	ap + rt + zrn + ath	qtz
	ZJC-02 – -05	(DBS-10-02 – -05)	drill core	retrogressed HP eclogite, profile towards 3rd gen. vein	ab [10–40] + hbl [10–40] + ep/czo [15] + qtz [5] + chl [3] + phe [2] + grt [1] + omp [1]	ap + rt + py	qtz
Shuanghe	**SH-A59**	(DBS-10-59B)	bulk	pristine UHP eclogite	grt [45] + omp [45] + qtz [8] + rt [1–2]	phe + zrn + coe*	qtz, grt
	SH-A60	(DBS-10-59A)	bulk	1st generation vein	qtz [98] + rt [1–2]	zrn	qtz
	SH-B56	(DBS-10-56)	bulk	retrogressed UHP eclogite	grt [35] + omp [35] + brs [15] + ep/czo [10] + phe [4] + ky [1]	rt+zrn+ap+py+coe*	-
	SH-C58	(DBS-10-58)	bulk	2nd generation vein (type I)	qtz [45] + ky [25] + zo [15] + phe [15]	ath + rt + ap + zrn	qtz
	SH-B55	(DBS-10-55)	bulk	2nd generation vein (type II)	brs [50] + ep/czo [30] + phe [5] + qtz [5] + ap [5] + omp [3] + rt [2]	zrn + py	qtz
	SH-B44	(DBS-10-44)	bulk	2nd generation vein (type II)	brs [50] + ep/czo [30] + phe [5] + qtz [5] + ap [5] + omp [3] + rt [2]	zrn + py	qtz
Bixiling	**BX-07**	(DS-09-07)	bulk	pristine UHP eclogite	grt [50] + omp [45] + qtz [3] + phe [1] + zo [1]	rt + py + zrn + coe*	-
	DS08A/ -B	(DS-09-08A, -B)	bulk	A: eclogite, B: amphibolite	no thin sections available	-	-
Huwan	**HW-42**	(DBS-10-42)	bulk	altered HP eclogite	grt [25] + omp [10] + phe [3] + zo [2] + matrix [60]	rt + py	-

3.4   Petrographic implications

3.4.1   Nature of eclogites and their protoliths

The sample set represents UHP/HP eclogites with different extents of retrograde overprint, and enclosed veins that formed at different metamorphic stages.

The degree of eclogite retrogression is assessed by the occurrence of retrograde minerals that do not belong to the initial eclogite assemblage, and by the extent of symplectic reactions between garnet and omphacite with amphibole or plagioclase. Eclogites from Bixiling (BX) and Shuanghe (SH-A) are the most pristine eclogite samples. They virtually lack retrograde features, except for thin symplectic amp + plag reaction rims after garnet and omphacite. The eclogite from SH-B and ZJC, in contrast, record an early retrograde stage that triggered the formation of barroisite and epidote/clinozoisite. The ZJC eclogite additionally preserves a later retrograde metamorphic stage, that is characterized by extensive decomposition of omphacite and garnet to fine-grained symplectic assemblages of hornblende + plagioclase. The latest preserved retrograde stage is represented by chlorite in the 3rd generation vein and the transition zone (**Figure 3.8**). Retrogression is likely to be facilitated at ZJC by higher tectonic stresses compared to BX and SH-A, as indicated by a deformed retrograde matrix structure, bent plagioclases and undulating quartz textures.

The occurrence of 2nd and 3rd generation polymineralic veins is restricted to eclogites that (i) contain epidote/clinozoisite, phengite (or possibly other hydrous phases such as lawsonite or allanite) in their peak assemblage and (ii) experienced retrogressive overprint. The latter is, to different extents, likewise observed by all previous studies on retrograde UHP/HP metamorphic veins (eg. CHEN ET AL., 2012; FRANZ ET AL., 2001; GUO ET AL., 2015; SHENG ET AL., 2013). The occurrence of epidote inclusions in eclogitic minerals has not been described before, except for GUO ET AL. (2015).
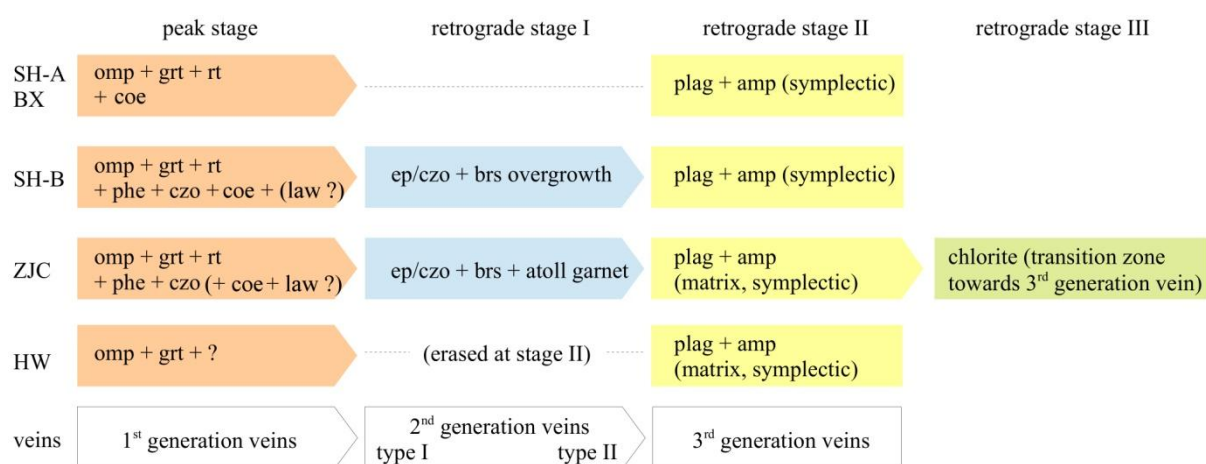
↑ **Figure 3.8** Schematic overview on the retrograde stages that are preserved in the eclogites from different localities and on the relative timing of vein formation (cf. **Chapter 3.4.2**). See **Chapter 3.4.3** for a description of type I and type II 2nd generation veins.

In this study epidote and phengite were identified as inclusions in garnet and omphacite of ZJC and SH-B/-C eclogites. These phases can be expected to appear in eclogite only if the subducted protolith provides sufficient amounts of water and Ca + Al + K, pointing to either the involvement of a sedimentary or granitic protolith source, or to a regional fluid flow during prograde stages. The latter would be in principal accordance with BEINLICH ET AL. (2010) and VITALE BROVARONE ET AL. (2014), who describe pervasive Ca-metasomatism and related formation of lawsonite in basaltic rocks during eclogitization of (oceanic) crust.

Pristine and largely undeformed eclogites are both devoid of polymineralic mineral veins and they virtually lack hydrous, Ca-Al-K-bearing minerals within their peak assemblage, except for minor (<<1%) phengite and zoisite. This reflects the fundamental requirement of a fluid phase for driving retrograde reactions. It is furthermore interpreted to demonstrate less felsic protolith compositions for BX and SH-A compared to ZJC and HW, what is in accordance with the presumed cumulate origin for the Bixiling eclogite (XIAO ET LA., 2000; ZHANG ET AL., 1995). Felsic protolith compositions, possibly introduced by felsic metasomatism, can thus be regarded as being a critical requirement regarding the formation of retrograde metamorphic veins.

3.4.2   Vein formation by aqueous fluids or hydrous melts?

All veins are argued to have been deposited by aqueous fluids rather than to represent segregated high-pressure hydrous partial melts, although distinction becomes increasingly difficult at higher temperatures near the top of the H_2O-silicate melt solvus and supercritical conditions. Melting is not excluded and may have occurred due to estimated P-T conditions of 2.3 GPa and 620°C (ZJC) as well as 3.1 GPa and 730°C (SH) (CARSWELL ET AL., 1997; OKAY ET AL., 1993, 1995; CARSWELL ET AL., 2000) near the water-saturated solidus of eclogite (SCHMIDT ET AL., 2004).

The interpretation of fluid-formed veins is firstly supported by petrographic arguments: (i) sharp contacts between veins and host eclogites would not be expected for solidified partial melts, (i) abundant hydrous phases in the veins (epidote, phengite, barroisite) as well as quartz remained in eclogites, the latter not being in accord with the hypothesis of their partial melting (RYABCHIKOV ET AL., 1996). In contrast to dehydration via fluids, the extraction of partial melts would have severely changed the bulk hostrock composition. Additionally, (i) abundant fluid inclusions are indeed observed in quartz while multiphase solid inclusions in UHP minerals that would be typical for partial melting (FERRANDO ET AL,. 2005; GAO ET AL., 2012), felsic magmatic veinlets and migmatic structures (e.g. garnet-enriched restites) are absent.

Secondly, the distinct zonation in the 2nd generation vein from ZJC (from phengite, zoisite and barroisite along the vein margin to solely quartz in the vein center) suggests a "fractional crystallization" from the percolating fluid with a high dissolved silica content. This is in agreement with decreasing trace element contents in epidote group minerals, indicating a changing fluid composition with time which corresponds to the compositional variation in the analyzed fluid inclusions. These additional observations corroborate the interpretation that these veins formed from hydrous fluids rather than from hydrous silicate melts.

3.4.3 P-T-t conditions during vein formation

The initial formation of 1st generation veins is texturally directly related to peak UHP conditions that were reached between 240–225 Ma in the Dabie area (cf. **Chapter 2**). This conclusion is based (i) on their occurrence strictly within the eclogitic foliation and (ii) on the textural evidence of the former existence of coesite for the 1st generation veins in Shuanghe (SH-A) and (iii) on the lack of retrogression at the contact between vein and host eclogite.

The formation of 2nd generation veins postdates the 1st generation based on petrographic and structural evidence. They crosscut the host eclogites foliation at high angles and they do not exhibit any indication for the former existence of coesite, suggesting a formation beyond UHP peak conditions. Their inventory of minerals comprises HP phases such as phengite, paragonite, omphacite and kyanite. While UHP indicators are absent, the HP minerals are evident tracers for high pressure conditions.

The minimum stabilizing pressure for the formation of kyanite is at 0.8 GPa at a temperatures of 700°C (HOLDAWAY, 1971). Jadeite-rich omphacite will form only above 1.4 GPa at 750°C (ESSENE AND FYFE, 1967; CARSWELL, 1990). The pressure conditions required for the formation of paragonite at 700°C are >1.8 GPa (POLI AND FUMAGALLI, 2003 and references therein). MASSONNE AND SCHREYER (1987) derived minimum formation pressures of 1.5 GPa for high-silica phengites coexisting with garnet, kyanite and quartz, whereas HERMANN (1997), MASSONNE AND SCHREYER (1989) and VELDE (1967) experimentally derived formation pressures of 3.0 GPa at 700°C for phengites with $Si_{3.4}$ [pfu] in the KCMASH system.

Given the above mentioned pressures as a lower pressure limit, the upper pressure limit of vein formation is assessed by the earliest availability of a free fluid phase after the UHP peak. According to GUO ET AL. (2013B, 2015), LI ET AL. (2004) and LI ET AL. (2005), the observed vein assemblages of kyanite, epidote/zoisite and quartz are interpreted to reflect the reaction products of the decompressional breakdown of lawsonite. Since lawsonite $[CaAl_2Si_2O_7(OH)_2 \cdot H_2O]$ contains about 11.5 wt% H_2O in its crystal structure (SCHMIDT AND POLI, 1998), it is the major storage of water at UHP conditions. Phase equilibrium modeling for the Dabie area revealed that lawsonite decomposed

at 2.7–3.0 GPa and 660–720 °C in the Zhujiachong area (GUO ET AL., 2015) and hence close to or at UHP conditions.

In conclusoin, the lower pressure limit for the formation of the 2nd generation veins is the minimum stability of phengite at 1.5 GPa (which can be expected to be distinctly higher for high silica contents in phengite) as well as paragonite at 1.8 GPa, whereas the upper limit given by the water-providing breakdown of lawsonite at ~2.7 GPa. These retrograde conditions were passed at about 225 Ma in Dabie Shan (**Figure 2.2**) at the onset of exhumation, ie. 17 Ma after the incipient peak UHP metamorphism (LIU ET AL., 2004, 2006; WAN ET AL., 2005; YANG ET AL., 2003) and correspond to the early HP stage at eclogite- to amphibole-eclogite facies.

The estimated time of formation of the 3rd generation vein is addressed by its mineral inventory. The main assemblage of (ab-rich) plagioclase + hornblende is typical for veins that evolve at the amphibolite stage along the retrograde metamorphic path, as described by BARNICOAT AND FRY (1986) and (COOMBS ET AL., 1975). For Dabie UHP rocks the amphibolite facies field was entered between 215–205 Ma (**Figure 2.2**), attesting the 3rd generation vein the youngest age of all investigated veins in this study. CONG ET AL. (1995) and LI ET AL. (2000) estimated a still younger timeframe of 190–170 Ma for the amphibolite facies retrogression of Shuanghe eclogites.

The latest alteration of the vein is recorded by textural secondary chlorite and calcite crystallization and extensive saussuritization in plagioclase. These minerals form at the expense of garnet and hornblende as a result of rehydration at lower greenschist facies conditions. The most common product of greenschist facies rehydration reactions in continental rocks is chlorite (BENNETT AND BARKER, 1992).

3.4.4   Origin and compositional characteristics of the vein-forming fluids

The 1st generation rutile-bearing quartz veins are interpreted to have initially evolved from a high-density fluid with melt-like qualities during the UHP peak. Structural evidence demonstrates that these veins have previously been coesite, proving UHP formation. The accumulation of incompatible

elements in the form of abundant rutile in these veins demands a liquid with extreme element solubilities. According to RYABCHIKOV ET AL. (1996), experimental hydrous melts at UHP conditions in equilibrium with garnet, omphacite and quartz are silica-rich with >70% SiO_2 and >20% H_2O. At UHP conditions, silicate–water systems are beyond the second critical endpoint to become completely miscible (eg. KESSEL, 2005). Water is possibly provided by remnants of prograde dehydration fluids, quartz is available due to the prograde reaction 'albite $\rightarrow$ jadeite + quartz'.

The observed primary fluid inclusions in quartz do not necessarily trap the fluid that precipitated the coesite veins, but rather traces a fluid phase that existed during the coesite $\rightarrow$ quartz transformation. The nature of such fluid is speculative. It may either be inherited from a prograde fluid that was once trapped in coesite and re-trapped during the coesite $\rightarrow$ quartz transformation later on. This fluid should than basically correspond to the primary fluid inclusions trapped in garnet of the eclogite host to these veins. Or it may represent a retrograde, lawsonite-breakdown related fluid that existed during coesite $\rightarrow$ quartz transformation. This is conceivable because lawsonite breakdown in Shuanghe and Zhujiachong expectedly occurred prior to the coesite $\rightarrow$ quartz transformation (**Figure 3.9**). In any case, primary fluid inclusions in 1st generation veins correspond to the earliest fluids trapped in all investigated veins.
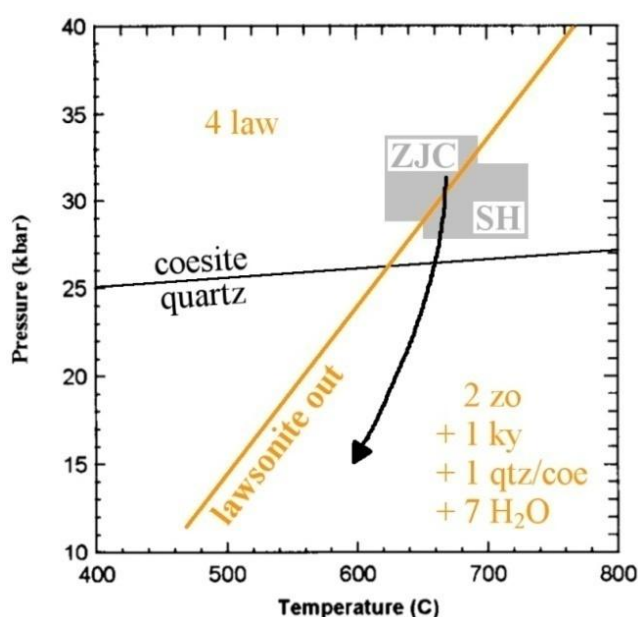
$\leftarrow$ **Figure 3.9** Lawsonite breakdown is expected to have occurred prior to the coesite-quartz transformation at SH and ZJC. Modified after SCHMIDT AND POLI (1994). Coesite-quartz transition after BOHLEN AND BOETTCHER (1982). P–T fields for Shuanghe (SH) and Zhujiachong (ZJC) after CARSWELL ET AL. (1997) and LI ET AL. (2004).

The mineral inventory of the polymineralic 2nd and 3rd generation veins widely coincides with the minerals identified in their retrograded eclogite host rocks, and according to eg. ZHANG ET AL. (2008) such vein-forming fluids were most probable locally derived, at least at the outcrop scale of several tens of meters. The vein within the eclogite lens at SH-B that does not propagate into the surrounding gneiss, supporting the concept of an essentially closed system.

Decompressional dehydration of hydrous phases is assumed to be the major source of aqueous fluids that (i) trigger pervasive retrogression at the outcrop scale of several tens of meters, and (ii) supply channelized HP, 2nd generation vein-forming fluids. These channelized fluids flow over distances of at least several meters (eg. JOHN ET AL., 2008) along hydraulic fractures that open as a result of enhanced fluid pressure in a dehydrating host rock (YARDLEY, 1983), and volume shrinkage of the host eclogite due to its dehydration (GUO ET AL., 2013A). Apart from that, potential partial melting in the felsic host gneiss may induce a significant fluid flow during exhumation, and thus contribute to the retrogression and related vein formation in enclosed eclogite bodies (ZONG ET AL., 2010).

The initial composition of the 2nd generation vein-forming fluid is expected to depend on the decomposing mineral. UHP-stable lawsonite [$CaAl_2Si_2O_7(OH)_2 \cdot H_2O$] is the best candidate to provide a (Ca-Al-H_2O-rich) fluid that could account for the observed, hydrous and calcic vein assemblages. Primary and early pseudosecondary fluid inclusions in minerals of 2nd generation veins (and as mentioned above possibly also in 1st generation veins) have the potential to represent those fluids. This type of fluid is supposed to not only account for HP vein formation, but also for the pervasive and Ca-metasomatic eclogite retrogression that produces large amounts of calcic amphibole and Ca-Al-epidote/clinozoisite at Shuanghe (SH-56) and Zhujiachong (ZJC-16) near the contacts to the veins.

The observed mineral zoning in the ZJC 2nd generation vein likely reflects a crack-seal process, where zoisite, phengite and barroisite precipitated at the onset of fracturing, followed later on by quartz. Assuming a closed system on the outcrop scale, this could be explained by a changing fluid composition with time, or respectively a fractional crystallization process driven by vein mineral precipitation that depleted the fluid in its elemental load.

A changing fluid composition is also indicated by the observed compositional zoning in epidote group minerals from the 2nd generation veins at Shuanghe B (SH-B44, -55) and the retrogressed eclogite from Shuanghe (SH-B56) and the eclogite in contact to the 3rd generation vein from Zhujiachong (ZJC-02 to -05). The zoning consistently displays an apparently early, clinozoisite-dominated mineral generation (low Fe-contents result in lower birefringence) as well as an later, epidote-dominated generation (higher Fe-contents result in higher birefringence). Based on the existence or absence of these minerals in a vein, two different types of 2nd generation veins are established as a working hypothesis (cf. **Table 3.1**):

Type I contains qtz + zo + phe + ky and is interpreted to have formed as a direct consequence of the breakdown of lawsonite (SH-C58, ZJC-09 – -13). Type II, in contrast, contains predominantly brs + (zoned) ep/czo + phe + qtz and strikingly lacks zo + ky. It is interpreted to have precipitated from a retrograde fluid that virtually represents the remainder of the lawsonite breakdown reaction '4 law $\rightarrow$ 2 zo + 1 ky + 1 qtz + 7 H_2O', slightly after the precipitation of type I veins. Such a fluid would explain the pervasive retrogression and the formation of the zoned epidote/clinozoisite that is observed in type II veins (SH-B44, -55), in the retrogressed eclogites from Shuanghe (SH-B56) and in the retrogressed eclogite in contact to the 3rd generation vein from Zhujiachong (ZJC-02 – -05).

The textural equilibrium of barroisite with epidote-rich (late) epidote and the simultaneous disequilibrium of barroisite with omphacite, the clinozoisite-rich (early) epidote and quartz in type II veins (cf. **Chapter 3.3**) implies (i) a multistage vein crystallization and (ii) younger formation ages of type II veins compared to type I veins (cf. **Figure 3.8**).

With regard to the mineral assemblage of albite-rich plagioclase, magnesiohornblende and quartz, the composition of the expectedly Na-rich amphibolite-facies 3rd generation vein-forming fluid differs markedly from the early, Ca-rich HP fluid. The required sodium is reasonably provided by the retrograde destabilization of jadeite-rich omphacite and water is supplied by remnants of the early retrograde fluid that precipitated the 2nd generation veins. The occurrence of zoned epidote/clinozoisite in the eclogite adjacent to the 3rd generation vein (comparably also found in type II 2nd generation veins and in the retrograded Shuanghe eclogite) is interpreted as a remnant of former fluid activity,

suggesting that the 3rd generation vein replaced a vein of the 2nd generation type. The profound saussuritization and chloritization is limited to the vein and the adjacent eclogite transition, reflecting a late 'reactivation' of the vein at shallow, greenschist facies levels. Since mineral veins represent weak points in the rock structure, they are expected to be preferentially reactivated. It is conceivable that hydrothermal waters with meteoric origin are involved in such late retrograde reactions. Waters with a meteoric component are almost devoid of solute content at low pressures and can infiltrate the Earth's crust to depths down to 10–15 km by utilizing pre-existing thrust and fault zones as fluid pathways (BENNETT AND BARKER, 1992; FRICKE ET AL., 1992; MORRISON, 1994; UPTON ET AL., 1995).

3.5 Conclusions

(1) The occurrence of veins is restricted to retrograded eclogite bodies that have hydrous, Al- + Ca- + K-bearing minerals such as phengite and clinozoisite affiliated to their peak assemblage. This observation indicates a felsic component in the eclogitic precursor to be a requirement for vein formation. Such a felsic component is possibly derived from continental crust and introduced by fluid-assisted Ca-metasomatism.

(2) The three observed vein generations are interpreted to have formed during the UHP metamorphic peak and along the retrograde path. The 1st generation veins are texturally related to peak UHP conditions. The 2nd generation veins show evidence for a formation at the onset of exhumation. The 3rd generation vein formed during amphibolite facies conditions by reactivation and replacement of a former 2nd generation vein, and experienced a greenschist facies overprint later on.

(3) The occurrence of 1st generation veins is restricted to pristine, ±dry eclogites. The fluid that precipitated these veins is rich in silica and HFSE, and most likely originates from internal prograde dehydration reactions during eclogitization. Primary fluid inclusions trapped in these veins represent the fluid present during the coesite → quartz transformation, that does not necessarily represent the prograde fluid, but rather an early retrograde fluid.

(4) Lawsonite is by petrographic and mineralogical evidence the best candidate for releasing the Ca - Al - H_2O-rich post-peak fluid that accounts for the formation of 2nd generation veins. Primary and early pseudosecondary fluid inclusions entrapped in vein and retrograded eclogite minerals can be expected to correspond to this fluid.

(5) Two types of 2nd generation veins are classified: Type I is likely to be directly related to the breakdown of lawsonite following the reaction '4 law → 2 zo + 1 ky + 1 qtz + 7 H_2O', whereas type II formed from a fluid that represents the remainder of the lawsonite breakdown

reaction. The type II fluid experienced compositional alteration as reflected by multi-stage crystallization of epidote group minerals.

(6) The Na-dominated fluid that is the source for the 3rd generation vein is proposed to originate from the retrograde decomposition of omphacite during amphibolitization and inherits its aqueous component from the early retrograde fluids.

(7) The 3rd generation vein and the adjacent eclogite record three stages of retrograde overprint, including (i) an early HP stage that accounted for the formation of high-Si phengite and zoned epidote/clinozoisite and corresponds to the 2nd generation veins, (ii) an amphibolite facies stage that replaced most of the 2nd generation vein mineral assemblage with magnesiohorn-blende and plagioclase and (iii) a late greenschist facies stage where the vein was reactivated, as recorded by secondary chlorite, calcite and saussurite.

3.6 References

Barnicoat AC, Fry N (1986) High-pressure metamorphism of the Zermatt-Saas ophiolite zone, Switzerland. *J Geol Soc 143(4)*: 607–618.

Beinlich A, Klemd R, John T, Gao J (2010) Trace-element mobilization during Ca-metasomatism along a major fluid conduit: Eclogitization of blueschist as a consequence of fluid–rock interaction. *Geochim Cosmochim Ac 74(6)*: 1892–1922.

Bennett DG, Barker AJ (1992) High salinity fluids: the result of retrograde metamorphism in thrust zones. *Geochim Cosmochim Ac 56(1)*: 81–95.

Bose K, Ganguly J (1995) Quartz-coesite transition revisited: Reversed experimental determination at 500–1200 ℃ and retrieved thermochemical properties. *Am Mineral 80(3)*: 231–238.

Carswell DA (1990) Eclogites and the eclogite facies: definitions and classification. In: *Eclogite facies rocks*. Springer, Amsterdam: 1–13.

Carswell DA, O'Brien PJ, Wilson RN, Zhai M (1997) Thermobarometry of phengite-bearing eclogites in the Dabie Mountains of central China. *J Metamorph Geol 15(2)*: 239–252.

Carswell DA, Wilson RN, Zhai M (2000) Metamorphic evolution, mineral chemistry and thermobarometry of schists and orthogneisses hosting ultra-high pressure eclogites in the Dabieshan of central China. *Lithos 52*: 121–155.

Chen RX, Zheng YF, Hu Z (2012) Episodic fluid action during exhumation of deeply subducted continental crust: geochemical constraints from zoisite–quartz vein and host metabasite in the Dabie orogen. *Lithos 155*: 146–166.

Cong BL, Zhai MG, Carswell DA, Wilson RN, Wang QC, Zhao ZY, Windley BF (1995) Petrogenesis of ultrahigh-pressure rocks and their country rocks at Shuanghe in the Dabie Mountains, Central China. *Eur J Mineral 7*: 119–138.

Coombs DS, Nakamura Y, Vuagnat M (1976) Pumpellyite-actinolite facies schists of the Taveyanne Formation near Loèche, Valais, Switzerland. *J Petrol 17(4)*: 440–471.

Essene EJ, Fyfe WS (1967) Omphacite in Californian metamorphic rocks. *Contrib Mineral Petrol 15(1)*: 1–23.

Ferrando S, Frezzotti ML, Dallai L, Compgnoni R (2005) Multiphase solid inclusions in UHP rocks (Su-Lu, China): Remnants of supercritical silicate-rich aqueous fluids released during continental subduction. *Chem Geol 223*: 68–81.

Franz L, Romer RL, Klemd R, Schmid R, Oberhansli R, Wagner T, Shuwen D (2001) Eclogite-facies quartz veins within metabasites of the Dabie Shan (eastern China): pressure-temperature-time-deformation path, composition of the fluid phase and fluid flow during exhumation of high-pressure rocks. *Contrib Mineral Petrol 141(3)*: 322–346.

Fricke HC, Wickham SM, O'Neil JR (1992) Oxygen and hydrogen isotope evidence for meteoric water infiltration during mylonitization and uplift in the Ruby Mountains-East Humboldt Range core complex, Nevada. *Contrib Mineral Petr 111(2)*: 203–221.

Gao XY, Zheng YF, Chen YX (2012) Dehydration melting of ultrahigh-pressure eclogite in the Dabie orogen: evidence from multiphase solid inclusions in garnet. *J Metamorph Geol 31*: 193–212.

Guo S, Ye K, Chen Y, Liu JB, Mao Q, Ma YG (2012) Fluid-rock interaction and element mobilization in UHP metabasalt: Constraints from an omphacite-epidote vein and host eclogites in the Dabie orogen. *Lithos 136*: 145–167.

Guo S, Ye K, Chen Y, Yang Y, Liu J (2013a) Lawsonite Breakdown in the Dabie UHP Eclogite: Constrains on the Fluid Actions and Trace Element Mobilization in Deep Subduction Zone. *Ac Geol Sinica 87*: 462–464.

Guo S, Ye K, Wu TF, Chen Y, Yang YH, Zhang LM, Liu JB, Mao Q, Ma YG (2013b) A potential method to confirm the previous existence of lawsonite in eclogite: the mass imbalance of Sr and LREEs in multistage epidote(Ganghe, Dabie UHP terrane). *J Metamorph Geol 31*: 415–435.

Guo S, Chen Y, Ye K, Su B, Yang Y, Zhang L, Liu JB, Mao Q (2015) Formation of multiple high-pressure veins in ultrahigh-pressure eclogite (Hualiangting, Dabie terrane, China): Fluid source, element transfer, and closed-system metamorphic veining. Chem Geol 417: 238–260.

Hermann J (1997) Experimental constraints on phase relations in subducted continental crust. *Contrib Mineral Petrol 143(2)*: 219–235.

Holdaway MJ (1971) Stability of andalusite and the aluminum silicate phase diagram. *Am J Sci 271(2)*: 97–131.

John T, Klemd R, Gao J, Garbe-Schönberg CD (2008) Trace-element mobilization in slabs due to non steady-state fluid–rock interaction: constraints from an eclogite-facies transport vein in blueschist (Tianshan, China). *Lithos 103(1)*: 1–24.

Kessel R, Schmidt MW, Ulmer P, Pettke T (2005) Trace element signature of subduction-zone fluids, melts and supercritical liquids at 120–180 km depth. *Nature 437*: 724–727.

Li S, Jagoutz E, Chen Y, Li Q (2000) Sm–Nd and Rb–Sr isotopic chronology and cooling history of ultrahigh pressure metamorphic rocks and their country rocks at Shuanghe in the Dabie Mountains, Central China. *Geochim Cosmochim Ac 64(6)*: 1077–1093.

Li XP, Zheng YF, Wu YB, Chen F, Gong B, Li YL (2004) Low-T eclogite in the Dabie terrane of China: petrological and isotopic constraints on fluid activity and radiometric dating. *Contrib Mineral Petrol 148(4)*: 443–470.

Li XP, Li Y, Shu G (2005) Breakdown of lawsonite subsequent to peak UHP metamorphism in the Dabie terrane and its implication for fluid activity. *Chinese Sci Bull 50*: 1366–1372.

Liu F, Xu Z, Xue H (2004) Tracing the protolith, UHP metamorphism, and exhumation ages of orthogneiss from the SW Sulu terrane (eastern China): SHRIMP U–Pb dating of mineral inclusion-bearing zircons. *Lithos 78(4)*: 411–429.

Liu D, Jian P, Kröner A, Xu S (2006) Dating of prograde metamorphic events deciphered from episodic zircon growth in rocks of the Dabie–Sulu UHP complex, China. *Earth Planet Sci Lett 250(3)*: 650–666.

Massonne HJ, Schreyer W (1987) Phengite geobarometry based on the limiting assemblage with K-feldspar, phlogopite, and quartz.*Contrib Mineral Petrol 96(2)*: 212–224.

Massonne HJ, Schreyer W (1989) Stability field of the high-pressure assemblage talc+ phengite and two new phengite barometers. *Eur J Mineral 1(3)*: 391–410.

Morrison J (1994) Meteoric water-rock interaction in the lower plate of the Whipple Mountain metamorphic core complex, California. *J Metam Geol 12*: 827–840.

Okay AI (1993) Petrology of a diamond and coesite-bearing metamorphic terrain, Dabie Shan, China. *Eur J Mineral 5*: 659–675.

Okay AI (1995) Paragonite eclogites from Dabie Shan, China: re-equilibrations during exhumation. *J Metamorph Geol 13*: 449–460.

Poli S, Fumagalli P (2003) Mineral assemblages in ultrahigh pressure metamorphism: a review of experimentally determined phase diagrams. In: *EMU Notes in Mineralogy 5, Ultrahigh Pressure Metamorphism*: 307–340.

Ryabchikov ID, Miller C, Mirwald PW (1996) Composition of hydrous melts in equilibrium with quartz eclogites. *J Mineral Petrol 58(1)*: 101–110.

Schmidt MW, Poli S (1994) The stability of lawsonite and zoisite at high pressures: Experiments in CASH to 92 kbar and implications for the presence of hydrous phases in subducted lithosphere. *Earth Planet Sci Lett 124(1)*: 105–118.

Schmidt MW, Poli S (1998) Experimentally based water budgets for dehydrating slabs and consequences for arc magma generation. *Earth Planet Sci Lett 163*: 361–379.

Schmidt, M. W., Vielzeuf, D., & Auzanneau, E. (2004). Melting and dissolution of subducting crust at high pressures: the key role of white mica. Earth and Planetary Science Letters, 228(1), 65-84.

Sheng YM, Zheng YF, Li SN, Hu Z (2013) Element mobility during continental collision: insights from polymineralic metamorphic vein within UHP eclogite in the Dabie orogen. J *Metamorph Geol 31(2)*: 221–241.

Upton P, Koons PO, Cahmberlain CP (1995) Penetration of deformation-driven meteoric water into ductile rocks: isotopic and model observations from the Southern Alps, New Zealand. *New Zeal J Geol Geop 38*: 535–543.

Velde B (1967) Si^{+4} content of natural phengites. *Contrib Mineral Petrol 14(3)*: 250–258.

Vitale Brovarone A, Alard O, Beyssac O, Martin L, Picatto M (2014) Lawsonite metasomatism and trace element recycling in subduction zones. *J Metamorph Geol 32(5)*: 489–514.

Wan Y, Li R, Wilde SA, Liu D, Chen Z, Yan L, Song T, Yin X (2005) UHP metamorphism and exhumation of the Dabie Orogen, China: evidence from SHRIMP dating of zircon and monazite from a UHP granitic gneiss cobble from the Hefei Basin. *Geochim Cosmochim Ac 69(17)*: 4333–4348.

Whitney DL, Evans BW (2010) Abbreviations for names of rock-forming minerals. *Am Mineral 95(1)*: 185–187.

Xiao Y, Hoefs J, van den Kerkhof AM, Fiebig J, Zheng Y (2000) Fluid history of UHP metamorphism in Dabie Shan, China: a fluid inclusion and oxygen isotope study on the coesite-bearing eclogite from Bixiling. *Contrib Mineral Petrol 139(1)*: 1–16.

Yang, JS, Wooden JL, Wu CL, Liu FL, Xu ZQ, Shi RD, Katayama I, Liou JG, Maruyama S (2003) SHRIMP U–Pb dating of coesite-bearing zircon from the ultrahigh-pressure metamorphic rocks, Sulu terrane, east China. *J Metamorph Geol 21(6)*: 551–560.

Yardley BW (1983) Quartz veins and devolatilization during metamorphism. *J Geol Soc 140(4)*: 657–663.

Zhang RY, Liou JG, Cong BL (1995b) Talc-, magnesite-and Ti-clinohumite-bearing ultrahigh-pressure meta-mafic and ultramafic complex in the Dabie Mountains, China. *J Petrol 36(4)*: 1011–1037.

Zhang ZM, Shen K, Sun WD, Liu YS, Liou JG, Shi C, Wang JL (2008) Fluids in deeply subducted continental crust: petrology, mineral chemistry and fluid inclusion of UHP metamorphic veins from the Sulu orogen, eastern China. *Geochim Cosmochim Ac 72(13)*: 3200–3228.

Zong K, Liu Y, Hu Z, Kusky T, Wang D, Gao C, Wang J (2010) Melting-induced fluid flow during exhumation of gneisses of the Sulu ultrahigh-pressure terrane. *Lithos 120(3)*: 490–510.

4. Element budget of UHP/HP veins and eclogites

4.1 Introduction

Subduction zones are powerful factories of fluid-assisted element recycling and redistribution. Both melts and aqueous fluids that are produced during devolatilization reactions in the subducting slab and the overlying mantle wedge constitute critical agents of mass transport and can transfer their signatures to infiltrated rocks while leaving behind altered residues. Such devolatilization reactions are capable of producing large quantities of fluid at different stages in the metamorphic cycle (eg. BEBOUT ET AL., 1999; KERRICK AND CONNOLLY, 2001; PEACOCK, 1990, 1993, 2001; SCAMBELLURI AND PHILIPPOT, 2001; SCHMIDT AND POLI, 1998).

Aqueous fluids linked to deep burial and subsequent exhumation form and evolve under HP/UHP conditions and are characterized by enhanced element solubilities (KESSEL ET AL., 2005; NEWTON AND MANNING, 2004), resulting in both transport and fractionation of fluid-mobile and nominally immobile elements (BECKER ET AL., 1999, 2000; GAO ET AL., 2007; HUANG ET AL., 2012; JOHN ET AL., 2004; LIANG ET AL., 2009; SCAMBELLURI AND PHILIPPOT, 2001; XIAO ET AL., 2006).

Metamorphic mineral veins represent fossil vestiges of fluid flow and provide the most substantial access to HP/UHP fluid-rock interaction. Although a vein does obviously not reflect the full element budget to the underlying fluid (a major part of the fluid and its contained elements may migrate away, leaving only a "dry" extract of the initial fluid in their wake), this work attempts to address the evolution and potential implications of HP/UHP fluids for crust and mantle reservoirs related to the

subduction and eclogitisation of basaltic rocks. This is done by a complete and systematic characterization of the major and trace element inventory including compositional zoning of vein and host eclogite minerals, as well as isotopic data on Sr and Pb.

The dataset is utilized to (i) trace and distinguish different fluid pulses, and (ii) to modeling a bulk vein element budget in order to detect potential element fractionations in vein minerals with particular emphasis on mass-balancing HFSE (Nb/Ta, Zr/Hf) and element pairs that are critical for important isotopic systems (Rb/Sr and U/Pb).

The behavior of HFSE during deep subduction is of particular interest with regard to the enigmatic 'Nb-paradox', that evolves from the fact that all known reservoirs of the silicate Earth are subchondritic, while an ubiquitous "missing" high-Nb reservoir has not been identified yet (**Figure 4.1**). MÜNKER ET AL. (2003) propose a Nb-enrichment in the metallic Earth core, PFÄNDER ET AL. (2007) argue an accumulated Nb/Ta fractionation over the Earth's history and suspect a high Nb/Ta reservoir hidden in the deep mantle. A third theory, as proposed by RUDNICK ET AL. (2000), suggest that residual eclogites or amphibolites after the extraction of HP/UHP fluids or melts in the course of deep subduction of basalts may represent an essential high-Nb reservoir. This hypothesis will be tested in the present study. MÜNKER ET AL. (2004) additionally found that HFSE can be enriched in the mantle by aqueous subduction zone fluids, and that subduction zone melting is an unlikely candidate to fractionating Nb from Ta.

Since rutile has been repeatedly found to fractionate Nb from Ta towards superchondritic ratios in metamorphic HP/UHP veins (eg. HUANG ET AL., 2012; XIAO ET AL., 2006), this mineral may hold major clues to the mobility and capacity of fractionating HFSE by HP/UHP subduction zone fluids, and other critical element pairs as mentioned above may be fractionated by different vein minerals as well.

Isotopic data on Sr and Pb are of particular interest in evaluating HP/UHP eclogites and related fluid-rock interaction with regard to the global, so-called 'lead paradox'. It arises from the fact that Pb isotope ratios in most MORB and OIB are variable and more radiogenic than in the undifferentiated

mantle or bulk silicate Earth. According to ALLÈGRE (1969) this is not to be expected from the higher

incompatibility of uranium compared to lead in the depleted mantle.
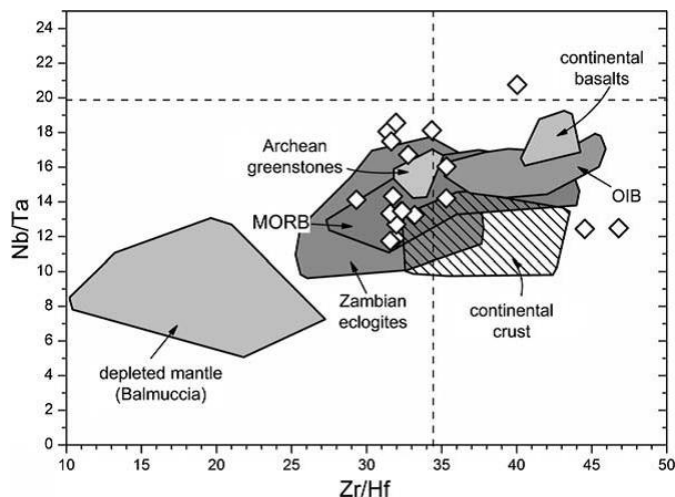

↑ **Figure 4.1** Plot of Nb/Ta vs. Zr/Hf for major terrestrial reservoirs (modified after SCHMIDT ET AL., 2009), illustrating the Nb deficit in the silicate Earth. Open diamonds are bulk eclogite analyses from SCHMIDT ET AL. (2009) on pristine samples.

STRACKE ET AL. (2005) postulated that none of the possible oceanic basalt lithologies (MORB, oceanic gabbros, altered oceanic basalt) can explain the Th/Pb characteristics of a required HIMU (high-μ = high-^{238}U/^{204}Pb = high radiogenic lead) source (**Figure 4.2**). Since Th/Pb calculated from HIMU isotopic signatures at 2 Ga and observed Th/Pb in HIMU basalts are different, the recent signature cannot be explained by subduction and recycling of oceanic crust, and a source is still unclear. Explanatory approaches comprise late transport of lead into the core (VOLLMER, 1977; VIDAL AND DOSSO, 1978; ALLÈGRE ET AL., 1980; VIDAL ET AL., 1984), an age of the mantle that is significantly younger than the ages of meteorites (ZARTMAN AND HAINES, 1988), hydrothermal transfer of lead from mantle to continental crust (PEUCKER-EHRENBRINK ET AL., 1994; CHAUVEL ET AL., 1995; HOFMANN, 1997), and uranium uptake by subducted oceanic crust (HOFMANN AND WHITE, 1980; ELLIOTT ET AL., 1999).

Element fractionation during deep subduction of continental crust is basically unknown, and thus chemical characteristics of residual eclogites, the precise trace element signature of related HP veins,

and a deeper understanding of fluid-rock interaction during deep continental subduction might hold clues on identifying potential contributors and processes to a HIMU source.
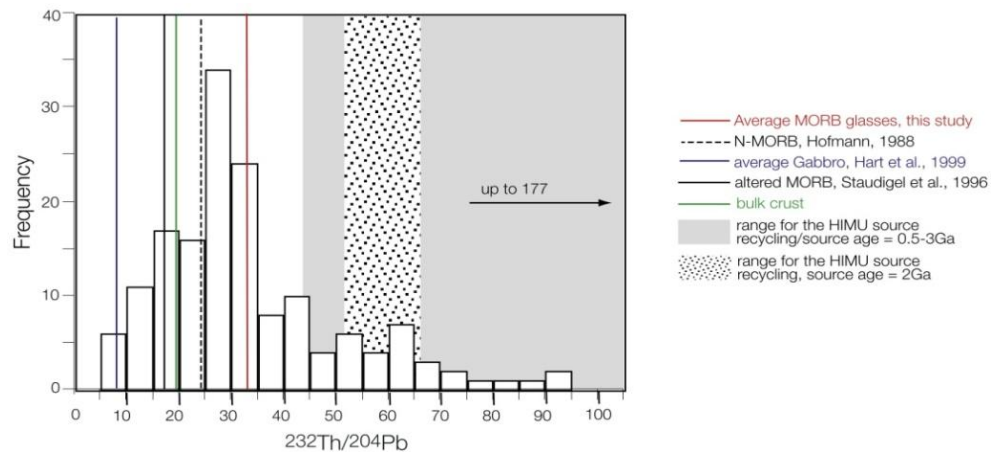
↑ Figure 4.2 Histogram of variation and frequency of ^{232}Th/^{204}Pb ratios in present-day MORB glasses compared to the range of ^{232}Th/^{204}Pb ratios calculated for the HIMU source (gray field), illustrating that none of the reservoirs of subducted oceanic crust have the Th/Pb ratios required to explain the ^{208}Pb/^{204}Pb enrichment in HIMU ocean island basalts. Taken from STRACKE ET AL. (2005).

4.2   Data aquisition

4.2.1   X-ray fluorescence spectrometry (XRF)

A sequential *PANalytical AXIOS-Advanced* spectrometer with a rhodium target X-ray tube has been used to determine the major and minor element abundances in eclogite bulk rock samples at the Geosciences Center Göttingen. A wavelength-dispersive standard routine containing 34 major, minor and trace elements was set up. Peak overlap interferences have been avoided by the use of suitable diffraction crystals, line overlap interferences have been corrected by the *PANalytical* software package *SuperQ 4*.

The analytical precision for major elements is better than 2%. For minor elements 1σ standard deviations are in the range of 2 to 5 % at concentration levels of 30 to 10 ppm. Detection limits vary between 5 to 0.1 ppm for the measured elements.

4.2.2   Electron microprobe (EMP)

Major element compositions of eclogite and vein minerals were determined at the Geosciences Center Göttingen, using a *Jeol JXA-8900RL* electron microprobe equipped with a LaB_6 cathode. Measurements were performed at 15 kV (20 kV for BSE imaging) acceleration voltage and 15 nA beam current on polished, carbon-coated thin sections. Probe diameter was defocused to 5–20 µm depending on sample surface properties. A measurement routine for 11 elements (Si, Al, Fe, K, Na, Mg, Ca, Ti, Cr, Ni, Mn) with peak dwell times of 15 s (30 s for Cr, Mn and Ni) and background detection times of 5 s (15 s for Cr, Mn and Ni) was set up for the majority of all analyses. For measurements of Sr- and REE-rich epidote group minerals this routine has been modified towards 14 elements (Si, Ti, Al, Fe, Mn, Mg, Ca, Na, Sr, Cl, La, Ce, Pr, Nd).

Standards comprised natural silicates as well as synthetic oxides and glasses (Si, Mg: olivine, Na: albite, K: sanidine, Ti: TiO_2, Fe: hematite, Al: anorthite, Ca: wollastonite, Cr: Cr_2O_3, Mn: rhodonite, Ni: NiO). A natural garnet standard originating from a garnet-pyroxenite from Kakanui, New Zealand,

has been used to recalculate Si and Al contents in garnet analyses, because the utilization of anorthite and olivine standards resulted in total sums exceeding 100 %. The PRZ correction procedure (ARMSTRONG, 1995) was used to diminish matrix effects.

The major constituents Si, Al and Ca yield 1σ standard deviations between 0.27 and 0.37 %, REE concentrations in the range of 1 wt.-% have deviations between 3 and 5%. The accuracy is usually better than 0.5 % for major elements and better than 1.0 % for Sr, Cl and REEs. Detection limits are usually between 150 and 350 ppm.

4.2.3   Laser ablation inductively coupled plasma mass spectrometry (LA-ICPMS)

Trace element compositions comprising a total of 32 elements (35 for apatite) were obtained for eclogite and vein minerals at the Geosciences Center Göttingen, using a *Perkin Elmer Sciex Elan DRC2* ICPMS. The instrument is coupled to a *Lambda Physics Compex 110 ArF-Excimer Laser* ablation device (λ = 193 nm) that includes a low volume sample chamber and an optical imaging system. Ar is used as carrier gas. Analyses of vein and eclogite minerals were performed in-situ on 40–50 µm thin sections, following the routine described by SIMON ET AL. (1997). Except for traverses, all analyses were performed on former EMP spots, using an in-house developed software that enables the transfer of spatial coordinates of the EMP stage locations to the stage of the LA-ICPMS. Trace element analyses of bulk eclogites were performed via solution ICPMS as well as via LA-ICPMS on glassy beads prepared after PACK ET AL. (2010).

Prior to and after every ablation spot measurement, the background has been recorded for 20 s. The laser spot diameter has been set to 120 µm (60 µm for zircon) to maximize the volume of ablated material at a laser energy of ~3 J/cm² and a laser pulse repetition rate of 8 Hz. Dwell times were set to 10 ms and raised to 50 or 100 ms for low intensity elements. Si concentrations obtained from EMP measurements at each the same spots were used as internal standard and all data were calibrated against the external standard NIST610 (PEARCE ET AL. 1997), which has been analysed repeatedly after every 5–6 sample measurements.

Due to the limited thickness of the thin sections and depending on the specific ablation resistance of the analyzed mineral, signal recording times were restricted to 25–60 s, occasionally resulting in poor counting statistics. 2σ standard errors[1] are generally <5 % and <10 % for concentrations >10 ppm and around 1 ppm, respectively. Analyses with errors beyond 30 % correspond to absolute concentrations <<1 ppm, and are regarded as below detection limit. The accuracy for all elements is better than 5 % relative to the NIST610. Analytical precision of solution ICPMS is generally better than 10% in the range of 1-100 ppm, and below 5% at higher concentrations.

Raw data were reduced using the software *IGOR Pro by Wavemetrics* and the LA-ICPMS specific evaluation package *Iolite* (HELLSTROM ET AL., 2008). It monitors time-dependent signal plateaus, allowing a visually controlled selection of the respective background, sample and standard sections.

4.2.4   Thermal Ionization Mass Spectrometry (TIMS)

$^{87}Sr/^{86}Sr$ and $^{208}Pb/^{206}Pb$ isotopic compositions of bulk eclogite samples and of selected mineral separates were acquired using a *Thermo-Finnigan Triton* mass spectrometer at the Geosciences Center Göttingen, operated in static mode. Sample preparation of bulk powders and mineral separates included pressure digestion in HF-HNO_3 prior to element separation via standard ion chromatography. Chromatographic element separation was attained on the basis of HDEHP resin-filled columns that were rinsed with HCl, following a standard protocol for each element.

Data evaluation comprised recalculation after international standards (NBS-987 for Sr, NBS-981 for Pb) and a standard correction of respective element mass fractionations. Analytical errors were below 1%. The external reproducibility was 0.710247 ± 0.000007 for $^{87}Sr/^{86}Sr$ and 2.165880 ± 0.0012 for $^{208}Pb/^{206}Pb$.

---

[1] 2σ standard errors are internally calculated by the Iolite software to $\frac{2\sigma}{\sqrt{n}}$, with n = number of single measurements

4.3 Results

## 4.3.1 Bulk eclogite chemistry

Major element characteristics

Bulk eclogite compositions are basaltic and coincide with a global intraplate basalt reference (**Figure 4.3**). Zhujiachong eclogites are more felsic compared to rocks from Shuanghe, Bixiling and Huwan. The enrichment in quartz of the pristine Shuanghe eclogite (SH-A59) compared to the retrogressed sample (SH-B56) is conceivably ascribed to the heterogeneously distributed qtz-rich layers and 1st generation veins at SH-A. The variability in quartz contents at ZJC is explainable with regard to the small sample size of the drillcores that reflect a small scale heterogeneity of qtz- and plag-rich layers, especially in the transition zone towards the 3rd generation vein (ZJC-02 to -05). These observations are in good agreement with the previously deduced petrographic implications (**Chapter 3**).
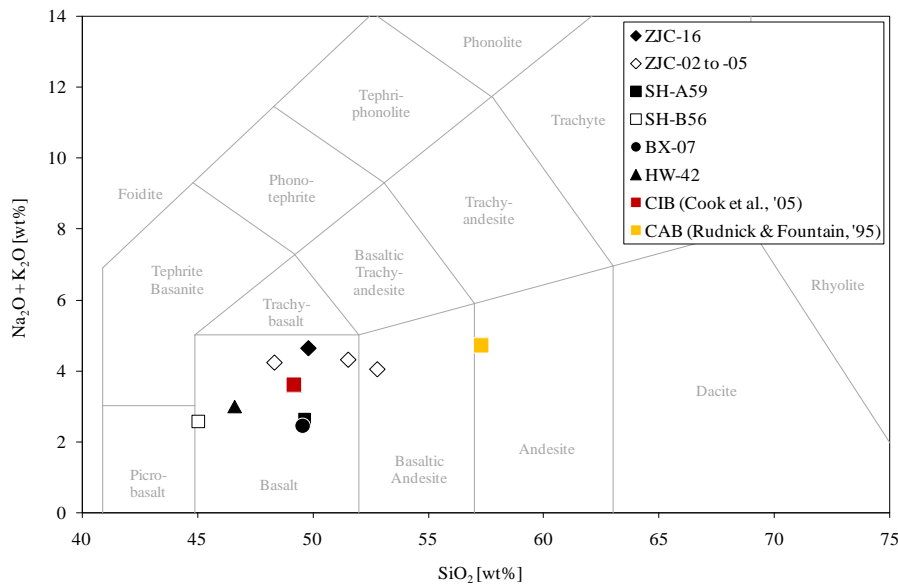
↑ **Figure 4.3** Total alkali vs. silica plot (IUGS classification after LE BAS ET AL., 1985, plotted after VERMA ET AL., 2002) shows a basaltic composition for all investigated eclogites. The variability in quartz contents is ascribed to heterogeneities on the specimen scale, especially for drill core samples from Zhujiachong. Comparison with continental intraplate basalts (**CIB**, after COOK ET AL., 2005) and continental arc basalts (**CAB**, RUDNICK AND FOUNTAIN, 1995) shows a coincidence with global CIB compositions, rather than with the more felsic CAB reference.

Selected major and minor element variation plots (**Figure 4.4**) reflect the extent of retrogression among the eclogites. The eclogites from SH-A and BX are the most pristine samples, as indicated by high ('unaltered') Ni contents. The overall lowest concentrations of fluid-mobile elements (Pb, Ba, Sr) in these rocks display both little retrogression, ie. little fluid influence, whereas the eclogites from ZJC are relatively enriched in these elements and HW as well as SH-B generally plot intermediate.
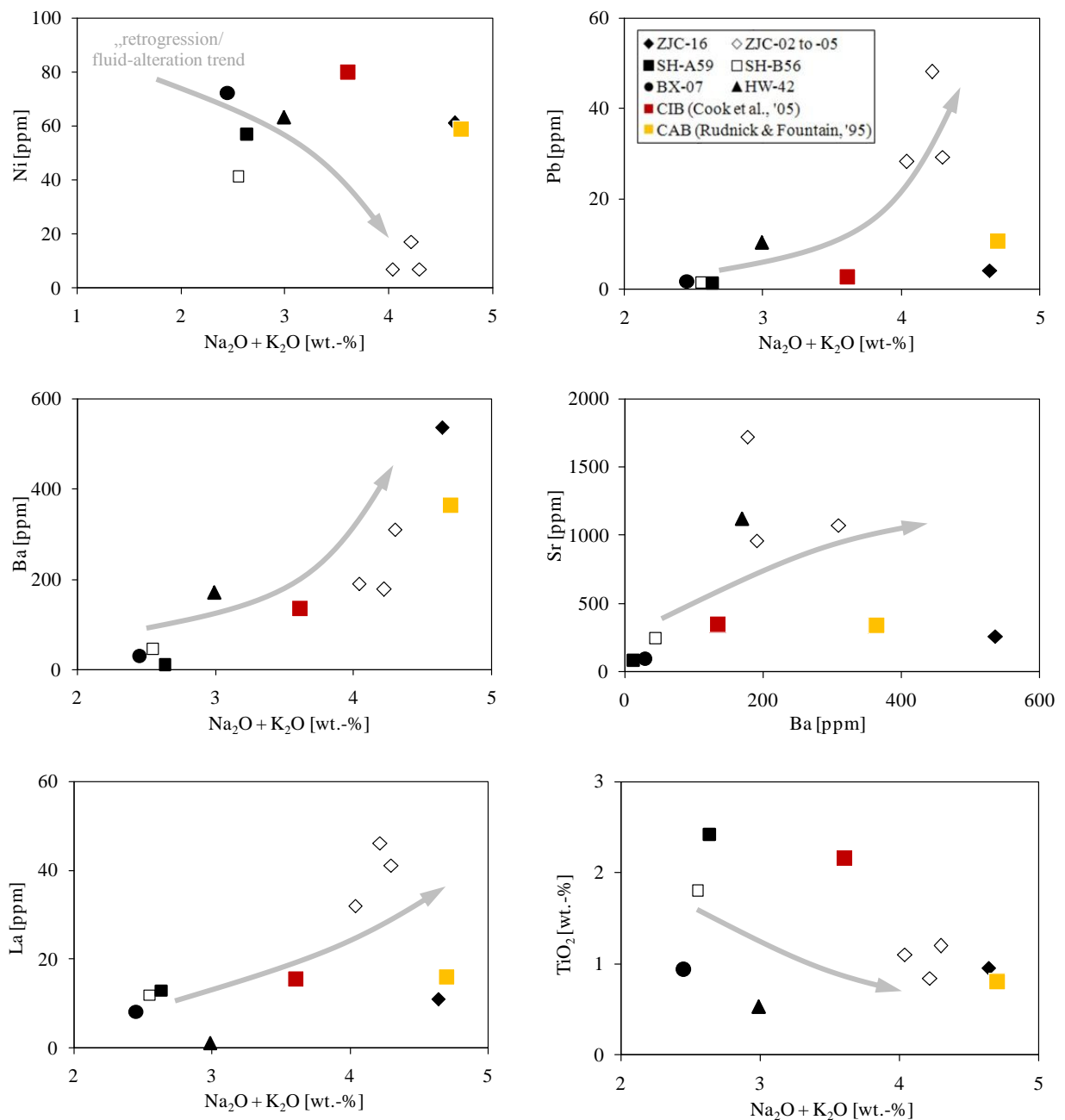
↑ **Figure 4.4 (previous page)** Selected element variation diagrams against the total alkali (Na$_2$O + K$_2$O) content are used to assess the extent of retrogression and fluid influence in the investigated eclogites. **Grey arrows** conceptually indicate increasing retrogression and/or alteration, in accordance with petrographic results. Eclogites with more felsic protoliths tend to display the overall highest retrograde fluid alteration. CIB and CAB compositions are plotted for comparison and especially CIB displays a good coincidence with the pristine eclogites SH-A and BX-07.

Lanthanum contents reflect the amount of epidote/clinozoisite in a sample, since these minerals are supposed to be the major host of REE in the samples. Given that only retrograded samples contain ep/czo, the La-content can be regarded as a proxy for retrogression. As to be expected from petrographic observation, the rutile-rich Shuanghe eclogites exhibit the highest titanium concentrations that are twice as high as for the other samples. Eclogites with more felsic protoliths tend to display the overall highest retrograde fluid alteration. CAB and CIB basically (particularly CIB) fall in the compositional ranges spanned by the eclogites.

The profile sampled along the eclogite transition zone towards the 3rd generation vein at ZJC (**Figure 4.5**) displays distinct gradients in oxide and element concentrations. Relative to the bulk eclogite, Sr, Pb, La and Th are strongly, Al$_2$O$_3$ and CaO are slightly enriched towards the vein, whereas K$_2$O, MgO, FeO$_{(t)}$, Ba and Rb are continuously depleted. TiO$_2$, Nb, Ta, Zr and U exhibit a selective enrichment relative to vein and bulk eclogite that is limited to the transition zone (ZJC-04 and ZJC-05). Zr and U are, in contrast to Nb, enriched in ZJC-02 relative to the bulk eclogite ZJC-16. SiO$_2$ and Na$_2$O are approximately constant.

The continuous depletion of a particular element from eclogite towards the vein is an indicator for its capability to being altered in (ie. scavenged from) the host eclogite under the retrograde influence of a vein-forming fluid. In this view, the decreasing K-, Mg-, Fe-, Ba- and Rb-contents reflect the retrograde decomposition of garnet, omphacite and phengite in the transition zone, as likewise monitored by petrographic evidence. The enrichment of Al and Ca in turn, corresponds to the retrograde formation of plagioclase and hornblende, whereas the strong enrichment of Sr, Pb, La and

Th towards the vein records an enhanced fluid mobility of these elements, and implies a relative enrichment of these elements in the vein.

The selective enrichment of Ti, Nb and Ta in the transition zone can be explained by preferential precipitation of these elements (eg. in the form of rutile) in the eclogite adjacent to the circulating fluid, but not in the vein itself.
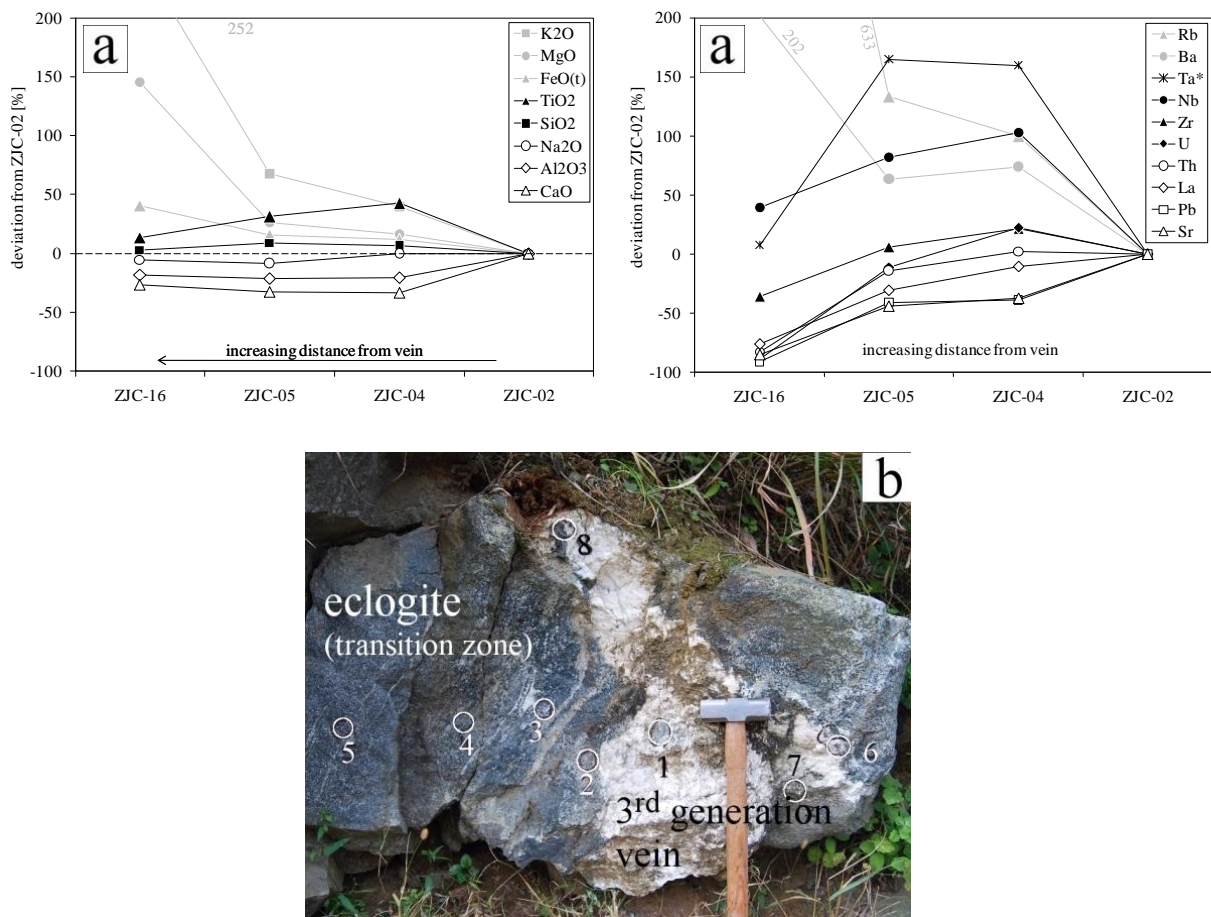
↑ **Figure 4.5 a** Compositional gradients (XRF) along the profile of the ZJC eclogite transition zone reflect the retrograde replacement of the eclogitic assemblage by plagioclase and hornblende, and a distinct mobility of Ti, Nb, Ta[†] and REE in the vein-forming fluid, that deposited these elements preferentially in the eclogite adjacent to the vein contact, but not in the vein itself. Note that ZJC-16 has been collected in a distance of about 10 m from any vein. **b** Outcrop photo with labeled sampling spots for comparison. Note that a bulk analysis of ZJC-03 was not possible due to small drill core size.

[†] Ta concentrations have not been determined by XRF and were exemplarily recalculated on the basis of Nb/Ta ratios in rutile (from ZJC-04,- 04, -05 and -16) obtained by LA-ICPMS.

Trace element characteristics

Eclogites exhibit trace element patterns that are consistently enriched against the chondritic composition and show relative depletions in Rb, Ti and HFSE (Nb, Ta, Zr, Hf) (**Figure 4.6a, b**).

In contrast to pristine samples (BX-07, SH-A59), eclogites that experienced retrogression (ZJC-02 to -05, ZJC-16, SH-B56) and alteration (HW-42) are relatively enriched in LILE (Ba, Th, U, Pb, Sr) that are known to be preferentially mobilized by fluids. HW-42 is the only sample with a positive Eu-anomaly, that is explained by major contents of plagioclase in the retrograde matrix. Pristine samples show the highest HFSE concentrations, and in this regard SH-A59 is distinctly enriched compared to its retrogressed analog SH-B56.

All eclogite trace element patterns basically correspond with continental arc basalt (CAB) and continental intraplate basalt (CIB) compositions proposed by RUDNICK AND FOUNTAIN (1995) and COOK ET AL. (2005) (**Figure 4.6c**), except for the pronounced depletions in HFSE. This points to a continental basaltic origin of the eclogite protoliths and mirrors a distinct impact of HP/UHP metamorphism on the rocks HFSE budget.
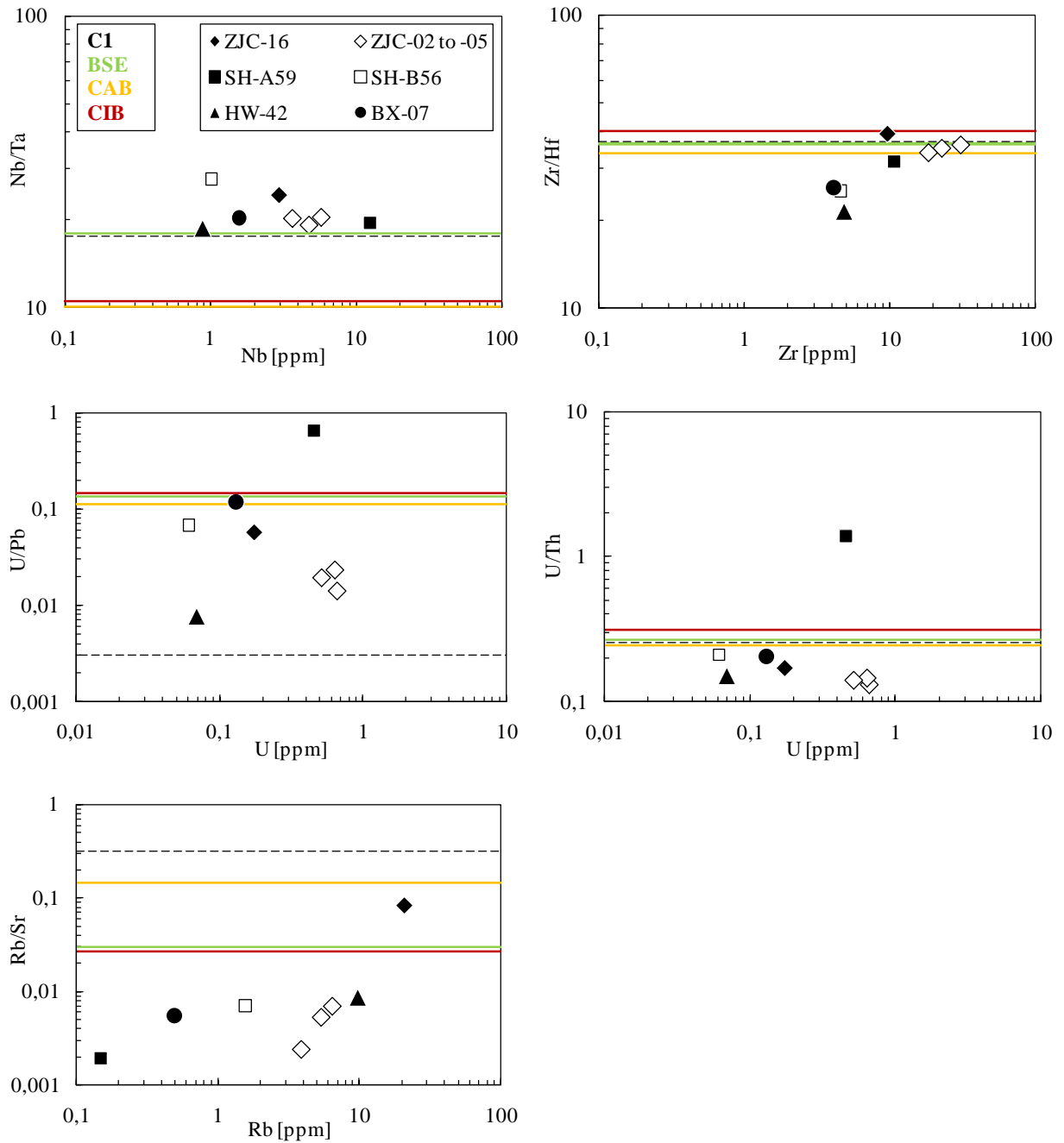
Variation plots for selected element ratios (**Figure 4.7**) display deviations from the reference ratios in C1 chondrites (C1), bulk silicate earth (BSE), continental arc basalts (CAB) and continental intraplate basalts (CIB), implying significant relative fractionation in eclogitic minerals.

Nb/Ta ratios of all eclogites consistently exceed the values of all compared reservoirs, especially for eclogites that contain veins in their immediate surroundings (SH-B56 and ZJC-16) and can thus be regarded as 'residues after vein extraction'. These observations point to a preferred mobilisation of Ta during HP/UHP metamorphism that is particularly pronounced with increasing involvement of a fluid phase.

Zr/Hf ratios roughly coincide with chondritic and silicate reservoir values, except for a significant depletion for BX, HW and SH-B. Since these samples represent each a pristine, an altered and a vein-bearing eclogite, while the Zr/Hf - inconspicuous eclogites are both retrograded and pristine, Zr/Hf ratios are apparently not systematically influenced by retrogressive effects. Their selective Zr-loss, or
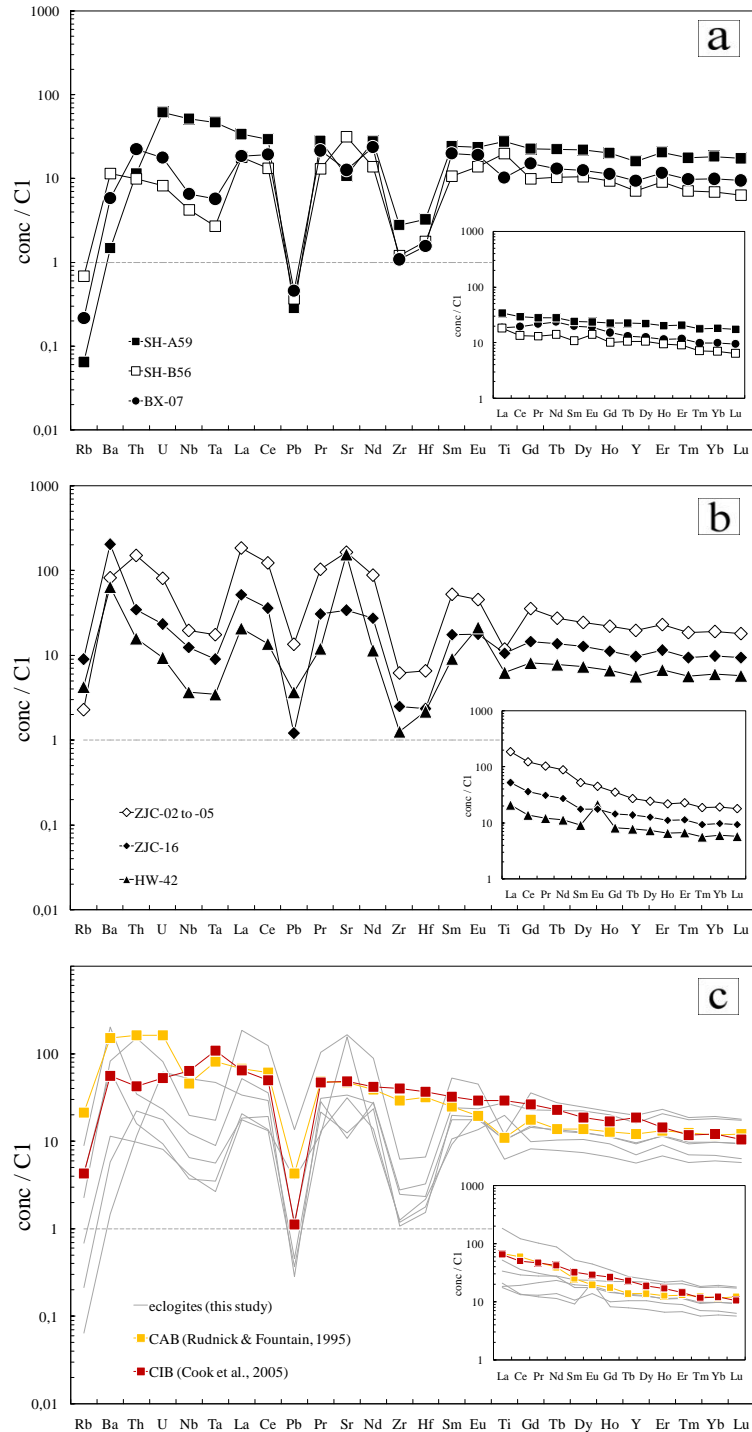
↑ Figure 4.6 a,b Chondrite-normalized multi element and REE plots show overall enriched patterns. Relatively enriched fluid mobile elements (Ba, Th, U, Sr) in retrograded eclogites reflect fluid-induced retrogression, and in case of Huwan also alteration, that is in contrast to pristine eclogite samples. Note that the analyses of ZJC-02 to -05 are plotted averaged. Chondritic values from MᴄDᴏɴᴏᴜɢʜ ᴀɴᴅ Sᴜɴ (1995). **c** Comparison with datasets of continental arc basalts (CAB, after Rᴜᴅɴɪᴄᴋ ᴀɴᴅ Fᴏᴜɴᴛᴀɪɴ, 1995) and continental intraplate basalts (CIB type A, after Cᴏᴏᴋ ᴇᴛ ᴀʟ., 2005) suggests a continental intraplate basaltic origin of the eclogite protoliths as well as a distinct effect of HP/UHP metamorphism on the HFSE budget of the eclogites.

↑ **Figure 4.7** Variation plots for selected element ratios in comparison with global bulk silicate earth (BSE), chondritic

values (C1) (MCDONOUGH AND SUN, 1995), continental intraplate basalt (CIB) (COOK ET AL.,2005) and continental arc basalt

(CAB) (RUDNICK AND FOUNTAIN, 1995). Deviations from the reference lines indicate element fractionation in one or more of

the eclogitic mineral phases. Systematical differences between pristine and retrograded eclogites (Nb/Ta, U/Pb, Rb/Sr) are

evident for an alteration of the ratios through fluid-mediated retrogression.

respectively Hf-gain, may be related to a particular element fractionation in HFSE-bearing minerals such as rutile or zircon and their modal abundances.

U/Pb ratios plot in a field in near or below the silicate reservoir values, except for the distinctly exceeding SH-A59. This excess is possibly related to the pronounced occurrence of a U-bearing mineral phase that is capable to fractionate U from Pb. In this regard, zircon is a possible candidate. The variably lowered U/Pb ratios in the other eclogites are likely explained by a preferential input of fluid-mobile Pb into the samples with the high extents of fluid-rock interaction (especially the altered HW-42 and the strongly retrogressed ZJC eclogites). The pristine eclogite from Bixiling, however, exhibits the typical ratio of its assumingly continental basaltic protolith. U/Th ratio characteristics are analogous to U/Pb.

Rb/Sr ratios display overall subchondritic values that, except for ZJC-16, also fall below the CIB and CAB references. These values are well explained by selective Sr-enrichement in the course of retrogression, since most retrograded eclogites contain epidote group minerals that are major carriers of LILE and potentially fractionate Sr from Rb.

4.3.2 Mineral chemistry

Major element characteristics

Garnet:

Mineral stoichiometry was recalculated on the basis of 12 oxygen. The compositional variation of garnet is $Alm_{42-60}Prp_{12-38}Grs_{12-34}Sps_{0-7}$, where the grossular component can be replaced by up to 0.64 pfu of the theoretical andradite endmember.

Garnet from ZJC and SH show similar characteristics with a tendency of (alm + sps)-richer compositions at ZJC. Independent of the locality, garnet occurs in two modes that correlate to petrographic observations and are categorized as homogeneous 'pristine garnet' and zoned 'garnet with retrograde fluid influence'. Both groups are distinguishable in backscattered electron images and they differ predominantly on their pyrope and grossular contents (**Figure 4.8**). Pristine garnet (Prp_{12-}

[22]) comprises minerals from the pristine eclogite SH-A59 as well as relictic crystal mantles in atoll garnets from ZJC-16 and fluid-unaffected crystal regions in garnet from eclogite at SH-B and -C. The retrogressive garnet group (Prp_{25-38}) comprises the texturally younger cores and rims of ZJC-16 atoll garnets as well as apparently fluid-affected, patchy zoned regions of SH-B and /-C garnet in immediate contact to 2nd generation veins.
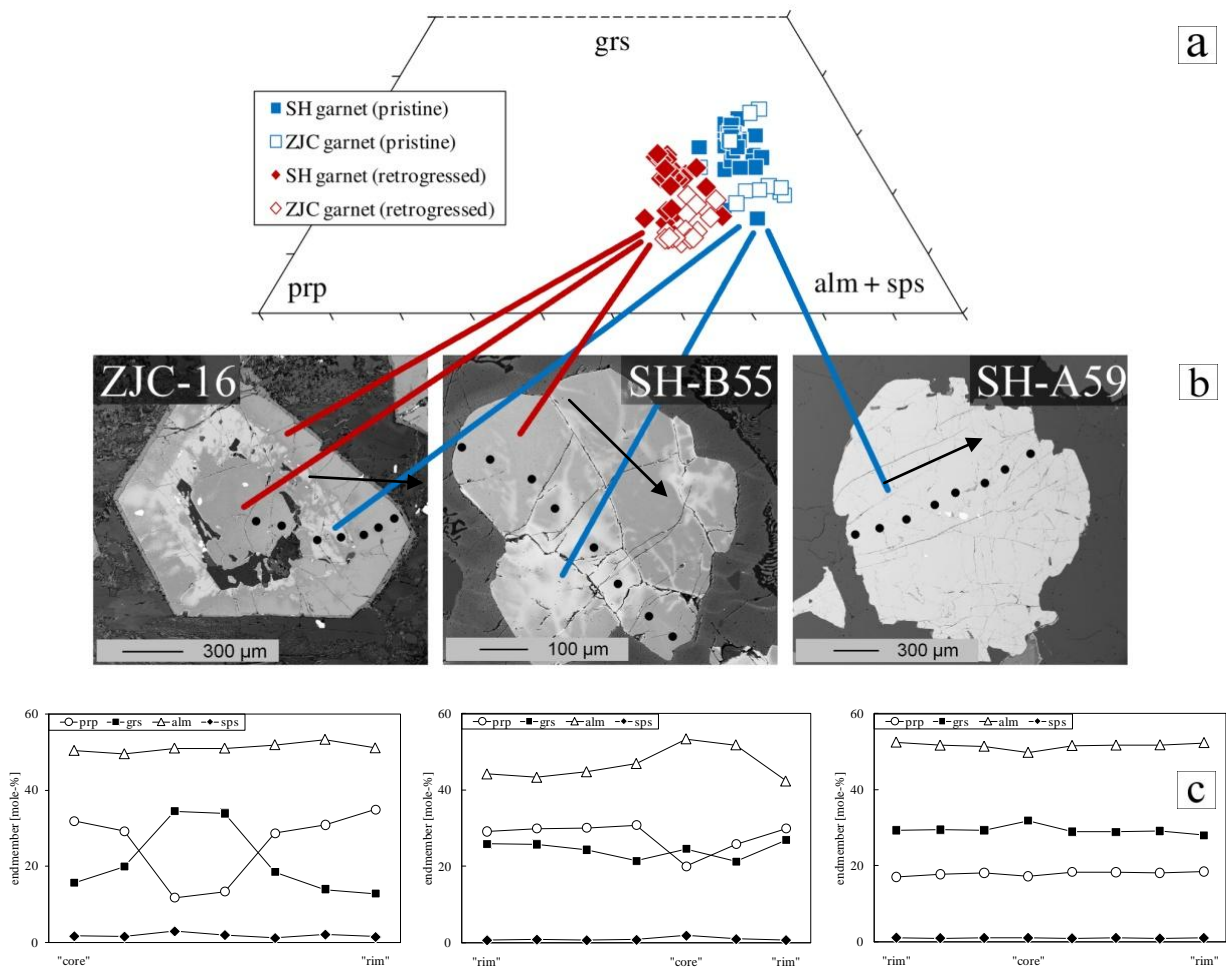
↑ **Figure 4.8 a** Compositional variation of garnet from SH and ZJC. Garnet with retrogressive/ fluid influence exhibits compositions with higher pyrope (prp) and lower grossular (grs) contents compared to pristine garnet. ZJC garnet tends to have slightly higher almandine + spessartine (alm + sps) contents than SH garnet. **b** BSE images of garnet with retrograde influence (ZJC-16, SH-B55) displays element zoning, whereas pristine garnet (SH-A59) is homogeneous. **c** EMP profiles analyzed across the garnets from depicted in b.

According to CHENG ET AL. (2007) and FARYAD ET AL. (2010), the garnet atoll structures at ZJC are a result of fluid-mediated partial dissolution of prograde garnet due to the breakdown of hydrous

minerals such as lawsonite, that is followed by early retrograde overgrowth of a younger (prp-richer and grs-poorer) garnet generation. This compositional shift in the course of decompressional exhumation has been accordingly described by XIA ET AL. (2012), and is interpreted to be a response to a pressure decrease during initial exhumation, but an ongoing temperature increase until the peak temperature is reached, pointing to a formation at the onset of exhumation.

Omphacite:

Omphacite compositions have been recalculated after MORIMOTO (1988) on the basis of 6 oxygen, and span a wide range of $(Wo+En+Fs)_{42-76}Jd_{12-55}Aeg_{0-14}$. Remarkable stoichiometric deviations are not observed, with TiO_2, NiO, Cr_2O_3 and MnO consistently being <0.1 wt-% and K_2O below detection limit. Ferric iron was determined after DROOP (1987).
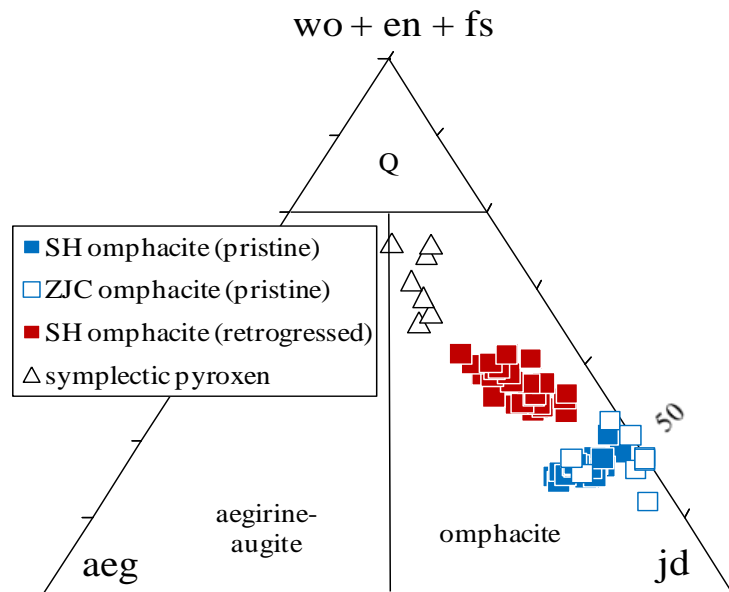
↑ **Figure 4.9** Omphacite from eclogite samples away from veins (SH-59A and ZJC-16) have the highest jadeite (jd) contents, whereas omphacite in direct contact to veins and in the retrogressed eclogite from Shuanghe (SH-B56) group around intermediate values. Lowest jadeite contents are observed for fine-grained omphacite in retrograde reaction rims after garnet.

Three groups of homogeneous omphacite that differ in their jadeite contents are classified (**Figure 4.9**). Omphacite from the pristine eclogite SH-A59 and the eclogite away from any veins ZJC-16 exhibit the highest jadeite contents of up to 55 wt-%, whereas symplectic omphacites after garnet in all eclogite samples show the lowest contents between 12–21 wt-%. Omphacite in SH-B56 and in direct contact to 2nd or 3rd generation veins form a group around intermediate jadeite contents (25–45 wt-%), indicating lower formation pressures compared to omphacite from pristine eclogites.
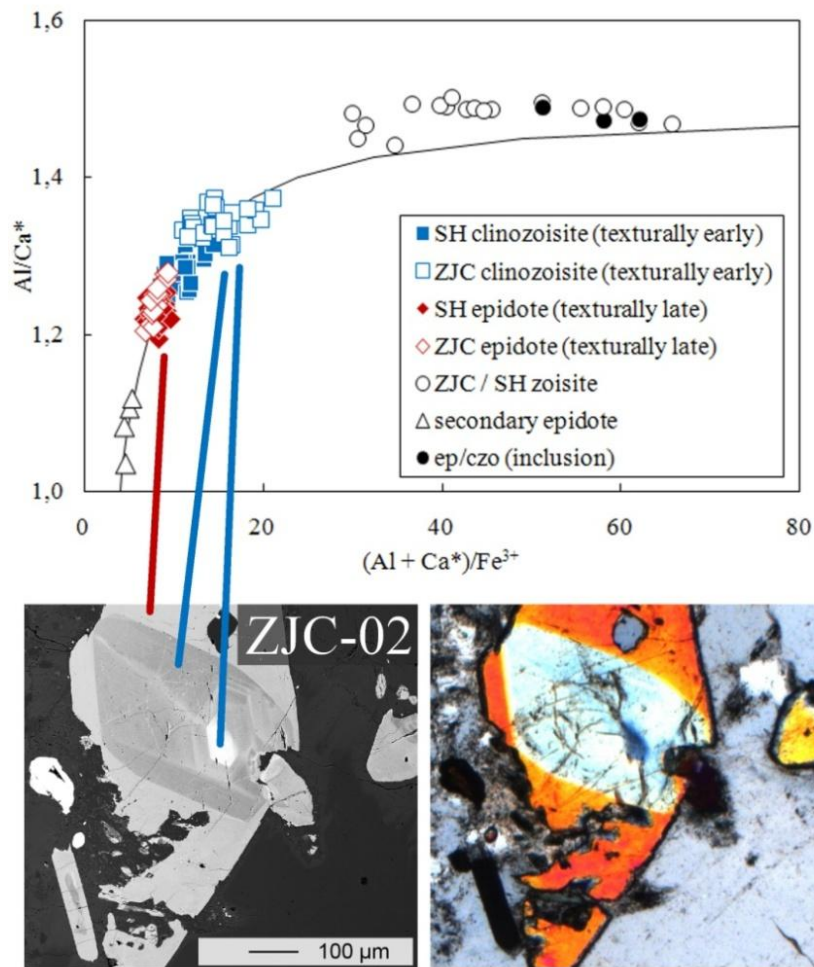
Epidote/clinozoisite, zoisite:

Epidote minerals (here: the monoclinic epidote group minerals together with the orthorhombic polymorph zoisite) are important Ca-Al-silicates in many metabasites, metapelites and metacherts that are characterized by high P/T ratios. Mineral stoichiometry was recalculated on the basis of 12.5 oxygen, ranging widely between the endmember compositions $Ep_{5-91}Czo_{9-95}$. Five groups that correlate with petrographic observations are distinguished based on differing Fe-contents (**Figure 4.10**).

Secondary epidote, mainly related to saussuritization and symplectic reaction rims after garnet and omphacite, shows the most Fe-rich compositions. The lowest iron contents are observed in inclusions in garnet and omphacite and in texturally early zoisite from the 2nd generation veins of type I from ZJC and SH as well as from the eclogite ZJC-16.

Two intermediate groups are (i) Fe-poor and clinozoisite dominated ($\sim Ep_{40}Czo_{60}$) and (ii) Fe-rich and epidote dominated ($\sim Ep_{60}Czo_{40}$). Group (i) corresponds to the texturally early mineral generation that occurs as large-grained clinozoisites in 2nd generation veins (cf. **Figure 3.5d**) of type II (cf. **Table 3.1**), as cores and mantles in zoned crystals (**Figure 4.10**, cf. also **Figure 3.7**), and in the retrogressed eclogite ZJC-16. Group (ii) corresponds to the texturally late mineral generation that comprises epidote aggregations and fine-grained idioblasts in type II 2nd generation veins in textural equilibrium with barroisite (cf. **Figure 3.5c**), as well as the rims of zoned minerals (**Figure 4.10**). They are virtually absent in the eclogite ZJC-16. An overview on the occurrences of the different mineral types is provided in **Table 4.1**. A systematical difference between vein and eclogite minerals is not evident.

Epidote/clinozoisite chemistry reflects a development from early, Fe-poor zoisite and clinozoisite towards epidote-dominated minerals that can overgrow the early generation. Since consistent zoning patterns are observed both in SH and ZJC 2nd veins, in the eclogite in contact to the 3rd generation vein at ZJC, and in the retrogressed eclogite from Shuanghe (SH-B56), it is deduced that 2nd generation vein formation and eclogite retrogression are generally triggered by the same fluid type.

↑ **Figure 4.10** Secondary epidote, texturally early zoisite and clinozoisite, texturally later epidote and prograde zoisite inclusions in SH and ZJC garnet and omphacite form five different petrochemical groups. The early generation comprises zoisite that occurs in all 2nd generation veins of type I and in the eclogite from Zhujiachong (ZJC-16), as well as clinozoisite that occurs in cores (allanite) and mantles of zoned minerals. Texturally late epidote-rich minerals are found as rims of zoned minerals, or as fine-grained idioblasts in 2nd generation veins and at the eclogite margin towards the 3rd generation vein at ZJC (cf. **Table 4.1**). A systematic difference between vein and eclogite minerals is not evident and an indication in the plot is renounced to retain clarity.

↓ **Table 4.1** Overview on the occurrence of different epidote/clinozoisite groups.

	zoisite (texturally early)	clinozoisite-rich ep/czo & allanite (texturally early)	ep-rich epidote/clinozoisite (texturally late)
occurrence	idioblasts often coexisiting with clinozoisite in: • 2nd generation veins (type I) • retrogressed eclogite ZJC-16	mineral cores (allanite) and mantles, as well as large single crystals in: • eclogite contact 3rd generation vein • 2nd generation veins of type II • retrogressed eclogites SH-B56, ZJC-16	mineral rims and late idioblasts in: • eclogite contact 3rd generation vein • 2nd generation veins of type II • retrogressed eclogite SH-B56 • secondary accessory in most samples

Phengite:

Phengite stoichiometry has been recalculated on the basis of 11 oxygen and is presented in terms of silica content in comparison to natural phengite and muscovite references (**Figure 4.11**). Phengite is a high-pressure and high-silica variety of muscovite and compositions fall on line with the solid solution series of the theoretical endmembers muscovite $(KAl_2(Si_3Al)O_{10}(OH)_2)$ and celadonite $(K(Al,Fe^{3+})(Mg,Fe^{2+})Si_4O_{10}(OH)_2)$.
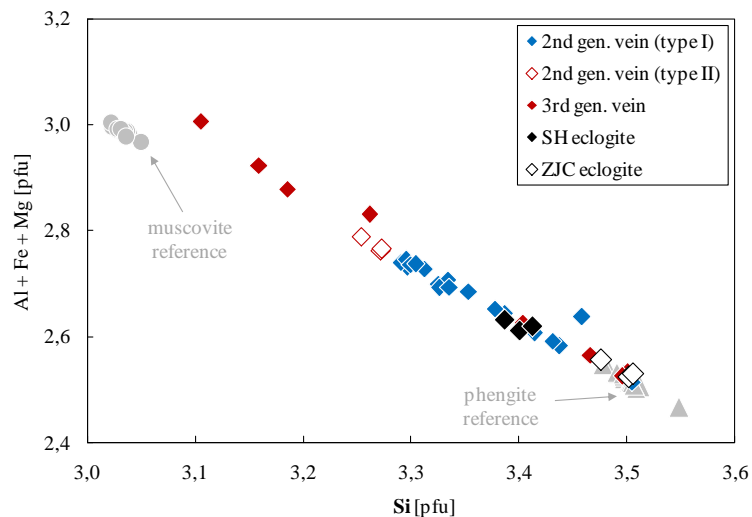
↑ **Figure 4.11** Phengite with the highest silica contents is observed in eclogites, 2nd generation veins of type I and at the eclogite margin towards the 3rd generation vein. Higher Si [pfu] correspond to higher pressure conditions during mineral (re)crystallization.

Observed compositions have Si contents between 3.4–3.5 pfu for ZJC and SH eclogites, indicating high formation pressures of at least 1.2–1.5 GPa (MASSONNE AND SCHREYER, 1987; HERMANN, 1997; MASSONNE AND SCHREYER, 1989; VELDE, 1967). Si contents in 2nd generation veins of type I and the eclogite margin towards the 3rd generation vein at ZJC are highly variable between 3.3–3.5, and 3.1–3.5 respectively and point either to formation under different pressures, or to variable retrograde recrystallization. With this regard, phengite in the type II 2nd generation veins apparently evolved under lower pressures compared to type I veins.

Amphibole, plagioclase and others:

Amphibole stoichiometry was determined after ESAWI (2004) on the anhydrous basis of 23 oxygen, using the ferric iron estimation of STOUT (1972) and the nomenclature after LEAKE ET AL. (1997). All investigated amphiboles belong to the calcic (magnesio-hornblende, tschermakite, pargasite, magnesio-hastingsite), sodic-calcic (magnesio-taramite, barroisite) or Mg-Fe (actinolite, cummingtonite/anthophyllite) supergroups.

Barroisite is by far the dominating amphibole in most samples and an indicator of HP/LT conditions. The occurrence of pargasite, hastingsite and taramite is restricted to retrograde reaction products after garnet and omphacite, while hornblende and tschermakite coexist in the 3rd generation vein from ZJC. Anthophyllite is found occasionally as retrograde reaction products with unclear precursors in 2nd generation veins of type I. Actinolite represents the texturally latest amphibole, forming secondary microveins along crystal fractures or superfine-grained alteration products after epidote/clinozoisite.

None of the analyzed amphiboles show a significant incorporation of Mn, Cr or Ni (<0.02 pfu), whereas barroisite and hornblende may contain up to 0.44 pfu Ti. Significant compositional zoning has not been detected.

Plagioclase compositions have been recalculated on the basis of 8 oxygen and are mostly albitic to minor andesinic, covering a compositional range of $Ab_{73-100}An_{0-27}Or_{0-1}$. Albite-rich plagioclase is the major constituent of the 3rd generation vein. The occurrence of andesinic plagioclase is restricted to rare secondary microveins and symplectites after garnet and omphacite.

The sodium mica paragonite ($NaAl_2(Si_3Al)O_{10}(OH)_2$) as observed in the 2nd generation vein from Zhujiachong, as well as chlorite, apatite and kyanite show neither significant compositional variations, nor remarkable deviations from their ideal stoichiometries.

Trace element characteristics

Garnet:

According to the BSE images depicted in **Figure 4.8b**, garnet trace chemistry defines two groups that correlate with major element compositions and petrography (**Figure 4.12a**).

The first group comprises pristine garnet and the second group represent garnet that is, by petrographic evidence, suspected to has been influenced by (ie. grown in the presence of) retrograde HP fluids. Element patterns are qualitatively identical with no remarkable trace contents except for minor uranium contents and almost flat M- to HREE enriched up to 60 times chondritic. Pristine garnet has significantly more enriched patterns than garnet with retrograde fluid influence, which may be explained by retrograde garnet grows in the presence of ("REE consuming") epidote group minerals that are absent in pristine eclogites. Relictic pristine garnet portions in retrograded samples thus imply that prograde garnet growths during eclogitization occurred without significant fluid influence, both in pristine and retrogressed samples.

Epidote group minerals:

Independent of their origin (vein or eclogite) trace chemistry of epidote group minerals defines four groups (**Figure 4.12b**):

(1) **ALN**: Cores of zoned minerals are allanite with extremely enriched compositions of up to 10000 times chondritic, corresponding to ∑REE 0.7–2 wt-%. (2) **ZO/CZO**: Texturally early clinozoisite-dominated ep/czo (eg. mantles of zoned minerals, cf. **Table 4.1**) and coexisting zoisite (eg. occurring in 2nd generation veins of early type I) show lower overall enrichment in the range of 1000–100 times chondritic, whereas zoisite is slightly more enriched than clinozoisite. Trace element patterns basically coincide with that of allanite, except for relatively enriched Sr. (3) **EP**: Epidote-dominated ep/czo (eg.

forming mineral rims or texturally late porphyroblasts) characteristically exhibit the lowest trace element contents along with a differing multi-element pattern with enrichment of Ba, Sr, in part Pb and HREE, and relative depletion of Th, LREE and MREE. Zoned minerals show a general trace element decrease from core, to mantle, to rim (**Figure 4.12c**). (4) **IN**: Inclusions in garnet and omphacite with the overall lowest trace element concentrations.

REE patterns of ALN and ZO/CZO decrease continuously from LREE to HREE and differ solely in total concentrations, whereas most REE patterns of EP show an complementary increase from low LREE and MREE towards enriched HREE contents. Corresponding late epidote assumingly forms in the absence of (HREE-rich) garnet, whereas few epidote with depleted HREE formed when garnet was still stable.

Amphibole:

All analyzed amphiboles, of which the majority is barroisite, are plotted together and show similar patterns that are on average mostly below or near chondritic values, except for a about tenfold enrichment of Ba and U, as well as a fivefold enrichment of Sr and M- to HREE (**Figure 4.12d**). The lowest trace element patterns usually correspond to non-barroisitic and texturally late amphiboles (eg. hornblende and symplectic amphibole), and a systematic difference between vein and eclogite minerals was not observed.

Phengite / paragonite:

Apart from pronounced enrichment of Ba (2000 times chondrite), U and Ta (20 times chondrite), and Sr (50 times chondrite), trace element contents of both micas are well below the chondritic values and often near or below the detection limit (**Figure 4.12e**). Scattering of REE patterns results from high uncertainties at the given, low concentrations. Phengite differs from paragonite by generally higher trace element concentrations, whereas the patterns in itself coincide. A systematic difference between eclogite and vein minerals is not evident.

Apatite:

Apatite is a considerable host of Th, U and REE (about 10 times the chondritic values), whereas further elements and especially HFSE are subchondritic down to 0.01 times chondrite (**Figure 4.12f**). Core regions of apatite generally show higher overall trace element contents than rims.

Zircon:

Only four zircon analyses were performed due to the limited amount of minerals with sizes (>60 µm) sufficient for LA-ICPMS spot measurements. Trace element chemistry reveals two different zircon types that reflect either eclogitic zircon from SH-A59 with almost flat REE patterns, or vein zircon that is relatively enriched in Pb and especially M- to HREE (**Figure 4.12g**). The latter is likely explained by eclogitic zircon growth in equilibrium with garnet, whereas the investigated metamorphic veins (SH-C58 and SH-A60) are devoid of garnet. Enriched Pb contents mirror a high fluid mobility of lead.

Rutile:

Rutile is the major host of HFSE (Ti, Nb, Ta, Zr, Hf, U) (**Figure 4.12h**). Concentrations of further trace elements fall below the chondritic value and are either afflicted with high uncertainties or below the detection limit. A systematic difference between eclogitic and vein minerals is not evident, but in contrast to rutiles from ZJC, BX, SH-A and SH-C, minerals from both eclogite and veins at SH-B show conspicuously lower Nb and Ta contents. The averaged total Nb concentration in the first mentioned rutile group is 350 ppm, whereas the rutiles from SH-B contain 50 ppm on average.

Omphacite, albite, kyanite, chlorite, quartz:

These minerals do not contain any remarkable amounts of trace elements. Their concentrations fall consistently below chondritic values, and are thus near or below the detection limit.
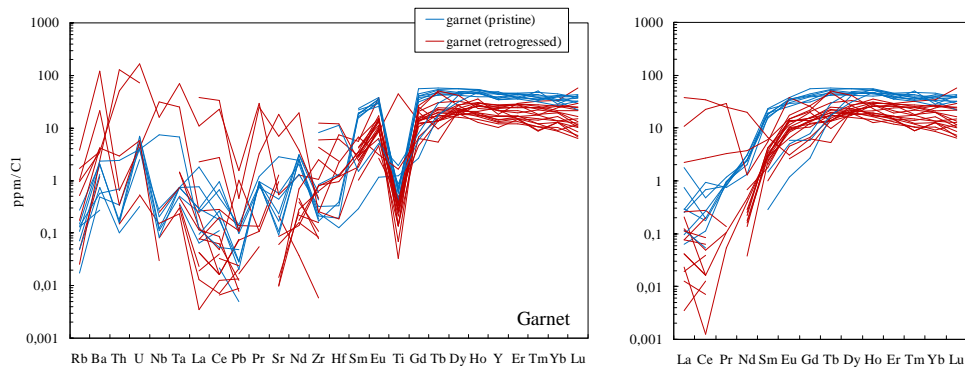
↑ Figure 4.12 a Chondrite-normalized garnet trace element chemistry shows two groups, **pristine garnet** that lacks petrographic evidence of HP fluid influence, and **garnet that has been influenced by or grown in the presence of a retrograde fluid** (cf. **Figure 4.6**). Both groups show qualitatively coinciding element patterns. The groups differ solely by higher element enrichment in pristine garnet, that can be ascribed to pristine garnet crystallization in the absence of epidote group minerals. Unusual enriched HFSE or LREE correspond to rutile or epidote inclusions that skipped petrographic observation. Chondritic values used in this study are from MCDONOUGH AND SUN (1995).
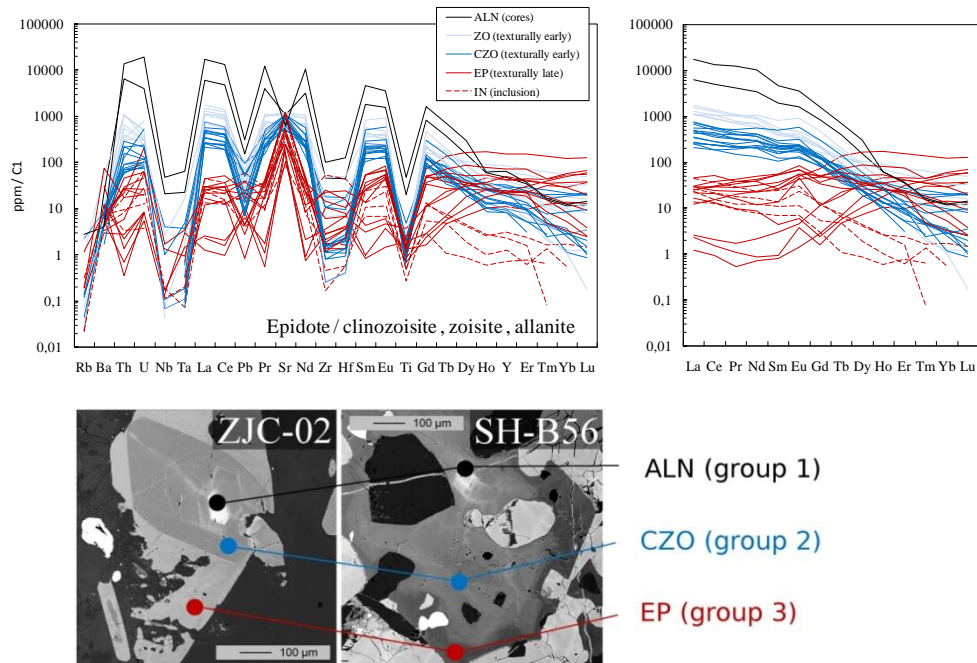
↑ Figure 4.12 b Trace element chemistry of epidote group minerals defines five major groups, including (1) early allanite mineral cores (**ALN**), (2/3) texturally early clinozoisite-rich ep/czo and coexisting zoisite (**ZO/CZO**), (4) texturally late epidote-rich ep/czo (**EP**), and (5) inclusions in garnet and omphacite (**IN**). The qualitatively comparable patterns (except for a relative stronger enrichment of Ba, Pb, Sr and HREE in late epidote that is suspected to be due to proceeding decomposition of garnet during late epidote crystallization) can be ordered by their relative enrichement: aln > czo/zo > ep. A systematic difference between vein and eclogite minerals is not observed, and an indication in the plot was thus renounced.
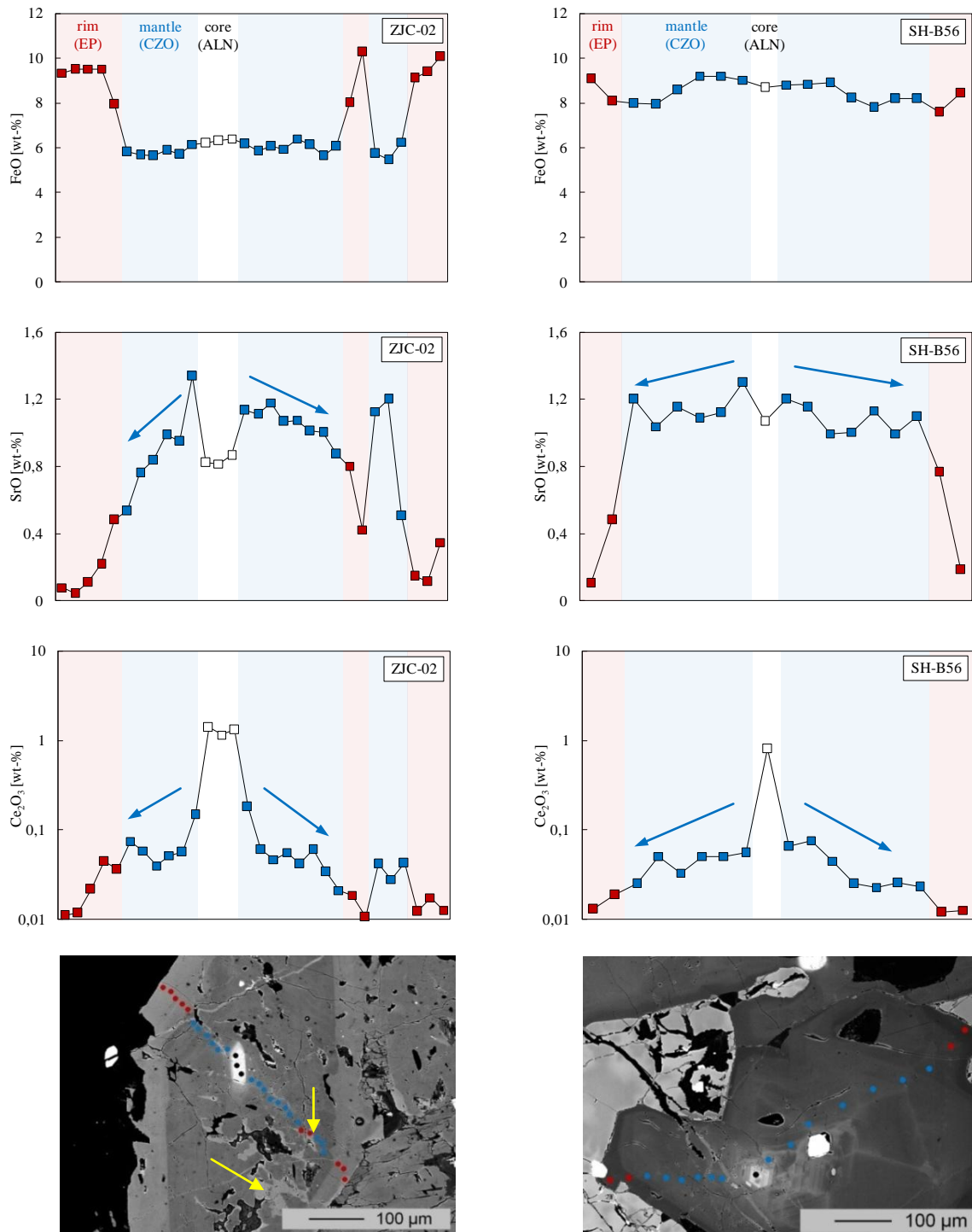
↑ **Figure 4.12 c** EMP profiles measured across a zoned ep/czo from the eclogite in contact to the 3rd generation vein at ZJC (ZJC-02, left) and from the retrograded SH eclogite (SH-B56, right). Compositional zoning reflects comparably decreasing REE and Sr contents within mantles (blue arrows) and towards the mineral rims, while the pronounced Fe-zoning in ZJC is not evident for SH. Yellow arrows indicate EP composition not only in mineral rims, but also diffusive along microcracks.
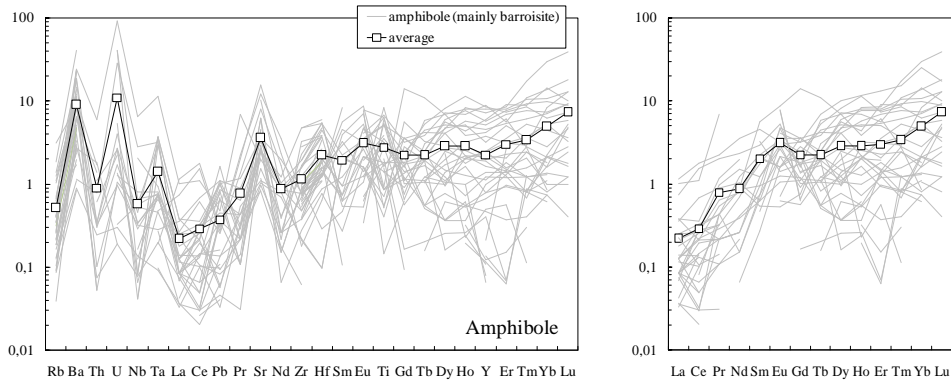
↑ **Figure 4.12 d** Amphibole trace element chemistry reveals barroisite to be a remarkable source for Ba, U (ten times chondrite) as well as Sr and M- to HREE (five times chondrite). REE patterns exhibit a positive Eu anomaly.
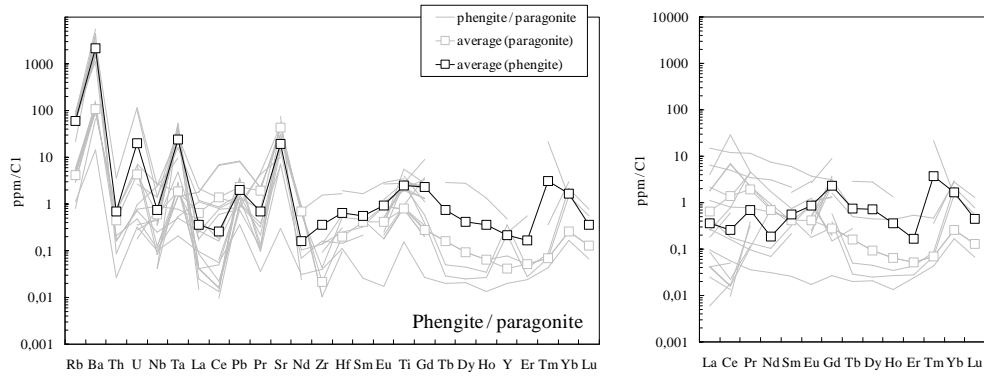
↑ **Figure 4.12 e** Mica trace element chemistry displays phengite and paragonite to be important reservoirs of LILE (Rb, Pb, Sr, U) and apparently also the HFS element Ta. The up to tenfold enrichment relative to C1 is decoupled from subchondritic Nb, Zr and Hf, whereas Ti contents are slightly superchondritic. REE contents scatter around chondritic values and are often below detection limit.
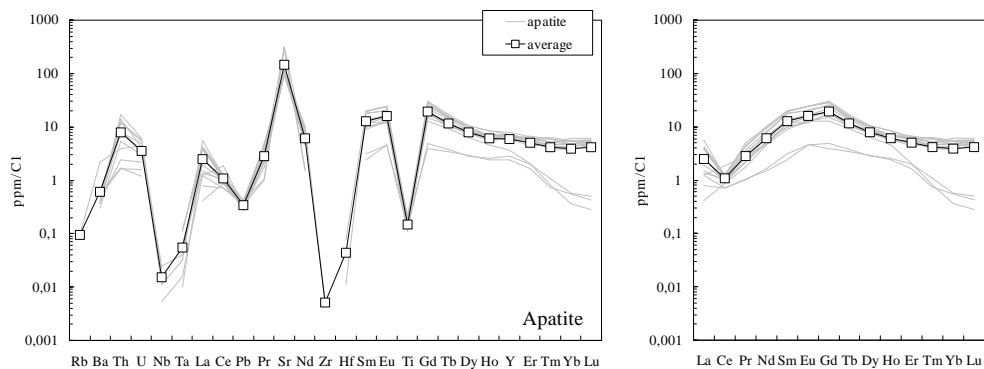
↑ **Figure 4.12 f** Apatite is a remarkable host for Th, U, Sr and contains remarkable amounts of REE. The REE pattern is most enriched for MREE (up to 30 times chondrite) and shows a distinct negative Ce anomaly.
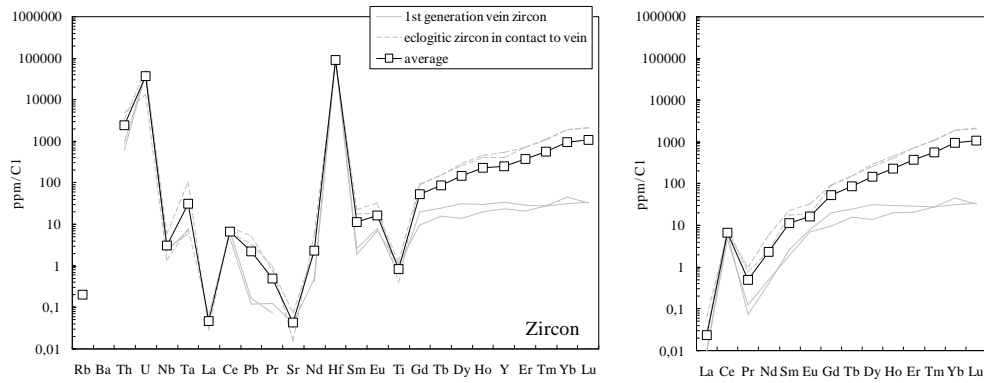
↑ **Figure 4.12 g** Zircon is the major host for Th, U, HFSE (up to 100000 times chondrite) and M- to HREE. REE patterns show a smooth increase from L- to HREE, which is disrupted by a pronounced positive Ce anomaly that typically relates to the occurrence of both Ce^{3+} and (zircon-compatible) Ce^{4+} which is in contrast to all other lanthanides. Zircons from the 1st generation vein (SH-A60) are less enriched in especially HREE than zircons from retrograded eclogites in direct contact (<5 cm) to 2nd generation veins (SH-C58, SH-B56), probably reflecting a higher availability of trace REE in retrograded environments. The slight negative Eu anomaly in vein zircons may in this regard be related to the presence of small amounts of feldspar that formed during retrogression in reaction rims after garnet and omphacite and can incorporate Eu, whereas feldspar is completely absent in pristine eclogite. Relatively enriched Pb concentrations in vein zircon likely mirror a high fluid mobility of lead.
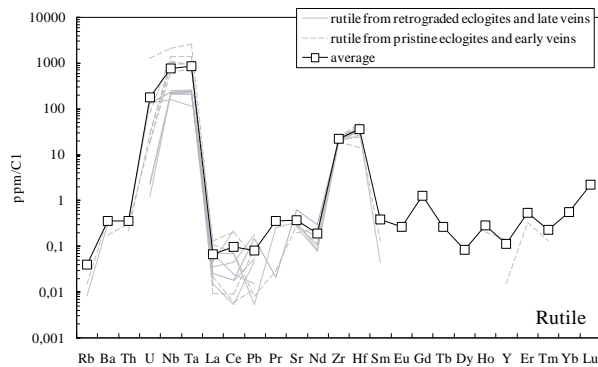
↑ **Figure 4.12 h** Rutile is a major host for HFSE. All further trace element contents are subchondritic and mostly below the detection limit. HFSE concentrations in "early" rutiles from pristine eclogite, 1st generation veins, and type I 2nd generation veins (BX-07, SH-A59,SH-C58, ZJC-10) are higher than in "later" rutiles from type II 2nd generation veins (SH-B44, -B55) or retrograded eclogites (ZJC-16, SH-B56), likely reflecting higher HFSE mobility at higher pressures.

4.3.3 Bulk eclogite and vein mass balance

A major and trace element mass balance based on averaged EMP analyses of bulk eclogites and LA-ICPMS chemistry of eclogitic and vein minerals is applied to access bulk vein compositions, since direct bulk analyses of the heterogeneous and in part large-grained veins are not feasible. Pristine (SH-A59) and retrogressed (ZJC-16, SH-B56) bulk eclogite chemistries were effectively remodeled to verify the reliability of the approach (**Figure 4.13a-c**).
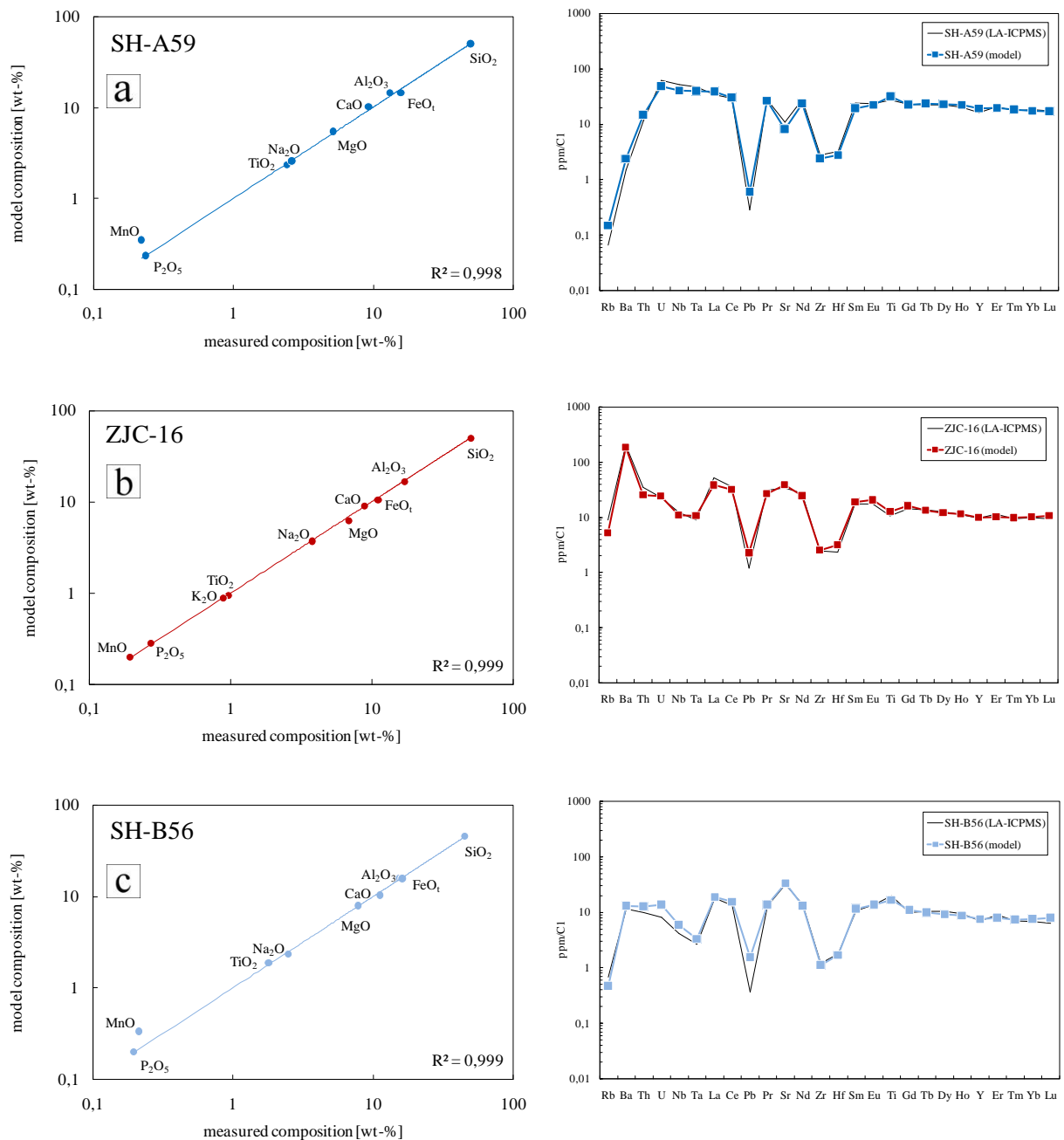
↑ **Figure 4.13 a (previous page)** Quantitative comparison of measured and modeled major and trace element compositions of the pristine Shuanghe eclogite (SH-A59). Modeled modal abundances in [wt-%]: allanite 0.3, apatite 0.6, rutile 2.3, omphacite 37, garnet (pristine) 49, quartz 10, albite 0.5, hornblende 0.5. **b** Quantitative comparison of measured and modeled major and trace element compositions of the retrograded Zhujiachong eclogite (ZJC-16). Modeled modal abundances in [wt-%]: clinozoisite 1.0, zoisite 2.5, phengite 8, paragonite 2, barroisite 1, hornblende 20, apatite 0.7, rutile 0.85, omphacite 25, garnet (pristine) 16, garnet (retrograded) 8, quartz 4, albite 11. **c** Quantitative comparison of measured and modeled major and trace element compositions of the retrograded Shuanghe eclogite (SH-B56). Modeled modal abundances in [wt-%]: allanite 0.1, clinozoisite 2, phengite 0.4, barroisite 20, hornblende 5, apatite 0.5, rutile 1.8, omphacite 21, garnet (pristine) 38, garnet (retrograded) 9, quartz 2, albite 0.5.

Vein modeling is done for both type I and type II 2nd generation veins. Modeling of 1st generation veins is renounced due to their simple qtz + rt + zrn mineralogy. Their element inventory is restricted to Si and HFSE, which the latter are entirely controlled by accessories that cannot be satisfyingly estimated. Modeling of 3rd generation veins is omitted, as they contain almost exclusively albite and quartz, that both contain a negligible trace element inventory. These late retrograde veins furthermore formed at comparatively shallow (amphibolite-facies) levels are not expected to contribute to deep-fluid rock element exchange.

Major element modeling of the different 2nd generation veins (**Figure 4.14**) reveals that the amphibole- and epidote/clinozoisite-rich type II veins are about of basaltic/eclogitic composition, whereas qtz-, phe-, zoi- and ky-dominated type I veins plot within the dacitic field.
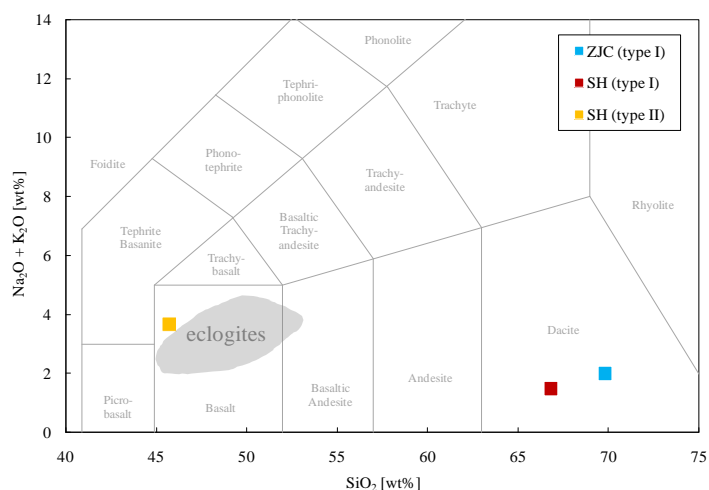
← **Figure 4.14** Modeled major element compositions for type I and type II 2nd generation veins. Type II veins resemble about basaltic (eclogitic) compositions in terms of total alkali vs silica, whereas type I veins are extremely felsic and plot within the dacitic field.
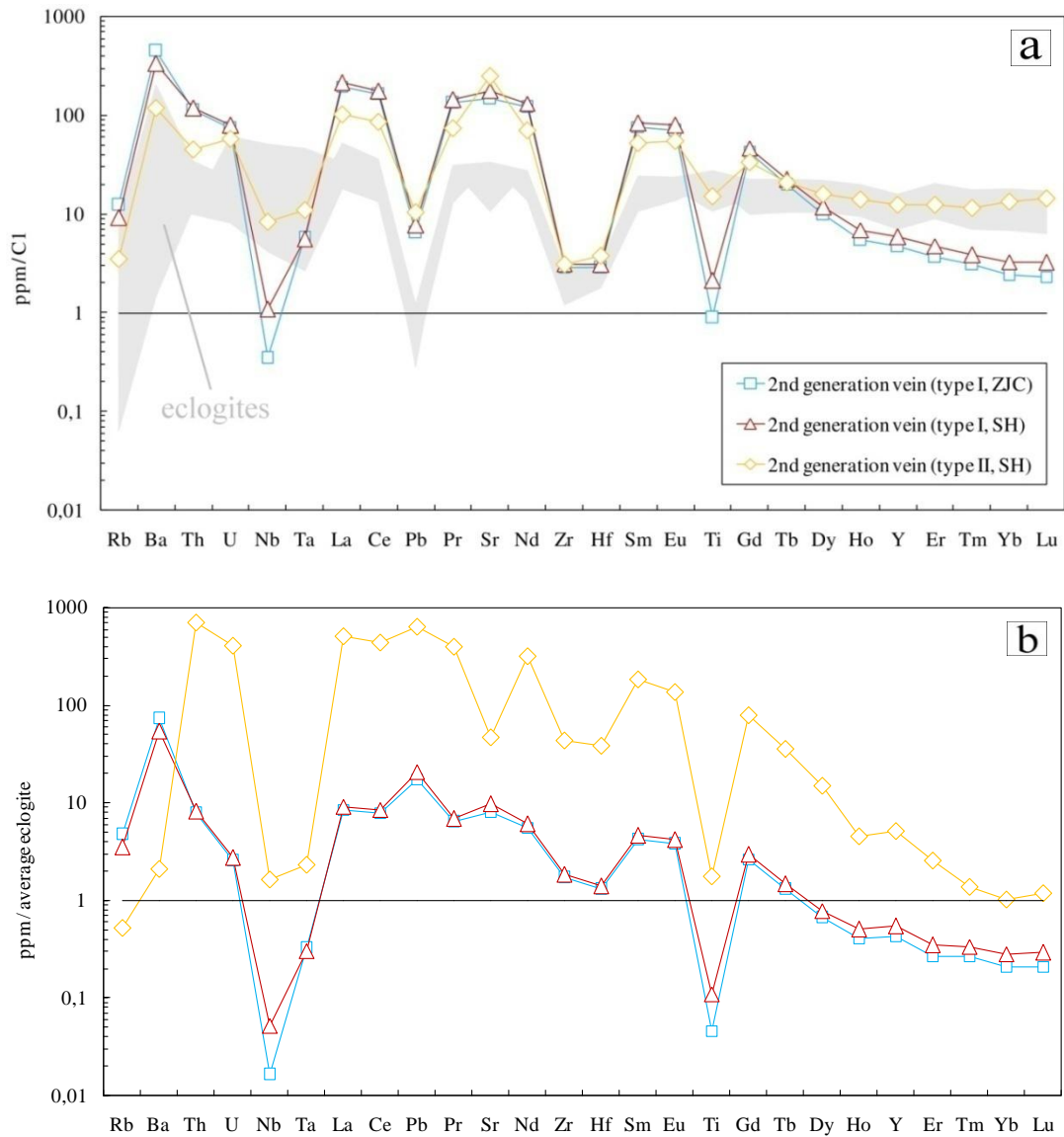
modal abundance	[wt-%]
zoisite	0.15
phengite	0.2
paragonite	0.05
amphibole	0.05
apatite	0.001
zircon	0.00001
quartz	0.5
kyanite	0.05
sum	1.001

modal abundance	[wt-%]
zoisite	0.15
clinozoisite	0.035
epidote	0.01
phengite	0.15
amphibole	0.05
apatite	0.007
rutile	0.001
zircon	0.00001
quartz	0.5
kyanite	0.1
sum	1.003

modal abundance	[wt-%]
allanite	0.001
clinozoisite	0.19
epidote	0.15
phengite	0.05
amphibole	0.5
apatite	0.05
rutile	0.01
quartz	0.05
sum	1.001

↑ **Figure 4.15** Modeled trace element compositions of type I and type II 2nd generation veins from Zhujiachong and Shuanghe, and chosen modal mineral contents. **a** Normalized to C1 (MCDONOUGH & SUN, 1995), **b** normalized to the average of all investigated eclogites. A general enrichment of most trace elements in veins (except for M-/HREE) can be reliably modeled. This observation is basically not changed for varying model parameters in a range of +-5%. The HFSE inventory, however, is very sensitive with respect to the assumed modal content of accessory rutile, and cannot be regarded as reliable.

106

Modeled vein trace element compositions (**Figure 4.15a,b**) consistently demonstrate that 2nd generation veins accumulate most trace elements, especially LREE and LILE, relative to the host eclogites. HFSE and M-/HREE are depleted, except for the ep/czo-rich type II vein. A reliable reconstruction of HFSE contents is not possible, since HFSE are solely controlled by accessory rutile. The chosen model assumptions of 0, 0.1 and 1.0 wt-% rutile display a resulting range of more than one order of magnitude in Ti, Nb and Ta contents - a modal rutile content of 3 wt-% would already lead to a relative HFSE enrichment against the bulk eclogites.

4.3.4   Strontium and lead isotopic signatures

$^{87}Sr/^{86}Sr$ characteristics of bulk eclogites and minerals

Measured $^{87}Sr/^{86}Sr$ isotopic compositions of Dabie eclogites and both vein and eclogite minerals were recalculated to 230 Ma, which is equivalent to the earliest expected time of vein formation, namely the metamorphic peak. They consistently fall on a narrow range between 0.704-0.707, except for enriched mica (0.708 paragonite, 0.718-0.745 phengite) (**Figure 4.16a**). Gneissic rocks from Dabieshan are in contrast enriched in ^{87}Sr (0.711-0.745). A comparison of ZJC, SH and BX eclogites from this study and from literature reveals that the most pristine samples have the lowest $^{87}Sr/^{86}Sr$, whereas the ratios significantly increase for retrograded samples (**Figure 4.16b**).

Since phengite is the major carrier of Rb in the investigated lithologies (cf. Figure **4.12e**), the ^{87}Sr enrichment in gneisses is attributed to high mica contents in gneiss, as supported by a positive correlation of Rb/Sr and $^{87}Sr/^{86}Sr$ (**Figure 4.17**). This correlation conceptually forms an isochrone, indicating that the vein-forming fluids did not influence the Sr isotopic composition of the initial eclogite source, which is likewise evident from the narrow range of isotopic compositions (0.7040-0.7065) for both vein minerals and eclogites, as presented in **Figure 4.16a**. The deviation of $^{87}Sr/^{86}Sr$ of two phengites (0.730 and 0.744) from the common, lower values are likely explained by inheritance from the gneissic host rock or partial disturbance by gneiss-derived fluids.
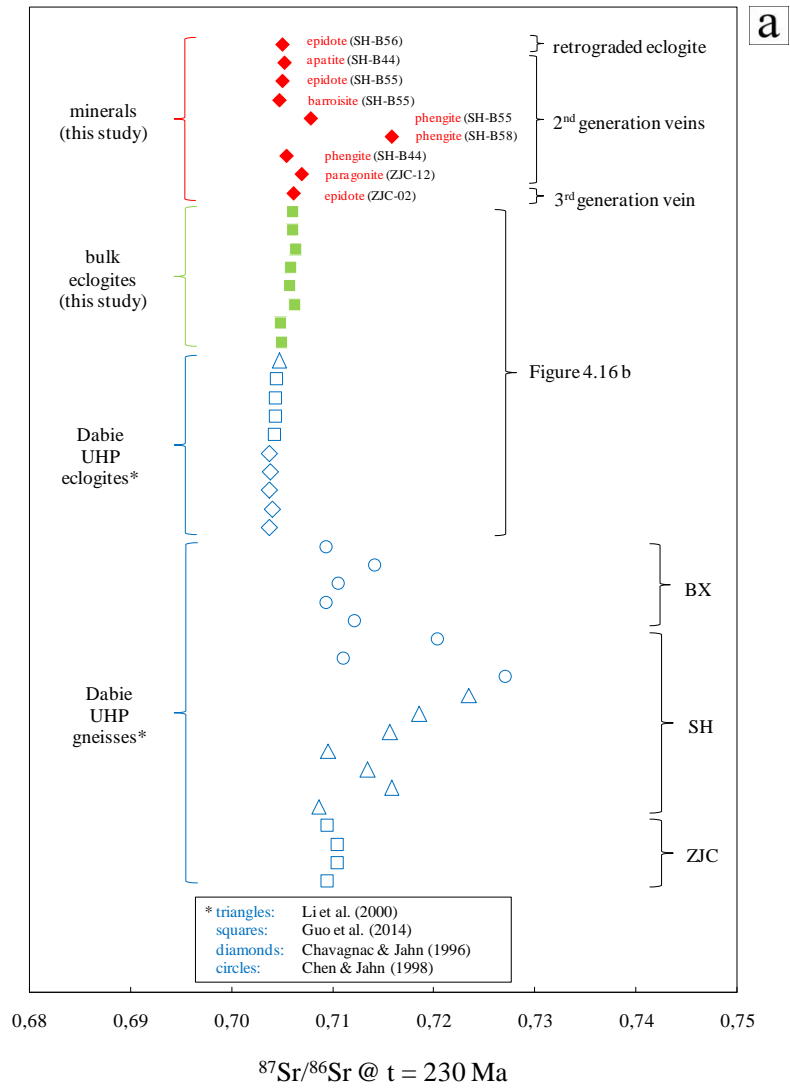
↑ **Figure 4.16 a** Comparison of $^{87}Sr/^{86}Sr$ recalculated to the expected, earliest time of vein formation (230 Ma, after LI ET AL., 2000) isotopic compositions of Dabie eclogites from this study with literature data for the same locations (ZJC, SH, BX). Errors (2σ) within symbol size.
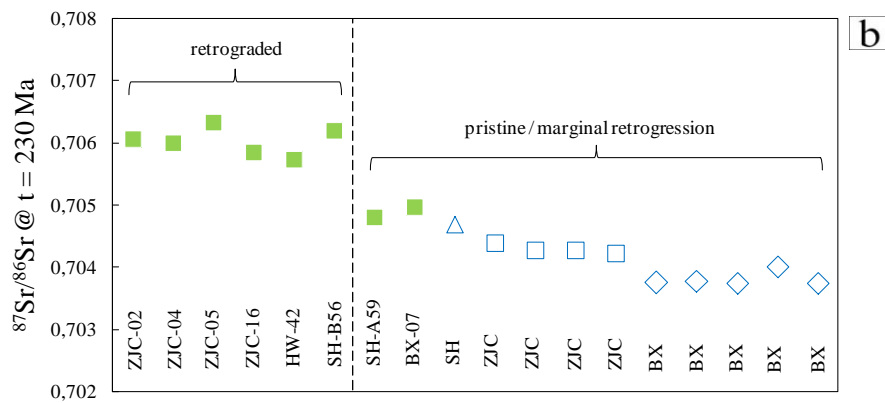
↑ **Figure 4.16 b** Enlarged section of figure 4.16a. Errors (2σ) within symbol size.
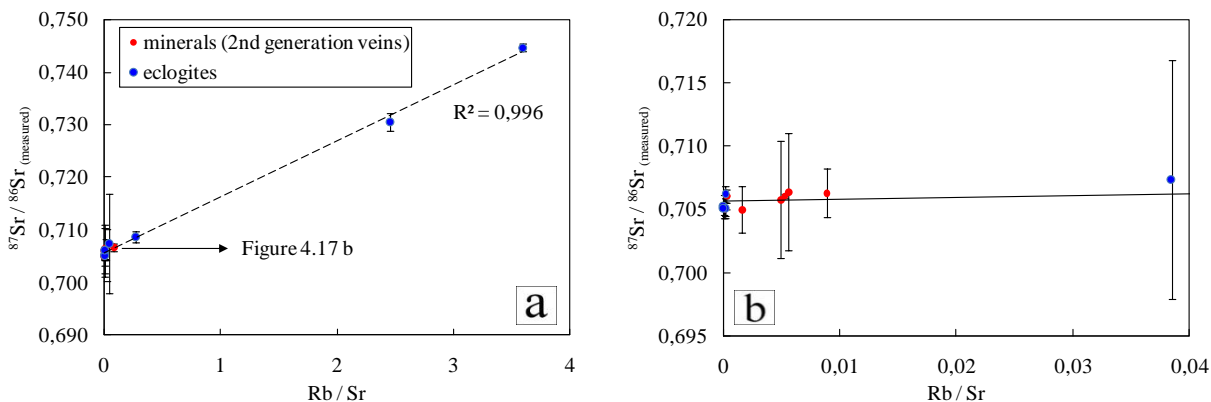
↑ **Figure 4.17** The correlation of $^{87}Sr/^{86}Sr$ and Rb/Sr demonstrates that the sources of veins and eclogites do not differ in their isotopic composition, or in other words that vein formation does not influence the Sr isotopy.

$^{206,208}Pb/^{204}Pb$ characteristics of bulk eclogites

Pb isotopic ratios were determined in order to evaluate whether HP/UHP fluid-rock interaction during continental subduction has the potential to contribute to the HIMU signature as observed in some OIB type basalts. These basalts have a strongly radiogenic Pb-composition.

A comparison of eclogites from this study with a compilation by STRACKE ET AL. (2005) clarifies that both pristine eclogites and residual eclogites after fluid-rock interaction are not appropriate candidates for a HIMU source (**Figure 4.18a,b**). In contrast to retrogressed eclogite samples, pristine eclogites (BX-07 and SH-A59) show the most radiogenic Pb signatures, as well as the least radiogenic Sr signatures. Pristine eclogites fall into the isotopic arrays of MORB (BX-07) and OIB (SH-A59) towards enriched compositions, whereas retrogressed eclogites plot far off the common basaltic systematics towards enriched $^{87}Sr/^{86}Sr$ and extremely low ($^{206}Pb/^{204} < 17.1$; $^{208}Pb/^{204}Pb < 37.6$) radiogenic lead signatures, indicating that HP/UHP metasomatism significantly shifts eclogitic isotope characteristics towards "opposite" HIMU compositions.

Eclogitization instead, does apparently not affect the Pb-Sr isotopic composition of a subducted basalt, since own data of pristine eclogites as well as literature data define a field for Dabie UHP eclogites that widely matches the field of the expected source MORBs (**Figure 4.18c**). The figure furthermore illustrates that the retrogression of eclogites raises the $^{87}Sr/^{86}Sr$ and lowers the $^{206}Pb/^{204}Pb$, what might
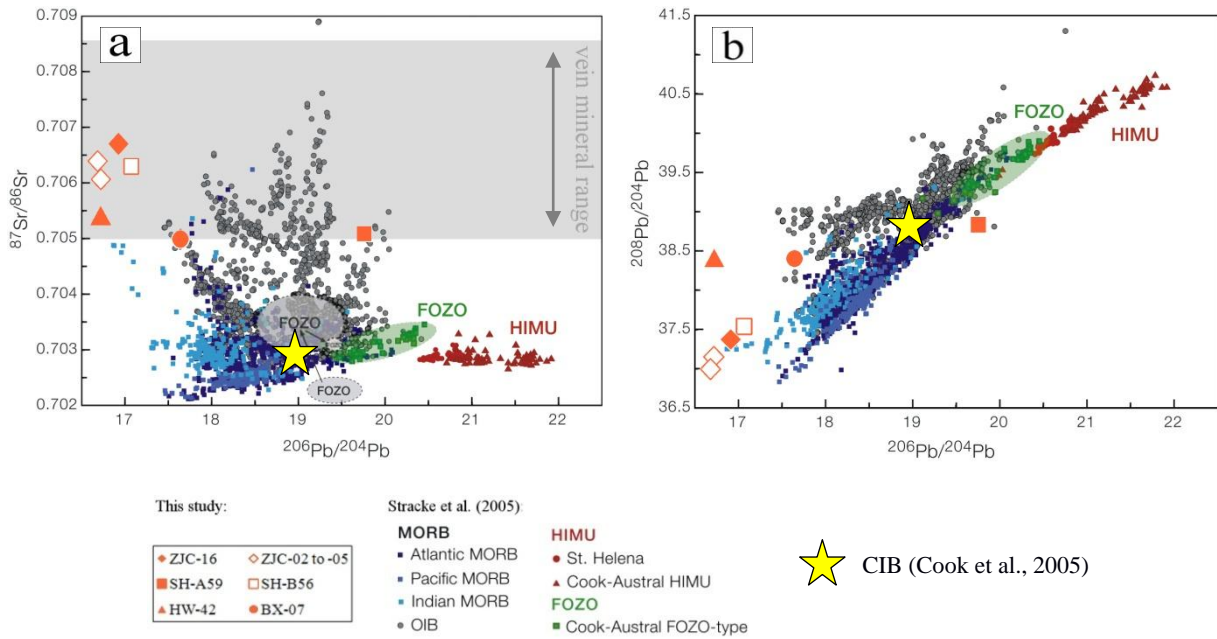
↑ **Figure 4.18 a, b** Measured $^{206}Pb/^{204}Pb$ vs. $^{87}Sr/^{86}Sr$ and measured $^{206}Pb/^{204}Pb$ vs. $^{208}Pb/^{204}Pb$ of pristine and retrograded Dabie bulk eclogites in comparison with MORB and (HIMU-) OIB compiled by STRACKE ET AL. (2005) and continental intraplate basalts (CIB) after COOK ET AL., (2005). Pristine samples (SH-A59, BX-07) plot within the isotopic arrays of MORB/OIB, whereas retrogressed eclogites after fluid-rock interaction plot far off the common basaltic systematics towards moderately enriched $^{87}Sr/^{86}Sr$ compositions along with extremly unradiogenic Pb characteristics. This indicates that in both eclogitization and fluid-driven retrogression are capable of shifting the isotopic composition of a subducting basalt.
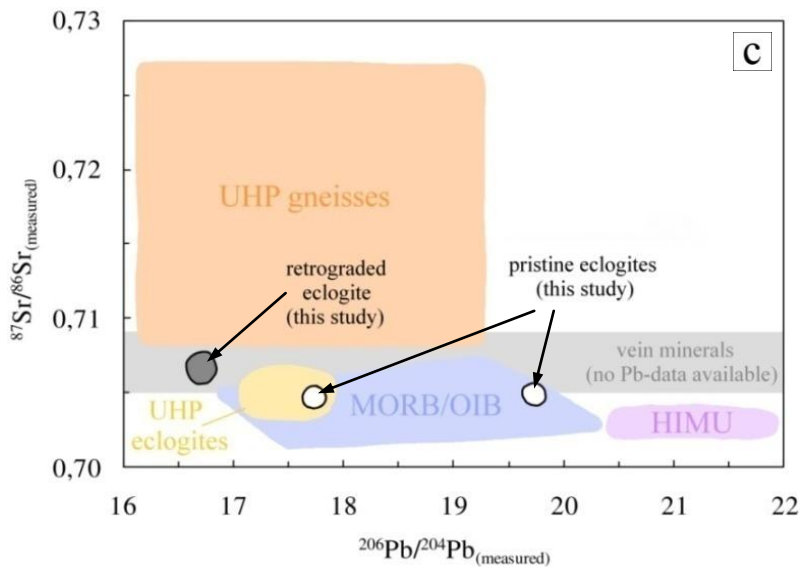
↑ **Figure 4.18 c** Schematic comparison of Pb- and Sr-isotopic compositions of this study (errors mainly within field sizes) with literature data on Dabie UHP gneisses and eclogites (ZHANG ET AL., 2002) and MORB, OIB and HIMU sources (STRACKE ET AL., 2005), suggesting a "gneissic influence" during retrogression and vein formation.

be explained by a geochemical interaction with the surrounding UHP gneisses. The vein minerals accordingly show a Sr-isotopic range that matches the field of retrograded eclogites, strongly linking retrogression and vein formation.

4.3.5 Element partitioning in eclogite and vein minerals

Variation plots for element ratios of interest are utilized to assess element partitioning in all investigated minerals (**Figure 4.19**).

The budget of Nb and Ta is controlled by accessory rutile. Other minerals have negligible, mostly subchondritic, Nb contents compared to about several 100 times C1-enrichment in rutile. A significant range of Nb/Ta ratios from subchondritic (13.66) to superchondritic (24.65) implies a certain fractionation to occur in rutile. Garnet analyses with Nb > 1 ppm are assumingly distorted by tiny rutile inclusions.

Zr and Hf is controlled by zircon, rutile, epidote/clinozoisite, barroisite and garnet. The contribution of omphacite and mica is negligible. While omp, brs, ep/czo, grt and most rt have subchondritic ratios, accessory allanite, zircon and two rutiles are (super-)chondritic. Bulk eclogite ratios consequently plot intermediate. It is noteworthy to mention that the two rutiles with the highest Zr/Hf ratios originate from retrogressed eclogite (ZJC-16: 43.8, ZJC-56: 51.2), whereas rutiles from pristine samples have the lowest ratios (BX-07: 18.3, SH-A59: 19.9). All other rutile analyses plot variably intermediate.

U/Pb and U/Th exhibit similar characteristics that display zircon and epidote/clinozoisite to constitute the controlling phases in a host rock. With U concentrations <1 ppm, garnet and omphacite as the major components of eclogite contribute little to the element inventory if ep/czo or zrn are present. Bulk eclogite compositions are superchondritic with the highest ratios observed in epidote-free pristine rocks (where garnet and zircon dominate the U-Th-Pb inventory), in contrast to retrogressed rocks that rather reflect the ratios of epidote/clinozoisite. Rutile analyses have errors near 60% and are suspected to be distorted by contamination with zircon. Note that U can be used as a proxy for epidote/clinozoisite composition (cf. **Figure 4.12b**) and the highest U contents correspond to allanite, whereas the lowest represent epidote.
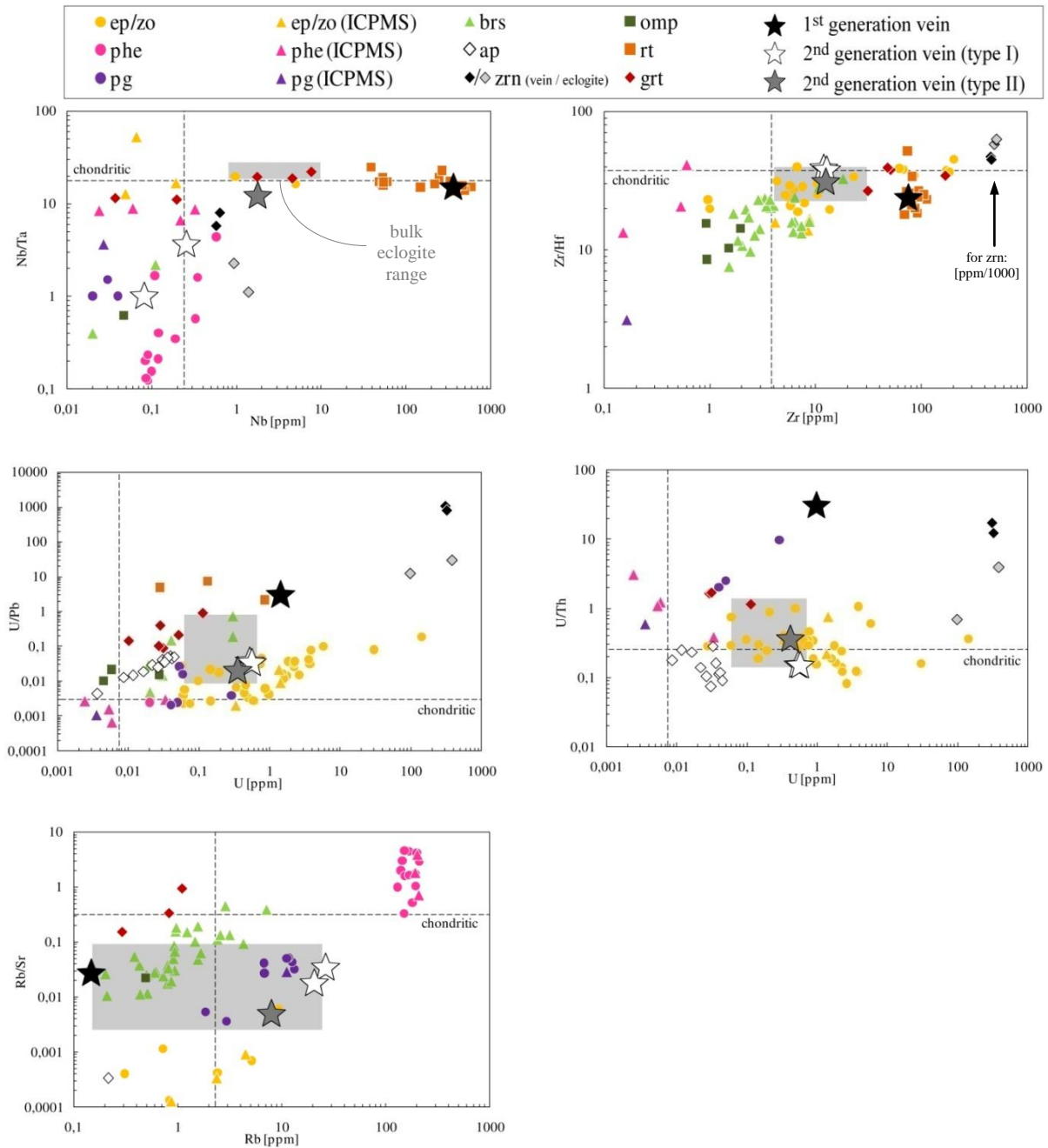
↑ Figure 4.19 Variation plots for selected element ratios in different minerals (in-situ LA-ICPMS analyses) in comparison with chondritic values (dashed lines, after MCDONOUGH AND SUN, 1995) and compositional ranges of investigated bulk eclogite samples (**Figure 4.7**). A distinction of vein and eclogitic minerals is renounced for clarity. Most analyses represent vein minerals and systematic differences between vein and eclogites could not be identified, except for rutile (cf. **Figure 4.20**), and for zircon. Concentrations well below 1 ppm are afflicted with high errors. Note that ratios with Gaussian errors[‡] exceeding 60% are not presented. Some additional ICPMS analyses of mineral separates (epidote/clinozoisite, phengite, paragonite) were performed in order to provide data for low concentrations. Stars mark bulk vein ratios as modeled above (cf. **Figure 4.15**), widely matching the eclogite fields. Modeled eclogites (not depicted) also match the fields.

[‡] ratio error $\frac{A}{B} = \sqrt{(\frac{\sigma_A}{conc_A} \cdot 100)^2 + (\frac{\sigma_B}{conc_B} \cdot 100)^2}$

The Rb and Sr inventory of a host rock is controlled by omphacite and garnet, in case no mica is present. Low Rb concentrations <1 ppm in grt and omp become superimposed, if paragonite and phengite occur, as it is especially the case for the retrogressed eclogites. While paragonite shows subchondritic ratios and moderate Rb contents, similar to those of grt and omp, phengite is apparently capable to distinctly fractionate Rb from Sr towards superchondritic values (and thus also to produce highly radiogenic compositions with time) and simultaneously exhibits Rb concentrations that are almost three orders of magnitude higher than for grt and omp.

It is obvious from **Figure 4.19** that the trace element budget of the investigated rocks is dominated by phengite (Rb-Sr), epidote/clinozoisite/zoisite (U-Pb) and the accessory phases rutile (Nb-Ta, Zr-Hf), zircon (U-Pb/-Th), and allanite (U-Pb). These phases contain by orders of magnitude the highest element concentrations and can, in part, fractionate the element ratios of interest: phengite fractionates Rb/Sr to superchondritic values, zircon fractionates Zr/Hf, U/Pb and U/Th towards superchondritic, epidote group minerals fractionate U/Pb to superchondritic ratios (aln > zo/czo > ep, cf. **Figure 4.19**), and rutile fractionation occurs both towards super- and subchondritic values. Zr/Hf ratios in vein zircon are higher than in zircon from (fluid-affected) eclogites, whereas U/Pb, U/Th and Nb/Ta ratios behave vice versa.

An analogous observation applies for rutile (**Figure 4.20**): fluid-affected eclogites and the rutiles therein (rutile can be assumed to determine the whole rock Nb-Ta budget, cf. **Figure 4.19**) are clearly superchondritic in Nb/Ta, whereas rutiles from pristine eclogites show the lowest, subchondritic and sub-continental crust ratios. Vein rutiles from 1st and 2nd generation veins show variable and intermediate, but always subchondritic, Nb/Ta values. It is obvious from these observations that deep fluid-rock interaction influences the HFSE budget of a rock towards superchondritic values.

It is noteworthy to mention that rutile from pristine eclogites (SH-A59, BX-07), 1st generation veins (SH-A60) and early 2nd generation (type I) veins (ZJC-10, SH-C58) have on average higher Nb contents (149–588 ppm, Ø 360 ppm) than rutile from late (type II) 2nd generation veins and retrograded eclogites (39–387 ppm, Ø 134 ppm). This correlation may indicate that relatively later, retrograde fluid rock interaction at lower pressures does not significantly change the fractionation of

Nb and Ta (Nb/Ta for the respective lithologies is similar), but that higher pressures mobilizes higher amounts of HFSE.
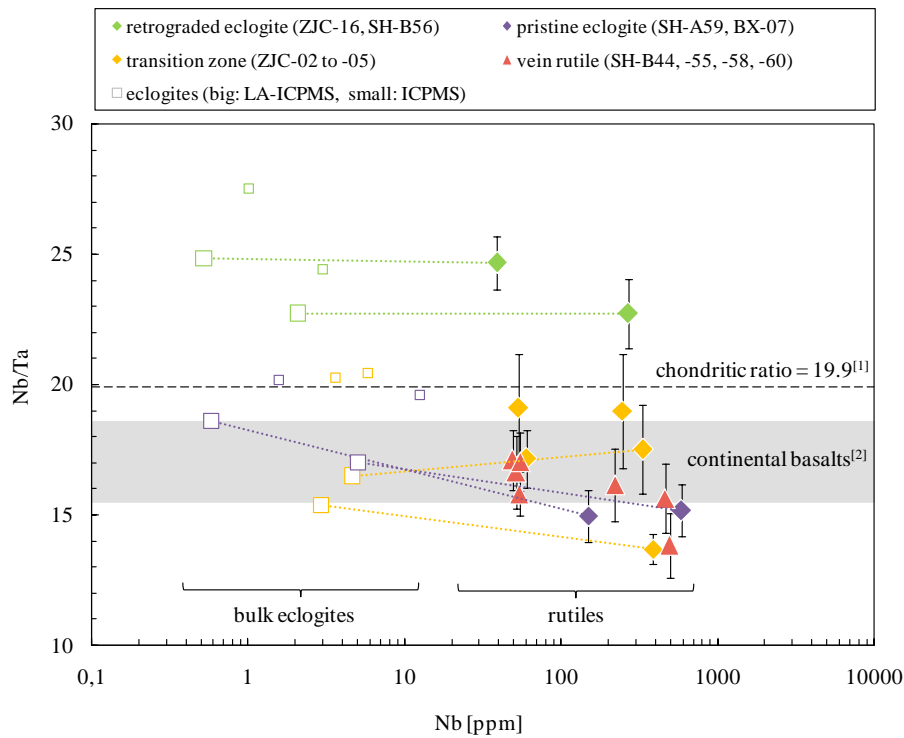
↑ **Figure 4.20** The nature of Nb/Ta fractionation in rutile depends on rock type. Retrograded eclogites (and rutile therein) show superchondritic Nb/Ta ratios, whereas Nb/Ta in pristine eclogite (and rutile therein) are subchondritic at the lower boundary of their precursor (continental basalt) field, implying that retrograde fluid-rock interaction influences the ratios. Rutile from 1st and 2nd generation veins and the transition zone at ZJC show variable subchondritic ratios in the basaltic field, but generally higher than in pristine samples. Solution ICPMS analyses of bulk eclogites are suspected to be systematically biased towards high Nb/Ta values, due to adhesive retention of Ta in teflon vessels during sample preparation. To avoid this effect, LA-ICPMS analyses were additionally performed on glassy beads, prepared as described in PACK ET AL. (2010). [1]MÜNKER ET AL. (2003) [2]PFÄNDER ET AL. (2007).

4.4 Discussion

4.4.1 Multi-stage fluid flow in the Dabieshan continental subduction zone

Fluid source and scope of fluid activity

The range of samples investigated in this study suggest that the extent of retrogression and the occurrence of complex veins is tied to the composition of the subducting protolith. Vein formation and extensive retrogression is restricted to eclogites that contain hydrous minerals (phengite, epidote) in their prograde assemblage, and are thus expected to have more felsic compositions. This is at first evident by phengite and epidote inclusions observed in garnet and omphacite from ZJC and SH-B, in contrast to a lack of these prograde phases in eclogites from SH-A and BX. Higher alkali contents in retrograde affected eclogites compared to pristine samples and the supposed intraplate basaltic protolith (**Figure 4.21**) support this conclusion and imply an additional felsic source component to these eclogites' protoliths prior to eclogitization.
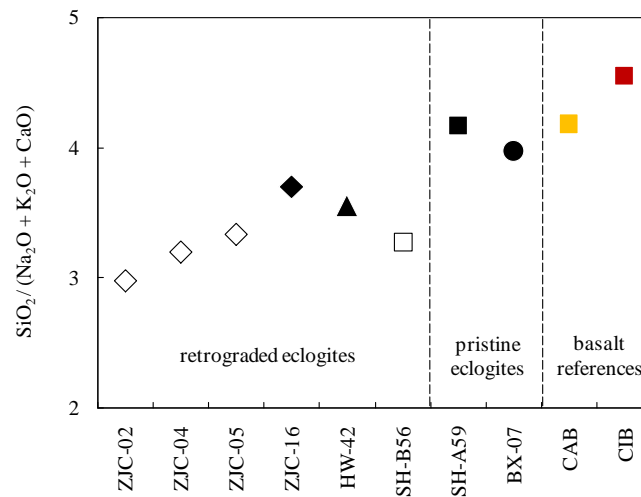
↑ **Figure 4.21** Alkali contents in pristine samples SH-A and BX and reference basalts are lower than in eclogites that experienced retrogression. The highest alkali contents are observed in ZJC and SH-B eclogites, that represent the eclogites with the most profound retrograde features. The compositional similarity of the pristine eclogites with the CIB and CAB references as the expected precursor rocks, in combination with prograde ep/czo and phe inclusions in eclogitic phases of retrogressed eclogites imply an alkali-enrichment of eclogite precursors prior to eclogitization.

115

Assuming the subduction of a chemically homogeneous basaltic block, the similarity of the expected Dabie eclogite protolith (CAB and CIB) compositions with the most pristine samples (BX and SH-A) in terms of SiO_2 vs. $K_2O + Na_2O + CaO$ suggests alkali-enrichment in retrograded samples during, or prior to, subduction. This is in accordance with BEINLICH ET AL. (2010) and BROVARONE ET AL. (2014), who describe extensive Ca-metasomatism and related formation of lawsonite in basaltic rocks during eclogitization of oceanic crust. They conclude that adjacent serpentinite, as well as metamafic and metasedimentary rocks are probable fluid and element sources for the observed metasomatism that extends for several tens of meters.

In case of Dabieshan serpentinites are not eligible, but felsic gneisses as well as metasedimentary units in which the eclogites are embedded, come into question as well. The sample ZJC-16 has been taken about 10 m away from the margin towards the host gneiss. For SH-B56 the distance is not known, but considering the geology (the intercalated eclogite bodies at Shuanghe are not wider than 50 m) it can be expected to be in the range of tens of meters.

It is thus proposed that high-Ca fluids were released in the host gneisses during subduction-dehydration and that these fluids resulted in the prograde and pervasive formation of metasomatic epidote group minerals (eg. lawsonite) and phengite in the basaltic bodies prior to or during eclogitization. Since pervasive fluid transport is assumed not to exceed distances of several tens of meters, the metasomatic formation of hydrous minerals can be expected to occur heterogeneously in the basalt, ie. preferentially along zones of enhanced fluid flow. Such as fault zones or at the eclogite-gneiss lithologic contact. In this regard, XIAO ET AL. (2000) supportingly reported that retrograded (eg. amphibolitized, phengite- or epidote-bearing) eclogite mainly developed at the margins of the Bixiling eclogite complex, whereas the majority of pristine (omphacite + garnet + quartz-) eclogites occurs in the central part of the complex.

The prograde lawsonitization enables the transport of water and trace elements to great depths. The retrograde, decompressional destabilization of lawsonite in turn results in the formation of zoisite/clinozoisite in the retrograded eclogites, and 'excess water' from the lawsonite breakdown reaction is channelized to precipitate the observed, early retrograde, 2nd generation vein systems. This

scenario also provides an explanation for the chemical consistency of most vein and eclogite minerals, speaking for a local derivation of the retrograde vein-forming fluids that were originally inherited from prograde gneiss dehydration.

Initial Sr isotope compositions in vein phengite and retrogressed eclogites at the expected, earliest time of vein formation are consistently higher than in pristine samples (**Figure 4.16b**), supporting the assumption that the fluids responsible for vein formation were initially derived from the high-^{87}Sr/^{86}Sr gneissic host rocks.

As suspected in **Chapter 3**, the formation of ALN/CZO and ZO-rich retrograde veins is well explained by breakdown of lawsonite, providing sufficient water and trace elements. This is in accordance with GUO ET AL. (2013), who concluded the former existence of lawsonite by mass-balancing a prograde, Sr and LREE-poor epidote generation (Sr: 990–1890 ppm, La: 60–110 ppm) that is assumed to have formed in equilibrium with lawsonite, and a retrograde, trace element-rich epidote generation (Sr: 7200–10300 ppm, La: 160–1300 ppm), interpreted to have grown after lawsonite.

Epidote IN (Ø Sr: 2008 ppm, Ø La: 5 ppm) and ALN/ZO/CZO (Ø Sr: 7881/6819/5860 ppm, Ø La: 2805/312/105 ppm) from this study correspond well to the mineral stages described by GUO ET AL. (2013) in terms of both petrography and chemistry. This leads to the analogous conclusion of former lawsonite existence, although this cannot be verified by direct petrographic evidence. CASTELLI ET AL. (1998) and LI ET AL. (2004) supportingly reported indirect petrographic evidence in the form of suspected lawsonite pseudomorphs for Zhujiachong.

Different fluid pulses recorded by compositional zoning in epidote group minerals and garnet

As evident from structural and petrographic observation discussed in **Chapter 3**, the eclogite–vein systems from Shuanghe and Zhujiachong record various stages of fluid circulation, related to the peak stage and three different retrograde stages. The earliest fluids, corresponding to 1st generation veins, are suspected to be progradely inherited from an dehydrating eclogite (LI ET AL., 2001). They

represent a melt-like and silica rich remnant of complete dehydration of ± 'dry' eclogite and precipitated quartz, rutile and zircon without triggering retrogression in the host eclogite. This is in good agreement with the experimental study of RYABCHIKOV ET AL. (1996), who reported silica-rich and Ti-bearing hydrous melts in equilibrium with garnet, omphacite and quartz at UHP conditions.

Compositional zoning in epidote (**Figure 4.12a-c**) reflects multiple changes of fluid composition and/or ambient conditions during the formation of 2nd generation veins. Since epidote group minerals are stable over a wide range of subsolidus conditions (POLI AND SCHMIDT, 2002, 2004), each mineral generation reflects vital information on fluid composition and ambient conditions (ENAMI ET AL., 2004; FEINEMAN ET AL., 2007; MATTINSON ET AL., 2004).

Epidote inclusions in omphacite and garnet (IN) are the earliest mineral generation observed in this study. The overall low trace element contents, especially in LREE (despite ambient conditions during formation comparable to that of CZO/ZO), are attributed to a preferential partitioning of these elements into coexisting lawsonite or allanite during prograde growth (MARTIN ET AL., 2011), as consistently also reported for a Dabie UHP eclogite by GUO ET AL. (2014).

Texturally early allanite mineral cores (ALN) and mineral mantles (CZO) share similar features, including variable iron contents that apparently depends on the locality (higher Fe-contents at Shuanghe compared to Zhujiachong), along with the highest Sr and REE concentrations and coinciding REE patterns. Inclusions of garnet and omphacite in CZO (**Figure 3.1g**) imply that CZO grew within the eclogite-facies stability field. According to GUO ET AL. (2012, 2013) clinozoisite cores and mantles with high trace element contents are likely metamorphic reaction products after lawsonite, with estimated formation conditions of 2.9 GPa at 670°C that are related to lawsonite breakdown at the onset of exhumation. Oscillatory zoning patterns in CZO (**Figure 4.12b**) indicate that the availability of trace elements in the HP fluid fluctuated. A theoretical mechanism to explain these patterns remains unclear, but it is conceivable to be related to a complex and episodic interplay of successive lawsonite decomposition (delivering trace elements and water) and simultaneous crystallization of CZO (consuming trace elements and less water compared to lawsonite).
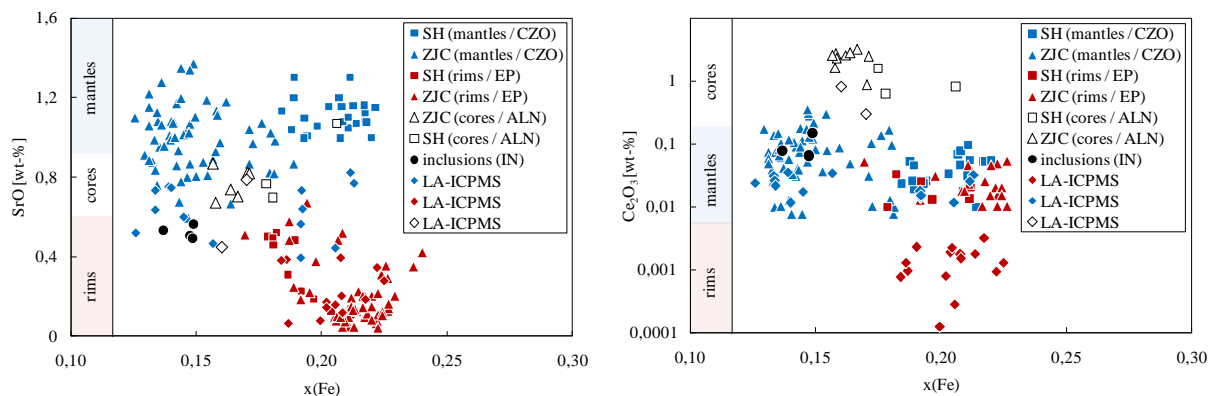
↑ Figure 4.22 Fe content vs. Sr anf Fe vs. Ce contents in compositionally zoned epidote group minerals (EMP analyses) for samples ZJC-02 and SH-B56, and in epidotes from all samples (LA-ICPMS analyses), displaying that mineral cores and mantles have higher Sr and REE contents compared to the rims. Zoisites plot beyond scaling at about 0.05 x(Fe) and show intermediate (mineral mantle-like) Ce and Sr. Note that most mineral rim EMP-analyses (EP) are below the detection limit of ~100 ppm, and the remaining plotted analyses are likely biased towards high Ce_2O_3 contents. x(Fe) = Fe / (Ca+Fe+Al)

The general decrease of Sr and Ce in CZO towards mineral rims (**Figure 4.12c, 4.22**) may be attributed to decreasing fluid mobility of these elements due to decreasing pressures (NAGASAKI AND ENAMI, 1998) and temperatures (FEINEMAN ET AL., 2007; MARTIN ET AL., 2011). Since CZO crystallization is ascribed to the limited eclogite facies P-T range, a successive element consumption of the element load provided by lawsonite breakdown by incorporation into CZO is, however, the preferable explanation. The overall alike trace element patterns for ALN, ZO and CZO that solely vary in absolute concentrations (**Figure 4.12b**), as well as the lack of another trace element sink (eg. a mineral with increasing trace element concentrations towards the rim, or a newly forming retrograde high trace element mineral) support the consumption scenario.

The significantly lowest trace element contents of texturally late epidote (EP), forming mineral rims (**Figure 4.12a-c, 4.22**), small idioblasts in 2nd generation veins and diffusive reaction zones along microcracks (**Figure 4.12c**, yellow arrows) along with clearly distinct REE patterns compared to ALN and CZO are evident for a different fluid composition during a late retrograde stage, that could not evolve from successive fluid consumption and related CZO-precipitaiton alone. Textural equilibrium

of epidote and hornblende in ZJC samples implies an amphibolite facies formation of the late epidote. The underlying fluid is supposed to having low trace element contents, since the element mobility at LP/LT amphibolite facies conditions can be expected to be limited (NAGASAKI AND ENAMI, 1998). Supportingly, the compatibility of LREEs in zoisite decreases with decreasing temperature (FEINEMAN ET AL., 2007; MARTIN ET AL., 2011), what can be also reasonably expected for structurally similar epidote.

The relative depletion of LREE along with an enrichment of M-/HREE against the earlier epidote generations are accordingly interpreted to reflect epidote crystallization from a fluid with low element mobilities, during or after the retrograde and M-/HREE liberating (cf. **Figure 4.12a**) decomposition of garnet in the adjacent host eclogite.

The distinction between type I and type II 2nd generation veins as proposed in **Chapter 3** is supported by compositional zoning in epidote group minerals: zoisite in type I veins has the overall highest trace element contents and is assumed to form directly related to the breakdown of lawsonite, from an oversaturated fluid concerning Ca- and REE- contents and thus a constant element availability in the fluid. It can thus be expected to grow homogeneously, as likewise monitored in the investigated samples. Epidote group minerals in relatively later type II veins display both an internal lowering of element contents (in CZO), as well as an overall lowering (from ALN to CZO to EP) (**Figure 4.12b, c**). This is ascribed to both P-T decrease and consumption of the fluids' element load through the precipitation of veins and retrograde minerals in eclogite, both resulting in a decreased element activity (ie. availability) in the late retrograde fluid.

The sharp and continuous transition from euhedral ALN to CZO (**4.12b, c**) reflects CZO-crystallization at stability conditions of allanite, whereas resorbed CZO-EP margins imply discordant epidote growth. BUDZYN ET AL. (2011) conducted an experimental study demonstrating that allanite stability is more dependent on the fluid composition and the ratio of silicate minerals than on the P-T conditions. They found that Ca-rich fluids promote allanite and REE-epidote (ALN, CZO and ZO in this study) growth, while lowering Ca and increasing Na destabilizes these phases in favor of epidote (EP). While ALN, CZO and ZO thus can be assumed to have precipitated early from a Ca-rich,

lawsonite-breakdown related fluid, the overgrowth with EP is associated to a distinctly later retrograde stage, when the vein-forming had become Na-enriched due to decomposition of omphacite and the successive incorporation of Ca into earlier epidote group minerals.

The compositional zoning in garnet (**Figure 4.8**) reflects prograde and retrograde (re-)crystallization by petrographic evidence and mineral chemistry and records both decompression and the involvement of a fluid phase. XIA ET AL. (2012) interpreted the increase in pyrope along with the decrease in grossular (**Figure 4.8c**) to be a response to decompression during initial exhumation, while temperatures increase until peak temperature is reached. In this regard, pristine garnet was formed during prograde metamorphism, and the retrograde garnet signature developed at the onset of exhumation, consequently triggered by the same, lawsonite-derived and Ca-rich fluid that precipitated the 2nd generation veins and caused pervasive retrogression. This is in accordance with the absence of retrograde garnet in SH-A, in contrast to the eclogites at SH-B and ZJC: the pristine SH-A (and also BX) eclogite does not show any evidence for the pre-peak existence of hydrous minerals, nor does it contain any retrograde mineral veins, displaying the virtual absence of retrograde fluid circulation.

Higher REE patterns for pristine garnet compared to retrograded (fluid-affected) garnet might be explained by garnet crystallization in the virtual absence of epidote group minerals. Partitioning of REE, and especially LREE into epidote minerals (cf. REE plot in **Figure 4.12b**) expectedly lowers the availability of REE during garnet growth. The observation of pristine garnet cores in retrograded eclogites suggests that garnet-fluid interaction occurred only after eclogitization, ie. garnet formation, supporting a timeframe around the onset of exhumation.

The two latest fluids, corresponding to 3rd generation veins, evolved at final stages of exhumation and are not discussed in detail since they are not expected to influence the element budget of potential mantle sources. They caused an amphibolite- and greenschist facies overprint and preferentially reactivated former HP/UHP 2nd generation veins and they are likely to be rich in Na (as reflected by albite formation) and generally poor in trace elements (as reflected by late epidote).

4.4.2   Element mobility during UHP/HP fluid – eclogite interaction

Element budget of UHP/HP vein formation in subducted continental basalts

Major and trace element characteristics of bulk eclogites confirm continental basalts to be the most probable precursors to all investigated eclogite samples (**Figures 4.3, 4.6**). Utilizing the fluid-mobile elements Sr and Ba as indicators for the degree of fluid-rock interaction in a rock, the eclogites from Bixiling (BX-07) and Shuanghe (SH-A59) are the least fluid affected, whereas the eclogites from Zhujiachong (ZJC-16) and Huwan (HW-42) experienced the most pronounced fluid-rock interaction (**Figure 4.4**), as likewise also monitored by petrographic evidence (increasing contents of hydrous amphibole and epidote, as well as retrograde reaction rims around peak eclogite phases).

Element mobilization and redistribution by a vein-forming fluid is monitored by compositional gradients towards the 3rd generation vein. Also the 3rd generation vein itself does mainly contain late retrograde albite and hornblende, relict HP-phengite within the vein points to the former existence, and thus an amphibolite-facies reactivation, of a former 2nd generation vein. This assumption is confirmed by the abundance of texturally early, zoned epidote group minerals (in textural disequilibrium with albite and likewise also found in 2nd generation veins) in the transition zone between vein and eclogite. The record of element mobilization in the transition zone can thus be regarded to also reflect the effects of a former 2nd generation vein in addition to effects of the late, low-pressure albite-hornblende vein.

Eclogite related major elements (K in phengite, Mg and Fe in garnet and omphacite) naturally decrease towards the vein, whereas the increase of Ca, Al and Na is well explained by metasomatic increase of epidote and plagioclase towards the vein (**Figure 4.5**). The enrichment of nominally fluid-immobile Ti, Nb, Ta and Zr in the transition zone displays a distinct mobility of HFSE in the fluid as well as a scope of fluid activity that is limited to ~50 cm. Fluid-mobile Sr, Pb, U and Th as well as nominally immobile La are enriched towards the vein, reflecting a metasomatic accumulation for LILE and LREE in the metasomatized eclogite in contact to the vein. Rb and Ba instead, are leached

from the transition zone which is attributed to the decomposition of phengite (KORH ET AL., 2009) and related chloritization during late, amphibolite facies retrogression.

The above described element mobilization related to the formation of 2nd generation veins is confirmed by quantitative trace and major element modeling of these veins (**Figures 4.14, 4.15**). Compared to the eclogites (both pristine and retrogressed), the models clearly show an enrichment of most trace elements (except for HFSE and M- to HREE) within the veins. For HFSE, this model is not usable, since the HFSE-budget is controlled by accessory rutile. The selective enrichment of HFSE in the Zhujiachong eclogite at the vein contact, however, implies a significant mobilization. This is also required by the HFSE discrepancy between eclogites and their precursors (**Figure 4.6c**).

Prograde to peak 1st generation quartz-rutile-zircon veins act as a sink for HFSE. Although the determination of rutile and zircon contents in these veins cannot be reliably modeled, the bulk analyses of the vein-bearing eclogite SH-A59 display a certain enrichment of Ti (**Figure 4.4**), Nb and U, pointing to an accumulation of rutile and zircon related to eclogite interaction with the peak fluid.

The models of type I and type II 2nd generation veins agree with the predicted genetic history as discussed in **Chapter 4.4.1** and **Chapter 3.4.3**. Type I veins that are linked to lawsonite breakdown at the onset of exhumation accumulated mainly SiO_2, CaO and Al_2O_3 and thus plot in the dacitic field in the TAS classification (**Figure 4.14**), whereas the relatively later type II veins are compositionally close to their basaltic host eclogites, speaking for a dominating local derivation (ie. scavenging) of their element load from their host eclogites. Trace element models support this interpretation as they show LREE enrichment over M- to HREE in type I veins in contrast to a general lowering of most trace elements, as well as decreased LREE/M-HREE ratios in type II veins. This is well explained by the before mentioned qualitative consumption of trace elements due to the early precipitation of type I zoisite-veins, since LREEs preferentially partition into zoisite (FEINEMANN ET AL., 2007; MARTIN ET AL., 2011).

HP/UHP vein formation and related retrogression in cold subduction zone eclogites can thus locally shift bulk rock chemistry towards Ca-metasomatized and trace element (LILE, LREE and also HFSE)

enriched compositions. The trace element composition of the pre-metamorphic eclogite precursors cannot be evaluated with any certainty, but the original source of the elemental load in the fluid is either an already altered (metasomatized) precursor, or the bedrock gneisses. In any case, the described metasomatized basalts and the enclosed veins represent therein are a major carrier of Ca, trace elements and water to great depths and may possibly transfer their enriched signatures to mantle sources.

The contribution of UHP/HP fluid-rock interaction to the niobium- and lead-paradoxa

As evident from **Figures 4.7**, **4.19**, and **4.20** fractionation of Rb/Sr, U/Pb and Nb/Ta is common in the investigated Dabie HP/UHP eclogites and veins. The minerals that control this fractionation are phengite (Rb/Sr), zircon and allanite/ zoisite/clinozoisite (U/Pb), and rutile (Nb/Ta). These phases (i) show fractionated ratios and (ii) have at least two orders of magnitude higher element concentrations (mainly between 100 and 1000 ppm) than all coexistent mineral phases, whose contributions to the respective element budget thus become negligible.

The occurrence of coarse-grained rutile in 1st and 2nd generation HP veins demonstrates that HFSE are mobilized by high-grade metamorphic fluids. Several studies found that Nb/Ta is fractionated by rutile, required that an aqueous fluid phases is present during rutile crystallization (eg. HUANG ET AL., 2012; JOHN ET AL., 2004; XIAO ET AL., 2006), whereas SCHMIDT ET AL. (2009) reported that eclogites without remarkable fluid-rock interaction basically retain their precursors Nb/Ta signatures. The present work confirms these observations and clearly identifies fluid-affected eclogites (and to a lesser extent also rutile-bearing 1st and 2nd generation veins) to be a potential superchondritic 'endmember' with respect to global Nb/Ta ratios (**Figure 4.20**), whereas eclogitization has apparently no influence on Nb/Ta, if fluids are absent. This is consistent with the study of BRENAN ET AL. (1994), who report $D_{Nb}/D_{Ta} > 1$ for rutile/fluid partitioning (which is in contrast to $D_{Nb}/D_{Ta} < 1$ between rutile and melts (KLEMME ET AL., 2005; SCHMIDT ET AL., 2004; XIONG ET AL., 2005), or likewise a higher fluid solubility of Ta compared to Nb as deduced by XIAO ET AL (2006). Rutile in equilibrium with such a

fluid would thus adopt an enriched Nb/Ta signature (>1), what is in agreement with the observed superchondritic ratios in metasomatized/fluid-affected eclogites and the respective rutiles.

The scope of the Nb/Ta-shifting fluid circulation is, in contrast to HUANG ET AL. (2012), distinctly wider than 20–50 cm, as reflected by superchondritic Nb/Ta (22.71) of rutile and bulk eclogite from ZJC-16. This sample has been collected about 10 meters away from any visible vein, but nevertheless showed pronounced retrogression, possibly related to pervasive retrograde fluid flow. Along with the similarity of eclogitic an vein minerals, this proves that channelized vein-forming fluids and pervasive fluids are genetically related.

Given that pristine eclogites resemble the initially subducted continental basalts in terms of Nb/Ta, and related metasomatized eclogites have strongly enriched Nb/Ta, there has to exist a complementary reservoir/component in term of a "residuum after fluid-rock interaction" (**Figure 4.23**) with a subchondritic Nb/Ta signature. This is consistent with the observation that the bulk silicate Earth has a deficit in niobium (niobium paradox), as illustrated in **Figure 4.1**, suggesting that UHP/HP fluid-rock interaction is a critical process to creating this global imbalance.
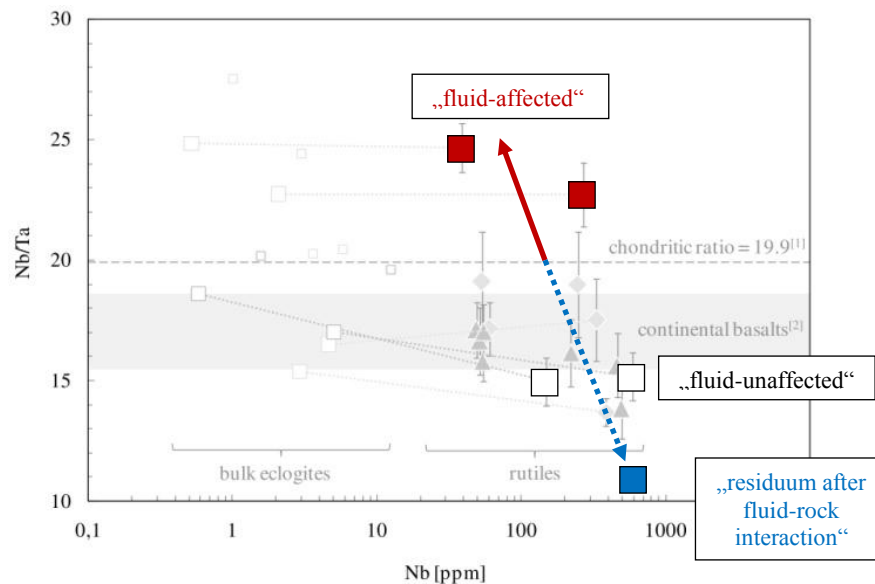

↑ **Figure 4.23** Conceptual model of Nb/Ta fractionation through high-pressure fluids. Assuming pristine eclogites to reflect their protolith Nb/Ta signatures, there should exist a complementary Ta-enriched, subchondritic reservoir that is related to the residual fluid after fluid-rock interaction.

Metasomatized eclogites are in turn a clearly superchondritic component that should be considered to theoretically balance the crustal Nb-deficit, although they apparently escape the continental crust magmatic sources and a large-scale residence in the crust/mantle is so far not located.

Isotopic signatures of bulk eclogites demonstrate that HP/UHP fluid-rock interaction has the potential to profoundly alter the Sr and Pb isotopic compositions of a subducting basalt (**Figure 4.18**). Pristine eclogites plot within the typical OIB range that is consistent with continental basalts, and are thus virtually not affected by eclogitization alone. Bixiling and Shuanghe eclogites plot towards the enriched ends of different isotopic arrays, implying different types of protoliths. All eclogites that experienced fluid-rock interaction plot far off the range of considered precursor rocks, in a comparatively narrow field towards extremely unradiogenic $^{206}Pb/^{204}Pb$ and highly radiogenic $^{87}Sr/^{86}Sr$ ratios.

This is well explained on a mineral chemical basis, considering that gneissic fluids are the initial source of metasomatism-retrogression and add phengite and epidote group minerals to a host basalt/eclogite. Phengite fractionates Rb over Sr and produces highly radiogenic compositions with time, relative to unmetasomatized rocks (CIB) (**Figure 4.24a**). Epidote group minerals in turn fractionate Pb over U relative to CIB (**Figure 4.24b**), resulting in comparatively less radiogenic compositions.
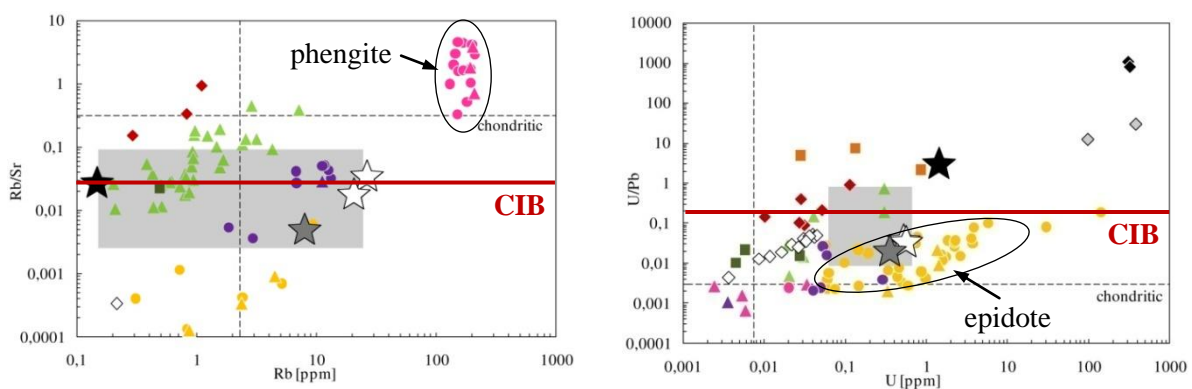
↑ **Figure 4.24 a** Modification of **Figure 4.19**. Phengite fractionates Rb over Sr relative to continental intraplate (CIB) precursors. **b** Epidote group minerals fractionate Pb over U relative to CIB. CIB ratios after COOK ET AL., 2005.

126

Relating to a global context, UHP/HP fluid rock interaction produces metasomatized eclogites with isotopic characteristics that are complementary to a HIMU source. A conceptual model (**Figure 4.25**) illustrates that suchlike altered rocks resemble the enriched mantle source EM-I. As proposed by HART ET AL. (1986), EM-I and HIMU may be complementary parts of the same metasomatic process (infiltrate versus residue). The present study confirms the theory of Hart and coworkers, by suggesting solidly that the EM-I source is fed by subducted metasomatized basalts. A potential contributor to the HIMU source, however, remains theoretical.
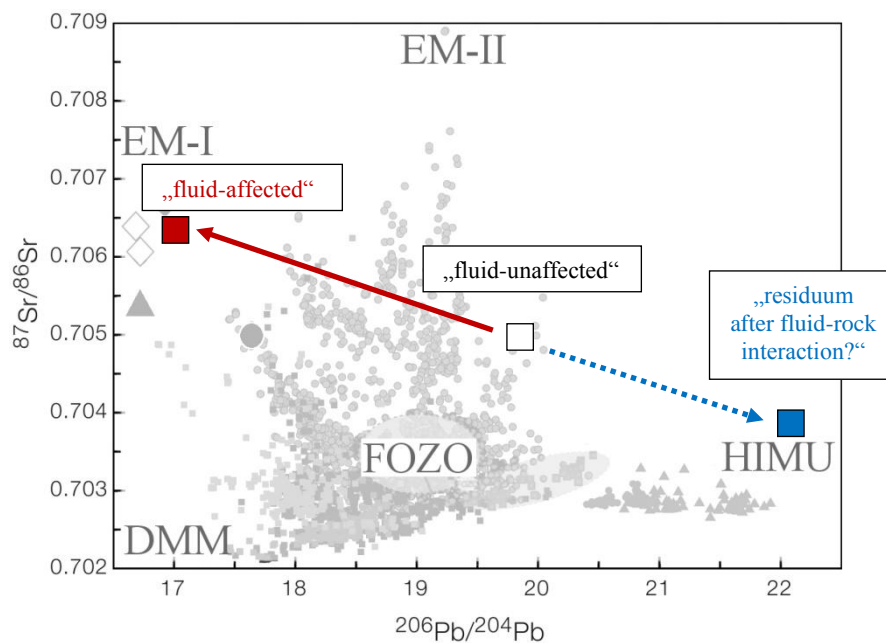
↑ **Figure 4.25** Conceptual model of Sr- and Pb isotopic arrays expected from high-pressure fluid-rock interaction. Compared to pristine samples, metasomatised eclogites are extremely shifted from assumed (continental) enriched basaltic compositions towards unradiogenic $^{206}Pb/^{204}Pb$ ratios along with an increase of $^{87}Sr/^{86}Sr$. In turn, the complementary composition that is to be expected for the residuum after fluid-rock interaction (metasomatism) tends to the highly radiogenic HIMU signature, as observed in several OIB type basalts. DMM: depleted MORB mantle, HIMU: high-μ (μ = $^{238}U/^{204}Pb_{@t=0}$) mantle component, EMI + II: enriched mantle, FOZO: focal zone. After HART ET AL. (1992), STRACKE ET AL. (2005).

4.5   Conclusions

(1) The precursor rocks to the investigated eclogites are continental intraplate basalts, as evident from geochemical fingerprinting.

(2) Lawsonitization prior to or during eclogitization is the most likely process to cause consistently observed, more felsic compositions of fluid-affected eclogites compared to pristine samples. This is not only evident from lawsonite being the only plausible candidate to provide the element prerequisite for the observed retrogression and vein formation, but also from prograde clinozoisite inclusions in garnet and omphacite that exhibit very low trace element contents. Such low concentrations along with comparable ambient HP conditions require growth in equilibrium with a high-REE phase.

(3) As evident from Sr and Pb isotope characteristics, the source of the early post-peak fluids are dehydrating granitic gneisses that are the host to the investigated eclogite bodies. Deduced from corresponding mineral chemistry in both veins and retrograded eclogite minerals, these fluids are the conjoint initial source for both pervasive retrogression in a spatial range of tens of meters, and for channelized fluid flow leading to the formation of 2nd generation veins.

(4) Compositional zoning in epidote group minerals tracks a compositional evolution in the post-peak, 2nd generation vein-forming fluid. Initially high trace element contents are successively diluted through "solute consumption" in the course of crystallization of retrograde and vein minerals. The late retrograde destabilization of garnet leads again to an increased availability of LREE in the fluid. A final introduction of virtually solute-free meteoric waters at shallow amphibolite facies depths cannot be excluded.

(5) Compositional zoning in garnet is restricted to retrograded eclogites, documenting the absence of fluid-rock interaction in pristine samples. Retrograded garnet core compositions coincide

128

with pristine (homogeneous) garnets while rimward overgrowths are LREE-depleted due to post-eclogitization equilibrium growth with epidote minerals.

(6) Bulk vein modeling and profile analyses towards a particular vein illustrate that 2nd generation veins accumulate many trace elements (HFSE, LILE, REE), both within themselves and within the adjacent host eclogite with a scope of fluid-rock interaction <1 m. If subducted, these veins as well as metasomatized eclogites, may be a significant agent of selective trace element and water recycling into the mantle.

(7) The trace element budget in 2nd generation veins is controlled by rutile (HFSE, U), zircon (Th, U, Zr, Hf, LREE), phengite and paragonite (Rb, Ba, Sr), apatite (Sr, MREE), and allanite/clinozoisite (U, Th, L-/MREE).

(8) Nb over Ta fractionation in rutile from fluid-affected eclogites (and to a lesser extent also from veins) attests metasomatized eclogites a potential to balance the global niobium deficiency. The same is, to a lesser extent, likely to be true for 1st and 2nd generation veins, but the HFSE budget of a bulk vein could not be reliably modeled.

(9) Phengite fractionates Rb over Sr, and epidote group minerals fractionate Pb over U relative to the basaltic precursor. The observed, gneiss-derived fluid metasomatism thus leads to an isotopic shift towards highly radiogenic Sr signatures along with extremely unradiogenic Pb characteristics in metasomatized eclogites. Such eclogites (and gneisses) isotopically resemble the global, enriched mantle component EM-I. On a global scale, the residuum after fluid rock interaction should have a HIMU signature and is apparently subducted to mantle, since it has not yet been located in the crust yet.

4.6   References

Allègre CJ (1969) Comportement des systemes U-Th-Pb dans le manteau superieur et modele d'evolution de ce dernier au cours des temps geologiques. *Earth Planet Sci Lett 5*, 261–269.

Allègre CJ, Brévart O, Dupré B, Minster JF (1980) Isotopic and chemical effects produced in a continuously differentiating convecting Earth mantle. *Philos Trans R Soc London 297*: 447–477.

Armstrong JT (1995) CITZAF - a package of correction programs for the quantitative Electron Microbeam X-Ray-Analysis of thick polished materials, thin-films, and particles. *Microb Anal 4(3)*: 177–200.

Barth MG, McDonough WF, Rudnick RL (2000) Tracking the budget of Nb and Ta in the continental crust. *Chem Geol 165(3)*: 197–213.

Bebout G, Ryan JG, Leeman WP, Bebout AE (1999) Fractionation of trace elements by subduction-zone metamorphismç effect of convergent-margin thermal evolution. *Earth Planet Sci Lett 171*: 63–81.

Becker H, Jochum KP, Carlson RW (1999) Constraints from high-pressure veins in eclogites on the composition of hydrous fluids in subduction zones. *Chem Geol 160*: 291–308.

Becker H, Jochum KP, Carlson RW (2000) Trace element fractionation during dehydration of eclogites from high-pressure terranes and the implications for element fluxes in subduction zones. *Chem Geol 163(1)*: 65–99.

Beinlich A, Klemd R, John T, Gao J (2010) Trace-element mobilization during Ca-metasomatism along a major fluid conduit: Eclogitization of blueschist as a consequence of fluid–rock interaction. *Geochim Cosmochim Ac 74(6)*: 1892–1922.

Brenan JM, Shaw HF, Phinney DL, Ryerson FJ (1994) Rutile-aqueous fluid partitioning of Nb, Ta, Hf, Zr, U and Th: implications for high field strength elements depletions in island-arc basalts. *Earth Planet Sci Lett 128*: 327–339.

Brovarone AV, Alard O, Beyssac O, Martin L, Picatto M (2014) Lawsonite metasomatism and trace element recycling in subduction zones. *J Metamorph Geol 32(5)*: 489–514.

Budzyń B, Harlov DE, Williams ML, Jercinovic MJ (2011) Experimental determination of stability relations between monazite, fluorapatite, allanite, and REE-epidote as a function of pressure, temperature, and fluid composition. *Am Mineral 96(10)*: 1547–1567.

Castelli D, Rolfo F, Compagnoni R, Xu ST (1998) Metamorphic veins with kyanite, zoisite and quartz in the Zhujiachong eclogite, Dabie Shan, China. *Isl Arc 7*: 159–173.

Chauvel C, Goldstein SJ, Hofmann AW (1995) Hydration and dehydration of oceanic crust controls Pb evolution of the mantle. *Chem Geol 126*: 65–75.

Chavagnac V, Jahn BM (1996) Coesite-bearing eclogites from the Bixiling Complex, Dabie Mountains, China: Sm- Nd ages, geochemical characteristics and tectonic implications. *Chem Geol 133(1)*: 29–51.

Chen J, Jahn BM (1998) Crustal evolution of southeastern China: Nd and Sr isotopic evidence. *Tectonophysics 284(1)*: 101–133.

Cheng A, Nakamura E, Kobayashi K, Zhou Z (2007) Origin of atoll garnets in eclogites and implications for the redistribution of trace elements during slab exhumation in a continental subduction zone. *Am Mineral 92(7)*: 1119–1129.

Cook C, Briggs RM, Smith IE, Maas R (2005) Petrology and geochemistry of intraplate basalts in the South Auckland volcanic field, New Zealand: evidence for two coeval magma suites from distinct sources. *J Petrol 46(3)*: 473–503.

Droop GTR (1987) A general equation for estimating Fe^{3+} concentrations in ferromagnesian silicates and oxides from microprobe analyses, using stoichiometric criteria. *Mineral Mag 51(361)*: 431–435.

Elliott T, Zindler A, Bourdon B (1999) Exploring the Kappa Conundrum: The role of recycling in the lead isotope evolution of the mantle. *Earth Planet Sci Lett 169*: 129–145.

Enami M, Liou JG, Mattinson CG (2004) Epidote minerals in high P/T metamorphic terranes: Subduction zone and high-to ultrahigh-pressure metamorphism. *Rev Mineral Geochem 56(1)*: 347–398.

Esawi EK (2004) AMPH-CLASS: An Excel spreadsheet for the classification and nomenclature of amphiboles based on the 1997 recommendations of the International Mineralogical Association. *Comput Geosci 30(7)*: 753–760.

Faryad SW, Klápová H, Nosál L (2010) Mechanism of formation of atoll garnet during high-pressure metamorphism. *Mineral Mag 74(1)*: 111–126.

Feineman MD, Ryerson FJ, DePaolo DJ, Plank T (2007) Zoisite-aqueous fluid trace element partitioning with implications for subduction zone fluid composition. *Chem Geol 239(3)*: 250-265.

Gao J, John T, Klemd R, Xiong X (2007) Mobilization of Ti–Nb–Ta during subduction: evidence from rutile-bearing dehydration segregations and veins hosted in eclogite, Tianshan, NW China. *Geochim Cosmochim Ac 71(20)*: 4974–4996.

Guo S, Ye K, Chen Y, Liu J, Mao Q, Ma Y (2012) Fluid–rock interaction and element mobilization in UHP metabasalt: constraints from an omphacite–epidote vein and host eclogites in the Dabie orogen. *Lithos 136*: 145–167.

Guo S, Ye K, Wu TF, Chen Y, Yang YH, Zhang LM, Liu JB, Mao Q, Ma YG (2013) A potential method to confirm the previous existence of lawsonite in eclogite: the mass imbalance of Sr and LREEs in multistage epidote (Ganghe, Dabie UHP terrane). *J Metamorph Geol 31(4)*: 415–435.

Guo S, Ye K, Yang Y, Chen Y, Zhang L, Liu J, Mao, Q, Ma YG (2014) In situ Sr isotopic analyses of epidote: tracing the sources of multi-stage fluids in ultrahigh-pressure eclogite (Ganghe, Dabie terrane). *Contrib Mineral Petrol 167(2)*: 1–23.

Hart SR, Gerlach DC, White WM (1986) A possible new Sr-Nd-Pb mantle array and consequences for mantle mixing, *Geochim Cosmochim Ac 50*: 1551–1557.

Hart SR, Hauri EH, Oschmann LA, Whitehead JA (1992) Mantle plumes and entrainment – Isotopic evidence. *Science 256*: 517–520.

Hellstrom J, Paton C, Woodhead J, Hergt J (2008) Iolite: software for spatially resolved LA-(quad and MC) ICPMS analysis. Mineralogical *Association of Canada short course series 40*: 343–348.

Hermann J (1997) Experimental constraints on phase relations in subducted continental crust. *Contrib Mineral Petrol 143(2)*: 219–235.

Hofmann AW, White WM (1980) The role of subducted oceanic crust in mantle evolution. *Year Book Carnegie Inst Washington 79*: 477–483.

Hofmann AW (1997) Mantle geochemistry: The message from oceanic volcanism. *Nature 385*: 219–229.

Huang J, Xiao Y, Gao Y, Hou Z, Wu W (2012) Nb–Ta fractionation induced by fluid-rock interaction in subduction-zones: constraints from UHP eclogite-and vein-hosted rutile from the Dabie orogen, Central-Eastern China. *J Metamorph Geol 30(8)*: 821–842.

John T, Scherer E, Haase KM, Schenk V (2004) Trace element fractionation during fluid-induced eclogitization in a s ubducting slab: trace element and Lu–Hf/Sm–Nd isotope systematics. *Earth Planetary Sci Lett 227*: 441–456.

Kerrick DM, Connolly JAD (2001) Metamorphic devolatilization of subducted oceanic metabasalts: implications for seismicity, arc magmatism and volatile recycling. *Earth Planet Sci Lett 189*: 19–29.

Kessel R, Schmidt MW, Ulmer P, Pettke T (2005) Trace element signature of subduction-zone fluids, melts and supercritical liquids at 120–180 km depth. *Nature 437*: 724–727.

Klemme S, Prowatke S, Hametner K, Günther D (2005) Partitioning of trace elements between rutile and silicate melts: implications for subduction zones. *Geochim Cosmochim Ac 69*: 2361–2371.

Korh AE, Schmidt ST, Ulianov A, Potel S (2009) Trace element partitioning in HP–LT metamorphic assemblages during subduction-related metamorphism, Ile de Groix, France: a detailed LA-ICPMS study. *J Petrol 50(6)*: 1107–1148.

Leake BE (1997) Nomenclature of amphiboles: Report of the subcommitee on amphiboles of the international mineralogical commission on new minerals and mineral names. *Min Mag 61 (4)*: 295–321.

Le Bas MJ, Le Maitre RW, Streckeisen A, Zanettin B (1986) A chemical classification of volcanic rocks based on the total alkali-silica diagram. *J Petrol 27(3)*: 745–750.

Li S, Jagoutz E, Chen Y, Li Q (2000) Sm–Nd and Rb–Sr isotope chronology of ultrahigh-pressure metamorphic rocks and their country rocks at Shuanghe in the Dabie Mountains, central China. *Geochim Cosmochim Ac 64*: 1077–1093.

Li YL, Zheng YF, Fu B, Zhou JB, Wei CS (2001) Oxygen isotope composition of quartz-vein in ultrahigh-pressure eclogite from Dabieshan and implications for transport of high-pressure metamorphic fluid. *Physics and Chemistry of the Eart*h 26(9): 695–704.

Li XP, Zheng YF, Wu YB, Chen FK, Gong B, Li YL (2004) Low-T eclogite in the Dabie terrane of China: petrological and isotopic constraints on fluid activity and radiometric dating. *Contrib Mineral Petrol 148*: 443–470.

Liang JL, Ding X, Sun XM, Zhang ZM, Zhang H, Sun WD (2009) Nb/Ta fractionation observed in eclogites from the Chinese Continental Scientific Drilling project. *Chem Geol 268(1)*: 27–40.

Martin LA, Wood BJ, Turner S, Rushmer T (2011) Experimental measurements of trace element partitioning between lawsonite, zoisite and fluid and their implication for the composition of arc magmas. *J Petrol 52(6)*: 1049–1075.

Massonne HJ, Schreyer W (1987) Phengite geobarometry based on the limiting assemblage with K-feldspar, phlogopite, and quartz.*Contrib Mineral Petrol 96(2)*: 212–224.

Massonne HJ, Schreyer W (1989) Stability field of the high-pressure assemblage talc+ phengite and two new phengite barometers. *Eur J Mineral 1(3)*: 391–410.

Mattinson CG, Zhang RY, Tsujimori T, Liou JG (2004) Epidote-rich talc-kyanite-phengite eclogites, Sulu terrane, eastern China: PT-fO$_2$estimates and the significance of the epidote-talc assemblage in eclogite. *Am Mineral 89(11-12)*: 1772–1783.

McDonough WF, Sun SS (1995) The composition of the Earth. *Chem Geol 120(3)*: 223–253.

Morimoto N (1988) Nomenclature of pyroxenes. *Miner Petrol 39(1)*: 55–76.

Münker C, Pfänder JA, Weyer S, Büchl A, Kleine T, Mezger K (2003) Evolution of planetary cores and the Earth-Moon system from Nb/Ta systematics. *Science 301(5629)*: 84–87.

Münker C, Wörner G, Yogodzinski G, Churikova T (2004) Behaviour of high field strength elements in subduction zones: constraints from Kamchatka-Aleutian arc lavas. *Earth Planet Sci Lett 224(3-4)*: 275–293.

Nagasaki A, Enami M (1998) Sr-bearing zoisite and epidote in ultra-high pressure (UHP) metamorphic rocks from the Su-Lu province, eastern China: An important Sr reservoir under UHP conditions. *Am Mineral 83(3-4)*: 240–247.

Newton RC, Manning CE (2004) Thermodynamics of SiO2-H2O fluid near the upper critical end point from quartz solubility measurements at 10 kbar. *Earth Planet Sci Lett 274*: 241–249.

Pack A, Kremer K, Albrecht N, Simon K, Kronz A (2010) Description of an aerodynamic levitation apparatus with applications in Earth sciences. *Geochem Transact 11(1)*: 1–16.

Peacock SM (1990) Fluid processes in subduction zones. *Science 248*: 329–337.

Peacock SM (1993) Large-scale hydration of the lithosphere above subducting slabs. *Chem Geol 108*: 49–59.

Peacock SM (2001) Are double seismic zones caused by serpentine dehydration reactions in subducting oceanic mantle? *Geology 29*: 299–302.

Pearce NJ, Perkins WT, Westgate JA, Gorton MP, Jackson SE, Neal CR, Chenery SP (1997) A compilation of new and published major and trace element data for NIST SRM 610 and NIST SRM 612 glass reference materials. *Geostandard Newslett 21(1)*: 115–144.

Peucker-Ehrenbrink B, Hofmann AW, Hart SR (1994) Hydrothermal lead transfer from mantle to continental crust: The role of metalliferous sediments. *Earth Planet Sci Lett 125*: 129–142.

Pfänder JA, Münker C, Stracke A, Mezger K (2007) Nb/Ta and Zr/Hf in ocean island basalts—implications for crust–mantle differentiation and the fate of Niobium. *Earth Planet Sci Lett 254(1)*: 158–172.

Poli S, Schmidt MW (2002) Petrology of subducted slabs. *Annu Rev Earth Pl Sc 30*: 207–235.

Poli S, Schmidt MW (2004) Experimental subsolidus studies on epidote minerals. *Rev Mineral Geochem 56(1)*: 171–195.

Rudnick RL, Fountain DM (1995) Nature and composition of the continental crust: a lower crustal perspective. *Rev Geophys 33(3)*: 267–309.

Rudnick RL, Barth M, Horn I, McDonough WF (2000) Rutile-bearing refractory eclogites: Missing link between continents and depleted mantle. *Science 287*: 278–281.

Scambelluri M, Philippot P (2001) Deep fluids in subduction zones. *Lithos 55*: 213–227.

Schmidt MW, Poli S (1998) Experimentally based water budgets for dehydrating slabs and consequences for arc magma generation. *Earth Planet Sci Lett 163*: 361–379.

Schmidt MW, Dardon A, Chazot G, Vannucci R (2004) The dependence of Nb and Ta rutile-melt partitioning on melt composition and Nb/Ta fractionation during subduction processes. *Earth Planet Sci Lett 226*: 415–432.

Schmidt A, Weyer S, John T, Brey GP (2009) HFSE systematics of rutile-bearing eclogites: new insights into subduction zone processes and implications for the earth's HFSE budget. *Geochim Cosmochim Ac 73(2)*: 455–468.

Simon, K., Wiechert, U., Hoefs, J., & Grote, B. (1997). Microanalysis of minerals by laser ablation ICPMS and SIRMS. *Fresen J Anal Chem 359(4)*: 458-461.

Stout JH (1972) Phase petrology and mineral chemistry of coexisting amphiboles from Tidemark, Norway. *J Petrol 13 (1)*: 99–145.

Stracke A, Hofmann AW, Hart SR (2005) FOZO, HIMU, and the rest of the mantle zoo. *Geochem Geophys Geosys 6(5)*: 1–20.

Velde B (1967) Si^{+4} content of natural phengites. *Contrib Mineral Petrol 14(3)*: 250–258.

Verma SP, Torres-Alvarado IS, Sotelo-Rodríguez ZT (2002) SINCLAS: standard igneous norm and volcanic rock classification system. *Comput Geosci 28(5)*: 711–715.

Vidal P, Chauvel C, Brousse R (1984) Large mantle heterogeneity beneath French Polynesia. *Nature 307*: 536–538.

Vidal P, Dosso L (1978) Core formation: Catastrophic or continuous? Sr and Pb isotope geochemistry constraints. *Geophys Res Lett 5*: 169–172.

Vollmer R (1977) Terrestrial lead isotopic evolution and formation of the Earth's core. *Nature 270*: 144–147.

Xia QX, Zheng YF, Lu XN, Hu Z, Xu H (2012) Formation of metamorphic and metamorphosed garnets in the low-T/UHP metagranite during continental collision in the Dabie orogen. *Lithos 136*: 73–92.

Xiao Y, Hoefs J, van den Kerkhof AM, Fiebig J, Zheng YF (2000) Fluid history of UHP metamorphism in Dabie Shan, China: a fluid inclusion and oxygen isotope study on the coesite-bearing eclogite from Bixiling. *Contrib Mineral Petr 139*: 1–16.

Xiao Y, Sun W, Hoefs J, Simon K, Zhang Z, Li S, Hofmann AW (2006) Making continental crust through slab melting: constraints from niobium–tantalum fractionation in UHP metamorphic rutile. *Geochim Cosmochim Ac 70(18)*: 4770–4782.

Xiong XL, Adam J, Green TH (2005) Rutile stability and rutile/melt HFSE partitioning during partial melting of hydrous basalt: implications for TTG genesis. *Chem Geol 218*: 339–359.

Zartman RE, Haines SM (1988) The plumbotectonic model for Pb systematics among major terrestrial reservoirs – A case for bi-directional transport. *Geochim Cosmochim Ac 52*: 1327–1339.

Zhang H, Gao S, Zhong Z, Zhang B, Zhang L, Hu S (2002) Geochemical and Sr–Nd–Pb isotopic compositions of Cretaceous granitoids: constraints on tectonic framework and crustal structure of the Dabieshan ultrahigh-pressure metamorphic belt, China. *Chem Geol* 186(3): 281–299.

5. Compositional evolution and origin of vein-forming UHP/HP fluids

5.1 Introduction

Fluid-mediated mass transfer linked to deep subduction is crucial regarding element redistribution within the crust and among Earth's mantle and crustal reservoirs. Deep fluids are liberated when subducted crustal rocks undergo high-pressure (HP) to ultrahigh-pressure (UHP) metamorphism. Experimental studies have shown that elevated pressures lead to polymerization (NEWTON AND MANNING, 2003) along with enhanced solubilities of silicate components in aqueous liquids (eg. NEWTON AND MANNING, 2002; HUNT AND MANNING, 2012) up to the formation of supercritical fluids with melt-like qualities (MANNING, 2004; KESSEL ET AL., 2005; HACK ET AL., 2007). Such fluids can mobilize even nominally fluid-immobile elements (eg. AYERS & WATSON, 1993) whereas this ability is strongly governed by fluid chemistry (GAO ET AL., 2007; MANNING ET AL., 2008; RAPP ET AL., 2010).

Owing to their high element solubility, supercritical fluids are expected to be the most effective agents of mass transport in UHP regimes (KEPPLER, 1996), but natural examples of multiphase solid inclusions potentially trapping such fluids are rare (eg. STÖCKHERT ET AL., 2001; FERRANDO ET AL., 2005). Inclusions of hydrous high pressure fluids in metamorphic minerals are known, however, their composition and their compositional changes during metamorphic evolution are poorly constrained. Solid evidence for former fluid activity in a rock during metamorphism is provided by mineral veins.

136

Although these veins, and fluid inclusions entrapped within their minerals, represent only vestiges of the fluid present at the time of their precipitation rather than the fluid itself and modifications along the exhumation path can disturb their record, fluid inclusions in high-grade metamorphic rocks allow the most robust access to the nature of deep fluids.

The Dabieshan orogenic belt in central-eastern China offers excellent opportunities to study high-grade metamorphic fluids, as it exposes lithologies that were subjected to deep continental subduction, resulting in coesite and micro-diamond inclusions in eclogitic minerals (eg. OKAY ET AL., 1989; WANG ET AL., 1989; SHUTONG ET AL., 1992) that confirm the UHP metamorphic history of the terrane. The presence of volatile-bearing mineral phases such as epidote, zoisite, phengite and lawsonite (CARSWELL 1997; NAGASAKI AND ENAMI 1998; GUO ET AL. 2013), as well as water that may be contained in nominally water-free minerals such as omphacite, garnet and rutile (ZHANG ET AL. 2001; SU ET AL., 2002) and numerous findings of mineral veins (CASTELLI ET AL., 1998; BECKER ET AL., 1999; FRANZ ET AL., 2001; ZHENG ET AL., 2007A; JOHN ET AL., 2008; ZHANG ET AL., 2008; WU ET AL., 2009; XIAO ET AL., 2011; GUO ET AL., 2012) in HP/UHP rocks demonstrate a substantial involvement of fluid phases during metamorphic and retrograde evolution.

These fluids can be trapped within host rock and vein minerals to form fluid inclusions at any metamorphic stage. Although high-grade metamorphic conditions should lead to reequilibration of these inclusions during exhumation in most cases (VITYK AND BODNAR, 1995), changes are mainly restricted to fluid inclusion volume rather than to a significant modification of content by leakage or diffusion (STERNER AND BODNAR, 1989; GAO AND KLEMD, 2001). Accordingly, inclusions that are subjected to extreme differential pressures hardly maintain peak densities, but many of them are preserved and can be considered to be compositionally closed containers of the fluid circulating at the time of entrapment.

Previous investigations of entrapped fluid inclusions in deeply subducted (U)HP rocks suggest complex and variable fluid compositions during eclogitization and peak metamorphism. Depending on the eclogitic precursor, compositions range from highly saline Ca-dominated brines (continental environment) or Na- and Mg-dominated brines (oceanic environment) $\pm$ CO_2 and N_2 to low-salinity aqueous fluids, whereas late retrograde fluids are characterized by generally lower salinities

(continental rocks: FU ET AL., 2002, 2003; GAO AND KLEMD, 2001; XIAO ET AL., 2000, oceanic rocks: PHILIPPOT AND SELVERSTONE, 1991; PHILIPPOT ET AL., 1995; SCAMBELLURI ET AL., 2001). The variety of fluid inclusions, trapped over a wide range of P–T conditions, is interpreted to be the result of multistage fluid-rock interaction, characterized by dissolution and precipitation processes (SCAMBELLURI AND PHILIPPOT, 2001). Studies by eg. PHILIPPOT (1993) and XIAO ET AL., (2000) indicate that fluid movement at high-grade metamorphic conditions is limited to the scale of a few meters and occurs within a largely closed system. ANDERSEN ET AL., (1989, 1993) and FU ET AL., (2003) demonstrated a marked difference of HP fluid regimes that evolved under either granulite-facies (CO_2-dominated anhydrous fluids) or eclogite-facies conditions (saline aqueous fluids $\pm$ N_2). Oxygen isotopes have been used by several authors to reconstruct fluid flow and fluid origin of UHP-related metamorphic fluids. XIAO ET AL. (2000) found that Dabieshan UHP eclogites in central, pristine portions of the Bixiling eclogite complex show precursor-like $\delta^{18}O$ of about 4 - 5‰, whereas retrograded portions towards the gneiss interface of the complex are significantly lowered to around 0‰. These results were refined by in-situ garnet isotope measurements of XIAO ET AL. (2002), revealing typical crustal $\delta^{18}O$ in the prograde part of a single garnet crystal, in contrast to distinctly lowered values towards the crystal rim. This implies that retrograde fluids have a light oxygen isotope composition that is likely to be inherited from meteoric waters. Exceptionally low $\delta^{18}O$ in UHP eclogites were suspected to document fluid-rock interaction with glaciation waters or at high temperatures (eg. YUI ET AL., 1995; ZHENG ET AL., 1996; BAKER ET AL., 1997; FU ET AL., 1999).

This work attempts to assess the compositional differences of the HP/UHP fluids at the different metamorphic stages as recorded by different vein types (**Chapter 3**). A comprehensive study of fluid inclusions, that can be regarded as the most direct access to the nature of the metamorphic fluid circulating during entrapment, is used to characterize the fluid regimes during vein crystallisation. This attempt is based on a systematical characterization of fluid inclusions in vein and related eclogite minerals, and is extended by the combination of mineral chemistry (**Chapter 4**) and in-situ fluid inclusion chemistry as determined by UV-fs-LA-ICPMS. Stable oxygen isotope compositions of vein and eclogite minerals are analyzed in order to provide information on possible fluid sources.

5.2 Data aquisition

5.2.1 Heating-/freezing stage microthermometry

Fluid inclusions were initially characterized by optical petrography on doubly polished and mounted ~200 µm thick sections. Microthermometric measurements were carried out on unmounted thick sections using a *Linkam THMS-G600* heating/freezing stage coupled to a *Linkam T95 LinkSys* controller and an *Olympus BH2* microscope, set up after SHEPERD (1981). Minimum temperatures of -195°C were achieved using liquid nitrogen as cooling medium. Samples were cooled with a rate of 20°C/min, and heated with a rate of 5°C/min.

For ice melting temperatures the accuracy is better than 0.2°C, for initial melting and homogenization temperatures better than 0.5°C and about 5°C for low-salinity inclusions. Stage calibration was done with pure CO_2 in synthetic inclusions.

5.2.2 UV-fs-LAICPMS

Chemical compositions of individual fluid inclusions were determined by ultraviolet femtosecond laser inductively coupled plasma mass spectrometry (UV-fs-LA-ICPMS) at the Institute for Mineralogy of the Leibniz University Hannover. The analytical setup provides a novel and efficient tool for the accurate determination of elemental data on low concentration levels, especially in small fluid inclusions, and is described in ALBRECHT ET AL., (2014). It comprises a *Thermo Scientific ELEMENT XR* magnetic sector field inductively coupled plasma mass spectrometer combined with a laser ablation system which is based on a *Spectra-Physics Solstice* femtosecond (Ti:Sapphire) laser operating in the deep UV at 194 nm, a modified New-Wave Research sample stage and a low-volume modified *Instec HCS622V* sample cell. Detailed information on the specifications of the laser system and the sample stage are described by HORN ET AL., (2006) and OESER ET AL., (2014). Due to a high energy density in combination with minimal heat transfer of the fs-laser (PRONKO ET AL., 1995) and fast mass spectrometric acquisition optimized for short transient signals, this technique allows a

controlled and complete solid state ablation of (frozen) fluid inclusions with minimal elemental fractionation effects at the sample site (HORN AND VON BLANCKENBURG, 2007).

The inclusions have been frozen to -90°C and subsequently ablated with repetition rates of 2-10 Hz (depending on inclusion depth) and a spot size of 25 μm. Dimensions and depths of successfully analyzed inclusions vary between 8 and 25 μm inclusion diameter and 15 to 80 μm distance to the section surface. Helium was used as carrier gas to the ICPMS and all analyses were calibrated against the external standard NIST610 (PEARCE ET AL., 1997). Raw data were processed with the data reduction software SILLS (GUILLONG ET AL,. 2008) and $NaCl_{eq}$ contents derived from water freezing point depression were used as internal standard to calculate absolute element concentrations in the aqueous inclusions. Since other dissolved major components like $CaCl_2$ or KCl have an influence on the ice melting temperature, a salt correction (HEINRICH ET AL., 2003) was performed prior to this calculation, resulting in corrected Na values which were then used as internal standard.

Standard errors (1σ) are generally between 0.1 and 10 % for major components (median for Na: 0.6 %, Ca: 9.5 %, K: 1.7 %) and mostly below 20 % for minor components (median for Sr: 2.6 %, Ba: 9.1 %, B: 12.7 %, Li: 21.7 %), except for lowly concentrated Rb (median: 50.8 %).

5.2.3 IR-Laser fluorination mass spectrometry (IR-LF-MS)

The oxygen isotopic composition of powdered bulk eclogites and mineral separates of most eclogite and vein minerals was determined by means of IR-laser fluorination. The procedure is described in detail by SHARP (1990), and includes sample pre-melting under high-vacuum conditions, laser fluorination of the sample with F_2, oxygen purification by removing excess F_2 through the reaction with heated NaCl, and subsequent fixing of chlorine in cryogenic traps. Triple oxygen isotope ratios ($^{18}O/^{16}O$, $^{17}O/^{18}O$) of the released O_2 gas were analyzed using a *Thermo Scientific MAT 253* mass spectrometer operated in continuous flow mode, and results are expressed in the linearized δ'-notation relative to VSMOW (MCKINNEY ET AL., 1950). Results were corrected on the basis of repeatedly analyzed standards (MORB glass with $δ^{18}O$ of 5.50‰ and NBS28 quartz with $δ^{18}O$ of 9.57‰), and in

case of significant daily drifts, a linear interpolation is applied. Analytical errors are typically between 0.102 and 0.247‰ for $\delta'^{18}O$.

5.2.4 Raman spectroscopy

Raman spectra of selected fluid inclusions from all petrographic groups were recorded in the range between 200 and 4200 cm⁻¹ with an acquisition time of 60 s for each spectral window using a confocal *Horiba Jobin Yvon HR800* UV Raman spectrometer equipped with an air-cooled Ar⁺-laser working at 488 nm and attached to an *Olympus BX41* microscope. Using a 100× Olympus long working distance objective with a numerical aperture of 0.55, the lateral resolution was on the order of 1 µm. Calibration of the spectral positions was done against the Raman mode of Si before and after sample measurements, yielding a value of 520.4 ± 0.3 cm⁻¹.

5.3   Results

The description of the results given in this chapter follows the concept of the different vein types (1st, 2nd and 3rd generation) and eclogite types (pristine and retrograded) as established in **Chapter 3** and in parts already confirmed in **Chapter 4**.

5.3.1   Fluid inclusion petrography

Fluid inclusions are found both in minerals of the pristine SH-59 eclogite and in all sampled vein types. No fluid inclusions were observed in the pristine Bixiling eclogite (BX-07), and the retrogressed samples from Zhujiachong (ZJC-16) and Shuanghe (SH-56). The main host mineral is quartz, very few workable inclusions have been observed in (coesite-bearing) garnet (cf. **Table 3.1**). Vein quartz commonly exhibits granular mosaic structures and is almost lacking deformation except for abundant, late-stage microcracks and sometimes slightly undulary extinction. Eclogitic quartz commonly occurs in small, polycrystalline domains with equilibrated qtz-qtz grain boundaries. These domains are characteristically undeformed, surrounded by garnet and omphacite and often elongated parallel to the eclogitic foliation.

Fluid inclusions are abundant in both vein and eclogite quartz whereas neither petrographic nor compositional difference amongst their fluid inclusions is observed. Many inclusions show reequilibration features such as leakage ("empty inclusions") and decripitation ("apophyses"). Excluding these inclusions from interpretation and further investigation, three petrogenetic groups of aqueous inclusions are distinguished on the basis of textural relations, petrographic evidence and Raman analysis, following ROEDDER (1984) and SHEPERD ET AL. (1985). These three groups document three main episodes of fluid entrapment:

(PI)   Primary inclusions with regular, roundish morphologies with diameters from 1-15 μm occur occasionally, either isolated (**Figure 5.1a**) or in spherical, intragranular clusters (**Figure 5.1b**) of up to ~10 inclusions of similar size. They are found in quartz from the SH eclogite and rarely also in UHP

garnet (**Figure 5.1c**) as well as in vein quartz from all 1st and 2nd generation veins. The three-phase inclusions comprise a liquid (L), a gas bubble (V) with estimated volumes between 3 and 7 % and a daughter crystal (S$_{halite}$) and tend to occur preferentially in core regions of their host minerals. They are the earliest inclusions observed and are assumed to have been directly trapped during mineral growth, and hence preserving a fluid closest related to the UHP metamorphic peak. Low peaks at Raman shifts of 2331 cm^{-1} detected in some primary inclusions within the SH eclogite samples attest the presence of nitrogen.

(PSI) Pseudosecondary inclusions have generally larger sizes between 3 and 30 μm and the highest abundance of all observed inclusion types. They can occur isolated, but are mostly found in curved or planary, intragranular healed microfractures that comprise several tens of inclusions of varying sizes. They tend to be roundish and regular and occasionally show negative crystal shapes (**Figure 5.1c**), however, they frequently have an irregular habitus (**Figure 5.1d**). While the majority of inclusions contain three phases (LVS$_{halite}$), many lack a visible daughter crystal. Vapour bubble volumes are between 3 and 10 %. The inclusions occur in both eclogitic and vein quartz of all investigated inclusion-bearing samples and are assumed to have been trapped during a time period extending from the beginning until the end of quartz growth. Some PSI in the 3rd generation vein sample are suspected to be of primary character, but due to a huge total amount of (especially secondary) inclusions, an unambiguous determination was not reasonable.
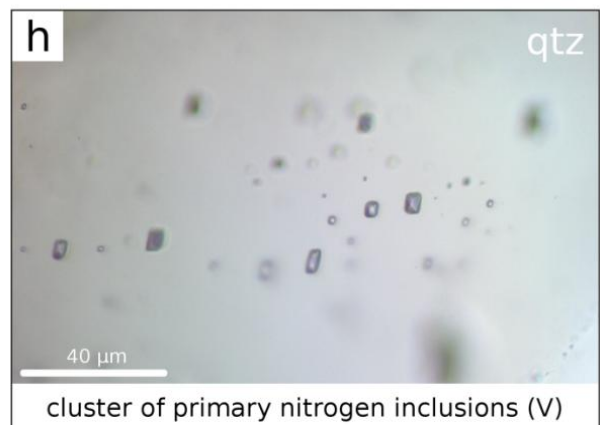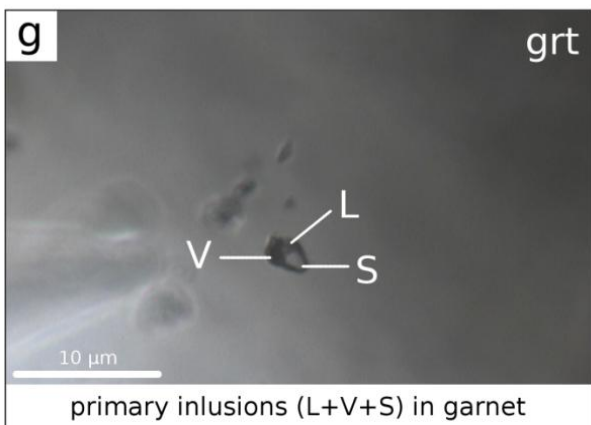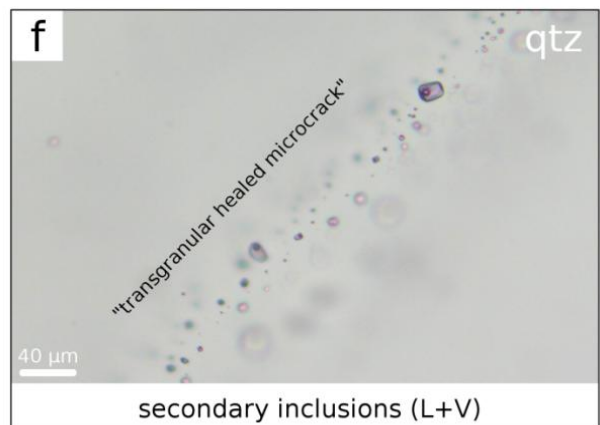
(SI) Secondary inclusions are abundant (although they are relatively rare compared to PSI) in quartz from all inclusion-bearing samples. They are consistently associated to healed microfractures and form transgranular, planary trails. Their common extension across grain boundaries proves a formation well after quartz the end of crystallization. Each trail encompasses up to a few tens to hundreds of two-phase (L +V) inclusions with varying shapes and sizes between 5 and 35 μm and gas bubble volumes of 8 - 20 % (**Figure 5.1e**). Larger inclusions tend to have irregular shapes, while trails of smaller inclusions in quartz often show negative crystal shapes as a result of surface energy

reduction during crack healing. The secondary inclusions were clearly formed after the other inclusion types described before.

Note that the optical characterization and classification of inclusions can be ambiguous in some cases, and some PSI may have falsely been interpreted to be PI or SI, respectively - or vice versa. The general absence of fluid inclusions in other minerals than quartz is owed to the brittle behavior of e.g. garnet and omphacite, which impedes recrystallization along microfractures.

(NI) A fourth, non-aqueous inclusion group comprises single-phase nitrogen inclusions (NI) with negative crystal morphologies and sizes between 1 and 5μm, occurring exclusively in SH eclogitic quartz (SH-A59, -A60). These inclusions form spherical clusters of up to tens of individuals with serial size distributions (**Figure 5.1f**). They are usually located in close spatial relationship to PI and the detection of small amounts of N_2 by Raman spectroscopy in the vapor bubbles of some PI point to a cogenetic formation.

↓ **Figure 5.1 a (next page)** Isolated primary inclusion in 1st generation vein quartz (SH-A60) next to a trail of secondary inclusions, **b** non-planary, spherical cluster of primary inclusions in eclogitic quartz (SH-A59), **c** intragranular planary array of pseudosecondary inclusions not crosscutting grain boundaries (SH-A60), **d** planary cluster of pseudosecondary inclusions within an intragranular healed microfracture, **e** irregular two-phase secondary inclusions related to transgranular healed microcracks (SH-C58), **f** transgranular trail of two-phase secondary inclusions (SH-C58) **g** miniscule primary inclusions in eclogitic garnet (SH-A59), **h** spherical cluster of nitrogen inclusions in eclogitic quartz (SH-A59).

a   qtz

PI

40 µm   L S V   5 µm

isolated primary inclusion (L+V+S)

b   qtz

PI

40 µm

cluster of primary inclusions (L+V+S)

c   qtz

"intragranular planary array"

40 µm

pseudosecondary inclusions (L+V±S)

d   qtz

40 µm

pseudosecondary inclusions (L+V±S)

e   qtz

40 µm

secondary inclusions (L+V)

f   qtz

"transgranular healed microcrack"

40 µm

secondary inclusions (L+V)

g   grt

L

V S

10 µm

primary inlusions (L+V+S) in garnet

h   qtz

40 µm

cluster of primary nitrogen inclusions (V)

145

5.3.2 Fluid inclusion major element compositions (traditional microthermometry)

Microthermometric results reflect different fluid compositions and conditions of inclusion formation that were found to directly correspond to the petrographic groups. Early PI throughout all samples show both the highest total salinities $NaCl_{eq}$ (estimated from final ice melting temperatures $T_{M(ice)}$, after BODNAR, 1993) and homogenization temperatures T_H, accompanied by the lowest eutectic temperatures T_E. Late SI exhibit the lowest salinities and T_H along with the highest T_E. The group of (most abundant) PSI spans a comparatively wide, intermediate range. If halite is present, its melting occurs before T_H within a temperature range of 195 - 241°C.

Exceptionally low eutectic temperatures down to -77°C in some PI indicate a complex salt system (**Fig 5.2**). Both the suspected microscopic observation of antarcticite ($CaCl_2 \cdot 6\,H_2O$) that is attributed to a dark brownish colouring caused by its microcrystalline structure during reheating of the inclusions as well as the occurrence of hydrohalite ($NaCl \cdot 2H_2O$) that forms characteristic hexagonal single crystals during reheating confirms the occurrence of calcium and sodium in the fluid. But at least one additional component that cannot be identified by microthermometric methods is required to attain the observed low T_E.

The eutectic temperatures of PSI cluster in a narrow range between -55 °C and -48°C which is, supported by the occasional observation of antarcticite and hydrohalite, diagnostic for a Ca-dominated salt system $H_2O + CaCl_2 + NaCl$.

SI with low salinities exhibit T_E mainly clustering between -30 to -20°C and not lower than -35°C, indicating NaCl dominance. Antarcticite is absent and hydrohalite is hardly observed due to low salt concentrations.

↓ **Figure 5.2 (next page)** Microthermometric dataset in vein quartz and eclogitic quartz from Zhujiachong and Shuanghe. Their T_E and $T_{M(ice)}$ correlate systematically with the petrographic groups. Note that primary high-salinity inclusions are found in both vein quartz, eclogitic quartz and in UHP garnet from Shuanghe. **b** Microthermometric data of all investigated aqueous inclusions (n = 357, in grey) comparatively including the UV-fs-LAICPMS dataset (n = 62) **c** Discrimination between petrographic fluid inclusion types PI, PSI and SI for both datasets.

146
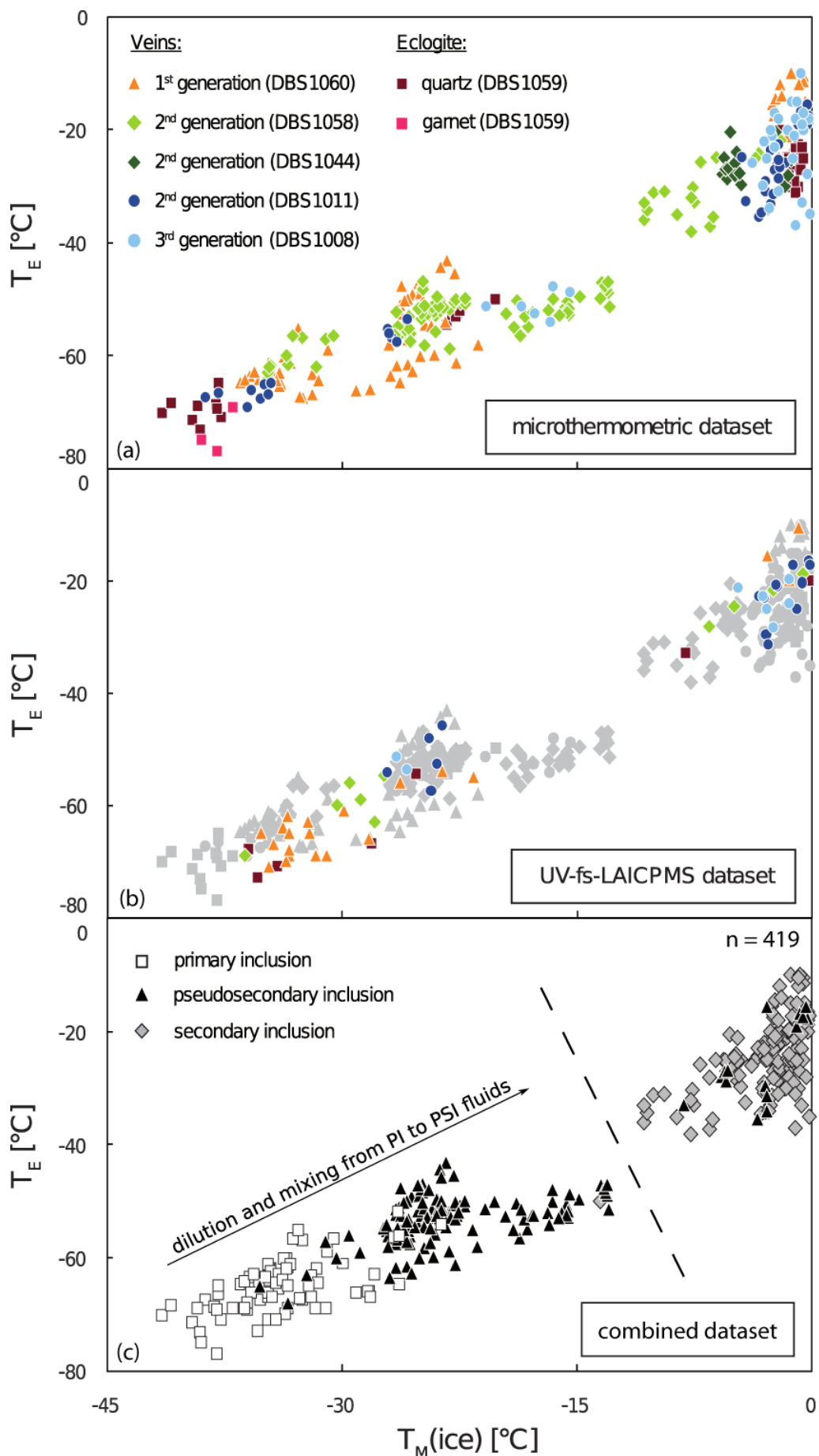
Hydrohalite melting in PI and PSI occurs in a wide temperature range of -34.5°C to -2.4 °C as well as metastable between 0.9 °C and 14.5°C. By contrast, hydrohalite in SI, if observed, melts between -25.0°C and -21.4°C. Neglecting additional unknown components, compositional calculations in the simplified model system H_2O - NaCl - $CaCl_2$ (based on the final melting temperatures of ice and hydrohalite, after STEELE-MACINNIS ET AL., 2010) indicate calcium to be the dominating salt component in these highly saline, early PI (Ca/Na > 1), while Ca contents decrease in later fluids trapped in PSI (Ca/Na < 1) until Ca is virtually absent in low-saline SI (**Figure 5.3**). Note that very low salinity SI do not appear in Figure 5 since $T_{M(hydrohalite)}$ could not be observed.
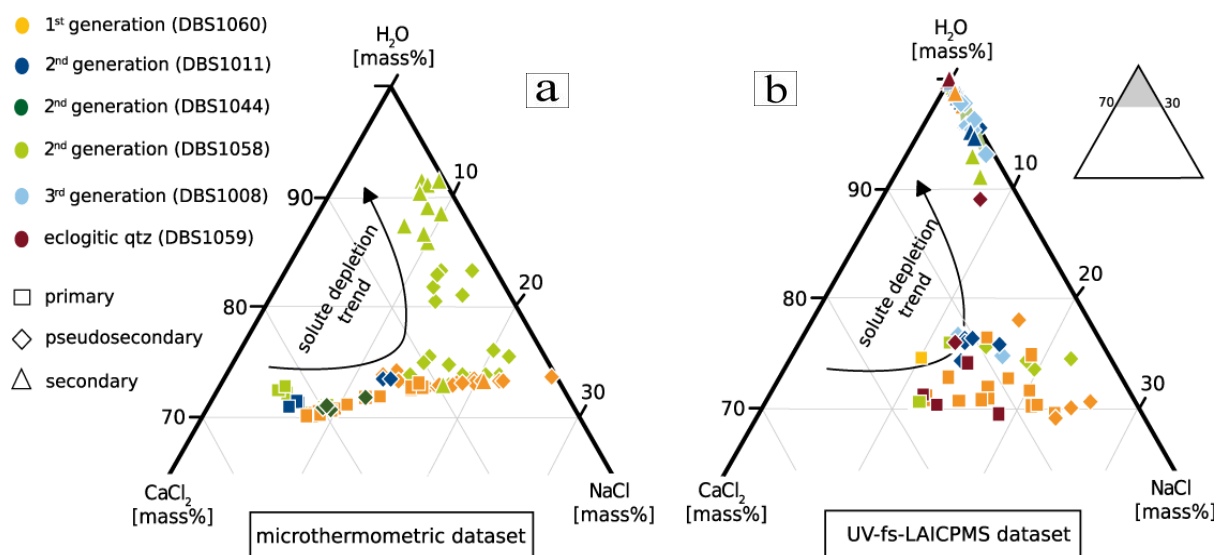
↑ **Figure 5.3 a** Fluid compositions in the simplified system H_2O - NaCl - $CaCl_2$ based on the final melting temperatures of ice ($T_{M(ice)}$) and hydrohalite ($T_{M(hydrohalite)}$) (calculated after STEELE-MACINNIS ET AL., 2010). Note that low salinity inclusions (<< 10 mass% NaCl) do not appear in this diagram since hydrohalite melting could not be observed due to low sodium concentrations and that additional components in the fluid (e.g. KCl) are neglected, possibly leading to too high Ca-contents **b** Fluid compositions of the inclusions analyzed by UV-fs-LAICPMS in the simplified system H_2O - NaCl - $CaCl_2$. Total concentrations were calculated on the basis of $T_{M(ice)}$. The respectively derived total salinities (calculated after BODNAR, 1993) were used as internal concentration standard. KCl as a minor component with up to 3 mass% is neglected.

Homogenization temperatures among all investigated aqueous inclusion types show a bimodal distribution, clustering around ~400°C and ~200°C (**Figure 5.4**). Inclusions with primary or

pseudosecondary character occur in both temperature groups with a predominance for high T_H, while secondary inclusions generally exhibit low T_H (**Figure 5.5**). Those PI and PSI with high T_H are inte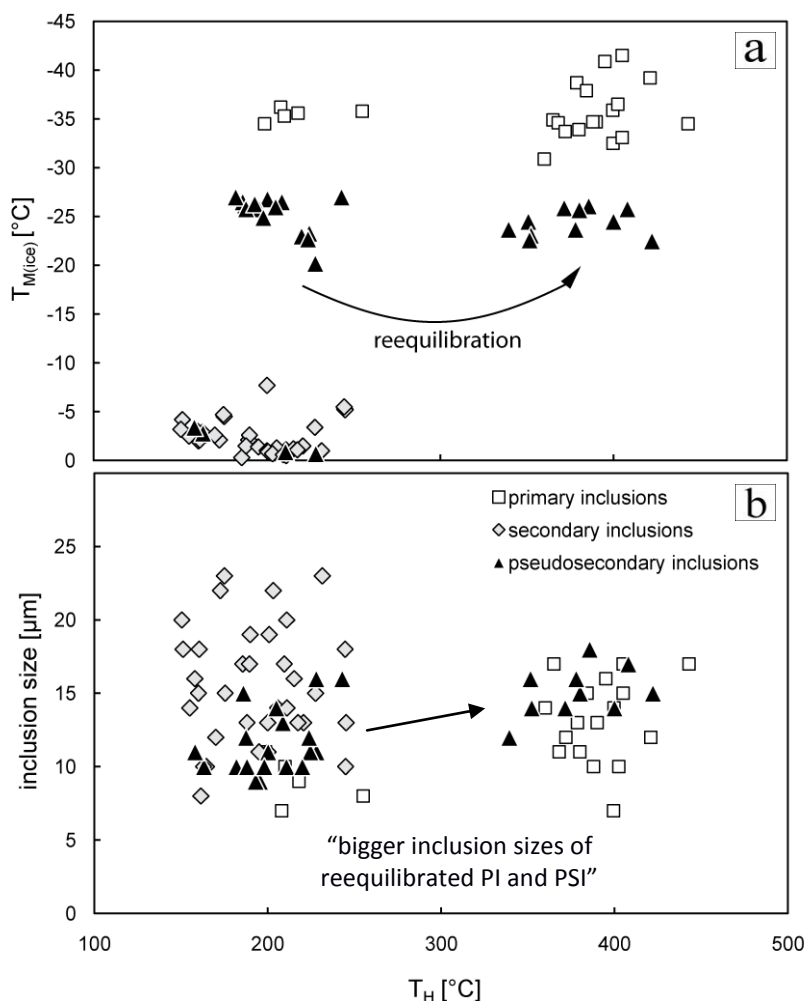rpreted to have reequilibrated due to microscopically unrecognized stretching and/or water leakage (BAKKER AND DOPPLER, 2016) that would both result in a decrease in inclusion density and hence in apparently higher T_H. This interpretation is supported by the fact that these inclusions tend to have larger dimensions making them more prone to reequilibration (**Figure 5.5b**).

PI and PSI in the low-T_H range exhibit higher temperatures on average (Ø 218 °C and Ø 202 °C) compared to SI (Ø 193 °C), implying at least two distinct periods of fluid entrapment during uplift at (i) an early stage when highly saline fluids and presumably also nitrogen were trapped, and (ii) a later stage when low salinity inclusions were formed.

Nitrogen inclusions (NI) homogenize into the liquid phase at T_H between -148 and -157 °C. According to ANGUS ET AL. (1979) and JACOBSEN ET AL. (1986) fluid densities range from 0.42 to 0.57 g/cm³ with internal pressures of 2.1 - 3.2 MPa. These conditions meet the critical point for pure nitrogen at room temperature and point to an entrapment of the inclusions beyond in the supercritical field.
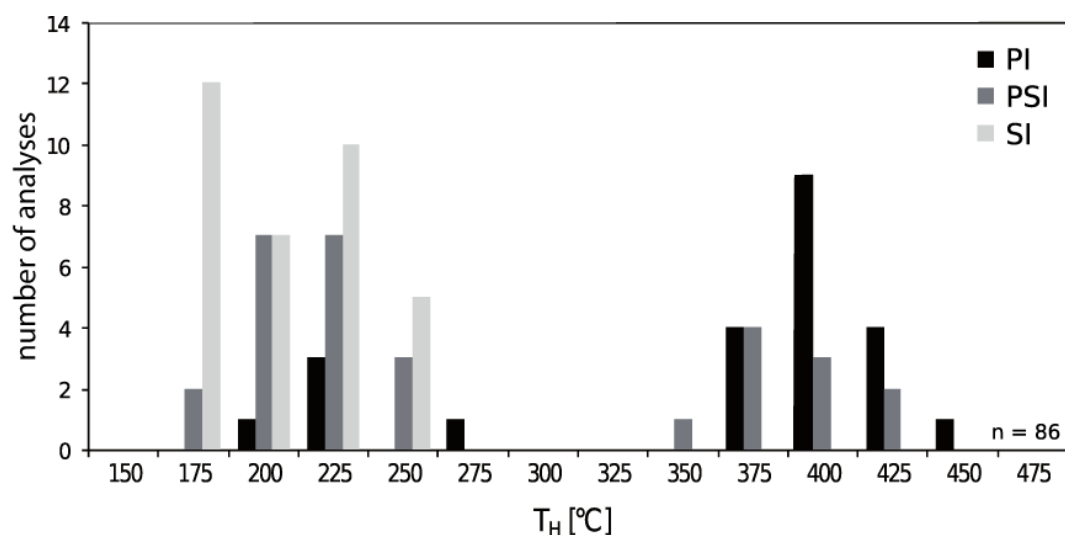
↑ **Figure 5.4** Histogram of homogenization temperatures of all investigated aqueous inclusion types display a bimodal distribution. Most primary and many pseudosecondary inclusions homogenize at ~400°C, while secondary inclusions show T_H of ~200°C. Primary and pseudosecondary inclusions with high T_H are interpreted to have reequilibrated due to microscopically unrecognized stretching and/or water leakage that would both result in a decrease in inclusion density and consequently in apparently higher T_H.

↑ Figure 5.5 High-T_H inclusions are interpreted to have reequilibrated since selective water leakage would result in a density loss and thus elevated homogenization temperatures **b** Inclusion dimensions of potentially reequilibrated inclusions tend to be bigger compared to the low-T_H inclusions. The apparent absence of reequilibrated secondary inclusions is assumed to be due to a better ability to characterize the generally larger secondary inclusions microscopically and hence to recognize reequilibration effects and avoid these inclusions for further analyses.

P-T calculations for aqueous inclusions were performed for each an averaged, representative inclusion (PI: T_H = 218 °C, $T_{M(ice)}$ = -35.6 °C; PSI: T_H = 202 °C, $T_{M(ice)}$ = -20.3 °C; SI: T_H = 193 °C, $T_{M(ice)}$ = -2.5 °C) of all three aqueous groups, combining averaged solute fractions independently obtained from UV-fs-LA-ICPMS. Fluid densities and isochores were determined using the programs *BULK* (calculates bulk fluid inclusion densities from measured T_H) and *ISOC* (the previously calculated T_H are used to derive corresponding isochores) of BAKKER (2003), applying the equations of state (EoS) for aqueous salt-bearing solutions from ZHANG AND FRANTZ (1987) and OAKES ET AL. (1990). The

calculations yielded similar P-T conditions of inclusion formation for all three inclusion types, namely within the amphibolite facies field (**Figure 5.12**). At least for PI and PSI these results do not coincide with the trapping conditions indicated by petrographic evidence and document a late density reequilibration. It has to be noted that the available EoS are not explicitly designed for pressures beyond 100 MPa and may deliver questionable results due to extrapolation biases.

5.3.3   Individual fluid inclusion chemistry by in-situ UV-fs-LA-ICPMS

Element concentrations determined by UV-fs-LA-ICPMS in 62 individual inclusions in quartz from all three aqueous groups document a clear difference in PI and SI fluid compositions. Inclusions in eclogitic garnet could not be analyzed due to sizes smaller than 5 μm. The solute content of PSI is generally only slightly lower compared to that of the PI (**Figure 5.5**, cf. **Figure 5.3b**). Results obtained from microthermometry (**Figure 5.2b**) are also similar. The inclusions analyzed by UV-fs-LA-ICPMS are not the same as those analysed above. We have chosen different thick section chips in order to assure that the inclusions are as pristine as possible and not modified by previous measurements cooling and heating procedures. Only T_E and $T_{M(ice)}$ were recorded without heating up to homogenization. However, our earlier salinity estimates from the conventional microthermometric measurements can thus be compared to the UV-fs-LA-ICPMS analytical results:

(PI)   Early inclusions with primary character and total salinities between 25 and 33 wt% $NaCl_{eq}$ contain between 11 - 24 wt% NaCl, 6 - 17 wt% $CaCl_2$ and 1 - 3 wt% KCl. Along with these main components, lithium (15 - 452 ppm), boron (322 - 1573 ppm), barium (473 - 2519 ppm), rubidium (4 - 73 ppm) and strontium (569 - 3239 ppm) are found in most inclusions. Few inclusions contain Mg (5 – 167 ppm), Al (47 – 788 ppm) and Ti (207 – 2768 ppm).

(PSI)   Intermediate inclusions with pseudosecondary character and total salinities between 5 and 32 wt% $NaCl_{eq}$ contain between 4 - 26 wt% NaCl, 0 - 12 wt% $CaCl_2$ and 0 - 3 wt% KCl. Along with these main components, lithium (3 - 507 ppm), boron (49 - 883 ppm), barium (2 - 983 ppm), rubidium

(1 - 52 ppm) and strontium (3 - 1676 ppm) are found in most inclusions. In few inclusions Mg (5 - 1884 ppm), Al (13 – 2245 ppm) and Ti (27 – 552 ppm) were detected.
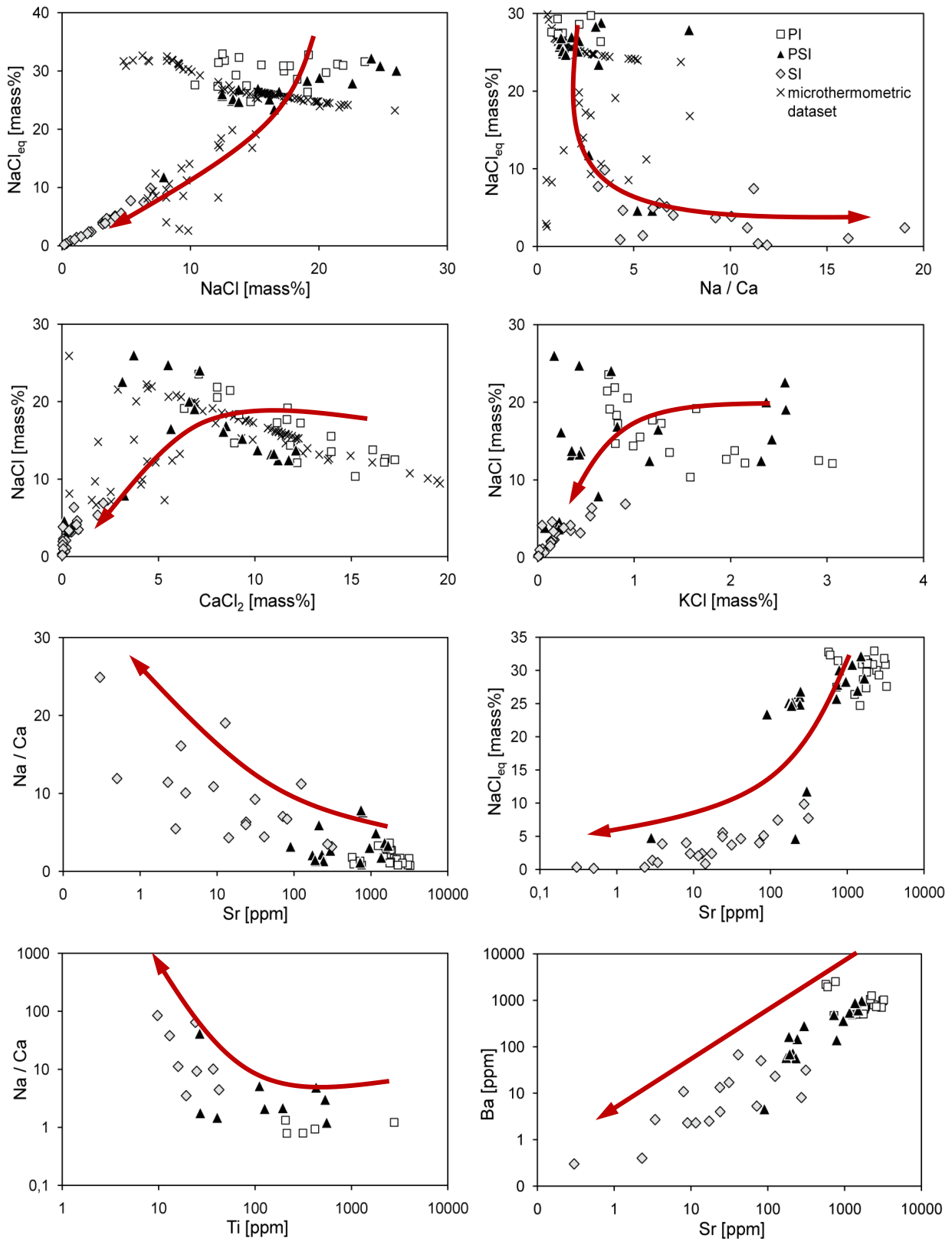
↑ **Figure 5.6 (previous page)** Multielement plots of both fs-UV-LAICPMS data, discriminating primary (PI), pseudosecondary (PSI), secondary inclusions (SI), and the bulk microthermometric dataset. The data demonstrate (1) high solute content in early inclusions, (2) decreasing Ca content with time up to pure Na solutions in SI, (3) similarity between PSI and PI, with PSI tending to generally lower solute contents, and (4) fluid mobility of K and Ti. Arrows trace the development from genetically old (PI) towards young inclusions (SI).

(SI) Secondary inclusions contain a fluid with a different composition and distinctly lower solute contents, compared to PSI and PI. Total salinities $NaCl_{eq}$ range between 0.2 - 10 wt% and the inclusions contain between 0.2 - 7 wt% NaCl, 0 - 2 wt% $CaCl_2$ and 0 - 0.9 wt% KCl. Trace element contents are generally very low and sometimes below the limit of detection (lithium: 0 - 99 ppm, boron: 15 - 939 ppm, barium: 0 - 67 ppm, rubidium: 0 - 17 ppm, and strontium: 0 - 311 ppm). Mg (3 – 16 ppm), Al (2 – 1201 ppm) and Ti (10 – 16 ppm) were detected in few inclusions.

Rather than being an original fluid component, the sporadic occurrence of comparatively high amounts of both Mg, Al and Ti in some inclusions (> 500 ppm) might be due to tiny solid phases in the inclusion that could not be discovered by optical observation and that are not necessarily daughter crystals (e.g. rutile, amphibole).

5.3.4 Oxygen isotopic compositions of eclogite and vein minerals

Oxygen isotopic compositions are expressed in a linearized form of the common delta notation, and express the deviation of the ratio $^{18}O/^{16}O$ to $^{17}O/^{16}O$ in a sample relative to the internationally defined standard VSMOW (Vienna Standard Mean Ocean Water):

$$\delta'^{17}O_{VSMOW}^{sample} = 1000 \cdot ln\left(\frac{\delta^{17}O}{1000} + 1\right) \qquad \text{and} \qquad \delta'^{18}O = 1000 \cdot ln\left(\frac{\delta^{18}O}{1000} + 1\right)$$

Oxygen isotopic compositions of bulk eclogite samples correlate with the grade of eclogite retrogression. Pristine samples have δ'^{18}O values between 4 – 8 ‰, which can be considered typical for unaltered continental basalts (HARMON AND HOEFS, 1995). Retrograded samples, in contrast, show

significantly lowered $\delta'^{18}O$ in the range of -3 – 0 ‰ (**Figure 5.7**), implying isotopic exchange with low-$\delta'^{18}O$ retrogression-related fluids. The isotopic composition of such a fluid is estimated by utilizing triple oxygen isotope $\Delta'^{17}O$ systematics of pristine and fluid-affected eclogites according to the approach of HERWARTZ ET AL. (2015). $\Delta'^{17}O$ is defined as

$$\Delta'^{17}O = \left[1000 \cdot ln\left(\frac{\delta^{17}O}{1000} + 1\right)\right] - 0.5305 \times \left[1000 \cdot ln\left(\frac{\delta^{18}O}{1000} + 1\right)\right]$$

which is equivalent to:

$$\Delta'^{17}O = \delta'^{17}O - 0.5305 \times \delta'^{18}O$$

In this approach, pristine eclogites are regarded as the fluid-unaffected endmember of simple mixing with an 100% fluid-altered eclogite in equilibrium with meteoric water of a certain isotopic composition. The approach delivers a theoretical $\delta'^{18}O$ for these waters of in a range of -15 to -25 ‰, within the 1σ uncertainty of the averaged retrogressed eclogite (**Figure 5.8**).
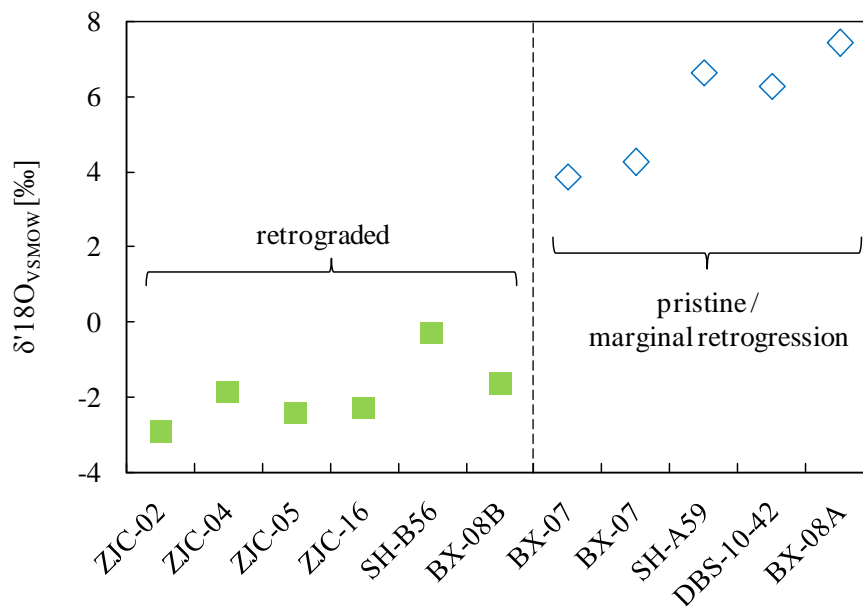
↑ **Figure 5.7** Only fluid-affected, retrogressed eclogites show unusually low oxygen isotopic compositions, whereas pristine samples have values typical for continental basaltic rocks.
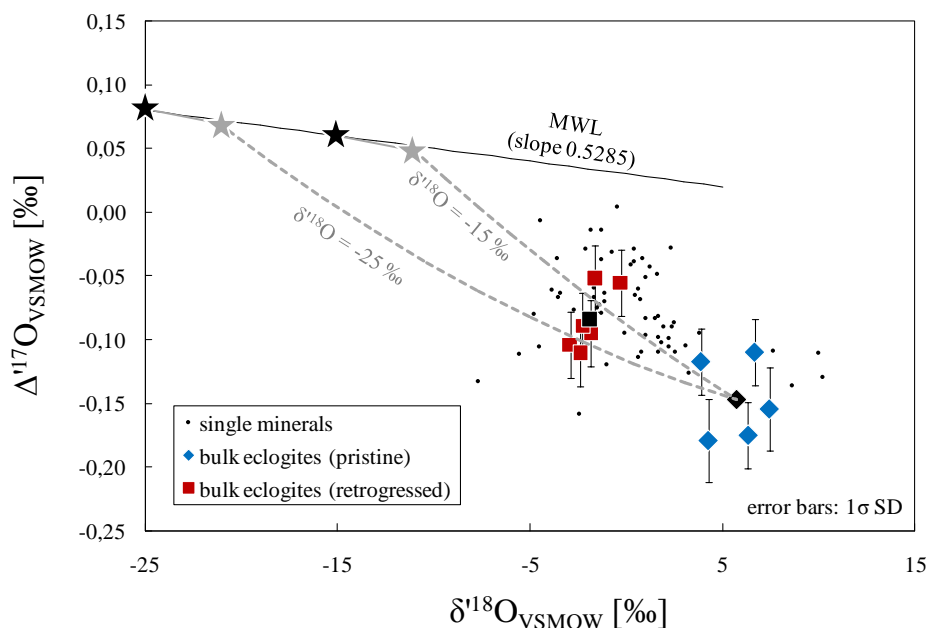
↑ Figure 5.8 Expected $\delta'^{18}O$ isotopic compositions of meteoric waters (black stars) interacting with the eclogitic precursors. Grey stars label 100% fluid-altered endmembers in equilibrium (slope 0.5305) with the meteoric water isotopic composition (black stars). The mixing line (in this case virtually linear) was calculated according to HERWARTZ ET AL. (2015) and corresponds to a degree of alteration of about 30% for retrograded samples. This is in broad agreement with the observed proportion of ~20 - 30% retrograde minerals in the retrogressed eclogites. Filled black diamond: averaged pristine bulk eclogites, filled black square: averaged metasomatized bulk eclogites. MWL: meteoric water line.

A comparison of all analyzed eclogitic and vein minerals illustrates that 1st generation vein quartz as well as eclogitic quartz (sample SH-A59, -A60) coincide and are in equilibrium with the eclogite assemblage (**Figure 5.9**), leading to the conclusion of an eclogite-internal derivation of the vein-forming fluid without influence of any retrograde low-$\delta'^{18}O$ fluid.

2nd generation vein minerals and minerals from retrogressed eclogites, in contrast, exhibit consistently lowered $\delta'^{18}O$, but are still broadly in equilibrium in each sample, except for quartz in ZJC-08 (higher than expected), and amphibole in ZJC-16 (higher than expected). This is evident for a direct relation of 2nd generation vein formation and pervasive retrogression in eclogites.

The apparent disequilibrium between quartz and amphibole/epidote in ZJC-08 is possibly due to a very late qtz-crystallization that is unrelated to the retrograde low-$\delta'^{18}O$ fluid that previously precipitated epidote and amphibole during the amphibolite facies metamorphic stage.

The apparent disequilibrium of amphibole in ZJC-16 with the eclogitic phases is likely to be a sampling bias, since a contamination with albite was virtually not avoidable during handpicking of amphibole. The albite content would furthermore explain the bulk composition that is above all other phases.
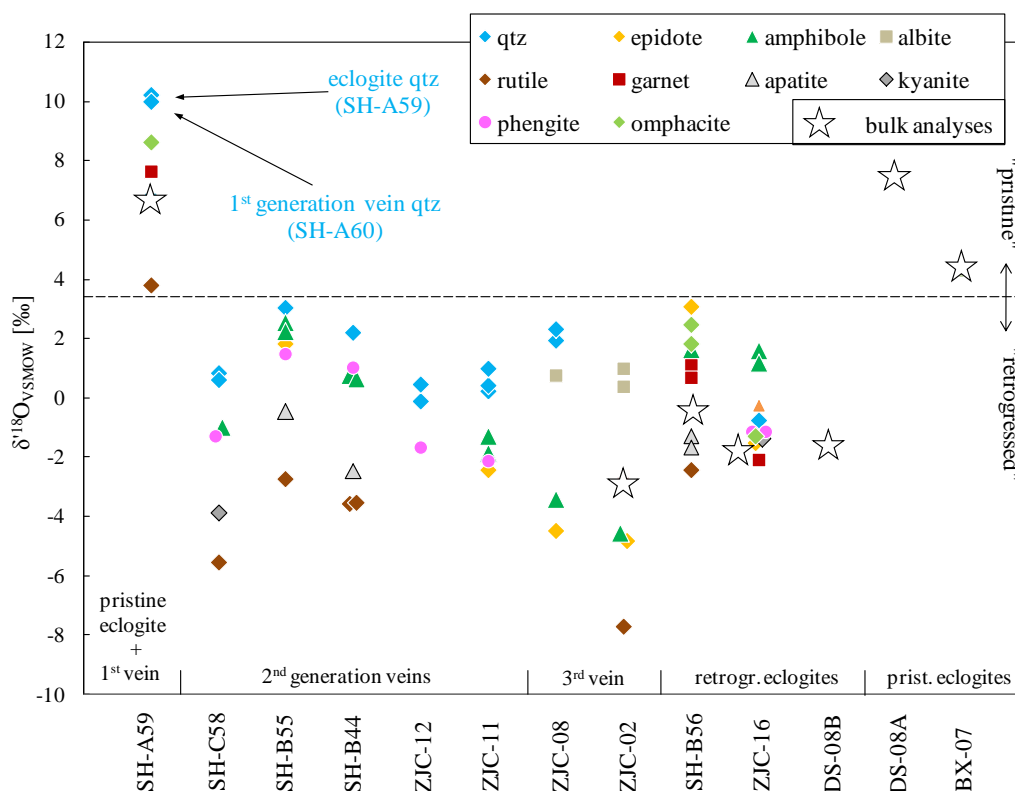
↑ **Figure 5.9** Illustration of $\delta'^{18}O$ in all available ("pickable") eclogitic and vein minerals broadly displays isotopic equilibrium in all samples and furthermore demonstrates that 1st generation veins are internally derived without influence of a low-$\delta'^{18}O$ retrogressive fluid, while 2nd generation veins and pervasive retrogression (ie. retrograde minerals in eclogites) apparently share a fluid source. Typical errors close to symbol size (~0.2 ‰).

5.4 Discussion

5.4.1 Origin of the vein-forming fluids

Prograde fluids

Prograde fluids are liberated due to the breakdown of hydrous minerals, and to a minor extent the liberation of primary fluid inclusions (ZHENG, 2004A) from minerals in the subducting slab and possibly an older, subducted basement of the Dabieshan (FRANZ ET AL., 2001). While early amphibole breakdown, occurring continuously over a range between 65 and 90 km depth (SCHMIDT AND POLI, 1998), releases mobile, hydrous and silica-poor fluids, the later dehydration under prograde eclogite facies conditions at depths >90 km is results in the formation of H_2O-rich fluids with a significant solute content (eg. HERMANN ET AL., 2006).

At increasing pressure conditions, part of this fluids' water can be dissolved either as structural hydroxyl or as molecular water into nominally anhydrous minerals in a rock (ZHENG, 2009). In addition, fluid components may be bound in newly forming HP hydrous minerals (such as phengite or zoisite) during burial. Both effects will result in the removal of water molecules from the metamorphic fluid phase. This essentially leads to a "dehydration" of the fluid and this prograde distillation process could account for high salinity and brine-like, Si- and Cl-rich residual fluids as typical for prograde high-grade metamorphic rocks (YARDLEY AND GRAHAM, 2002). Besides, the prograde decomposition of ammonium-bearing minerals is likely to provide nitrogen as a source of the observed N_2-inclusions. Owing to the basaltic precursor of the eclogites, feldspar and amphibole are the most likely candidates for a potential nitrogen source, and would also account for the remarkably high Ca content in the prograde fluids.

Such prograde fluids are inferred to be represented by the observed highly saline PI in pristine garnet, and the most likely source to 1st generation veins that formed shortly after the UHP metamorphic peak (LI ET AL., 2004; ZHENG ET AL., 2007A), and recrystallized during the coeiste–quartz transition. The exclusive occurrence of nitrogen in 1st generation veins in the form of pure high-density inclusions, rather than dissolved in the aqueous inclusions, is interpreted to be owed to the $N_2 - H_2O$ immiscibility beyond $2 - 2.2$ GPa, as described by HAEFNER ET AL., (2002), thus pointing to an early HP formation of the NI.

The prograde fluids do apparently not result in a formation of complex (2nd generation-type) veins in pristine eclogites, but only leave 1st generation qtz-HFSE veins behind. This is attributed to (i) virtually inhibited hydraulic fracturing during the UHP metamorphic peak, and (ii) associated low fluid volumes considering only internal (basaltic) fluid sources.

Retrograde fluids

Compared to prograde fluids that are argued to have precipitated 1st generation veins in pristine eclogites, the formation of 2nd generation veins is restricted to retrograded eclogites that were interpreted in **Chapter 4** to have experienced prograde Ca- and OH-metasomatism in the form of lawsonitization prior or during eclogitization. Resulting higher water contents in those eclogites and a pressure release at the onset of exhumation (the deduced timeframe for 2nd generation veining) enables hydraulic fracturing in the course of decompressional dehydration of water-bearing metasomatic minerals, such as lawsonite.

The major source of the post-peak, 2nd generation vein-forming fluids are proposed to be bedrock gneisses as indicated by strontium isotope characteristics (**Chapter 4**), and both fluid inclusion chemistry and oxygen isotopes support this assumption. The correlation of $\delta'^{18}O$ and $^{87}Sr/^{86}Sr$ (**Figure 5.10**) demonstrates that fluid-rock interaction consistently transfers both Sr- and O-isotopic fingerprints of Dabie gneisses onto the fluid-affected eclogites. As already discussed in **Chapter 4**, the

radiogenic Sr-signature is a result of Rb/Sr fractionation in phengite, which is a rock-forming mineral in gneiss, and dehydrational fluids adopt this signature.

The oxygen isotopic signature of retrograded eclogites requires the interaction with a fluid of nearly $\delta'^{18}O = -20‰$ (**Figure 5.8**). Non-glacial precipitation at Phanerozoic palaeolatitudes of central China (30 – 40°N) does not fall below -10 ‰ (IAEA, 2001) and does hence not come into question as a possible source. Such light oxygen isotope compositions are naturally only realized when heavy oxygen is effectively 'removed' from the precipitation reservoir on a large scale. This is exclusively realized during glaciation events, where ^{18}O is preferentially bound in ice. Several authors thus proposed glacial fluid-rock interaction of crustal rocks with light waters prior to subduction that produce the low oxygen signatures in the gneisses (BAKER ET AL., 1997; FU ET AL., 1999; HERWARTZ ET AL., 2015; TANG ET AL., 2008; YUI ET AL., 1995; ZHENG ET AL., 1998, 2003B, 2004B). The continental, Neoproterozoic glaciation corresponding to the Kaigas ice age is related to this fluid-rock interaction by ZHENG ET AL. (2007B), since the subducted precursor rocks in Dabieshan have about Neoproterozoic ages (eg. HIRAJIMA AND NAKAMURA, 2003).
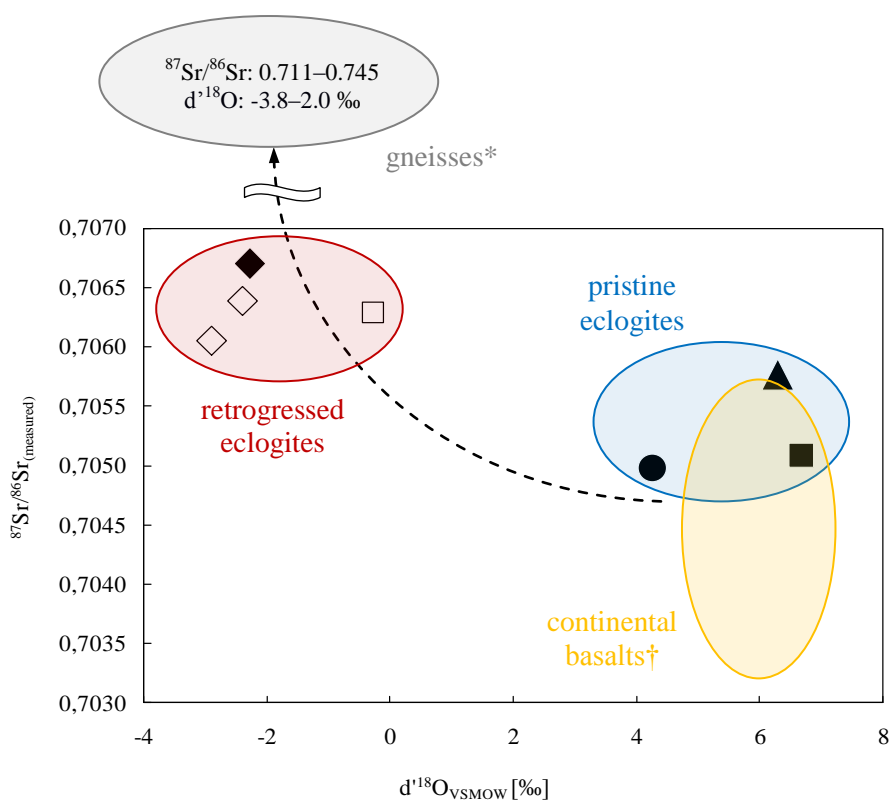
↑ **Figure 5.10** The degree of retrogression in bulk eclogites from different investigated localities correlates with $^{18}O/^{16}O$ as well as $^{87}Sr/^{86}Sr$ ratios. This indicates a fluid source that is related to (i) glaciation prior to subduction and (ii) to the gneissic lithologies in which the eclogites are embedded. Standard errors (2σ) within symbol size. *Gneiss d'^{18}O from FU ET AL. (1999) and ZHENG ET AL. (2003B), $^{87}Sr/^{86}Sr_{(measured)}$ after CHAVAGNAC AND JAHN (1996), CHEN AND JAHN (1998), GUO ET AL. (2014) AND LI ET AL. (2000). †Continental basalt d'^{18}O and $^{87}Sr/^{86}S_r$ from HARMON AND HOEFS (1995).

Considering strontium and oxygen isotope evidence, along with the chemical signature of fluid-affected eclogites and the field observation of an occurrence of retrograded, low δ'^{18}O eclogites predominantly at the eclogite-gneiss margin, the following scenario is deduced:

Neoproterozoic pervasive glacial fluid-rock interaction causes low δ'^{18}O in gneisses at low temperatures and shallow crustal levels. During Triassic subduction, compressional gneiss dehydration results in the formation of low-δ'^{18}O fluids that are rich in water, Ca, Al and Na, and have high $^{87}Sr/^{86}Sr$ (inherited from gneissic mica). These fluids infiltrate intercalated basaltic bodies and since eclogites are more resistant towards fluid infiltration, the gneiss fluid signature is predominantly transferred at the eclogite-gneiss interface by prograde pervasive metasomatism in the form of lawsonitization (cf. **Chapter 3** and **4**). 2nd generation veining occurs on the retrograde path, fed by two fluids with comparable compositional characteristics: fluids that are released during early retrograde lawsonite breakdown (type I veins) and external gneissic fluids (type II veins). Characteristically low $^{206}Pb/^{204}Pb$ are produced during epidote crystallization, since epidote group minerals fractionate Pb over U relative to the eclogite precursor.

5.4.2 Compositional evolution of the post-peak vein-forming fluids

In a summary model (**Figure 5.12**), the fluids involved in vein formation are considered to be conceptually linked to a sequence of prograde and retrograde dehydration processes. The different types of observed fluid inclusions are argued to correspond to these vein-forming fluids, and their relation is discussed here.

The fluid inclusion study reveals three aqueous inclusion groups (early and highly saline PI, intermediate and variably lower saline PSI, late and low-saline SI) that are defined on the basis of textural criteria. Each group shows characteristic compositional features, and according to STERNER AND BODNAR, (1989) and GAO AND KLEMD, (2001) the qualitative composition of the trapped fluids should not be affected even if reequilibration occurred. Systematical selective leakage has been described before, but only for gaseous species (CO_2, H_2O. H_2, CH_4) (RIDLEY AND HAGEMANN, 1999; BAUMGARTNER ET AL., 2014; SPENCER ET AL., 2015). LI ET AL. (2009) experimentally documented a Na-loss from reequilibrated fluid inclusions along with an distinct accumulation of Cu at 0.2 GPa. BAKKER AND DOPPLER (2016) found that the two main modification processes of fluid H_2O – NaCl inclusions at around 0.4 GPa are preferential loss of H_2O via diffusion and total volume loss by diffusion of quartz into the original inclusion volume. Individual fluid inclusion chemistries should thus be widely retained during reequilibration.

Based on petrographic observations that allow the derivation of a temporal sequence of these inclusion types, the most striking inference is a decreasing solute content of the metamorphic fluids with time. Although the time frame cannot be determined absolutely, at least the earliest, highly saline fluid trapped in PI in 1st generation veins can be directly assigned to the retrograde quartz–coesite transition (~2.7 GPa and 700°C), as deduced in **Chapter 4**, presuming that a fluid inclusion cannot be preserved during a mineral phase transition. The salinity characteristics as determined by microthermometry in the salt system H_2O – NaCl – $CaCl_2$ were precisely confirmed and refined by UV-fs-LAICPMS analyses of individual inclusions of all types, except for very unworkable inclusions (<5 µm) in garnet. Results support the trend of a development from early Ca-rich brines (as trapped in PI and PSI) to Na-dominated solutes (as trapped in SI) along the retrograde path, coinciding with the findings of XIAO ET AL., (2000). The authors describe high-salinity PI in prograde kyanite, deducing a Ca-brine fluid already to exist during the prograde metamorphic stage. The same may analogously derived from the few high salinity inclusions observed in prograde garnet in the present work. The fact that compositionally comparable inclusions were found in both such 1st generation vein quartz and in UHP eclogitic (formerly coesite-bearing) prograde garnet suggests a compositional similarity of prograde and early retrograde fluids, which supports the arguments in **Chapter 5.4.1**.

Moreover, potassium is identified to be a main solute in highly saline inclusions (PI and PSI). The detection of significant concentrations of Al, Mg, and Ti in PSI and PI, displays the ability of the HP fluid to transport these nominally fluid-immobile elements. In addition, UV-fs-LAICP-MS analyses allow the fluids to be further characterized, with respect to mobile elements Sr, Rb, Ba, Li and B, all following the general depletion trend with time. Their additional presence besides the major components accounts for the remarkably low eutectic temperatures of down to -77 °C. The results suggest that PI and PSI entrapped a very similar fluid, with the only difference of a lower and more variable solute content in the PSI. Their entrapment not only represents similar fluids but also occurred close in time as indicated by similar T_H, indicating a solute dilution with time and probably small-scale fluid mixing during early retrogression.
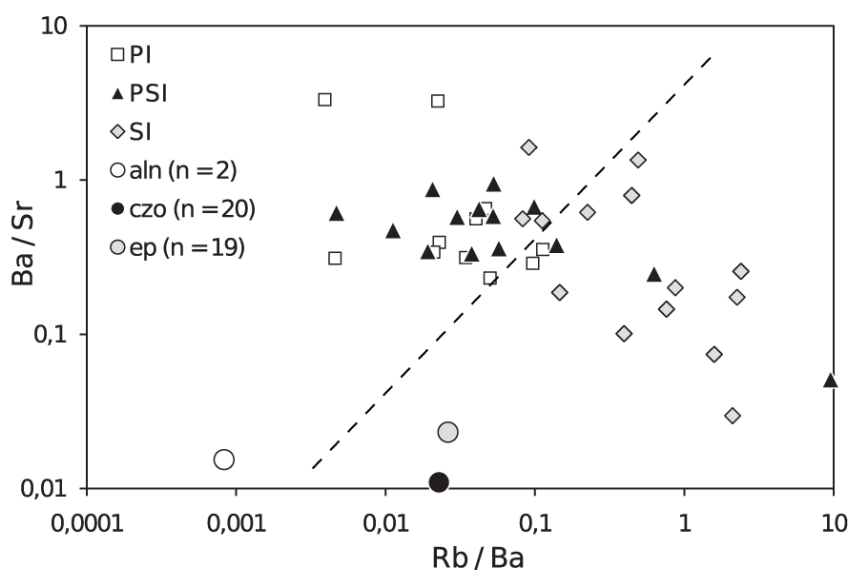
↑ **Figure 5.11** Ba/Sr vs. Rb/Ba from fs-UV-LAICPMS fluid inclusion dataset, as well as LA-ICPMS analyses for all three mineral growth zones (allanite, clinozoisite, epidote). Rb/Ba ratios in epidote and clinozoisite correlate with those in secondary inclusions, while Rb/Ba in both primary and pseudosecondary inclusions as well as in allanite is systematically lower.

Given the argumentation that the compositional zoning of allanite-clinozoisite-epidote in the veins (**Chapter 4**) documents the temporal compositional changes in the fluid after peak metamorphic conditions, it is a reasonable test to correlate mineral compositions to fluid compositions. This is illustrated in **Figure 5.11**. The comparison of Rb/Ba and Ba/Sr ratios in fluid inclusions and the three epidote growth zones are changing in the same systematic way. Early, trace element-rich allanite is low in both Ba/Sr and Rb/Ba ratios and the earliest post-peak fluids circulating during the coesite–quartz transition are also low in Rb/Ba (but not Ba/Sr). By contrast, later clinozoisite and epidote from more diluted fluids have high Rb/Ba and correspond to fluids in secondary inclusions which are equally higher in Rb/Ba. Since highly saline and diluted fluids are similar in Ba/Sr, the corresponding allanite-zoisite and epidote compositions are also uniform. Thus, the systematic variations in fluid composition and in zoned minerals are consistent. Also, the relative depletion in Ba over Sr and Rb over Ba in the minerals is conceptually consistent with experimental HP fluid-mineral trace element partitioning (BRENAN ET AL., 1995; FEINEMAN ET AL., 2007; MARTIN ET AL., 2011).

The fluid depletion trend recorded by the temporal sequence of fluid inclusions and epidote chemistry is explained as follws:

Since progressive uplift along the retrograde path results in both the formation of retrograde assemblages in the hosting eclogite and in the crystallization of epidote, phengite, kyanite, barroisite, quartz and minor rutile in 2nd generation veins, the metamorphic fluid solute content is continuously depleted.

Abundantly crystallizing epidote group minerals are claimed to be the major sink for Ca and most trace elements, owing for the evolution towards Na-dominated, trace element-poorer fluid compositions. Accordingly, the enriched allanite cores and successively clinozoisite mantles of the observed zoned epidote group minerals have precipitated from these early fluids.

At a late retrograde stage beyond the amphibolite facies, the remaining fluid has become diluted due to both decompressional water release from nominally anhydrous minerals and consumption via the crystallization of vein minerals and retrograde assemblage in the eclogite. It is assumed to be the source of 3rd generation vein precipitation and is entrapped in the low-salinity PSI and SI within.

As reflected by fluid chemistry and trace element patterns from epidotes, the composition of the final third-stage fluid that is entrapped in late SI is expected to distinctly differing from the first- and second-stage fluids. The most striking differences are a pronounced gap in elemental concentrations, especially for Ca, Na, K and Sr (**Figure 5.6**), and enriched HREE in the youngest epidote generation EP (**Figure 4.12b**). These features are explained by (i) a late dilution with more or less zero-salinity meteoric waters as well as the crystallization of Na-rich minerals (e.g. albite in the 3rd generation veins) and (ii) the incipient alteration of HREE-bearing garnet in the eclogite.

In conclusion, PI trap the initial fluid released from lawsonite breakdown and from surrounding gneisses, PSI trap this same fluid on successively diluted stages, and SI trap a Ca-poor remainder of this fluid, that is possibly mixed with meteoric waters during a late retrograde stage.
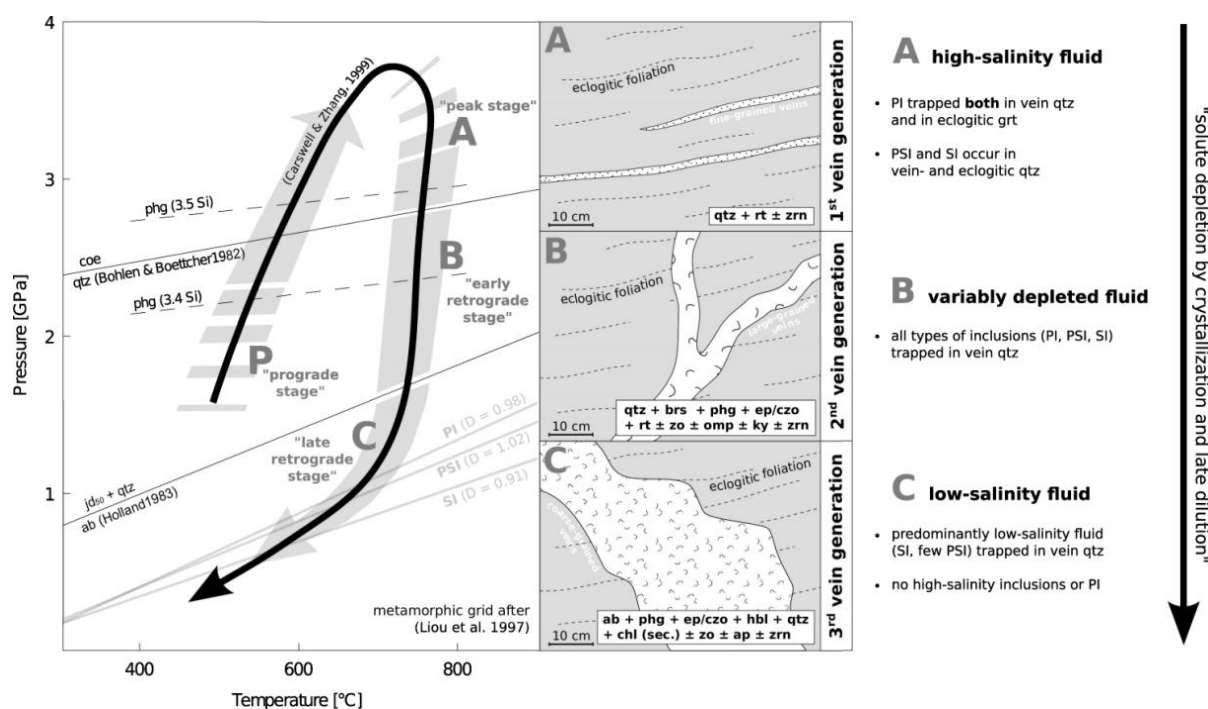
↑ **Figure 5.12** Schematic illustration of vein and fluid evolution along the retrograde metamorphic path. A prograde (stage P) high-salinity fluid is entrapped in primary fluid inclusions in prograde garnet. A post-peak high salinity fluid that originates from surrounding gneisses and decompressional lawsonite breakdown is trapped in PI and early PSI IN both 1st and 2nd generation vein minerals. The crystallization of 2nd generation veins and retrograde eclogite phases lead to a successive depletion of the initial fluid during exhumation (stage B) and the entrapment of fluid inclusions with variably depleted compositions. An assumed introduction of meteoric waters during a late retrograde stage C results in the formation of low-salinity fluid inclusions in 3rd generation veins.

5.4.3 Meaning of microthermometric P-T estimates

As to be expected from the maximum calculable pressure for pure H_2O ($T_H = 0$ °C) of about 2 GPa, the representatively calculated fluid isochores do not match the expected (ultra-)high pressure conditions, at least for PI and PSI (**Figure 5.12**). This is interpreted to be a result of in-situ reequilibration at later retrograde conditions, potentially near the entrapment conditions of the late SI fluid. The isochore most closely related to high-grade metamorphic conditions was calculated by FU ET AL. (2003) for an aqueous inclusion from Dabie Sulu. However, it touches only the lower end of the eclogite facies field with about 1.1 GPa at 600 °C. As a consequence and as also concluded by FU ET AL. (2003), the structural and petrographic characterization of the inclusions is the crucial factor in terms of fluid chronology in high-grade metamorphic regimes.

5.5   Conclusions

(1) Microthermometric results coincide with UV-fs-LAICPMS data and are essentially refined by enabling the quantification of trace element contents.

(2) Prograde fluids are preserved in UHP eclogitic pristine garnet as primary inclusions and demsontrate the existence of a high salinity fluid on the prograde path. The internal amount of this fluid in pristine (unmetasomatized) eclogites is not sufficient to cause hydraulic fracturing and 2nd generation type veins, but only produces small-scaled 1st generation veins.

(3) Initial post-peak fluids are a mixture of external gneiss-derived fluids and internal fluids that evolve from the breakdown of metasomatic minerals such as lawsonite. These fluids initiate 2nd generation vein formation and pervasive retrogression.

(4) The post-peak fluids are successively depleted during exhumation, due to solute consumption in the course of hydrous vein mineral and retrograde mineral crystallization along an early retrograde stage, and dilution with meteoric waters at a late retrograde stage beyond the stability of garnet.

(5) The fluid depletion trend is consistently recorded by both fluid inclusions and epidote chemistry: PI trap the earliest fluid present at the onset of exhumation and correspond to

allanite/zoisite. PSI trap the successively depleted fluid at variable retrograde HP stages, as likewise recorded in clinozoisite. SI trap the most depleted remainder of the earlier fluids that are potentially diluted with meteoric waters, and correlate with late epidote overgrowths.

(6) The P-T calculations on high grade metamorphic fluid inclusions provide unusable results that underestimate the real trapping conditions due to internal pressure reequilibration.

5.6 References

Albrecht M, Derrey IT, Horn I, Schuth S, Weyer S (2014) Quantification of trace element contents in frozen fluid inclusions by UV-fs-LA-ICP-MS analysis. *J Anal At Spectrom 29*: 1034–1041.

Andersen T, Austrheim H, Burke EAJ, Elvevold S (1993) N_2 and CO_2 in deep crustal fluids: evidence from the Caledonides of Norway. *Chem Geol 108*: 113–132.

Andersen T, Burke EAJ, Austrheim H (1989) Nitrogen-bearing, aqueous fluid inclusions in some eclogites from the Western Gneiss Region of the Norwegian Caledonides. *Contrib Mineral Petrol 103*: 153–165.

Angus SB, Armstrong B, de Reuck KM (1979) International Thermodynamic Tables of the Fluid State – 6. Nitrogen. *Pergamon Press*, Oxford

Ayers JC, Watson EB (1993) Rutile solubility and mobility in supercritical aqueous fluids. *Contrib Mineral Petrol 114*: 321–330.

Baker J, Matthews A, Mattey D, Rowley D, Xue F (1997) Fluid–rock interactions during ultra-high pressure metamorphism, Dabie Shan, China. *Geochim Cosmochim Ac 61*: 1685–1696.

Bakker RJ (2003) Package FLUIDS 1: Computer programs for analysis of fluid inclusion data and for modeling bulk fluid properties. *Chem Geol 194*: 2–23.

Bakker RJ, Doppler G (2016) Salinity and density modifications of synthetic H 2 O and H 2 O–NaCl fluid inclusions in re-equilibration experiments at constant temperature and confining pressure. *Chem Geol 424*: 73–85.

Baumgartner M, Bakker RJ, Doppler G (2014) Re-equilibration of natural H2O–CO2–salt-rich fluid inclusions in quartz — Part 1: experiments in pure water at constant pressures and differential pressures at 600° C. *Contrib Mineral Petrol 168(1)*: 1–14.

Becker H, Jochum KP, Carlson RW (1999) Constraints from high-pressure veins in eclogites on the composition of hydrous fluids in subduction zones. *Chem Geol 160*: 291–308.

Bodnar RJ (1993) Revised equation and table for determining the freezing point depression of H_2O - NaCl solutions. *Geochim Cosmochim Ac 57*: 683–684.

Brenan JM, Shaw HF, Ryerson FJ, Phinney DL (1995) Mineral-aqueous fluid partitioning of trace elements at 900°C and 2 GPa: Constraints on the trace element chemistry of mantle and deep crustal fluids. *Geochim Cosmochim Ac 59*: 3331–3350.

Carswell DA, O'Brien PJ, Wilson RN, Zhai M (1997) Thermobarometry of phengite-bearing eclogites in the Dabie Mountains of central China. *J Metamorph Geol 15(2)*: 239–252.

Castelli D, Rolfo F, Compagnoni R, Xu ST (1998) Metamorphic veins with kyanite, zoisite and quartz in the Zhu-Jia-Chong eclogite, Dabie Shan, China. *Isl Arc 7*: 159–173.

Feineman MD, Ryerson FJ, DePaolo DJ, Plank T (2007) Zoisite-aqueous fluid trace element partitioning with implications for subduction zone fluid composition. *Chem Geol 239*: 250–265.

Ferrando S, Frezzotti ML, Dallai L, Compgnoni R (2005) Multiphase solid inclusions in UHP rocks (Su-Lu, China): Remnants of supercritical silicate-rich aqueous fluids released during continental subduction. *Chem Geol 223*: 68–81.

Franz L, Romer RL, Klemd R, Schmid R, Oberhänsli R, Wagner T, Shuwen D (2001) Eclogite-facies quartz veins within metabasites of the Dabie Shan (eastern China): pressure-temperature-time-deformation path, composition of the fluid phase and fluid flow during exhumation of high-pressure rocks. *Contrib Mineral Petr 141*: 322–346.

Fu B, Zheng YF, Wang Z, Xiao Y, Gong B, Li S (1999) Oxygen and hydrogen isotope geochemistry of gneisses associated with ultrahigh pressure eclogites at Shuanghe in the Dabie Mountains. *Contrib Mineral Petrol 134*: 52–66.

Fu B, Zheng YF, Touret JLR (2002) Petrological, isotopic and fluid inclusion studies of eclogites from Sujiahe, NW Dabie Shan (China). *Chem Geol 187*: 107–128.

Fu B, Touret JLR, Zheng YF, Jahn BM (2003) Fluid inclusions in granulites, granulitized eclogites and garnet clinopyroxenites from the Dabie–Sulu terranes, eastern China. *Lithos 70*: 293–319.

Gao J, Klemd R (2001) Primary fluids entrapped at blueschist to eclogite transition: evidence from the Tianshan meta-subduction complex in northwestern China. *Contrib Mineral Petrol 142*: 1–14.

Gao J, John T, Klemd R, Xiong X (2007) Mobilization of Ti–Nb–Ta during subduction: Evidence from rutile-bearing dehydration segregations and veins hosted in eclogite, Tianshan, NW China. *Geochim Cosmochim Ac 71*: 4974–4996.

Guillong M, Meier DL, Allan MM, Heinrich CA, Yardley BWD (2008) SILLS - A MATLAB-based program for the reduction of laser ablation ICP-MS data of homogeneous materials and inclusions. *Mineral Assoc Can, Short Course 40*: 328–333.

Guo, S, Ye, K, Chen, Y, Liu, J, Mao, Q & Ma, Y (2012): Fluid–rock interaction and element mobilization in UHP metabasalt: Constraints from an omphacite–epidote vein and host eclogites in the Dabie orogen. *Lithos 136-139*: 145–167

Guo S, Ye K, Wu TF, Chen Y, Yang YH, Zhang LM, Liu JB, Mao Q, Ma YG (2013) A potential method to confirm the previous existence of lawsonite in eclogite: the mass imbalance of Sr and LREEs in multistage epidote (Ganghe, Dabie UHP terrane). *J Metamorph Geol 31*: 415–435.

Hack AC, Thompson AB, Aerts M (2007) Phase relations involving hydrous silicate melts, aqueous fluids, and minerals. *Rev Mineral Geochem 65*: 129–85.

Haefner A, Aranovich LY, Connolly JAD, Ulmer P (2002) H_2O activity in $H_2O - N_2$ fluids at high pressure and temperature measured by the brucite-periclase equilibrium. *Am Mineral 87*: 822–828.

Harmon RS, Hoefs J (1995) Oxygen isotope heterogeneity of the mantle deduced from global 18O systematics of basalts from different geotectonic settings. *Contrib Mineral Petrol 120(1)*: 95–114.

Heinrich CA, Pettke T, Halter WE, Aigner-Torres M, Audétat A, Günther D, Hattendorf B, Bleiner D, Guillong M, Horn I (2003) Quantitative multi-element analysis of minerals, fluid and melt inclusions by laser-ablation inductively-coupled-plasma mass-spectrometry. *Geochim Cosmochim Ac 67*: 3473–3497.

Hermann J, Spandler C, Hack A, Korsakov AV (2006) Aqueous fluids and hydrous melts in high-pressure and ultra-high pressure rocks: implications for element transfer in subduction zones. *Lithos 92(3)*: 399–417.

Herwartz D, Pack A, Krylov D, Xiao Y, Muehlenbachs K, Sengupta S, Di Rocco T (2015) Revealing the climate of snowball Earth from $\Delta^{17}O$ systematics of hydrothermal rocks. *P Natl Acad Sci 112(17)*: 5337–5341.

Hirajima T, Nakamura D (2003) The Dabie Shan–Sulu orogen. In: EMU Notes in Mineralogy 5: 105–144. Eötvös Univ. Press, Budapest.

Horn I, von Blanckenburg F, Schoenberg R, Steinhoefel G, Markl G (2006) In situ iron isotope ratio determination using UV-femtosecond laser ablation with application to hydrothermal ore formation processes. *Geochim Cosmochim Ac 70*: 3677–3688.

Horn I, von Blanckenburg F (2007) Investigation on elemental and isotopic fractionation during 196 nm femtosecond laser ablation multiple collector inductively coupled plasma mass spectrometry. *Spectrochim Acta B 62*: 410–422.

Hunt JD, Manning CE (2012) A thermodynamic model for the system SiO_2-H_2O near the upper critical end point based on quartz solubility experiments at 500-1100 °C and 5-20 kbar. *Geochim Cosmochim Ac 86*: 196–213.

IAEA (2001) GNIP Maps and Animations, *International Atomic Energy Agency*, Vienna.

Jacobsen RT, Stewart RB, Jahangiri M (1986) Thermodynamic Properties of Nitrogen from the Freezing Line to 2000 K at Pressures to 1000 MPa. *J Phys Chem Ref Data 15*: 735–909.

John T, Klemd R, Gao J, Garbe-Schönberg CD (2008) Trace-element mobilization in slabs due to non steady-state fluid–rock interaction: Constraints from an eclogite-facies transport vein in blueschist (Tianshan, China). *Lithos 103*: 1–24.

Keppler H (1996) Constraints from partitioning experiments on the composition of subduction-zone fluids. *Nature 380*: 237–240.

Kessel R, Schmidt MW, Ulmer P, Pettke T (2005) Trace element signature of subduction-zone fluids, melts and supercritical liquids at 120–180 km depth. *Nature 437*: 724–727.

Li XP, Zheng YF, Wu YB, Chen FK, Gong B, Li YL (2004) Low-T eclogite in the Dabie terrane of China: petrological and isotopic constraints on fluid activity and radiometric dating. *Contrib Mineral Petrol 148*: 443–470.

Li Y, Audétat A, Lerchbaumer L, Xiong XL (2009) Rapid Na, Cu exchange between synthetic fluid inclusions and external

Manning CE (2004) The chemistry of subduction-zone fluids. *Earth Planet Sc Lett 223*: 1–16.

Manning CE, Wilke M, Schmidt C, Cauzid J (2008) Rutile solubility in albite-H_2O and $Na_2Si_3O_7$-H_2O at high temperatures and pressures by in-situ synchrotron radiation micro-XRF. *Earth Planet Sc Lett 272*: 730–737.

Martin LAJ, Wood BJ, Turner S, Rushmer T (2011) Experimental measurements of trace element partitioning between

McKinney CR, McCrea JM, Epstein S, Allen HA, Urey HC (1950) Improvements in mass spectrometers for the measurement of small differences in isotope abundance ratios. *Rev Sci Inst 21(8)*: 724–730.

Nagasaki A, Enami M (1998) Sr-bearing zoisite and epidote in ultra-high pressure (UHP) metamorphic rocks from the Su-Lu province, eastern China: An important Sr reservoir under UHP conditions. *Am Mineral 83*: 240–247.

Newton RC, Manning CE (2002) Solubility of enstatite + forsterite in H_2O at deep crust / upper mantle conditions: 4-15 kbar and 700-900 °C. *Geochim Cosmochim Ac 66*: 4165–4176.

Newton RC, Manning CE (2003) Activity coefficient and polymerization of aqueous silica at 800 °C, 12 kbar, from solubility measurements on SiO_2-buffering mineral assemblages. *Contrib Mineral Petr 146*: 135–143.

Oakes CS, Bodnar RJ, Simonson JM (1990) The system NaCl-$CaCl_2$-H_2O: I. The ice liquidus at 1 atm total pressure. *Chem Geol 54*: 603–610.

Oeser M, Weyer S, Horn I, Schuth S (2014) High-Precision Fe and Mg Isotope Ratios of Silicate Reference Glasses Determined In Situ by Femtoscond LA-MC-ICP-MS and by Solution Nebulisation MC-ICP-MS. *Geostand Geoanal Res 38*: 311–328.

Okay AI, Xu S, Sengör AMC (1989) Coesite from the Dabie Shan eclogites, central China. *Eur J Mineral 1*: 595–598.

Pearce NJG, Perkins WT, Westgate JA, Gorton MP, Jackson SE, Neal CR, Chenery SP (1997) A compilation of new and published major and trace element data for NIST SRM 610 and NIST SRM 612 glass reference materials. *Geostandard Newslett 21*: 115–144.

Philippot P, Selverstone J (1991) Trace-element-rich brines in eclogitic veins: Implications for fluid composition and transport during subduction. *Contrib Mineral Petrol 106*: 417–430.

Philippot P (1993) Fluid-melt-rock interaction in mafic eclogites and coesite- bearing metasediments: Constraints on volatile recycling during subduction. *Chem Geol 108*: 93–112.

Philippot P, Chevallier P, Chopin C, Dubessy J (1995) Fluid composition and evolution in coesite-bearing rocks (Dora-Maira massif, Western Alps): Implications for element recycling during subduction. *Contrib Mineral Petrol 121*: 29–44.

Pronko PP, Dutta SK, Du D, Singh RK (1995) Thermophysical effects in laser processing of materials with picosecond and femtosecond pulses. *J Appl Phys 78*: 6233–6240.

Rapp JF, Klemme S, Butler IB, Harley SL (2010) Extremely high solubility of rutile in chloride and fluoride-bearing metamorphic fluids: An experimental investigation. *Geology 38*: 323–326.

Ridley J, Hagemann SG (1999) Interpretation of post-entrapment fluid-inclusion re-equilibration at the Three Mile Hill, Marvel Loch and Griffins Find high-temperature lode-gold deposits, Yilgarn Craton, Western Australia. *Chem Geol 154(1)*: 257–278.

Roedder E (1984) Reviews in Mineralogy Vol. 12, Fluid Inclusions. *Mineral Soc Am*, Washington.

Ryabchikov ID, Miller C, Mirwald PW (1996) Composition of hydrous melts in equilibrium with quartz eclogites. *J Miner Petrol 58*: 101–110.

Scambelluri M, Bottazzi P, Trommsdorff V, Vannucci R, Hermann J, Gomez-Pugnaire MT, Lòpez-Sanchez Vizcaìno V (2001) Incompatible element-rich fluids released by antigorite breakdown in deeply usbducted mantle. *Earth Planet Sc Lett 192*: 457–470.

Scambelluri M, Philippot P (2001) Deep fluids in subduction zones. *Lithos 55*: 213–227.

Schmidt MW, Poli S (1998) Experimentally based water budgets for dehydrating slabs and consequences for arc magma generation. *Earth Planet Sci Lett 163*: 361–379.

Sharp ZD (1990) A laser-based microanalytical method for the in situ determination of oxygen isotope ratios of silicates and oxides. *Geochim Cosmochim Ac 54(5)*: 1353–1357.

Sheperd TJ (1981) Temperature-programmable heating-freezing stage for microthermometric analysis of fluid inclusions. *Econ Geol 76*: 1244–1247.

Sheperd TJ, Rankin AH, Alderton DHM (1985) A practical guide to fluid inclusion studies. *Blackie and Son*, Glasgow.

Shutong X, Okay AI, Shouyuan J, Sengör AMC, Wen S, Yican L, Laili J (1992) Diamond from the Dabie Shan Metamorphic rocks and its implication for tectonic setting. *Science 256*: 80–82.

Spencer ET, Wilkinson JJ, Nolan J, Berry AJ (2015) The controls of post-entrapment diffusion on the solubility of chalcopyrite daughter crystals in natural quartz-hosted fluid inclusions. *Chem Geol 412*: 15–25.

Steele-MacInnis M, Bodnar RJ, Naden J (2011) Numerical model to determine the composition of H_2O-NaCl-$CaCl_2$ fluid inclusions based on microthermometric and microanalytical data. *Geochim Cosmochim Ac 75*: 21–40.

Sterner SM, Bodnar RJ (1989) Synthetic fluid inclusions – VII Re-equilibration of fluid inclusions in quartz during laboratory-simulated metamorphic burial and uplift. *J Metamorph Geol 7*: 243–260.

Stöckhert B, Duyster J, Trepmann C, Massonne HJ (2001) Microdiamond daughter crystals precipitated from supercritical COH + silicate fluids included in garnet, Erzgebirge, Germany. *Geology 29*: 391–394.

Su W, You Z, Cong B, Ye K, Zhong Z (2002) Cluster of water molecules in garnet from ultrahigh-pressure eclogite. *Geology 30*: 611–614.

Tang J, Zheng YF, Gong B, Wu YB, Gao TS, Yuan H, Wu FY (2008) Extreme oxygen isotope signature of meteoric water in magmatic zircon from metagranite in the Sulu orogen, China: implications for Neoproterozoic rift magmatism. *Geochim Cosmochim Ac 72(13)*: 3139–3169.

Vityk MO, Bodnar RJ (1995) Do fluid inclusions in high-grade metamorphic terranes preserve peak metamorphic density during retrograde decompression? *Am Mineral 80*: 641–644.

Wang X, Liou JG, Mao HK (1989) Coesite-bearing eclogites from the Dabie Mountains in central China. *Geology 17*: 1085–1088.

Wu YB, Gao S, Zhang HF, Yang SH, Liu XC, Jiao WF, Liu YS, Yuan HL, Gong HJ, He MC (2009) U–Pb age, trace-element, and Hf-isotope compositions of zircon in a quartz vein from eclogite in the western Dabie Mountains: constraints on fluid flow during early exhumation of ultrahigh-pressure rocks. *Am Mineral 94*: 303–312.

Xiao Y, Hoefs J, van den Kerkhof AM, Fiebig J, Zheng, Y (2000) Fluid history of UHP metamorphism in Dabie Shan, China: a fluid inclusion and oxygen isotope study on the coesite-bearing eclogite from Bixiling. *Contrib Mineral Petrol 139*: 1–16.

Xiao Y, Hoefs J, Hou Z, Simon K, Zhang Z (2011) Fluid/rock interaction and mass transfer in continental subduction zones: constraints from trace elements and isotopes (Li, B, O, Sr, Nd, Pb) in UHP rocks from the Chinese Continental Scientific Drilling Program, Sulu, East China. *Contrib Mineral Petrol 162*: 797–819.

Yardley BWD, Graham JT (2002) The origins of salinity in metamorphic fluids. *Geofluids 2(4)*: 249–256.

Yui, TF, Rumble, D, Lo CH (1995) Unusually low d^{18}O ultra-high-pressure metamorphic rocks from the Su-Lu Terrain, eastern China. *Geochim Cosmochim Ac 59*: 2859–2864.

Zhang YG and Frantz JD (1987) Determination of the homogenization temperatures and densities of supercritical fluids in the system NaCl-KCl-CaCl$_2$-H$_2$O using synthetic fluid inclusions. *Chem Geol 64*: 335–350.

Zhang J, Jin Z, Green HW, Jin S (2001) Hydroxyl in continental deep subduction zone: Evidence from UHP eclogites of the Dabie Mountains. *Chinese Sci Bull 46*: 592–596.

Zhang ZM, Shen K, Sun WD, Liu YS, Liou JG, Shi C, Wang JL (2008) Fluids in deeply subducted continental crust: petrology, mineral chemistry and fluid inclusion of UHP metamorphic veins from the Sulu orogen, eastern China. *Geochim Cosmochim Ac 72*: 3200–3228.

Zheng YF, Fu B, Gong B, Li S (1996) Extreme ^{18}O depletion in eclogite from the Su-Lu terrane in East China. *Eur J Mineral 8*: 317–323.

Zheng YF, Fu B, Li Y, Xiao Y, Li S (1998) Oxygen and hydrogen isotope geochemistry of ultrahigh-pressure eclogites from the Dabie Mountains and the Sulu terrane. *Earth Planet Sci Lett 155(1)*: 113–129.

Zheng, Y F, Gong B, Zhao ZF, Fu B, Li Y L (2003a) Two types of gneisses associated with eclogite at Shuanghe in the Dabie terrane: carbon isotope, zircon U–Pb dating and oxygen isotope. *Lithos 70(3)*: 321–343.

Zheng YF, Fu B, Gong B, Li L (2003b) Stable isotope geochemistry of ultrahigh pressure metamorphic rocks from the Dabie–Sulu orogen in China: implications for geodynamics and fluid regime. *Earth Sci Rev 62(1)*: 105–161.

Zheng Y (2004a) Fluid activity during exhumation of deep-subducted continental plate. *Chin Sci Bull 49(10)*: 985–998.

Zheng YF, Wu YB, Chen FK, Gong B, Li L, Zhao ZF (2004b) Zircon U-Pb and oxygen isotope evidence for a large-scale [18]O depletion event in igneous rocks during the Neoproterozoic. *Geochim Cosmochim Ac 68(20)*: 4145–4165.

Zheng YF, Gao TS, Wu YB, Gong B, Liu XM (2007a) Fluid flow during exhumation of deeply subducted continental crust: zircon U–Pb age and O–isotope studies of a quartz vein within ultrahigh-pressure eclogite. *J Metamorph Geol 25*: 267–283.

Zheng, Y. F., Wu, Y. B., Gong, B., Chen, R. X., Tang, J., & Zhao, Z. F. (2007b). Tectonic driving of Neoproterozoic glaciations: Evidence from extreme oxygen isotope signature of meteoric water in granite. Earth and Planetary Science Letters, 256(1), 196-210.

Zheng YF (2009) Fluid regime in continental subduction zones: petrological insights from ultrahigh-pressure metamorphic rocks. *J Geol Soc 166(4)*: 763–782.

Appendix

Nina Albrecht

Date of birth: 16.11.1984

Place of birth: Hameln (Germany)

Scientific education:

04/2004   **ABITUR** (Albert-Einstein-Gymnasium Hameln)

10/2004 – 03/2005   Study of Mathematics the Georg-August-University of Göttingen

04/2005 – 12/2011   Study of Geosciences at the Georg-August-University of Göttingen

06/2009   **BACHELOR OF SCIENCES** (Geosciences)

Thesis: 'Mikrochemische Charakterisierung von Prozessmaterialien der Stahlproduktion mittels LA-ICPMS' (supervisor: Prof. Dr. A. Pack)

09/2009   Mapping thesis: 'Geologische Kartierung W' Västervik (SE' Schweden): Magmatite und Metamorphite im Übergangsbereich der Transskandinavischen Magmatischen Zone und der Svekofennischen Domäne' (supervisor: Prof. Dr. B. T. Hansen)

12/2011   **DIPLOMA** (Geosciences, specialisation: geochemistry and mineralogy)

Thesis: 'Trace Element Mobility at High-Pressure Conditions: A Study on High-Grade Metamorphic Veins from Dabieshan, China' (supervisor: Prof. Dr. G. Wörner)

03/2012 – 2016   **DOCTORATE** at the Geoscience Center Göttingen.

Thesis: 'Evolution of metamorphic fluids at U/HP conditions and their significance for element transfer in subduction zones: A multidisciplinary study on metamorphic veins in eclogites from Dabieshan, China' (supervisor: Prof. G. Wörner)

Scientific experience:

2007 – 2016   Research assistant in the working group of Prof. Dr. A. Pack

2012 – 2016   Teaching assistant in advanced optical petrography

07/2008 – 09/2008   Student trainee at the 'Thyssen Krupp Steel AG Duisburg', Germany

2010 and 2012   Sampling trips to China in collaboration with the School of Earth and Space Sciences Hefei in cooperation with Prof. Dr. Y. Xiao (each 3-weeks)

Awards:

2012   Poster Prize of the 'European Mineralogical Union', awarded at the EMC[2012] Frankfurt

Articles:

- **Albrecht et al.** (in preparation): Evolution of metamorphic fluids during deep continental subduction recorded by fluid inclusions in UHP eclogite-hosted veins (Dabie Shan, China).

- Hezel DC, Poole G, Hoyes J, Coles BJ, Unsworth C, **Albrecht N**, Smith C, Rehkämper M, Pack A, Genge M, Russell SS (2015) Fe and O isotope composition of meteorite fusion crusts: possible natural analogues to chondrule formation? *Meteoritics and Planetary Sciences 50*, 229-242.

- Pack A, Kremer K, **Albrecht N**, Simon K, Kronz A (2010) Description of an aerodynamic levitation apparatus with applications in Earth sciences. *Geochemical Transactions 11*, 1-16.

Abstracts*:

- Hora J, Wörner G, **Albrecht N**, Pack A (2014) Effect of Pre-Eruption Storage on Estimates of magmatic d^{18}O from Minerals. *Goldschmidt Conference*, Prague.

- **Albrecht N**, Wörner G, Xiao Y, van den Kerkhof AM (2013) Fluid inclusions and epidote zoning in UHP eclogite-hosted veins (Dabieshan, China). *DMG/GV Joint Annual Meeting*, Tübingen.

- **Albrecht N**, Wörner G, Xiao Y, van den Kerkhof AM (2013) High pressure fluid evolution derived from veins in UHP eclogites (Dabieshan, China). *Goldschmidt Conference*, Florence.

- **Albrecht N**, Wörner G, Xiao Y, van den Kerkhof AM (2013): Evolution of high pressure fluids deduced from fluid inclusions and epidote zoning in metamorphic veins (Dabieshan UHP Orogenic Belt, China) *ECROFI XXII*, Antalya.

- **Albrecht N**, Wörner G, Xiao Y (2012) Trace Element Mobility and Compositional Evolution in (U)HP Fluids - A Study on High-Grade Metamorphic Veins from Dabieshan, China. *European Mineralogical Conference*, Frankfurt.

- Bischoff A, Horstmann M, Heusser G, Pack A, **Albrecht N** (2012) Almahata Sitta sample MS-181: the first carbonaceous chondrite (CBa) from asteroid 2008 TC3. *75th Annual Meeting of the Meteoritical Society*, Cairns.

- Horstmann M, Bischoff A, Pack A, **Albrecht N**, Weyrauch M, Hain H, Roggon L, Schneider K (2012) Mineralogy and oxygen isotope composition of new samples from the Almahata Sitta strewn field. *75th Annual Meeting of the Meteoritical Society*, Cairns.

- Pack A, **Albrecht N**, Hofmann, M. E. G., Bultmann, E. M., Horváth, B., and Gehler, A. (2012): Variations in triple isotope fractionation exponents. European Mineralogical Conference, Frankfurt.

- Pack A, **Albrecht N**, Hofmann MEG, Horváth B, Gehler A (2012) Experimental data on variations in triple oxygen isotope equilibrium fractionation exponents. *International Symposium on Isotopomers*, Washington D.C.

- Pack A, Horváth B, Hofmann M, Goldmann A, **Albrecht N**, Gellissen M, Zipfel J, Palme H (2011) Defining the terrestrial oxygen isotope fractionation line and observed oxygen isotopic heterogeneity within the Allende meteorite. *Lunar and Planetary Science Conference*, Houston.

- Goldmann A, Pack A, Gellissen M, **Albrecht N**, Zipfel J, Palme H (2011) Oxygen isotope variations in the Allende CV3 meteorite. *Goldschmidt Conference*, Prague.

- Pack A, **Albrecht N**, Hezel DC (2010) Evaporation experiments for studying the interaction between air and cosmic Fe,Ni metals. *20th General Meeting of the International Mineralogical Association*, Budapest.

*First author publications are based on the PhD work, all further contributions are related to my work as research assistant in the working group of Prof. A. Pack

Supplementary material:

Supplementary material is provided in digital form. The attached DVD contains .xlsx and .txt files with all obtained raw data, corrected datasets as well as related calculations and plots presented in this study. An overview on file names and the respective content is given here:

[*eclogite_XRF.xlsx*]:   Bulk eclogite major element chemistry (XRF)

[*eclogite_ICPMS.xlsx*]:   Bulk eclogite trace element chemistry (ICPMS)

[*eclogite_LAICPMS.xlsx*]:   Bulk eclogite trace element chemistry (LA-ICPMS on glassy beads)

[*mineral_EMP.xlsx*]:   Mineral major element chemistry (EMP)

[*epidote_EMP.xlsx*]:   Epidote major and minor element chemistry (EMP)

[*mineral_LAICPMS.xlsx*]:   Mineral trace element chemistry (LA-ICPMS)

[*bulk_vein_model.xlsx*]:   Bulk vein mass balance (major and trace elements)

[*Sr_Pb_TIMS.xlsx*]:   Sr- and Pb-isotopes (TIMS)

[*fluid_inclusion_MT_UV.xlsx*]: Semi-quantitative fluid inclusion chemistry (MicroThermometry) and quantitative in-situ fluid inclusion chemistry (UV-fs-LA-ICPMS)

[*fluid_incl_RAMAN.xlsx*]:   Qualitative in-situ fluid inclusion chemistry (Raman spectroscopy)

[*oxygen_IRLFMS.xlsx*]:   Oxygen isotopes of bulk eclogites and minerals (IR-LF-MS)

[*fluid_incl_P_T_estimates*]:   Fluid inclusion density and isochore calculations[1] (.txt files)

---

[1] Bakker, RJ (2003) Package FLUIDS 1- Computer programs for analysis of fluid inclusion data and for modelling bulk fluid properties. *Chem Geol 194(1)*: 3-23.